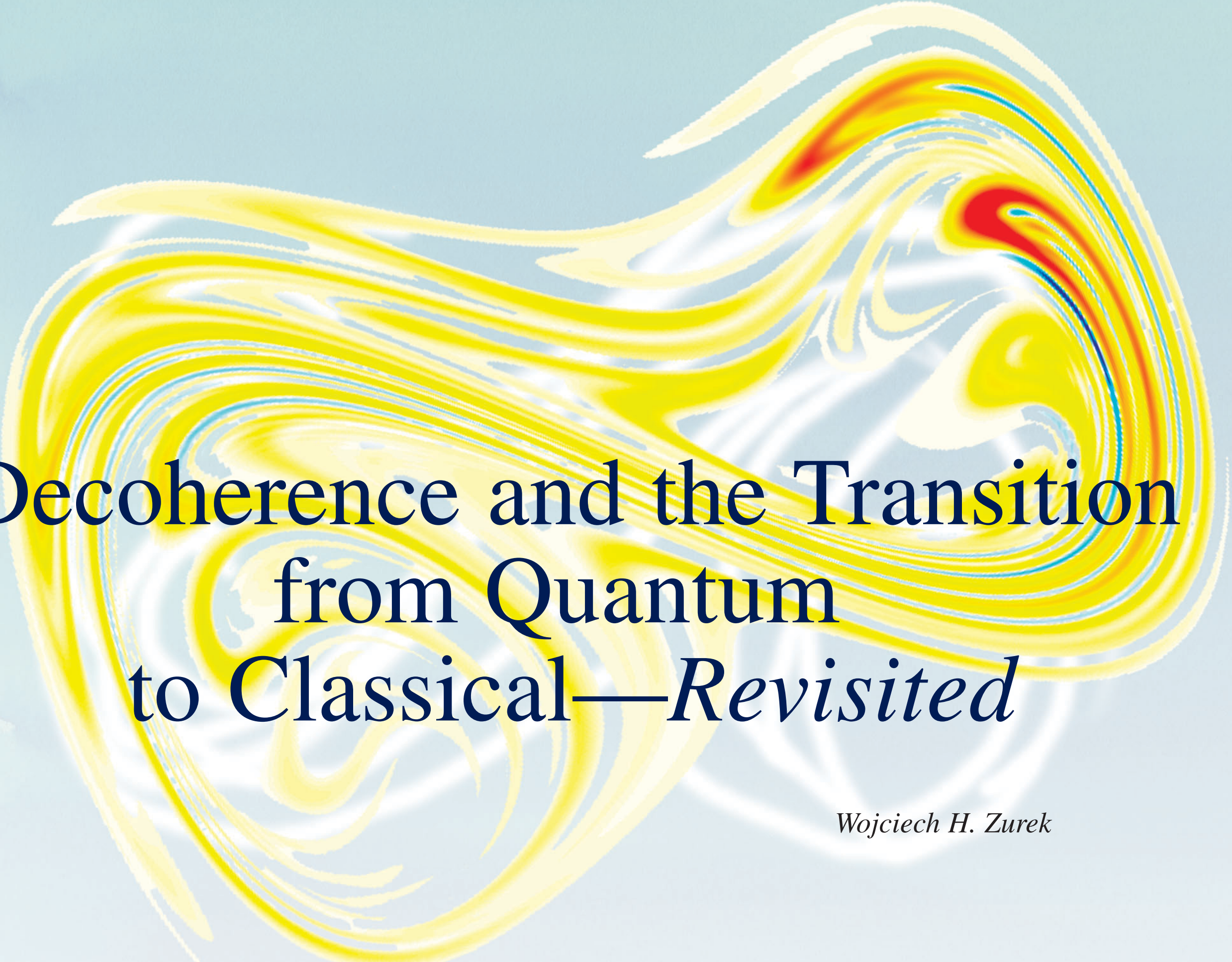

Decoherence and the Transition from Quantum to Classical—*Revisited*

Wojciech H. Zurek

This paper has a somewhat unusual origin and, as a consequence, an unusual structure. It is built on the principle embraced by families who outgrow their dwellings and decide to add a few rooms to their existing structures instead of starting from scratch. These additions usually "show," but the whole can still be quite pleasing to the eye, combining the old and the new in a functional way.

What follows is such a "remodeling" of the paper I wrote a dozen years ago for *Physics Today* (1991). The old text (with some modifications) is interwoven with the new text, but the additions are set off in boxes throughout this article and serve as a commentary on new developments as they relate to the original. The references appear together at the end.

In 1991, the study of decoherence was still a rather new subject, but already at that time, I had developed a feeling that most implications about the system's "immersion" in the environment had been discovered in the preceding 10 years, so a review was in order. While writing it, I had, however, come to suspect that the small gaps in the landscape of the border territory between the quantum and the classical were actually not that small after all and that they presented excellent opportunities for further advances.

Indeed, I am surprised and gratified by how much the field has evolved over the last decade. The role of decoherence was recognized by a wide spectrum of practic-

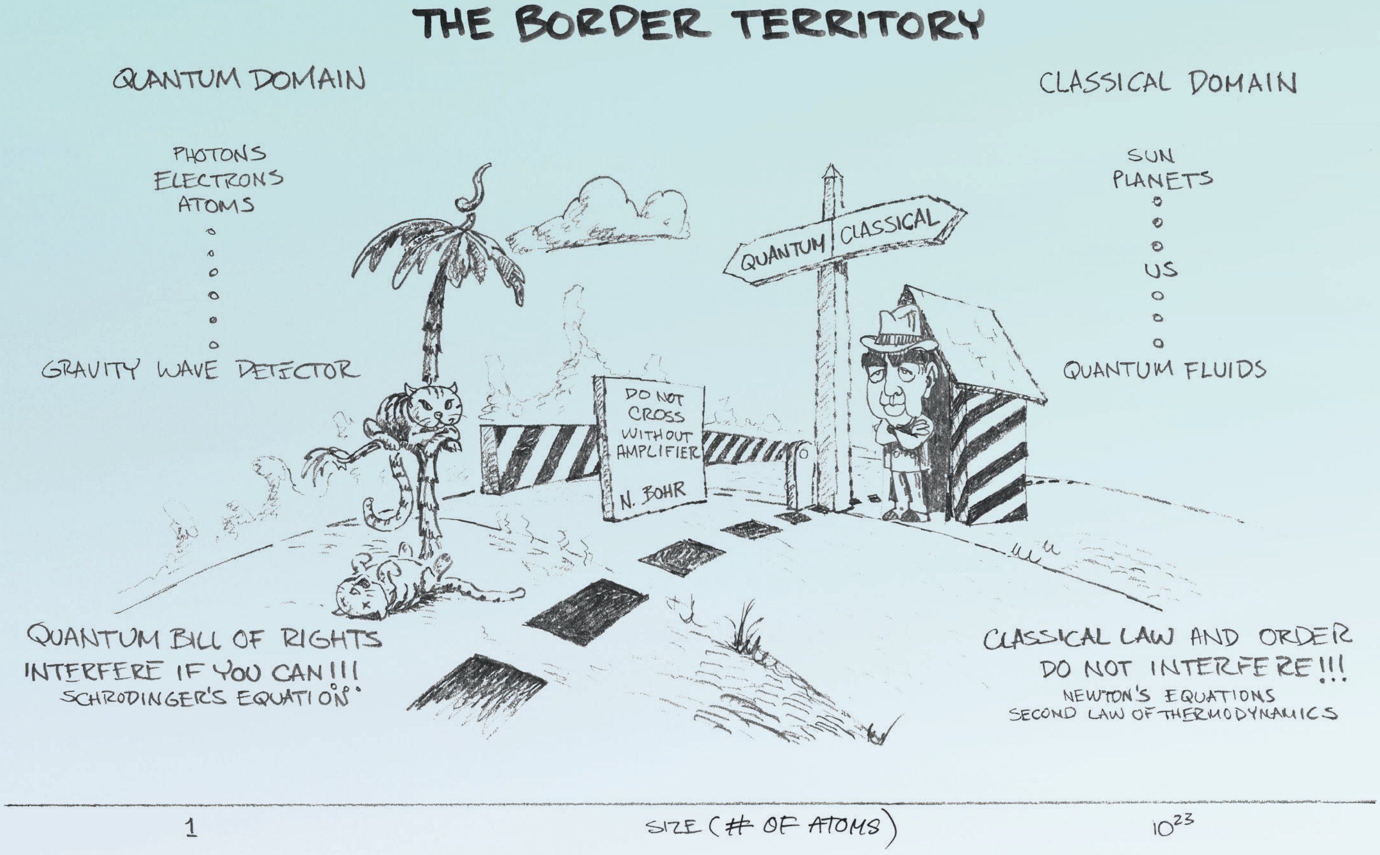
THE BORDER TERRITORY
QUANTUM DOMAIN
CLASSICAL DOMAIN
PHOTONS
ELECTRONS
ATOMS
GRAVITY WAVE DETECTOR
SUN
PLANETS
US
QUANTUM FLUIDS
QUANTUM | CLASSICAL
DO NOT CROSS WITHOUT AMPLIFIER
N. BOHR
QUANTUM BILL OF RIGHTS
INTERFERE IF YOU CAN!!!
SCHRODINGER'S EQUATION
CLASSICAL LAW AND ORDER
DO NOT INTERFERE!!!
NEWTON'S EQUATIONS
SECOND LAW OF THERMODYNAMICS
1
SIZE (# OF ATOMS)
10^{23}

ing physicists as well as, beyond physics proper, by material scientists and philosophers. The study of the predictability sieve, investigations of the interface between chaotic dynamics and decoherence, and most recently, the tantalizing glimpses of the information-theoretic nature of the quantum have elucidated our understanding of the Universe. During this period, Los Alamos has grown into a leading center for the study of decoherence and related issues through the enthusiastic participation of a superb group of staff members, postdoctoral fellows, long-term visitors, and students, many of whom have become long-term collaborators. This group includes, in chronological order, Andy Albrecht, Juan Pablo Paz, Bill Wootters, Raymond Laflamme, Salman Habib, Jim Anglin, Chris Jarzynski, Kosuke Shizume, Ben Schumacher, Manny Knill, Jacek Dziarmaga, Diego Dalvit, Zbig Karkuszewski, Harold Ollivier, Roberto Onofrio, Robin Blume-Kohut, David Poulin, Lorenza Viola, and David Wallace.

Finally, I have some advice for the reader. I believe this paper should be read twice: first, just the old text alone; then—and only then—on the second reading, the whole thing. I would also recommend to the curious reader two other overviews: the draft of my *Reviews of Modern Physics* paper (Zurek 2001a) and Les Houches Lectures coauthored with Paz (Paz and Zurek 2001).

Introduction

Quantum mechanics works exceedingly well in all practical applications. No example of conflict between its predictions and experiment is known. Without quantum physics, we could not explain the behavior of the solids, the structure and function of DNA, the color of the stars, the action of lasers, or the properties of superfluids. Yet nearly a century after its inception, the debate about the relation of quantum physics to the familiar physical world continues. Why is a theory that seems to account with precision for everything we can measure still deemed lacking?

The only "failure" of quantum theory is its inability to provide a natural framework for our prejudices about the workings of the Universe. States of quantum systems evolve according to the deterministic, linear Schrödinger equation

$$i\hbar \frac{d}{dt}|\psi\rangle = H|\psi\rangle \quad . \tag{1}$$

That is, just as in classical mechanics, given the initial state of the system and its Hamiltonian H, one can, at least in principle, compute the state at an arbitrary time. This deterministic evolution of $|\psi\rangle$ has been verified in carefully controlled experiments. Moreover, there is no indication of a border between quantum and classical at which Equation (1) would fail (see cartoon on the opener to this article).

There is, however, a very poorly controlled experiment with results so tangible and immediate that it has enormous power to convince: Our perceptions are often difficult to reconcile with the predictions of Equation (1). Why? Given almost any initial condition, the Universe described by $|\psi\rangle$ evolves into a state containing many alternatives that are never seen to coexist in our world. Moreover, while the ultimate evidence for the choice of one alternative resides in our elusive "consciousness," there is every indication that the choice occurs much before consciousness ever gets involved and that, once made, the choice is irrevocable. Thus, at the root of our unease with quantum theory is the clash between the principle of superposition—the basic tenet of the theory reflected in the linearity of Equation (1)—and everyday classical reality in which this principle appears to be violated.

The problem of measurement has a long and fascinating history. The first widely accepted explanation of how a single outcome emerges from the multitude of potentialities was the Copenhagen Interpretation proposed by Niels Bohr (1928), who insisted that a classical apparatus is necessary to carry out measurements. Thus, quantum theory was not to be universal. The key feature of the Copenhagen Interpretation is the dividing line between quantum and classical. Bohr emphasized that the border must be mobile so that even the "ultimate apparatus"—the human nervous system—could in principle be measured and analyzed as a quantum object, provided that a suitable classical device could be found to carry out the task.

In the absence of a crisp criterion to distinguish between quantum and classical, an identification of the classical with the macroscopic has often been tentatively accepted. The inadequacy of this approach has become apparent as a result of relatively recent developments: A cryogenic version of the Weber bar—a gravity-wave detector— must be treated as a quantum harmonic oscillator even though it may weigh a ton (Braginsky et al. 1980, Caves et al. 1980). Nonclassical squeezed states can describe oscillations of suitably prepared electromagnetic fields with macroscopic numbers of photons (Teich and Saleh 1990). Finally, quantum states associated with the currents of superconducting Josephson junctions involve macroscopic numbers of electrons, but still they can tunnel between the minima of the effective potential corresponding to the opposite sense of rotation (Leggett et al. 1987, Caldeira and Leggett 1983a, Tesche 1986).

If macroscopic systems cannot be always safely placed on the classical side of the boundary, then might there be no boundary at all? The Many Worlds Interpretation (or more accurately, the Many Universes Interpretation), developed by Hugh Everett III with encouragement from John Archibald Wheeler in the 1950s, claims to do away with the boundary (Everett 1957, Wheeler 1957). In this interpretation, the entire universe is described by quantum theory. Superpositions evolve forever according to the Schrödinger equation. Each time a suitable interaction takes place between any two quantum systems, the wave function of the universe splits, developing ever more "branches."

Initially, Everett's work went almost unnoticed. It was taken out of mothballs over a decade later by Bryce DeWitt (1970) and DeWitt and Neill Graham (1973), who managed to upgrade its status from "virtually unknown" to "very controversial." The Many Worlds Interpretation is a natural choice for quantum cosmology, which describes the whole Universe by means of a state vector. There is nothing more macroscopic than the Universe. It can have no a priori classical subsystems. There can be no observer "on the outside." In this universal setting, classicality must be an emergent property of the selected observables or systems.

At first glance, the Many Worlds and Copenhagen Interpretations have little in common. The Copenhagen Interpretation demands an a priori "classical domain" with a border that enforces a classical "embargo" by letting through just one potential outcome. The Many Worlds Interpretation aims to abolish the need for the border altogether. Every potential outcome is accommodated by the ever-proliferating branches of the wave function of the Universe. The similarity between the difficulties faced by these two viewpoints becomes apparent, nevertheless, when we ask the obvious question, "Why do I, the observer, perceive only one of the outcomes?" Quantum theory, with its freedom to rotate bases in Hilbert space, does not even clearly define which states of the Universe correspond to the "branches." Yet, our perception of a reality with alternatives—not a coherent superposition of alternatives—demands an explanation of when, where, and how it is decided what the observer actually records. Considered in this context, the Many Worlds Interpretation in its original version does not really abolish the border but pushes it all the way to the boundary between the physical Universe and consciousness. Needless to say, this is a very uncomfortable place to do physics.

In spite of the profound nature of the difficulties, recent years have seen a growing consensus that progress is being made in dealing with the measurement problem, which is the usual euphemism for the collection of interpretational conundrums described above. The key (and uncontroversial) fact has been known almost since the inception of quantum theory, but its significance for the transition from quantum to classical is being recognized only now: Macroscopic systems are never isolated from their environments. Therefore—as H. Dieter Zeh emphasized (1970)—they should not be expected to follow Schrödinger's equation, which is applicable only to a closed system. As a result, systems usually regarded as classical suffer (or benefit) from the natural loss of quantum coherence, which "leaks out" into the environment (Zurek 1981, 1982). The resulting "decoherence" cannot be ignored when one addresses the problem of the reduction of the quantum mechanical wave packet: Decoherence imposes, in effect, the required "embargo" on the potential outcomes by allowing the observer to maintain only the records of alternatives sanctioned by decoherence and to be aware of only one of the branches—one of the "decoherent histories" in the nomenclature of Murray Gell-Mann and James Hartle (1990) and Hartle (1991).

The aim of this paper is to explain the physics and thinking behind this approach. The reader should be warned that this writer is not a disinterested witness to this development (Wigner 1983, Joos and Zeh 1985, Haake and Walls 1986, Milburn and Holmes 1986, Albrecht 1991, Hu et al. 1992), but rather, one of the proponents. I shall, nevertheless, attempt to paint a fairly honest picture and point out the difficulties as well as the accomplishments.

Decoherence in Quantum Information Processing

Much of what was written in the introduction remains valid today. One important development is the increase in experimental evidence for the validity of the quantum principle of superposition in various contexts including spectacular double-slit experiments that demonstrate interference of fullerenes (Arndt et al. 1999), the study of superpositions in Josephson junctions (Mooij et al.1999, Friedman et al. 2000), and the implementation of Schrödinger "kittens" in atom interferometry (Chapman et al. 1995, Pfau et al. 1994), ion traps (Monroe et al. 1996) and microwave cavities (Brune et al. 1996). In addition to confirming the superposition principle and other exotic aspects of quantum theory (such as entanglement) in novel settings, these experiments allow—as we shall see later—for a controlled investigation of decoherence.

The other important change that influenced the perception of the quantum-to-classical "border territory" is the explosion of interest in quantum information and computation. Although quantum computers were already being discussed in the 1980s, the nature of the interest has changed since Peter Shor invented his factoring algorithm. Impressive theoretical advances, including the discovery of quantum error correction and resilient quantum computation, quickly followed, accompanied by increasingly bold experimental forays. The superposition principle, once the cause of trouble for the interpretation of quantum theory, has become the central article of faith in the emerging science of quantum information processing. This last development is discussed elsewhere in this issue, so I shall not dwell on it here.

The application of quantum physics to information processing has also transformed the nature of interest in the process of decoherence: At the time of my original review (1991), decoherence was a solution to the interpretation problem—a mechanism to impose an effective classicality on de facto quantum systems. In quantum information processing, decoherence plays two roles. Above all, it is a threat to the quantumness of quantum information. It invalidates the quantum superposition principle and thus turns quantum computers into (at best) classical computers, negating the potential power offered by the quantumness of the algorithms. But decoherence is also a necessary (although often taken for granted) ingredient in quantum information processing, which must, after all, end in a "measurement."

The role of a measurement is to convert quantum states and quantum correlations (with their characteristic indefiniteness and malleability) into classical, definite outcomes. Decoherence leads to the environment-induced superselection (einselection) that justifies the existence of the preferred pointer states. It enables one to draw an effective border between the quantum and the classical in straightforward terms, which do not appeal to the "collapse of the wave packet" or any other such deus ex machina.

Correlations and Measurements

A convenient starting point for the discussion of the measurement problem and, more generally, of the emergence of classical behavior from quantum dynamics is the analysis of quantum measurements due to John von Neumann (1932). In contrast to Bohr, who assumed at the outset that the apparatus must be classical (thereby forfeiting the claim of quantum theory to universal validity), von Neumann analyzed the case of a quantum apparatus. I shall reproduce his analysis for the simplest case: a measurement on a two-state system $\mathcal{S}$ (which can be thought of as an atom with spin 1/2) in which a quantum two-state (one bit) detector records the result.

The Hilbert space $\mathcal{H}_{\mathcal{S}}$ of the system is spanned by the orthonormal states $|\uparrow\rangle$ and $|\downarrow\rangle$, while the states $|d_\uparrow\rangle$ and $|d_\downarrow\rangle$ span the $\mathcal{H}_{\mathcal{D}}$ of the detector. A two-dimensional $\mathcal{H}_{\mathcal{D}}$ is the absolute minimum needed to record the possible outcomes. One can devise a quantum

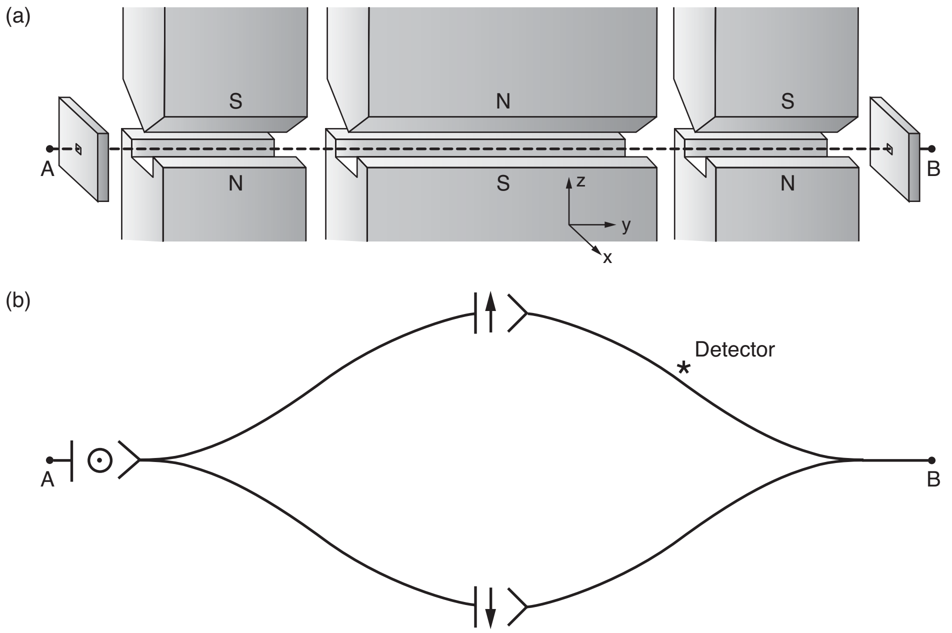

Figure 1. A Reversible Stern-Gerlach Apparatus
The "gedanken" reversible Stern-Gerlach apparatus in (a) splits a beam of atoms into two branches that are correlated with the component of the spin of the atoms (b) and then recombines the branches before the atoms leave the device. Eugene Wigner (1963) used this gedanken experiment to show that a correlation between the spin and the location of an atom can be reversibly undone. The introduction of a one-bit (two-state) quantum detector that changes its state when the atom passes nearby prevents the reversal: The detector inherits the correlation between the spin and the trajectory, so the Stern-Gerlach apparatus can no longer undo the correlation. (This illustration was adapted with permission from Zurek 1981.)

detector (see Figure 1) that "clicks" only when the spin is in the state $|\uparrow\rangle$, that is,

$$|\uparrow\rangle\,|d_{\downarrow}\rangle \rightarrow |\uparrow\rangle\,|d_{\uparrow}\rangle \quad , \tag{2}$$

and remains unperturbed otherwise.

I shall assume that, before the interaction, the system was in a pure state $|\psi_{\mathcal{S}}\rangle$ given by

$$|\psi_{\mathcal{S}}\rangle = \alpha|\uparrow\rangle + \beta|\downarrow\rangle \quad , \tag{3}$$

with the complex coefficients satisfying $|\alpha|^2 + |\beta|^2 = 1$. The composite system starts as

$$|\Phi^{i}\rangle = |\psi_{\mathcal{S}}\rangle|d_{\downarrow}\rangle \quad . \tag{4}$$

Interaction results in the evolution of $|\Phi^{i}\rangle$ into a correlated state $|\Phi^{c}\rangle$:

$$|\Phi^{i}\rangle = (\alpha|\uparrow\rangle + \beta|\downarrow\rangle)|d_{\downarrow}\rangle \Rightarrow \alpha|\uparrow\rangle|d_{\uparrow}\rangle + \beta|\downarrow\rangle|d_{\downarrow}\rangle = |\Phi^{c}\rangle \quad . \tag{5}$$

This essential and uncontroversial first stage of the measurement process can be accomplished by means of a Schrödinger equation with an appropriate interaction. It might be tempting to halt the discussion of measurements with Equation (5). After all, the correlated state vector $|\Phi^{c}\rangle$ implies that, if the detector is seen in the state $|d_{\uparrow}\rangle$, the system is guaranteed to be found in the state $|\uparrow\rangle$. Why ask for anything more?

The reason for dissatisfaction with $|\Phi^{c}\rangle$ as a description of a completed measurement is simple and fundamental: In the real world, even when we do not know the outcome of a measurement, we do know the possible alternatives, and we can safely act as if only one of those alternatives has occurred. As we shall see in the next section, such an assumption is not only unsafe but also simply wrong for a system described by $|\Phi^{c}\rangle$.

How then can an observer (who has not yet consulted the detector) express his ignorance about the outcome without giving up his certainty about the "menu" of the possibilities? Quantum theory provides the right formal tool for the occasion: A density matrix can be used to describe the probability distribution over the alternative outcomes.

Von Neumann was well aware of these difficulties. Indeed, he postulated (1932) that, in addition to the unitary evolution given by Equation (1), there should be an ad hoc "process 1"—a nonunitary reduction of the state vector—that would take the pure, correlated state $|\Phi^C\rangle$ into an appropriate mixture: This process makes the outcomes independent of one another by taking the pure-state density matrix:

$$\rho^c = |\Phi^c\rangle\langle\Phi^c| = |\alpha|^2|\uparrow\rangle\langle\uparrow||d_\uparrow\rangle\langle d_\uparrow| + \alpha\beta^*|\uparrow\rangle\langle\downarrow||d_\uparrow\rangle\langle d_\downarrow| + \alpha^*\beta|\downarrow\rangle\langle\uparrow|d_\downarrow\rangle\langle d_\uparrow| + |\beta|^2|\downarrow\rangle\langle\downarrow||d_\downarrow\rangle\langle d_\downarrow| \ , \tag{6}$$

and canceling the off-diagonal terms that express purely quantum correlations (entanglement) so that the reduced density matrix with only classical correlations emerges:

$$\rho^r = |\alpha|^2|\uparrow\rangle\langle\uparrow||d_\uparrow\rangle\langle d_\uparrow| + |\beta|^2|\downarrow\rangle\langle\downarrow||d_\downarrow\rangle\langle d_\downarrow| \ . \tag{7}$$

Why is the reduced ρ^r easier to interpret as a description of a completed measurement than ρ^c? After all, both ρ^r and ρ^c contain identical diagonal elements. Therefore, both outcomes are still potentially present. So what—if anything—was gained at the substantial price of introducing a nonunitary process 1?

The Question of Preferred Basis: What Was Measured?

The key advantage of ρ^r over ρ^c is that its coefficients may be interpreted as classical probabilities. The density matrix ρ^r can be used to describe the alternative states of a composite spin-detector system that has classical correlations. Von Neumann's process 1 serves a similar purpose to Bohr's "border" even though process 1 leaves all the alternatives in place. When the off-diagonal terms are absent, one can nevertheless safely maintain that the apparatus, as well as the system, is each separately in a definite but unknown state, and that the correlation between them still exists in the preferred basis defined by the states appearing on the diagonal. By the same token, the identities of two halves of a split coin placed in two sealed envelopes may be unknown but are classically correlated. Holding one unopened envelope, we can be sure that the half it contains is either "heads" or "tails" (and not some superposition of the two) and that the second envelope contains the matching alternative.

By contrast, it is impossible to interpret ρ^c as representing such "classical ignorance." In particular, even the set of the alternative outcomes is not decided by ρ^c! This circumstance can be illustrated in a dramatic fashion by choosing $\alpha = -\beta = 1/\sqrt{2}$ so that the density matrix ρ^c is a projection operator constructed from the correlated state

$$|\Phi^C\rangle = (|\uparrow\rangle|d_\uparrow\rangle - |\downarrow\rangle|d_\downarrow\rangle)/\sqrt{2} \ . \tag{8}$$

This state is invariant under the rotations of the basis. For instance, instead of the eigenstates of $|\uparrow\rangle$ and $|\downarrow\rangle$ of $\hat{\sigma}_z$ one can rewrite $|\Phi^C\rangle$ in terms of the eigenstates of $\hat{\sigma}_x$:

$$|\odot\rangle = (|\uparrow\rangle + |\downarrow\rangle)/\sqrt{2} \ , \tag{9a}$$

$$|\otimes\rangle = (|\uparrow\rangle - |\downarrow\rangle)/\sqrt{2} \ . \tag{9b}$$

This representation immediately yields

$$|\Phi^c\rangle = -\,(|\odot\rangle|d_\odot\rangle - |\otimes\rangle|d_\otimes\rangle)/\sqrt{2}\ , \tag{10}$$

where

$$|d_\odot\rangle = (|d_\downarrow\rangle - |d_\uparrow\rangle)/\sqrt{2}\ \text{ and } |d_\otimes\rangle = (|d_\uparrow\rangle + |d_\downarrow\rangle)/\sqrt{2} \tag{11}$$

are, as a consequence of the superposition principle, perfectly "legal" states in the Hilbert space of the quantum detector. Therefore, the density matrix

$$\rho^c = |\Phi^c\rangle\langle\Phi^c|$$

could have many (in fact, infinitely many) different states of the subsystems on the diagonal.

This freedom to choose a basis should not come as a surprise. Except for the notation, the state vector $|\Phi^c\rangle$ is the same as the wave function of a pair of maximally correlated (or entangled) spin-1/2 systems in David Bohm's version (1951) of the Einstein-Podolsky-Rosen (EPR) paradox (Einstein et al. 1935). And the experiments that show that such nonseparable quantum correlations violate Bell's inequalities (Bell 1964) are demonstrating the following key point: The states of the two spins in a system described by $|\Phi^c\rangle$ are not just unknown, but rather they cannot exist before the "real" measurement (Aspect et al. 1981, 1982). We conclude that when a detector is quantum, a superposition of records exists and is a record of a superposition of outcomes—a very nonclassical state of affairs.

Missing Information and Decoherence

Unitary evolution condemns every closed quantum system to "purity." Yet, if the outcomes of a measurement are to become independent events, with consequences that can be explored separately, a way must be found to dispose of the excess information. In the previous sections, quantum correlation was analyzed from the point of view of its role in acquiring information. Here, I shall discuss the flip side of the story: Quantum correlations can also disperse information throughout the degrees of freedom that are, in effect, inaccessible to the observer. Interaction with the degrees of freedom external to the system—which we shall summarily refer to as the environment—offers such a possibility.

Reduction of the state vector, $\rho^c \Rightarrow \rho^r$, decreases the information available to the observer about the composite system $\mathcal{SD}$. The information loss is needed if the outcomes are to become classical and thereby available as initial conditions to predict the future. The effect of this loss is to increase the entropy $\mathcal{H} = -Tr\rho \ln\rho$ by an amount

$$\Delta\mathcal{H} = \mathcal{H}(\rho^r) - \mathcal{H}(\rho^c) = -\,(|\alpha|^2 \ln|\alpha|^2 + |\beta|^2 \ln|\beta|^2)\ . \tag{12}$$

Entropy must increase because the initial state described by ρ^c was pure, $\mathcal{H}(\rho^c) = 0$, and the reduced state is mixed. Information gain—the objective of the measurement—is accomplished only when the observer interacts and becomes correlated with the detector in the already precollapsed state ρ^r.

To illustrate the process of the environment-induced decoherence, consider a system $\mathcal{S}$, a detector $\mathcal{D}$, and an environment $\mathcal{E}$. The environment is also a quantum system. Following the first step of the measurement process—establishment of a correlation as shown in Equation (5)—the environment similarly interacts and becomes correlated with the apparatus:

$$|\Phi^c\rangle|\mathcal{E}_0\rangle = (\alpha|\uparrow\rangle|d_\uparrow\rangle + \beta|\downarrow\rangle|d_\downarrow\rangle)|\mathcal{E}_0\rangle \Rightarrow \alpha|\uparrow\rangle|d_\uparrow\rangle|\mathcal{E}_\uparrow\rangle + \beta|\downarrow\rangle|d_\downarrow\rangle|\mathcal{E}_\downarrow\rangle = |\Psi\rangle \ . \tag{13}$$

The final state of the combined $\mathcal{SDE}$ "von Neumann chain" of correlated systems extends the correlation beyond the $\mathcal{SD}$ pair. When the states of the environment $|\mathcal{E}_i\rangle$ corresponding to the states $|d_\uparrow\rangle$ and $|d_\downarrow\rangle$ of the detector are orthogonal, $\langle\mathcal{E}_i|\mathcal{E}_{i'}\rangle = \delta_{ii'}$, the density matrix for the detector-system combination is obtained by ignoring (tracing over) the information in the uncontrolled (and unknown) degrees of freedom

$$\rho_{\mathcal{DS}} = Tr_{\mathcal{E}}\,|\Psi\rangle\langle\Psi| = \Sigma_i\langle\mathcal{E}_i|\Psi\rangle\langle\Psi|\mathcal{E}_{i'}\rangle = |\alpha|^2|\uparrow\rangle\langle\uparrow||d_\uparrow\rangle\langle d_\uparrow| + |\beta|^2|\downarrow\rangle\langle\downarrow||d_\downarrow\rangle\langle d_\downarrow| = \rho^r \ . \tag{14}$$

The resulting ρ^r is precisely the reduced density matrix that von Neumann called for. Now, in contrast to the situation described by Equations (9)–(11), a superposition of the records of the detector states is no longer a record of a superposition of the state of the system. A preferred basis of the detector, sometimes called the "pointer basis" for obvious reasons, has emerged. Moreover, we have obtained it—or so it appears—without having to appeal to von Neumann's nonunitary process 1 or anything else beyond the ordinary, unitary Schrödinger evolution. The preferred basis of the detector—or for that matter, of any open quantum system—is selected by the dynamics.

Not all aspects of this process are completely clear. It is, however, certain that the detector–environment interaction Hamiltonian plays a decisive role. In particular, when the interaction with the environment dominates, eigenspaces of any observable Λ that commutes with the interaction Hamiltonian,

$$[\Lambda, H_{int}] = 0 \ , \tag{15}$$

invariably end up on the diagonal of the reduced density matrix (Zurek 1981, 1982). This commutation relation has a simple physical implication: It guarantees that the pointer observable Λ will be a constant of motion, a conserved quantity under the evolution generated by the interaction Hamiltonian. Thus, when a system is in an eigenstate of Λ, interaction with the environment will leave it unperturbed.

In the real world, the spreading of quantum correlations is practically inevitable. For example, when in the course of measuring the state of a spin-1/2 atom (see Figure 1b), a photon had scattered from the atom while it was traveling along one of its two alternative routes, this interaction would have resulted in a correlation with the environment and would have necessarily led to a loss of quantum coherence. The density matrix of the $\mathcal{SD}$ pair would have lost its off-diagonal terms. Moreover, given that it is impossible to catch up with the photon, such loss of coherence would have been irreversible. As we shall see later, irreversibility could also arise from more familiar, statistical causes: Environments are notorious for having large numbers of interacting degrees of freedom, making extraction of lost information as difficult as reversing trajectories in the Boltzmann gas.

Quantum Discord—A Measure of Quantumness

The contrast between the density matrices in Equations (6) and (7) is stark and obvious. In particular, the entanglement between the system and the detector in ρ^c is obviously quantum—classical systems cannot be entangled. The argument against the "ignorance" interpretation of ρ^c still stands. Yet we would like to have a quantitative measure of how much is classical (or how much is quantum) about the correlations of a state represented by a general density matrix. Such a measure of the quantumness of correlation was devised recently (Ollivier and Zurek 2002). It is known as quantum discord. Of the several closely related definitions of discord, we shall select one that is easiest to explain. It is based on mutual information—an information-theoretic measure of how much easier it is to describe the state of a pair of objects $(\mathcal{S}, \mathcal{D})$ jointly rather than separately. One formula for mutual information $\mathcal{I}(\mathcal{S}\!:\!\mathcal{D})$ is simply

$$\mathcal{I}(\mathcal{S}\!:\!\mathcal{D}) = \mathcal{H}(\mathcal{S}) + \mathcal{H}(\mathcal{D}) - \mathcal{H}(\mathcal{S}, \mathcal{D}),$$

where $\mathcal{H}(\mathcal{S})$ and $\mathcal{H}(\mathcal{D})$ are the entropies of $\mathcal{S}$ and $\mathcal{D}$, respectively, and $\mathcal{H}(\mathcal{S}, \mathcal{D})$ is the joint entropy of the two. When $\mathcal{S}$ and $\mathcal{D}$ are not correlated (statistically independent),

$$\mathcal{H}(\mathcal{S}, \mathcal{D}) = \mathcal{H}(\mathcal{S}) + \mathcal{H}(\mathcal{D}),$$

and $\mathcal{I}(\mathcal{S}\!:\!\mathcal{D}) = 0$. By contrast, when there is a perfect classical correlation between them (for example, two copies of the same book), $\mathcal{H}(\mathcal{S}, \mathcal{D}) = \mathcal{H}(\mathcal{S}) = \mathcal{H}(\mathcal{D}) = \mathcal{I}(\mathcal{S}\!:\!\mathcal{D})$. Perfect classical correlation implies that, when we find out all about one of them, we also know everything about the other, and the conditional entropy $\mathcal{H}(\mathcal{S}|\mathcal{D})$ (a measure of the uncertainty about $\mathcal{S}$ after the state of $\mathcal{D}$ is found out) disappears. Indeed, classically, the joint entropy $\mathcal{H}(\mathcal{S}, \mathcal{D})$ can always be decomposed into, say, $\mathcal{H}(\mathcal{D})$, which measures the information missing about $\mathcal{D}$, and the conditional entropy $\mathcal{H}(\mathcal{S}|\mathcal{D})$. Information is still missing about $\mathcal{S}$ even after the state of $\mathcal{D}$ has been determined: $\mathcal{H}(\mathcal{S}, \mathcal{D}) = \mathcal{H}(\mathcal{D}) + \mathcal{H}(\mathcal{S}|\mathcal{D})$. This expression for the joint entropy suggests an obvious rewrite of the preceding definition of mutual information into a classically identical form, namely,

$$\mathcal{J}(\mathcal{S}\!:\!\mathcal{D}) = \mathcal{H}(\mathcal{S}) + \mathcal{H}(\mathcal{D}) - (\mathcal{H}(\mathcal{D}) + \mathcal{H}(\mathcal{S}|\mathcal{D})).$$

Here, we have abstained from the obvious (and perfectly justified from a classical viewpoint) cancellation in order to emphasize the central feature of quantumness: In quantum physics, the state collapses into one of the eigenstates of the measured observable. Hence, a state of the object is redefined by a measurement. Thus, the joint entropy can be defined in terms of the conditional entropy only after the measurement used to access, say, $\mathcal{D}$, has been specified. In that case,

$$\mathcal{H}_{|d_k\rangle}(\mathcal{S}, \mathcal{D}) = (\mathcal{H}(\mathcal{D}) + \mathcal{H}(\mathcal{S}|\mathcal{D}))_{|d_k\rangle}\,.$$

This type of joint entropy expresses the ignorance about the pair $(\mathcal{S}, \mathcal{D})$ after the observable with the eigenstates $\{|d_k\rangle\}$ has been measured on $\mathcal{D}$. Of course, $\mathcal{H}_{|d_k\rangle}(\mathcal{S}, \mathcal{D})$ is not the only way to define the entropy of the pair. One can also compute a basis-independent joint entropy $\mathcal{H}(\mathcal{S}, \mathcal{D})$, the von Neumann entropy of the pair. Since these two definitions of joint entropy do not coincide in the quantum case, we can define a basis-dependent quantum discord

$$\delta_{|d_k\rangle}(\mathcal{S}|\mathcal{D}) = \mathcal{I} - \mathcal{J} = (\mathcal{H}(\mathcal{D}) + \mathcal{H}(\mathcal{S}|\mathcal{D}))_{|d_k\rangle} - \mathcal{H}(\mathcal{S},\mathcal{D})$$

as the measure of the extent by which the underlying density matrix describing $\mathcal{S}$ and $\mathcal{D}$ is perturbed by a measurement of the observable with the eigenstates $\{|d_k\rangle\}$. States of classical objects—or classical correlations—are "objective:" They exist independent of measurements. Hence, when there is a basis $\{|\hat{d}_k\rangle\}$ such that the minimum discord evaluated for this basis disappears,

$$\hat{\delta}\,(\mathcal{S}|\mathcal{D}) = \min_{\{|d_k\rangle\}}\big(\mathcal{H}(\mathcal{S},\mathcal{D}) - (\mathcal{H}(\mathcal{D}) + \mathcal{H}(\mathcal{S}|\mathcal{D}))_{|d_k\rangle}\big) = 0,$$

the correlation can be regarded as effectively classical (or more precisely, as "classically accessible through $\mathcal{D}$"). One can then show that there is a set of probabilities associated with the basis $\{|d_k\rangle\}$ that can be treated as classical. It is straightforward to see that, when $\mathcal{S}$ and $\mathcal{D}$ are entangled (for example, $\rho^c = |\phi^c\rangle\langle\phi^c|$), then $\hat{\delta} > 0$ in all bases. By contrast, if we consider ρ^r, discord disappears in the basis $\{|d_\uparrow\rangle, |d_\downarrow\rangle\}$ so that the underlying correlation is effectively classical.

It is important to emphasize that quantum discord is not just another measure of entanglement but a genuine measure of the quantumness of correlations. In situations involving measurements and decoherence, quantumness disappears for the preferred set of states that are effectively classical and thus serves as an indicator of the pointer basis, which as we shall see, emerges as a result of decoherence and einselection.

Decoherence: How Long Does It Take?

A tractable model of the environment is afforded by a collection of harmonic oscillators (Feynman and Vernon 1963, Dekker 1981, Caldeira and Leggett 1983a, 1983b, 1985, Joos and Zeh 1985, Hu et al. 1992) or, equivalently, by a quantum field (Unruh and Zurek 1989). If a particle is present, excitations of the field will scatter off the particle. The resulting "ripples" will constitute a record of its position, shape, orientation, and so on, and most important, its instantaneous location and hence its trajectory.

A boat traveling on a quiet lake or a stone that fell into water will leave such an imprint on the water surface. Our eyesight relies on the perturbation left by the objects on the preexisting state of the electromagnetic field. Hence, it is hardly surprising that an imprint is left whenever two quantum systems interact, even when "nobody is looking," and even when the lake is stormy and full of preexisting waves, and the field is full of excitations—that is, when the environment starts in equilibrium at some finite temperature. "Messy" initial states of the environment make it difficult to decipher the record, but do not preclude its existence.

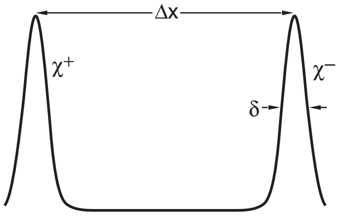

Figure 2. A "Schrödinger Cat" State or a Coherent Superposition
This cat state $\varphi(x)$, the coherent superposition of two Gaussian wave packets of Equation (18), could describe a particle in a superposition of locations inside a Stern-Gerlach apparatus (see Figure 1) or the state that develops in the course of a double-slit experiment. The phase between the two components has been chosen to be zero.

A specific example of decoherence—a particle at position x interacting with a scalar field ϕ (which can be regarded as a collection of harmonic oscillators) through the Hamiltonian

$$H_{int} = \epsilon x \, d\phi/dt \ , \tag{16}$$

where ϵ is the strength of the coupling, has been extensively studied by many, including the investigators just referenced. The conclusion is easily formulated in the so-called "high-temperature limit," in which only thermal-excitation effects of the field ϕ are taken into account and the effect of zero-point vacuum fluctuations is neglected.

In this case, the density matrix $\rho(x, x')$ of the particle in the position representation evolves according to the master equation

$$\dot{\rho} = \overbrace{\underbrace{-\frac{i}{\hbar}[H,\rho]}_{\dot{p}=-FORCE=\nabla V}}^{Von\ \ Neumann\ \ Equation} - \underbrace{\overbrace{\gamma(x-x')\left(\frac{\partial}{\partial x}-\frac{\partial}{\partial x'}\right)\rho}^{Relaxation}}_{\dot{p}=-\gamma p} - \underbrace{\overbrace{\frac{2m\gamma k_B T}{\hbar^2}(x-x')^2\rho}^{Decoherence}}_{Classical\ \ Phase\ \ Space} \ , \tag{17}$$

where H is the particle's Hamiltonian (although with the potential $V(x)$ adjusted because of H_{int}), γ is the relaxation rate, k_{B} is the Boltzmann constant, and T is the temperature of the field. Equation (17) is obtained by first solving exactly the Schrödinger equation for a particle plus the field and then tracing over the degrees of freedom of the field.

I will not analyze Equation (17) in detail but just point out that it naturally separates into three distinct terms, each of them responsible for a different aspect of the effectively classical behavior. The first term—the von Neumann equation (which can be derived from the Schrödinger equation)—generates reversible classical evolution of the expectation value of any observable that has a classical counterpart regardless of the form of ρ (Ehrenfest's theorem). The second term causes dissipation. The relaxation rate $\gamma = \eta/2m$ is proportional to the viscosity $\eta = \epsilon^2/2$ because of the interaction with the scalar field. That interaction causes a decrease in the average momentum and loss of energy. The last term also has a classical counterpart: It is responsible for fluctuations or random "kicks" that lead to Brownian motion. We shall see this in more detail in the next section.

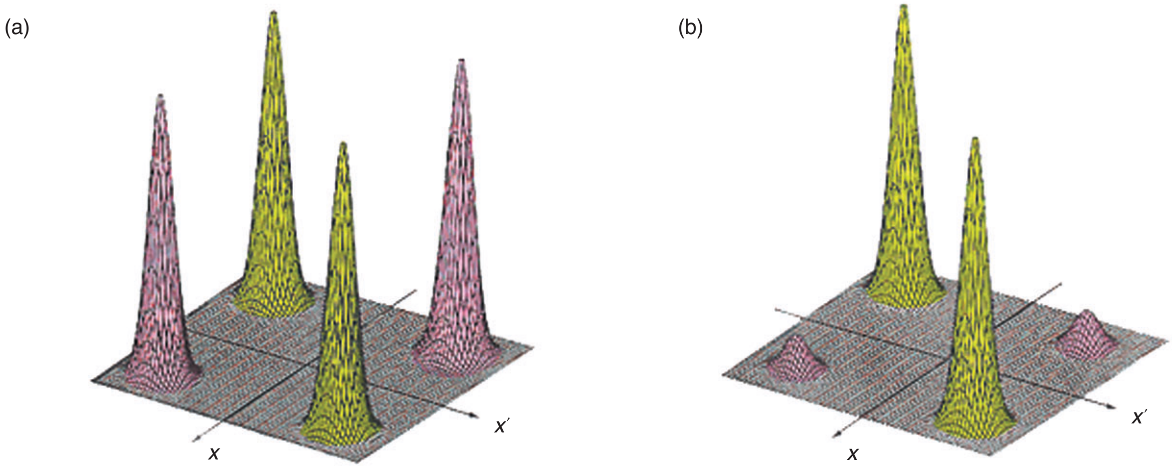

Figure 3. Evolution of the Density Matrix for the Schrödinger Cat State in Figure 2

(a)This plot shows the density matrix for the cat state in Figure 2 in the position representation $\rho(x, x') = \varphi(x)\varphi^*(x)$. The peaks near the diagonal (green) correspond to the two possible locations of the particle. The peaks away from the diagonal (red) are due to quantum coherence. Their existence and size demonstrate that the particle is not in either of the two approximate locations but in a coherent superposition of them. (b) Environment-induced decoherence causes decay of the off-diagonal terms of $\rho(x, x')$. Here, the density matrix in (a) has partially decohered. Further decoherence would result in a density matrix with diagonal peaks only. It can then be regarded as a classical probability distribution with an equal probability of finding the particle in either of the locations corresponding to the Gaussian wave packets.

For our purposes, the effect of the last term on quantum superpositions is of greatest interest. I shall show that it destroys quantum coherence, eliminating off-diagonal terms responsible for quantum correlations between spatially separated pieces of the wave packet. It is therefore responsible for the classical structure of the phase space, as it converts superpositions into mixtures of localized wave packets which, in the classical limit, turn into the familiar points in phase space. This effect is best illustrated by an example. Consider the "cat" state shown in Figure 2, where the wave function of a particle is given by a coherent superposition of two Gaussians: $\varphi(x) = (\chi^+(x) + \chi^-(x))/2^{1/2}$ and the Gaussians are

$$\chi^{\pm}(x) = \langle x|\pm\rangle \sim \exp\left[-\frac{\left(x \pm \frac{\Delta x}{2}\right)^2}{4\delta^2}\right] . \tag{18}$$

For the case of wide separation ($\Delta x >> \delta$), the corresponding density matrix $\rho(x, x') = \varphi(x)\,\varphi^*(x')$ has four peaks: Two on the diagonal defined by $x = x'$, and two off the diagonal for which x and x' are very different (see Figure 3). Quantum coherence is due to the off-diagonal peaks. As those peaks disappear, position emerges as an approximate preferred basis.

The last term of Equation (17), which is proportional to $(x - x')^2$, has little effect on the diagonal peaks. By contrast, it has a large effect on the off-diagonal peaks for which $(x - x')^2$ is approximately the square of the separation $(\Delta x)^2$. In particular, it causes the off-diagonal peaks to decay at the rate $\frac{d}{dt}\left(\rho^{+-}\right) \sim 2\gamma m k_B T \big/ \hbar^2 (\Delta x)^2 \rho^{+-} = \tau_D^{-1}\rho^{+}$.

It follows that quantum coherence will disappear on a decoherence time scale (Zurek 1984):

$$\tau_D \cong \gamma^{-1}\left(\frac{\lambda_{dB}}{\Delta x}\right)^2 = \tau_R\left(\frac{\hbar}{\Delta x\sqrt{2mk_BT}}\right)^2 , \tag{19}$$

where $\lambda_{dB} = \hbar/(2mk_BT)^{-1/2}$ is the thermal de Broglie wavelength. For macroscopic objects, the decoherence time τ_D is typically much less than the relaxation time $\tau_R = \gamma^{-1}$.

For a system at temperature $T = 300$ kelvins with mass $m = 1$ gram and separation $\Delta x = 1$ centimeter, the ratio of the two time scales is $\tau_D/\tau_R \sim 10^{-40}$! Thus, even if the relaxation rate were of the order of the age of the Universe, $\sim 10^{17}$ seconds, quantum coherence would be destroyed in $\tau_D \sim 10^{-23}$ second.

For microscopic systems and, occasionally, even for very macroscopic ones, the decoherence times are relatively long. For an electron ($m_e = 10^{-27}$ grams), τ_D can be much larger than the other relevant time scales on atomic and larger energy and distance scales. For a massive Weber bar, tiny Δx ($\sim 10^{-17}$ centimeter) and cryogenic temperatures suppress decoherence. Nevertheless, the macroscopic nature of the object is certainly crucial in facilitating the transition from quantum to classical.

Experiments on Decoherence

A great deal of work on master equations and their derivations in different situations has been conducted since 1991, but in effect, most of the results described above stand. A summary can be found in Paz and Zurek (2001) and a discussion of the caveats to the simple conclusions regarding decoherence rates appears in James Anglin et al. (1997).

Perhaps the most important development in the study of decoherence is on the experimental front. In the past decade, several experiments probing decoherence in various systems have been carried out. In particular, Michel Brune, Serge Haroche, Jean-Michel Raimond, and their colleagues at École Normale Supérieure in Paris (Brune et al. 1996, Haroche 1998) have performed a series of microwave cavity experiments in which they manipulate electromagnetic fields into a Schrödinger-cat-like superposition using rubidium atoms. They probe the ensuing loss of quantum coherence. These experiments have confirmed the basic tenets of decoherence theory. Since then, the French scientists have applied the same techniques to implement various quantum information-processing ventures. They are in the process of upgrading their equipment in order to produce "bigger and better" Schrödinger cats and to study their decoherence.

A little later, Wineland, Monroe, and coworkers (Turchette et al. 2000) used ion traps (set up to implement a fragment of one of the quantum computer designs) to study the decoherence of ions due to radiation. Again, theory was confirmed, further advancing the status of decoherence as both a key ingredient of the explanation of the emergent classicality and a threat to quantum computation. In addition to these developments, which test various aspects of decoherence induced by a real or simulated "large environment," Pritchard and his coworkers at the Massachusetts Institute of Technology have carried out a beautiful sequence of experiments by using atomic interferometry in order to investigate the role of information transfer between atoms and photons (see Kokorowski et al. 2001 and other references therein). Finally, "analogue experiments" simulating the behavior of the Schrödinger equation in optics (Cheng and Raymer 1999) have explored some of the otherwise difficult-to-access corners of the parameter space.

In addition to these essentially mesoscopic Schrödinger-cat decoherence experiments, designs of much more substantial "cats" (for example, mirrors in superpositions of quantum states) are being investigated in several laboratories.

Classical Limit of Quantum Dynamics

The Schrödinger equation was deduced from classical mechanics in the Hamilton-Jacobi form. Thus, it is no surprise that it yields classical equations of motion when $\hbar$ can be regarded as small. This fact, along with Ehrenfest's theorem, Bohr's correspondence principle, and the kinship of quantum commutators with the classical Poisson brackets, is part of the standard lore found in textbooks. However, establishing the quantum–classical correspondence involves the states as well as the equations of motion. Quantum mechanics is formulated in Hilbert space, which can accommodate localized wave packets with sensible classical limits as well as the most bizarre superpositions. By contrast, classical dynamics happens in phase space.

To facilitate the study of the transition from quantum to classical behavior, it is convenient to employ the Wigner transform of a wave function $\psi(x)$:

$$W(x,p) = \frac{1}{2\pi\hbar} \int_{-\infty}^{\infty} e^{ipy/\hbar} \psi^{*}\left(x + \frac{y}{2}\right) \psi\left(x - \frac{y}{2}\right) dy \ , \tag{20}$$

which expresses quantum states as functions of position and momentum.

The Wigner distribution $W(x,p)$ is real, but it can be negative. Hence, it cannot be regarded as a probability distribution. Nevertheless, when integrated over one of the two variables, it yields the probability distribution for the other (for example, $\int W(x,p)dp = |\psi(x)|^2$). For a minimum uncertainty wave packet, $\psi(x) = \pi^{-1/4}\delta^{-1/2}\exp\{-(x-x_0)^2/2\delta^2 + ip_0x/\hbar\}$, the Wigner distribution is a Gaussian in both x and p:

$$W(x,p) = \frac{1}{\pi\hbar} \exp\left\{ -\frac{(x-x_0)^2}{\delta^2} - \frac{(p-p_0)^2\delta^2}{\hbar^2} \right\} \ . \tag{21}$$

It describes a system that is localized in both x and p. Nothing else that Hilbert space has to offer is closer to approximating a point in classical phase space. The Wigner distribution is easily generalized to the case of a general density matrix $\rho(x,x')$:

$$W(x,p) = \frac{1}{2\pi\hbar} \int_{-\infty}^{-\infty} e^{ipy/\hbar} \rho\left(x - \frac{y}{2}, x + \frac{y}{2}\right) dy \ , \tag{22}$$

where $\rho(x,x')$ is, for example, the reduced density matrix of the particle discussed before.

The phase-space nature of the Wigner transform suggests a strategy for exhibiting classical behavior: Whenever $W(x,p)$ represents a mixture of localized wave packets—as in Equation (21)—it can be regarded as a classical probability distribution in the phase space. However, when the underlying state is truly quantum, as is the superposition in Figure 2, the corresponding Wigner distribution function will have alternating sign—see Figure 4(a). This property alone will make it impossible to regard the function as a probability distribution in phase space. The Wigner function in Figure 4(a) is

$$W(x,p) \sim \frac{\left(W^{+} + W^{-}\right)}{2} \ + \ \frac{1}{\pi\hbar} \exp\left\{ -\frac{p^2\delta^2}{\hbar^2} - \frac{x^2}{\delta^2} \right\} \cdot \cos\left(\frac{\Delta x}{\hbar} p \right) \ , \tag{23}$$

where the Gaussians W^{+} and W^{-} are Wigner transforms of the Gaussian wave packets χ^{+} and χ^{-}. If the underlying state had been a mixture of χ^{+} and χ^{-} rather than a superposition, the Wigner function would have been described by the same two Gaussians W^{+} and W^{-}, but the oscillating term would have been absent.

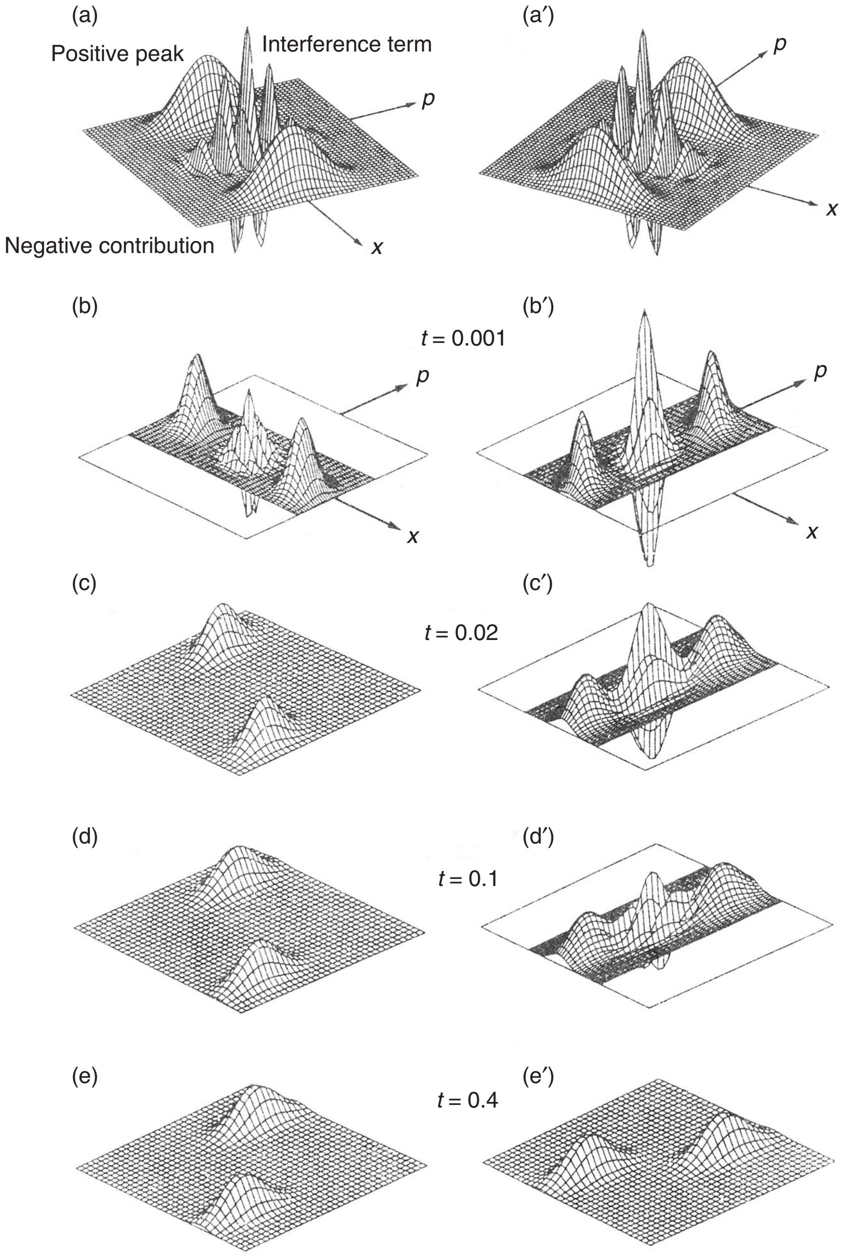

Figure 4. Wigner Distributions and Their Decoherence for Coherent Superpositions
(a) The Wigner distribution $W(x, p)$ is plotted as a function of x and p for the cat state of Figure 2. Note the two separate positive peaks as well as the oscillating interference term in between them. This distribution cannot be regarded as a classical probability distribution in phase space because it has negative contributions. (b–e) Decoherence produces diffusion in the direction of the momentum. As a result, the negative and positive ripples of the interference term in $W(x, p)$ diffuse into each other and cancel out. This process is almost instantaneous for open macroscopic systems. In the appropriate limit, the Wigner function has a classical structure in phase space and evolves in accord with the equations of classical dynamics. (a′–e′) The analogous initial Wigner distribution and its evolution for a superposition of momenta are shown. The interference terms disappear more slowly on a time scale dictated by the dynamics of the system: Decoherence is caused by the environment coupling to (that is, monitoring) the position of the system—see Equation(16). So, for a superposition of momenta, it will start only after different velocities move the two peaks into different locations.

The equation of motion for $W(x, p)$ of a particle coupled to an environment can be obtained from Equation (17) for $\rho(x, x')$:

$$\frac{\partial W}{\partial t} = \underbrace{-\frac{p}{m}\frac{\partial}{\partial x}W + \frac{\partial V}{\partial x}\frac{\partial}{\partial p}W}_{Liouville\ \ Equation} + \underbrace{2\gamma\frac{\partial}{\partial p}pW}_{Friction} + \underbrace{D\frac{\partial^2 W}{\partial p^2}}_{Decoherence} \quad , \tag{24}$$

where V is the renormalized potential and $D = 2m\gamma k_B T = \eta k_B T$. The three terms of this equation correspond to the three terms of Equation (17).

The first term is easily identified as a classical Poisson bracket $\{H, W\}$. That is,

The Predictability Sieve

Since 1991, understanding the emergence of preferred pointer states during the process of decoherence has advanced a great deal. Perhaps the most important advance is the predictability sieve (Zurek 1993, Zurek et al. 1993), a more general definition of pointer states that applies even when the interaction with the environment does not dominate over the self-Hamiltonian of the system. The predictability sieve sifts through the Hilbert space of a system interacting with its environment and selects states that are most predictable. Motivation for the predictability sieve comes from the observation that classical states exist or evolve predictably. Therefore, selecting quantum states that retain predictability in spite of the coupling to the environment is the obvious strategy in search of classicality. To implement the predictability sieve, we imagine a (continuously infinite) list of all the pure states $\{|\psi\rangle\}$ in the Hilbert space of the system in question. Each of them would evolve, after a time t, into a density matrix $\rho_{|\psi\rangle}(t)$. If the system were isolated, all the density matrices would have the form $\rho_{|\psi\rangle}(t) = |\psi(t)\rangle\langle\psi(t)|$ of projection operators, where $|\psi(t)\rangle$ is the appropriate solution of the Schrödinger equation. But when the system is coupled to the environment (that is, the system is "open"), $\rho_{|\psi\rangle}(t)$ is truly mixed and has a nonzero von Neumann entropy. Thus, one can compute $\mathcal{H}(\rho_{|\psi\rangle}(t)) = -Tr\rho_{|\psi\rangle}(t)\log\rho_{|\psi\rangle}(t)$, thereby defining a functional on the Hilbert space $\mathcal{H}_{\mathcal{S}}$ of the system, $|\psi\rangle \rightarrow \mathcal{H}(|\psi\rangle, t)$.

An obvious way to look for predictable, effectively classical states is to seek a subset of all $\{|\psi\rangle\}$ that minimize $\mathcal{H}(|\psi\rangle, t)$ after a certain, sufficiently long time t. When such preferred pointer states exist, are well defined (that is, the minimum of the entropy $\mathcal{H}(|\psi\rangle,t)$ differs significantly for pointer states from the average value), and are reasonably stable (that is, after the initial decoherence time, the set of preferred states is reasonably insensitive to the precise value of t), one can consider them as good candidates for the classical domain. Figure A illustrates an implementation of the predictability sieve strategy using a different, simpler measure of predictability—purity ($\mathrm{Tr}\rho^2$)—rather than the von Neumann entropy, which is much more difficult to compute.

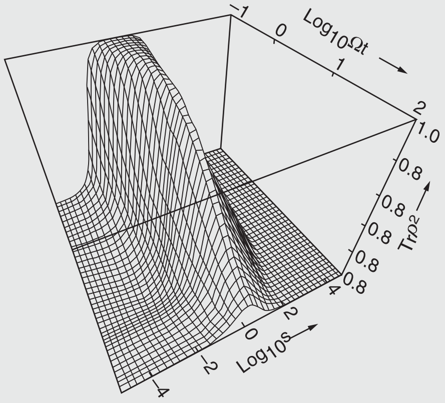

Figure A. The Predictability Sieve for the Underdamped Harmonic Oscillator
One measure of predictability is the so-called purity $\mathrm{Tr}\rho^2$, which is plotted as a function of time for mixtures of minimum uncertainty wave packets in an underdamped harmonic oscillator with $\gamma/\omega = 10^{-4}$. The wave packets start with different squeeze parameters s. $\mathrm{Tr}\rho^2$ serves as a measure of the purity of the reduced density matrix ρ. The predictability sieve favors coherent states ($s = 1$), which have the shape of a ground state, that is, the same spread in position and momentum when measured in units natural for the harmonic oscillator. Because they are the most predictable (more than the energy eigenstates), they are expected to play the crucial role of the pointer basis in the transition from quantum to classical.

if $w(x, p)$ is a familiar classical probability density in phase space, then it evolves according to:

$$\frac{\partial w}{\partial t} = -\frac{\partial w}{\partial x}\frac{\partial H}{\partial p} + \frac{\partial w}{\partial p}\frac{\partial H}{\partial x} = \{H, w\} = Lw \qquad (25)$$

where L stands for the Liouville operator. Thus, classical dynamics in its Liouville form follows from quantum dynamics at least for the harmonic oscillator case, which is described rigorously by Equations (17) and (24). (For more general $V(x)$, the Poisson bracket would have to be supplemented by quantum corrections of order $\hbar$.) The second term of Equation (24) represents friction. The last term results in the diffusion of $W(x, p)$ in momentum at the rate given by D.

Continued on page 104

Quantum Chaos and Phase-Space Aspects of Quantum-Classical Correspondence

Classical mechanics “happens” in phase space. It is therefore critically important to show that quantum theory can—in the presence of decoherence—reproduce the basic structure of classical phase space and that it can emulate classical dynamics. The argument put forward in my original paper (1991) has since been amply supported by several related developments.

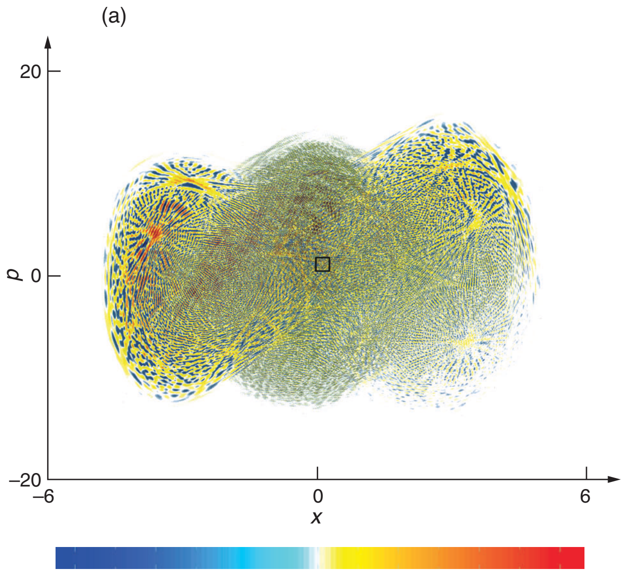

The crucial idealization that plays a key role in classical physics is a “point.” Because of Heisenberg’s principle, $\Delta x\, \Delta p \geq \hbar/2$, quantum theory does not admit states with simultaneously vanishing Δx and Δp. However, as the study of the predictability sieve has demonstrated, in many situations relevant to the classical limit of quantum dynamics, one can expect decoherence to select pointer states that are localized in both Δx and Δp, that is, approximate minimum uncertainty wave packets. In effect, these wave packets are a quantum version of points, which appear naturally in the underdamped harmonic oscillator coupled weakly to the environment (Zurek et al. 1993, Gallis 1996). These results are also relevant to the transition from quantum to classical in the context of field theory with the added twist that the kinds of states selected will typically differ for bosonic and fermionic fields (Anglin and Zurek 1996) because bosons and fermions tend to couple differently to their environments. Finally, under suitable circumstances, einselection can even single out energy eigenstates of the self-Hamiltonian of the system, thus justifying in part the perception of “quantum jumps” (Paz and Zurek 1999).

An intriguing arena for the discussion of quantum-classical correspondence is quantum chaos. To begin with, classical and quantum evolutions from the same initial conditions of a system lead to very different phase-space “portraits.” The quantum phase-space portrait will depend on the particular representation used, but there are good reasons to favor the Wigner distribution. Studies that use the Wigner distribution indicate that, at the moment when quantum-classical correspondence is lost in chaotic dynamics, even the averages computed using properties of the classical and quantum states begin to differ (Karkuszewski et al. 2002).

Decoherence appears to be very effective in restoring correspondence. This point, originally demonstrated almost a decade ago (Zurek and Paz 1994, 1995) has since been amply corroborated by numerical evidence (Habib et al. 1998). Basically, decoherence eradicates the small-scale interference accompanying the rapid development of large-scale coherence in quantum versions of classically chaotic systems (refer to Figure A). This outcome was expected. In order for the quantum to classical correspondence to hold, the coherence length ℓ_C of the quantum state must satisfy the following inequality: $\ell_C = \hbar/(2D\lambda)^{1/2} << \chi$, where λ is the Lyapunov exponent, D is the usual coefficient describing the rate of decoherence, and χ is the scale on which the potential $V(x)$ is significantly nonlinear:

$$\chi \cong \sqrt{\frac{V'}{V'''}}\ .$$

When a quantum state is localized on scales small compared to χ (which is the import of the inequality above), its phase space evolution is effectively classical, but because of chaos and decoherence, it becomes irreversible and unpredictable. Nevertheless—as argued by Tanmoy Bhattacharya, Salman Habib, and Kurt Jacobs in the article “The Emergence of Classical Dynamics in a Quantum World” on page 110—one can even recover more or less classical trajectories by modeling a continuous measurement. However, this is an extra ingredient not in the spirit of the decoherence approach as it invokes the measurement process without explaining it.

A surprising corollary of this line of argument is the realization (Zurek and Paz 1994) that the dynamical second law—entropy production at the scale set by the

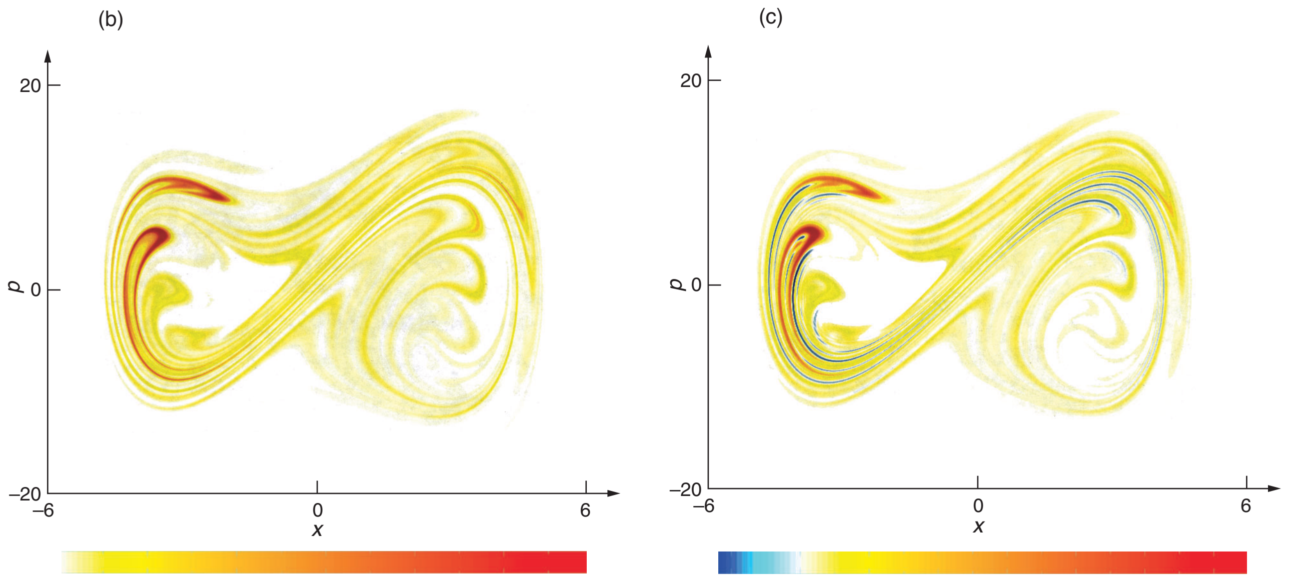

Figure A. Decoherence in a Chaotic Driven Double-Well System

This numerical study (Habib et al. 1998) of a chaotic driven double-well system described by the Hamiltonian $H = p^2/2m - Ax^2 + Bx^4 + Fx\cos(\omega t)$ with $m = 1$, $A = 10$, $B = 0.5$, $F = 10$, and $\omega = 6.07$ illustrates the effectiveness of decoherence in the transition from quantum to classical. These parameters result in a chaotic classical system with a Lyapunov exponent $\lambda \cong 0.5$. The three snapshots taken after 8 periods of the driving force illustrate phase space distributions in (a) the quantum case, (b) the classical case, and (c) the quantum case but with decoherence ($D = 0.025$). The initial condition was always the same Gaussian, and in the quantum cases, the state was pure. Interference fringes are clearly visible in (a), which bears only a vague resemblance to the classical distribution in (b). By contrast, (c) shows that even modest decoherence helps restore the quantum-classical correspondence. In this example the coherence length ℓ_C is not much smaller than the typical nonlinearity scale, so the system is on the border between quantum and classical. Indeed, traces of quantum interference are still visible in (c) as blue "troughs," or regions where the Wigner function is still slightly negative. The change in color from red to blue shown in the legends for (a) and (c) corresponds to a change from positive peaks to negative troughs. In the ab initio classical case (b), there are no negative troughs.

dynamics of the system and more or less independent of the strength of the coupling to the environment—is a natural and, indeed, an inevitable consequence of decoherence. This point has been since confirmed in numerical studies (Miller and Sarkar 1999, Pattanayak 1999, Monteoliva and Paz 2000).

Other surprising consequences of the study of Wigner functions in the quantum-chaotic context is the realization that they develop phase space structure on the scale associated with the sub-Planck action $a = \hbar^2/A << \hbar$, where A is the classical action of the system, and that this sub-Planck action is physically significant (Zurek 2001b). This can be seen in Figure A part (a), where a small black square with the area of $\hbar$ is clearly larger than the smallest "ripples" in the image. This point was to some extent anticipated by the plots of the Wigner functions of Schrödinger cats [see Figures 4(a) and 4(a′) in this article] a version of which appeared in the 1991 *Physics Today* version of this paper—the interference term of the Wigner function has a sub-Planck structure.

A lot has happened in establishing phase-space aspects of quantum-classical correspondence, but a lot more remains to be done. (A more thorough summary of the past accomplishments and remaining goals can be found in Zurek 2001b).

Continued from page 101

Classical equations of motion are a necessary but insufficient ingredient of the classical limit: We must also obtain the correct structure of the classical phase space by barring all but the probability distributions of well-localized wave packets. The last term in Equation (24) has precisely this effect on nonclassical $W(x,p)$. For example, the Wigner function for the superposition of spatially localized wave packets—Figure 4(a)—has a sinusoidal modulation in the momentum coordinate produced by the oscillating term $\cos((\Delta x/\hbar)p)$. This term, however, is an eigenfunction of the diffusion operator $\partial^2/\partial p^2$ in the last term of Equation (24). As a result, the modulation is washed out by diffusion at a rate

$$\tau_D^{-1} = -\frac{\dot{W}}{W} = \frac{\left(D\dfrac{\partial^2}{\partial p^2}W\right)}{W} = \frac{2m\gamma k_B T\left(\Delta x\right)^2}{\hbar^2} . \qquad (26)$$

Negative valleys of $W(x,p)$ fill in on a time scale of order τ_D, and the distribution retains just two peaks, which now correspond to two classical alternatives—see Figures 4(a) to 4(e). The Wigner function for a superposition of momenta, shown in Figure 4(a′), also decoheres as the dynamics causes the resulting difference in velocities to damp out the oscillations in position and again yield two classical alternatives—see Figures 4(b′) to 4(e′).

The ratio of the decoherence and relaxation time scales depends on $\hbar^2/m$—see Equation (19). Therefore, when m is large and $\hbar$ small, τ_D can be nearly zero—decoherence can be nearly instantaneous—while, at the same time, the motion of small patches (which correspond to the probability distribution in classical phase space) in the smooth potential becomes reversible. This idealization is responsible for our confidence in classical mechanics, and, more generally, for many aspects of our belief in classical reality.

The discussion above demonstrates that decoherence and the transition from quantum to classical (usually regarded as esoteric) is an inevitable consequence of the immersion of a system in an environment. True, our considerations were based on a fairly specific model—a particle in a heat bath of harmonic oscillators. However, this is often a reasonable approximate model for many more complicated systems. Moreover, our key conclusions—such as the relation between the decoherence and relaxation time scales in Equation (19)—do not depend on any specific features of the model. Thus, one can hope that the viscosity and the resulting relaxation always imply decoherence and that the transition from quantum to classical can be always expected to take place on a time scale of the order of the above estimates.

Quantum Theory of Classical Reality

Classical reality can be defined purely in terms of classical states obeying classical laws. In the past few sections, we have seen how this reality emerges from the substrate of quantum physics: Open quantum systems are forced into states described by localized wave packets. They obey classical equations of motion, although with damping terms and fluctuations that have a quantum origin. What else is there to explain?

Controversies regarding the interpretation of quantum physics originate in the clash between the predictions of the Schrödinger equation and our perceptions. I will therefore conclude this paper by revisiting the source of the problem—our awareness of definite outcomes. If these mental processes were essentially unphysical, there would be no hope of formulating and addressing the ultimate question—why do we perceive just one of the quantum alternatives?—within the context of physics. Indeed, one might be tempted to follow Eugene Wigner (1961) and give consciousness the last word in collapsing the state vector. I shall assume the opposite. That is, I shall examine the idea that the higher mental processes all correspond to well-defined, but at present, poorly understood information-processing functions that are being carried out by physical systems, our brains.

Described in this manner, awareness becomes susceptible to physical analysis. In particular, the process of decoherence we have described above is bound to affect the states of the brain: Relevant observables of individual neurons, including chemical concentrations and electrical potentials, are macroscopic. They obey classical, dissipative equations of motion. Thus, any quantum superposition of the states of neurons will be destroyed far too quickly for us to become conscious of the quantum "goings on." Decoherence, or more to the point, environment-induced superselection, applies to our own "state of mind."

One might still ask why the preferred basis of neurons becomes correlated with the classical observables in the familiar universe. It would be, after all, so much easier to believe in quantum physics if we could train our senses to perceive nonclassical superpositions. One obvious reason is that the selection of the available interaction Hamiltonians is limited and constrains the choice of detectable observables. There is, however, another reason for this focus on the classical that must have played a decisive role: Our senses did not evolve for the purpose of verifying quantum mechanics. Rather, they have developed in the process in which survival of the fittest played a central role. There is no evolutionary reason for perception when nothing can be gained from prediction. And, as the predictability sieve illustrates, only quantum states that are robust in spite of decoherence, and hence, effectively classical, have predictable consequences. Indeed, classical reality can be regarded as nearly synonymous with predictability.

There is little doubt that the process of decoherence sketched in this paper is an important element of the big picture central to understanding the transition from quantum to classical. Decoherence destroys superpositions. The environment induces, in effect, a superselection rule that prevents certain superpositions from being observed. Only states that survive this process can become classical.

There is even less doubt that this rough outline will be further extended. Much work needs to be done both on technical issues (such as studying more realistic models that could lead to additional experiments) and on problems that require new conceptual input (such as defining what constitutes a "system" or answering the question of how an observer fits into the big picture).

Decoherence is of use within the framework of either of the two interpretations: It can supply a definition of the branches in Everett's Many Worlds Interpretation, but it can also delineate the border that is so central to Bohr's point of view. And if there is one lesson to be learned from what we already know about such matters, it is that information and its transfer play a key role in the quantum universe.

The natural sciences were built on a tacit assumption: Information about the universe can be acquired without changing its state. The ideal of "hard science" was to be objective and provide a description of reality. Information was regarded as unphysical, ethereal, a mere record of the tangible, material universe, an inconsequential reflection, existing beyond and essentially decoupled from the domain governed by the laws of physics. This view is no longer tenable (Landauer 1991). Quantum theory has put an end to this Laplacean dream about a mechanical universe. Observers of quantum phenomena can no longer be just passive spectators. Quantum laws make it impossible to gain information without changing the state of the measured object. The dividing line between what is and what is known to be has been blurred forever. While abolishing this boundary, quantum theory has simultaneously deprived the "conscious observer" of a monopoly on acquiring and storing information: Any correlation is a registration, any quantum state is a record of some other quantum state. When correlations are robust enough, or the record is sufficiently indelible, familiar classical "objective reality" emerges from the quantum substrate. Moreover, even a minute interaction with the environment, practically inevitable for any macroscopic object, will establish such a correlation: The environment will, in effect, measure the state of the object, and this suffices to destroy quantum coherence. The resulting decoherence plays, therefore, a vital role in facilitating the transition from quantum to classical.

The Existential Interpretation

The quantum theory of classical reality has developed significantly since 1991. These advances are now collectively known as the existential interpretation (Zurek 2001a). The basic difference between quantum and classical states is that the objective existence of the latter can be taken for granted. That is, a system's classical state can be simply "found out" by an observer originally ignorant of any of its characteristics. By contrast, quantum states are hopelessly "malleable"—it is impossible in principle for an observer to find out an unknown quantum state without perturbing it. The only exception to this rule occurs when an observer knows beforehand that the unknown state is one of the eigenstates of some definite observable. Then and only then can a nondemolition measurement (Caves et al. 1980) of that observable be devised such that another observer who knew the original state would not notice any perturbations when making a confirmatory measurement.

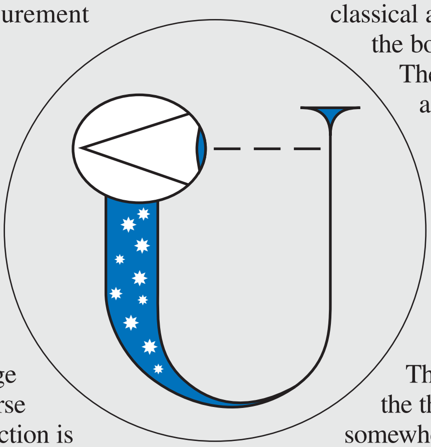

If the unknown state cannot be found out—as is indeed the case for isolated quantum systems—then one can make a persuasive case that such states are subjective, and that quantum state vectors are merely records of the observer's knowledge about the state of a fragment of the Universe (Fuchs and Peres 2000). However, einselection is capable of converting such malleable and "unreal" quantum states into solid elements of reality. Several ways to argue this point have been developed since the early discussions (Zurek 1993, 1998, 2001a). In effect, all of them rely on einselection, the emergence of the preferred set of pointer states. Thus, observers aware of the structure of the Hamiltonians (which are "objective," can be found out without "collateral damage", and in the real world, are known well enough in advance) can also divine the sets of preferred pointer states (if they exist) and thus discover the preexisting state of the system.

One way to understand this environment-induced objective existence is to recognize that observers—especially human observers—never measure anything directly. Instead, most of our data about the Universe is acquired when information about the systems of interest is intercepted and spread throughout the environment. The environment preferentially records the information about the pointer states, and hence, only information about the pointer states is readily available. This argument can be made more rigorous in simple models, whose redundancy can be more carefully quantified (Zurek 2000, 2001a).

This is an area of ongoing research. Acquisition of information about the systems from fragments of the environment leads to the so-called conditional quantum dynamics, a subject related to quantum trajectories (Carmichael 1993). In particular one can show that the predictability sieve also works in this setting (Dalvit et al. 2001).

The overarching open question of the interpretation of quantum physics—the "meaning of the wave function"—appears to be in part answered by these recent developments. Two alternatives are usually listed as the only conceivable answers. The possibility that the state vector is purely epistemological (that is, solely a record of the observer's knowledge) is often associated with the Copenhagen Interpretation (Bohr 1928). The trouble with this view is that there is no unified description of the Universe as a whole: The classical domain of the Universe is a necessary prerequisite, so both classical and quantum theory are necessary and the border between them is, at best, ill-defined. The alternative is to regard the state vector as an ontological entity—as a solid description of the state of the Universe akin to the classical states. But in this case (favored by the supporters of Everett's Many Worlds Interpretation), everything consistent with the universal state vector needs to be regarded as equally "real."

The view that seems to be emerging from the theory of decoherence is in some sense somewhere in between these two extremes. Quantum state vectors can be real, but only when the superposition principle—a cornerstone of quantum behavior—is "turned off" by einselection. Yet einselection is caused by the transfer of information about selected observables. Hence, the ontological features of the state vectors—objective existence of the einselected states—is acquired through the epistemological "information transfer."

Obviously, more remains to be done. Equally obviously, however, decoherence and einselection are here to stay. They constrain the possible solutions after the quantum–classical transition in a manner suggestive of a still more radical view of the ultimate interpretation of quantum theory in which information seems destined to play a central role. Further speculative discussion of this point is beyond the scope of the present paper, but it will be certainly brought to the fore by (paradoxically) perhaps the most promising applications of quantum physics to information processing. Indeed, quantum computing inevitably poses questions that probe the very core of the distinction between quantum and classical. This development is an example of the unpredictability and serendipity of the process of scientific discovery: Questions originally asked for the most impractical of reasons—questions about the EPR paradox, the quantum-to-classical transition, the role of information, and the interpretation of the quantum state vector—have become relevant to practical applications such as quantum cryptography and quantum computation. ■

Acknowledgments

I would like to thank John Archibald Wheeler for many inspiring and enjoyable discussions on “the quantum” and Juan Pablo Paz for the pleasure of a long-standing collaboration on the subject.

Further Reading

Albrecht, A., 1992. Investigating Decoherence in a Simple System. *Phys. Rev. D* **46** (12): 5504.

Anglin, J. R., and W. H. Zurek. 1996. Decoherence of Quantum Fields: Pointer States and Predictability. *Phys*. *Rev*. *D* **53** (12): 7327.

Anglin, J. R., J. P. Paz, and W. H. Zurek. 1997. Deconstructing Decoherence. *Phys*. *Rev*. *A* **55** (6): 4041.

Arndt, M., O. Nairz, J. VosAndreae, C. Keller, G. van der Zouw, A. Zeilinger. 1999. Wave-Particle Duality of C-60 Molecules. *Nature* **401** (6754): 680.

Aspect, A., J. Dalibard, and G. Roger. 1982. Experimental Test of Bell’s Inequalities Using Time-Varying Analyzers. *Phys*. *Rev*. *Lett*. **49**: 1804.

Aspect, A., P. Grangier, and G. Rogier. 1981. Experimental Tests of Realistic Local Theories via Bell’s Theorem. *Phys*. *Rev*. *Lett*. **47**: 460.

Bell. J. S. 1964. On the Einstein Podolsky Rosen Paradox. *Physics* **1**: 195.

Bohm, D. 1951. In *Quantum Theory*. Chap. 22, p. 611. Englewood Cliffs, NJ: Prentice Hall.

Bohr, N. 1928. The Quantum Postulate and Recent Development of Atomic Theory. *Nature* **121**: 580. Reprinted in *Quantum Theory and Measurement*. Edited by Wheeler, J. A., and W. H. Zurek. Princeton, NJ: Princeton University Press.

Braginsky, V. B., Y. I. Vorontsov, and K. S. Thorne. 1980. Quantum Nondemolition Measurements. *Science* **209**: 547.

Brune, M., E. Hagley, J. Dreyer, X. Maitre, C. Wunderlich, J. M. Raimond, and S. Haroche. 1996. Observing the Progressive Decoherence of the “Meter” in a Quantum Measurement. *Phys*. *Rev*. *Lett*. **77**: 4887.

Caldeira, A. O., and A. J. Leggett. 1983a. Path Integral Approach to Quantum Brownian Motion. *Physica A*. **121**: 587.

———. 1983b. Quantum Tunneling in a Dissipative System. *Ann*. *Phys*. *(N. Y.)* **149** (2): 374.

———. 1985. Influence of Damping on Quantum Interference: An Exactly Soluble Model. *Phys*. *Rev*. *A* **31**: 1059.

Carmichael, H. J. 1993. *An Open Systems Approach to Quantum Optics*. Berlin: Springer Verlag.

Caves, C. M., K. S. Thorne, R. W. P. Drewer, V. D. Sandberg, and M. Zimmerman. 1980. On the Measurement of a Weak Classical Force Coupled to a Quantum-Mechanical Oscillator. 1. Issues of Principle. *Rev*. *Mod*. *Phys*. **52**: 341.

Chapman, M. S., T. D. Hammond, A. Lenef, J. Schmiedmayer, R. A. Rubenstein, E. Smith , and D. E. Pritchard. 1995. Photon Scattering from Atoms in an Atom Interferometer. *Phys*. *Rev*. *Lett*. **75** (21): 3783.

Cheng, C. C., and M. G. Raymer. 1999. Long-Range Saturation of Spatial Decoherence in Wave-Field Transport in Random Multiple-Scattering Media. *Phys*. *Rev*. *Lett*. **82** (24): 4807.

Dalvit, D. A. R., J. Dziarmaga, W. H. Zurek. 2001. Unconditional Pointer States from Conditional Master Equations. *Phys. Rev. Lett.* **86** (3): 373.

Dekker, H. 1981. Classical and Quantum Mechanics of the Damped Harmonic Oscillator. *Phys*. *Rep*. **80**: 1.

DeWitt, B. S. 1970. Quantum Mechanics and Reality. *Phys*. *Today* **23**: 30.

DeWitt, B. S., and N. Graham, eds. 1973. *The Many-Worlds Interpretation of Quantum Mechanics*. Princeton: Princeton University Press.

Einstein, A., B. Podolsky, and N. Rosen. 1935. Can Quantum-Mechanical Description of Physical Reality Be Considered Complete? *Phys*. *Rev*. **47**: 777.

Everett III, H. 1957. “Relative State” Formulation of Quantum Mechanics. *Rev*. *Mod*. *Phys*. **29**: 454.

Feynman, R. P., and F. L.Vernon. 1963. The Theory of a General Quantum System Interacting with a Linear Dissipative System. *Ann*. *Phys*. **24**: 118.

Friedman, J. R., V. Patel, W. Chen, S. K. Tolpygo, and J. E. Lukens. 2000. Quantum Superposition of Distinct Macroscopic States. *Nature* **406** (6791): 43.

Fuchs, C. A., and A. Peres. 2000. Quantum Theory Needs No “Interpretation”. *Phys*. *Today* **53** (3): 70.

Gallis, M. R. 1996. Emergence of Classicality via Decoherence Described by Lindblad Operators. *Phys*. *Rev*. *A* **53** (2): 655.

Gell-Mann, M., and J. B. Hartle. 1990. Quantum Mechanics in the Light of Quantum Cosmology. In *Complexity, Entropy, and the Physics of Information*. p. 425. Edited by W. H. Zurek. Redwood City: Addison-Wesley.

Griffiths, R. B. 1984. Consistent Histories and the Interpretation of Quantum Mechanics. *J*. *Stat*. *Phys*. **36**: 219.

Haake, F., and D. F. Walls. 1986. In *Quantum Optics IV*. Edited by J. D. Harvey, and D. F. Walls. Berlin: Springer Verlag.

Habib, S., K. Shizume, and W. H. Zurek. 1998. Decoherence, Chaos, and the Correspondence Principle. *Phys*. *Rev*. *Lett*. **80** (20): 4361.

Haroche, S. 1998. Entanglement, Mesoscopic Superpositions and Decoherence Studies with Atoms and Photons in a Cavity. *Physica Scripta* **T76**: 159.

Hartle, J. B. 1991. The Quantum Mechanics of Cosmology. In *Quantum Cosmology and Baby Universes: Proceedings of the 1989 Jerusalem Winter School*. Edited by S. Coleman, J. B. Hartle, T. Piran, and S. Weinberg. Singapore: World Scientific.

Hu, B. L., J. P. Paz, and Y. Zhang. 1992. Quantum Brownian Motion in a General Environment: Exact Master Equation with Nonlocal Dissipation and Colored Noise. *Phys*. *Rev*. *D* **45**: 2843.

Joos, E., and H. D. Zeh. 1985. The Emergence of Classical Properties Through Interaction with the Environment. *Z*. *Phys*. *B* **59**: 223.

Karkuszewski, Z. P., J. Zakrzewski, and W. H. Zurek. 2002. Breakdown of Correspondence in Chaotic Systems: Ehrenfest Versus Localization Times. *Phys*. *Rev*. *A* **65** (4): 042113.

Kokorowski, D. A., A. D. Cronin, T. D. Roberts, and D. E. Pritchard. 2001. From Single-to Multiple-Photon Decoherence in an Atom Interferometer. *Phys*. *Rev*. *Lett*. **86** (11): 2191.

Landauer, R. 1991. Information is Physical. *Phys*. *Today* **44** (5): 23.

Leggett, A. J., S. Chakravarty, A. T. Dorsey, M. P. A. Fisher, A. Garg, and W. Zwerger. 1987. Dynamics of the Dissipative System. *Rev*. *Mod*. *Phys*. **59**: 1.

Milburn, G. J., and C. A. Holmes. 1986. Dissipative Quantum and Classical Liouville Mechanics of the Unharmonic Oscillator. *Phys*. *Rev*. *Lett*. **56**: 2237.

Miller, P. A., and S. Sarkar. 1999. Signatures of Chaos in the Entanglement of Two Coupled Quantum Kicked Tops. *Phys. Rev. E* **60**: 1542.

Monroe, C., D. M. Meekhof, B. E. King, and D. J. Wineland. 1996. A "Schrodinger Cat" Superposition State of an Atom. *Science* **272** (5265): 1131.

Monteoliva, D., and J. P. Paz. 2000. Decoherence and the Rate of Entropy Production in Chaotic Quantum Systems. *Phys*. *Rev*. *Lett*. **85** (16): 3373.

Mooij, J. E., T. P. Orlando, L. Levitov, L. Tian, C. H. van der Wal, and S. Lloyd. 1999. Josephson Persistent-Current Qubit. *Science* **285** (5430): 1036.

Myatt, C. J., B. E. King, Q. A. Turchette, C. A. Sackett, D. Kielpinski, W. M. Itano, et al. 2000. Decoherence of Quantum Superpositions Through Coupling to Engineered Reservoirs. *Nature* **403**: 269.

Ollivier, H., and W. H. Zurek. 2002. Quantum Discord: A Measure of the Quantumness of Correlations. *Phys*. *Rev*. *Lett*. **88** (1): 017901.

Omnès, R. 1990. From Hilbert Space to Common Sense. *Ann*. *Phys*. **201**: 354.

———. 1992. Consistent Interpretation of Quantum Mechanics. *Rev*. *Mod*. *Phys*. **64**: 339.

Pattanayak, A. K. 1999. Lyapunov Exponents Entropy Production and Decoherence. *Phys*. *Rev*. *Lett*. **83** (22): 4526.

Paz, J. P., and W. H. Zurek. 1993. Environment-Induced Decoherence, Classicality, and Consistency of Quantum Histories. *Phys*. *Rev*. *D* **48** (6): 2728.

———. 1999. Quantum Limit of Decoherence: Environment Induced Superselection of Energy Eigenstates. *Phys*. *Rev*. *Lett*. **82** (26): 5181.

———. 2001. In *Coherent Atomic Matter Waves*, *Les Houches Lectures*. Edited by R. Kaiser, C. Westbrook, and F. Davids. Vol. 72, p. 533. Berlin: Springer.

Paz, J. P., S. Habib, and W. H. Zurek. 1993. Reduction of the Wave Packet: Preferred Observable and Decoherence Time Scale. *Phys*. *Rev*. *D* **47**: 488.

Pfau, T., S. Spälter, Ch. Kurtsiefer, C. R. Ekstrom, and J. Mlynek. 1994. Loss of Spatial Coherence by a Single Spontaneous Emission. *Phys*. *Rev*. *Lett*. **73** (9): 1223.

Scully, M. O., B. G. Englert, and J. Schwinger. 1989. Spin Coherence and Humpty-Dumpty. III. The Effects of Observation. *Phys*. *Rev*. *A* **40**: 1775.

Teich, M. C., and B. E. A. Saleh. 1990. Squeezed and Antibunched Light. *Phys. Today* **43** (6): 26.

Tesche, C. D. 1986. Schroedinger's Cat: A Realization in Superconducting Devices. *Ann*. *N*. *Y*. *Acad*. *Sci*. **480**: 36.

Turchette, Q. A., C. J. Myatt, B. E. King, C. A. Sackett, D. Kielpinski, W. M. Itano, et al. 2000. Decoherence and Decay of Motional Quantum States of a Trapped Atom Coupled to Engineered Reservoirs. *Phys*. *Rev*. *A* **62**: 053807.

Unruh, W. G., and W. H. Zurek. 1989. Reduction of a Wave Packet in Quantum Brownian Motion. *Phys. Rev. D*.**40**:1071.

Von Neumann, J. 1932. *Mathematische Grundlagen der Quanten Mechanik*. Berlin: Springer-Verlag. English translation by R. T. Beyer. 1955. *Mathematical Foundations of Quantum Mechanics*. Princeton: Princeton University Press.

Wheeler, J. A. 1957. Assessment of Everett's "Relative State" Formulation of Quantum Theory. *Rev. Mod. Phys.* **29**: 463.

Wheeler, J. A., and W. H. Zurek, eds. 1983. *Quantum Theory and Measurement*. Princeton: Princeton University Press.

Wigner, E. P. 1932. On the Quantum Correction for Thermodynamic Equilibrium. *Phys. Rev.* **40**: 749.

———. 1961. Remarks on the Mind-Body Question. In *The Scientist Speculates*. p. 284. Edited by I. J. Good. London: Heineman.

———. 1963. The Problem of Measurement. *Am. J. Phys.* **31**: 615.

———. 1983. In *Quantum Optics*, *Experimental Gravitation*, *and the Measurement Theory*. Edited by P. Meystre, and M. O. Scully. p. 43. New York: Plenum Press.

Zeh, H. D. 1970. On the Interpretation of Measurement in Quantum Theory. *Found. Phys.* **1**: 69.

Zurek, W. H. 1981. Pointer Basis of Quantum Apparatus: Into What Mixture Does the Wave Packet Collapse? *Phys. Rev. D* **24**: 1516.

———. 1982. Environment-Induced Superselection Rules. *Phys. Rev. D* **26**: 1862.

———. 1984. Reduction of the Wave Packet: How Long Does It Take? In *Frontiers of Nonequilibrium Statistical Physics*. Edited by P. Meystre, and M. O. Scully. New York : Plenum.

———. 1991. Decoherence and the Transition From Quantum to Classical. *Phys. Today* **44** (10): 36.

———. 1993. Preferred States, Predictability, Classicality, and the Environment-Induced Decoherence. *Prog. Theor. Phys.* **89** (2): 281.

———. 1998. Decoherence, Chaos, Quantum-Classical Correspondence, and the Algorithmic Arrow of Time. *Physica Scripta* **T76**: 186.

———.2000. Einselection and Decoherence from an Information Theory Perspective. *Ann. Phys.* (Leipzig) **9** (11–12): 855.

———. 2001a. Decoherence, Einselection, and the Quantum Origins of the Classical. [Online]: http://eprints.lanl.gov (quant-ph/0105127).

———. 2001b. Sub-Planck Structure in Phase Space and its Relevance for Quantum Decoherence. *Nature* **412**: 712.

Zurek, W. H., and J. P. Paz. 1994. Decoherence, Chaos, and the Second Law. *Phys. Rev. Lett.* **72** (16): 2508.

———. 1995. Quantum Chaos: A Decoherent Definition. *Physica D* **83** (1–3): 300.

Zurek, W. H., S. Habib, and J. P. Paz. 1993. Coherent States via Decoherence. *Phys. Rev. Lett.* **70** (9): 1187.

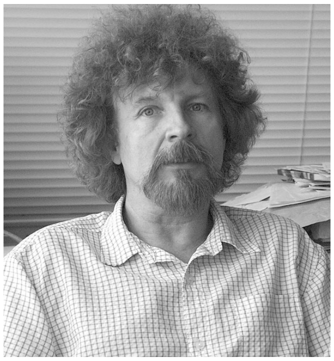

Wojciech Hubert Zurek was educated in Kraków, in his native Poland (M. Sc., 1974) and in Austin, Texas (Ph. D. in physics, 1979). He was a Richard Chace Tolman fellow at the California Institute of Technology and a J. Robert Oppenheimer postdoctoral fellow at the Los Alamos National Laboratory, where he became a technical staff member. Between 1990 and 1996, Wojciech led the Theoretical Astrophysics Group. In 1996, he was selected as a Los Alamos National Laboratory Fellow. He is a Foreign Associate of the Cosmology Program of the Canadian Institute of Advanced Research and the founder of the Complexity, Entropy, and Physics of Information Network of the Santa Fe Institute. His research interests include decoherence, physics of quantum and classical information, foundations of statistical and quantum physics and astrophysics.

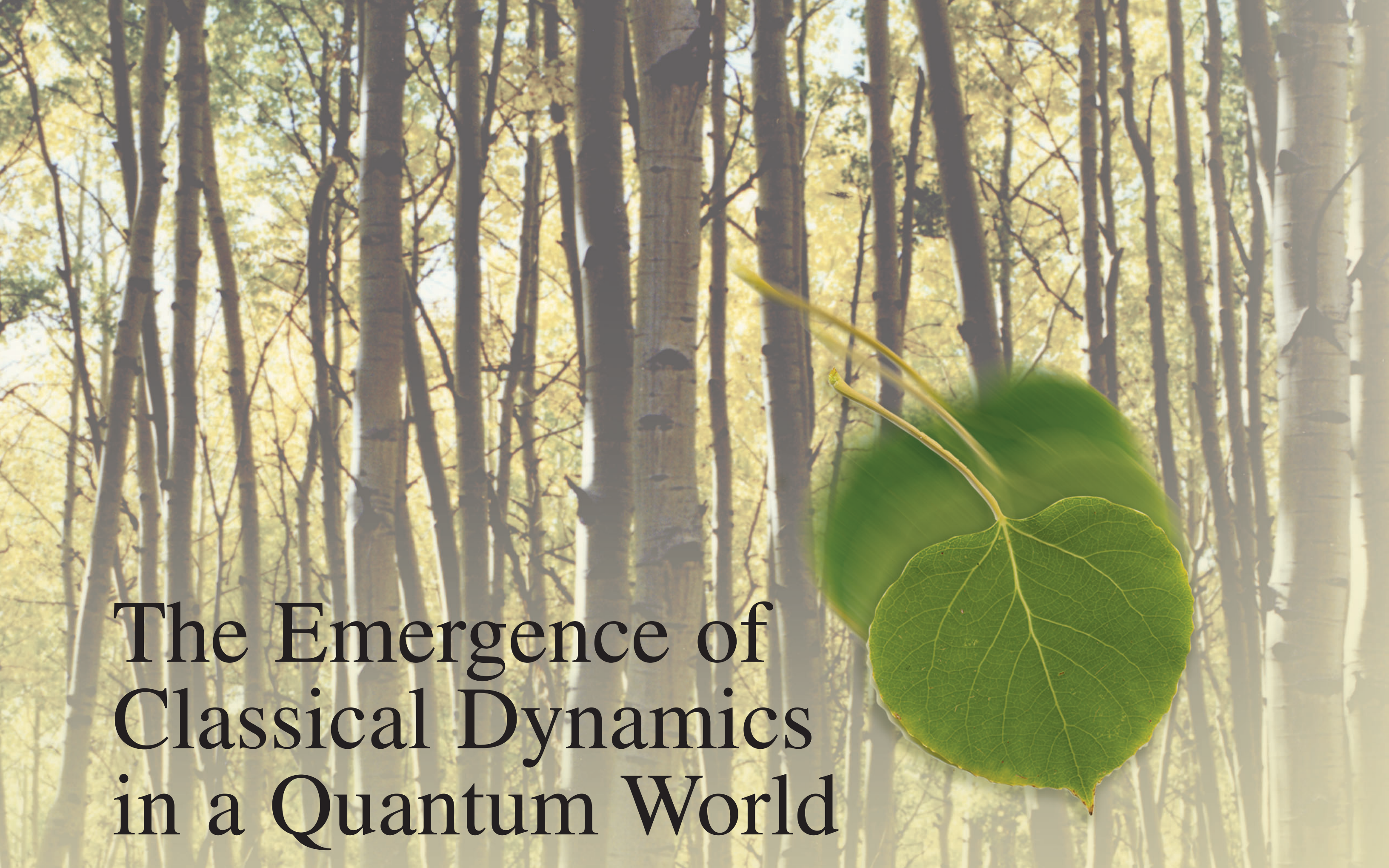

The Emergence of Classical Dynamics in a Quantum World

Tanmoy Bhattacharya, Salman Habib, and Kurt Jacobs

Ever since the advent of quantum mechanics in the mid 1920s, it has been clear that the atoms composing matter do not obey Newton’s laws. Instead, their behavior is described by the Schrödinger equation. Surprisingly though, until recently, no clear explanation was given for why everyday objects, which are merely collections of atoms, are observed to obey Newton’s laws. It seemed that, if quantum mechanics explains all the properties of atoms accurately, everyday objects should obey quantum mechanics. As noted in the box to the right, this reasoning led a few scientists to believe in a distinct macroscopic, or “big and complicated,” world in which quantum mechanics fails and classical mechanics takes over although there has never been experimental evidence for such a failure. Even those who insisted that Newtonian mechanics would somehow emerge from the underlying quantum mechanics as the system became increasingly macroscopic were hindered by the lack of adequate experimental tools. In the last decade, however, this quantum-to-classical transition has become accessible to experimental study and quantitative description, and the resulting insights are the subject of this article.

A Historical Perspective

The demands imposed by quantum mechanics on the disciplines of epistemology and ontology have occupied the greatest minds. Unlike the theory of relativity, the other great idea that shaped physical notions at the same time, quantum mechanics does far more than modify Newton's equations of motion. Whereas relativity redefines the concepts of space and time in terms of the observer, quantum mechanics denies an aspect of reality to system properties (such as position and momentum) until they are measured. This apparent creation of reality upon measurement is so profound a change that it has engendered an uneasiness defying formal statement, not to mention a solution. The difficulties are often referred to as "the measurement problem." Carried to its logical extreme, the problem is that, if quantum mechanics were the ultimate theory, it could deny any reality to the measurement results themselves unless they were observed by yet another system, ad infinitum. Even the pioneers of quantum mechanics had great difficulty conceiving of it as a fundamental theory without relying on the existence of a classical world in which it is embedded (Landau and Lifshitz 1965).

Quantum mechanics challenges us on another front as well. From our intuitive understanding of Bayes' theorem for conditional probability, we constantly infer the behavior of systems that are observed incompletely. Quantum mechanics, although probabilistic, violates Bayes' theorem and thereby our intuition. Yet the very basis for our concepts of space and time and for our intuitive Bayesian view comes from observing the natural world. How come the world appears to be so classical when the fundamental theory describing it is manifestly not so? This is the problem of the quantum-to-classical transition treated in this article.

One of the reasons the quantum-to-classical transition took so long to come under serious investigation may be that it was confused with the measurement problem. In fact, the problem of assigning intrinsic reality to properties of individual quantum systems gave rise to a purely statistical interpretation of quantum mechanics. In this view, quantum laws apply only to ensembles of identically prepared systems.

The quantum-to-classical transition may also have been ignored in the early days because regular, rather than chaotic, systems were the subject of interest. In the former systems, individual trajectories carry little information, and quantization is straightforward. Even though Henri Poincaré (1992) had understood the key aspects of chaos and Albert Einstein (1917) had realized its consequences for the Bohr-Sommerfeld quantization schemes, which were popular at that time, this subject was never in the spotlight, and interest in it was not sustained until fairly recently.

As experimental technology progressed to the point at which single quanta could be measured with precision, the façade of ensemble statistics could no longer hide the reality of the counterclassical nature of quantum mechanics. In particular, a vast array of quantum features, such as interference, came to be seen as everyday occurrences in these experiments.

Many interpretations of quantum mechanics developed. Some appealed to an anthropic principle, according to which life evolved to interpret the world classically, others imagined a manifold of universes, and yet others looked for a set of histories that were consistent enough for classical reasoning to proceed (Omnès 1994, Zurek in this issue). However, by themselves, these approaches do not offer a dynamical explanation for the suppression of interference in the classical world. The key realization that led to a partial understanding of the classical limit was that weak interactions of a system with its environment are universal (Landau and Lifshitz 1980) and remove the nonclassical terms in the quantum evolution (Zurek 1991). The folklore developed that this was the the only effect of a sufficiently weak interaction in almost any system. In fact, Wigner functions (the closest quantum analogues to classical probability distributions in phase space) did often become positive, but they failed to become localized along individual classical trajectories. In the heyday of ensemble interpretations, this was not a problem because classical ensembles would have been represented by exactly such distributions. When applied to a single quantum system in a single experiment, however, this delocalized positive distribution is distinctly dissatisfying.

Furthermore, even when a state is describable by a positive distribution, it is not obvious that the dynamics can be interpreted as the dynamics of any classical ensemble without hypothesizing a multitude of "hidden" variables (Schack and Caves 1999). And finally, the original hope that a weak interaction merely erases interference turned out to be untenable, at least in some systems (Habib et al. 2000).

The underlying reason for environmental action to produce a delocalized probability distribution is that even if we take a single classical system with its initial (or subsequent) positions unknown, our state of knowledge can be encoded by that distribution. But in an actual experiment, we do know the position of the system because we continuously measure it. Without this continuous (or almost continuous) measurement, we would not have the concept of a classical trajectory. And without a classical trajectory, such remarkable signals of chaos as the Lyapunov exponent would be experimentally immeasurable. These developments brought us to our current view that continuous measurements provide the key to understanding the quantum-to-classical transition.

We will illustrate the problems involved in describing the quantum-to-classical transition by using the example of a baseball moving through the air. Most often, we describe how the ball moves through air, how it spins, or how it deforms. Regardless of which degree of freedom we might consider—whether it is the position of the center of mass, angular orientation, or deviation from sphericity—in the final analysis, those variables are merely a combination of the positions (or other properties) of the individual atoms. As all the properties of each of these atoms, including position, are described by quantum mechanics, how is it that the ball as a whole obeys Newton's equation instead of some averaged form of the Schrödinger equation?

Even more difficult to explain is how the chaotic behavior of classical, nonlinear systems emerges from the behavior of quantum systems. Classical, nonlinear, dynamical systems exhibit extreme sensitivity to initial conditions. This means that, if the initial states of two identical copies of a system (for example, particle positions and momenta) differ by some tiny amount, those differences magnify with time at an exponential rate. As a result, in a very short time, the two systems follow very different evolutionary paths. On the other hand, concepts such as precise position and momentum do not make sense according to quantum mechanics: We can describe the state of a system in terms of these variables only probabilistically. The Schrödinger equation governing the evolution of these probabilities typically makes the probability distributions diffuse over time. The final state of such systems is typically not very sensitive to the initial conditions, and the systems do not exhibit chaos in the classical sense.

The key to resolving these contradictions hinges on the following observation: While macroscopic mechanical systems may be described by single quantum degrees of freedom, those variables are subject to observation and interaction with their environment, which are continual influences. For example, a baseball's center-of-mass coordinate is continually affected by the numerous properties of the atoms composing the baseball, including thermal motion, the air that surrounds it, which is also in thermal motion, and the light that reflects off it. The process of observing the baseball's motion also involves interaction with the environment: Light reflected off the baseball and captured by the observer's eye creates a trace of the motion on the retina.

In the next section, we will show that, under conditions that refine the intuitive concept of what is macroscopic, the motion of a quantum system is basically indistinguishable from that of a classical system! In effect, observing a quantum system provides information about it and counteracts the inherent tendency of the probability distribution to diffuse over time although observation creates an irreducible disturbance. In other words, as we see the system continuously, we know where it is and do not have to rely upon the progressively imprecise theoretical predictions of where it could be. When one takes into account this "localization" of the probability distribution encoding our knowledge of the system, the equations governing the expected measurement results (that is, the equations telling us what we observe) become nonlinear in precisely the right way to recover an approximate form of classical dynamics—for example, Newton's laws in the baseball example.

What happens when no one observes the system? Does the baseball suddenly start behaving quantum mechanically if all observers close their eyes? The answer is hidden in a simple fact: Any interaction with a sufficiently complicated external world has the same effect as a series of measurements whose results are not recorded. In other words, the nature of the disturbance on the system due to the system's interactions with the external world is identical to that of the disturbance observed as an irreducible component of measurement. Naturally, questions about the path of the baseball can't be verified if there are no observers, but other aspects of its classical nature can, and do, survive.

Classical vs Quantum Trajectories

Let us now turn to some significant details. To describe the motion of a single classical particle, all we need to do is specify a spatially dependent, and possibly time-dependent, force that acts on the particle and substitute it into Newton's equations. The resulting set of two coupled differential equations, one for the position x of the particle and the other for the momentum p, predicts the evolution of the particle's state. If the force on the particle is denoted by $F(x,t)$, the equations of motion are

$$\dot{x} = \frac{p}{m} \quad , \tag{1}$$

and

$$\dot{p} = F(x,t) = -\partial_x V(x,t) \quad , \tag{2}$$

where V is the potential.

To visualize the motion, one can plot the particle's position and momentum as they change in time. The resulting curve is called a trajectory in phase space (see Figure 1). The axes of phase space delineate the possible spatial and momentum coordinates that the single particle can take. A classical particle's state is given at any time by a point in phase space, and its motion therefore traces out a curve, or trajectory, in phase space.

By contrast, the state of a quantum particle is not described by a single point in phase space. Because of the Heisenberg uncertainty principle, the position and momentum cannot simultaneously be known with arbitrary precision, and the state of the system must therefore be described by a kind of probability density in phase space. This pseudoprobability function is called the Wigner function and is denoted by $f_W(x,p)$. As expected for a true probability density, the integral of the Wigner function over position gives the probability density for p, and the integral over p gives the probability density for x. However, because the Wigner function may be negative in places, we should not try to interpret it too literally. Be that as it may, when we specify the force on the particle, $F(x,t)$, the evolution of the Wigner function is given by the quantum Liouville equation, which is

$$\begin{aligned}\dot{f}_W(x,p) &= -\left[\tfrac{p}{m}\,\partial_x + F(x,t)\partial_p\right] f_W(x,p) \\ &\quad + \sum_{\lambda=1}^{\infty} \frac{1}{(2\lambda+1)!}\left(\frac{\hbar}{2i}\right)^{2\lambda} \partial_x^{2\lambda+1} V(x,t)\,\partial_p^{2\lambda+1} f_W(x,p) \quad .\end{aligned} \tag{3}$$

Clearly, in order for a quantum particle to behave as a classical particle, we must be able to assign it a position and momentum, even if only approximately. For example, if the Wigner function stays localized in phase space throughout its evolution, then the centroid of the Wigner function[1] could be interpreted at each time as the location of the particle in phase space.

---

[1] The centroid of the Wigner function is the point in phase space consisting of the mean values of x and p, that is $(\langle x\rangle,\langle p\rangle)$.

Figure 1. Potentials and Phase-Space Trajectories for Single-Particle Systems
The figure shows four systems in which a single particle is constrained to move in a one-dimensional potential. The four systems are (a) a harmonic oscillator, (b) a double well, (c) a driven harmonic oscillator, and (d) a driven double well, also known as a Duffing oscillator. As the potentials increase in complexity from (a) to (d), so do the phase-space trajectories. In (c) and (d), the potential is time dependent, oscillating back and forth between the solid and dashed curves during each period. In (d), the force is nonlinear, and the trajectory covers increasingly more of the phase space as time passes.

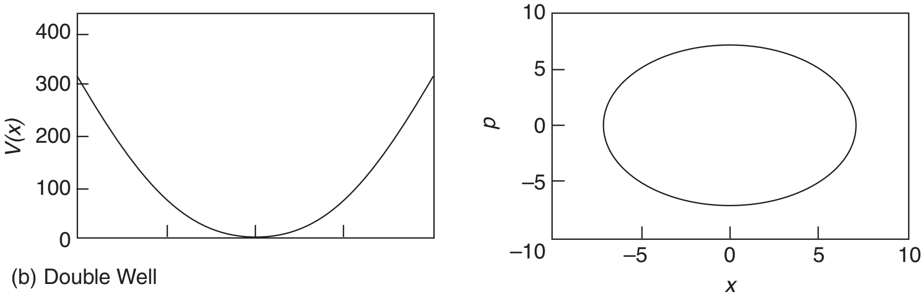
(a) Harmonic Oscillator

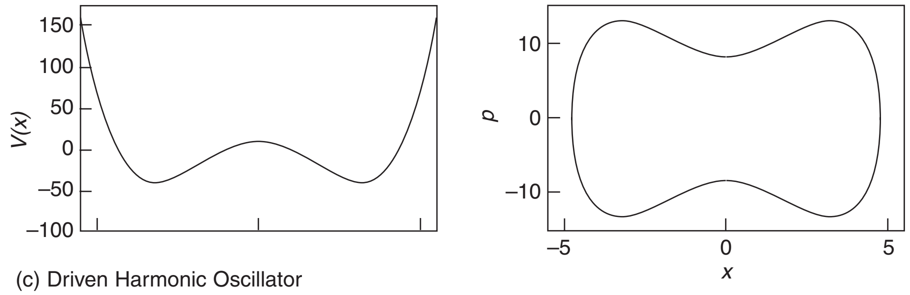
(b) Double Well

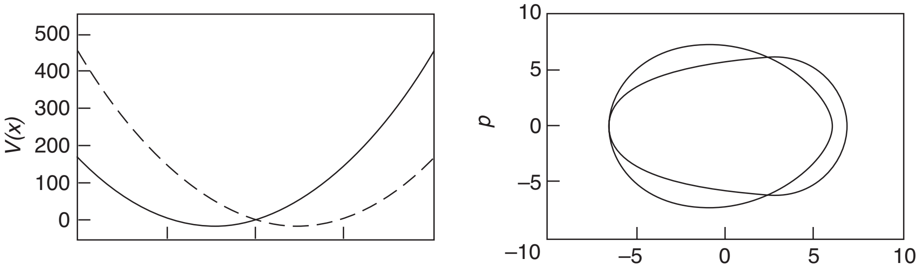
(c) Driven Harmonic Oscillator

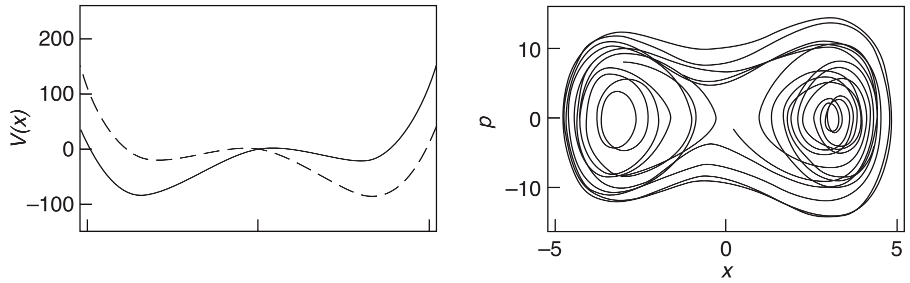
(d) Duffing Oscillator

Moreover, the Liouville equation yields the following equations of motion for the centroid:

$$\langle \dot{x} \rangle = \frac{\langle p \rangle}{m} \ , \tag{4}$$

and

$$\langle \dot{p} \rangle = \langle F(x,t) \rangle \ , \tag{5}$$

where m is the mass of the particle. This result, referred to as Ehrenfest's theorem,[2] says that the equations of motion for the centroid formally resemble the classical ones but differ from classical dynamics in that the force F has been replaced with the average value of F over the Wigner function. Suppose again that the Wigner function is sharply peaked about $\langle x \rangle$ and $\langle p \rangle$. In that case, we can approximate $\langle F(x) \rangle$ as a Taylor series expansion about $\langle x \rangle$:

$$\left\langle F(x) \right\rangle = F\left(\left\langle x \right\rangle\right) + \frac{\sigma_x^2}{2} \partial_x^2 F\left(\left\langle x \right\rangle\right) + \ldots, \tag{6}$$

where σ_x^2 is the variance of x so that $\sigma_x^2 = \langle (x - \langle x \rangle)^2 \rangle$. If the second and higher terms in the Taylor expansion are negligible, the equations for the centroid become

$$\left\langle \dot{x} \right\rangle = \frac{\left\langle p \right\rangle}{m} \quad , \tag{7}$$

and

$$\left\langle \dot{p} \right\rangle = F\left(\left\langle x \right\rangle, t\right) \quad . \tag{8}$$

And these equations for the centroid are identical to the equation of motion for the classical particle! If we somehow arrange to start the system with a sharply localized Wigner function, the motion of the centroid will start out by being classical, and Equation (6) indicates precisely how sharply peaked the Wigner function needs to be.

However, the Wigner function of an unobserved quantum particle rarely remains localized even if for some reason it starts off that way. In fact, when an otherwise noninteracting quantum particle is subject to a nonlinear force, that is, a force with a nonlinear dependence on x, the evolution usually causes the Wigner function to develop a complex structure and spread out over large areas of phase space. In the sequence of plots in Figure 2(a–d), the Wigner function is shown to spread out in phase space under the influence of a nonlinear force. Once the Wigner function has spread out in this way, the evolution of the centroid bears no resemblance to a classical trajectory.

So, the key issue in understanding the quantum-to-classical transition is the following: Why should the Wigner function localize and stay localized thereafter? As stated in the introduction, this is an outcome of continuous observation (measurement). We therefore now turn to the theory of continuous measurements.

Continuous Measurement

In simple terms, any process that yields a continuous stream of information may be termed continuous observation. Because in quantum mechanics measurement creates an irreducible disturbance on the observed system and we do not wish to disturb the system unduly, the desired measurement process must yield a limited amount of information in a finite time. Simple projective measurements, also known as von Neumann

---

[2] According to Ehrenfest's theorem, a quantum-mechanical wave packet obeys the equation of motion of the corresponding classical particle when the position, momentum, and force acting on the particle are replaced by the expectation values of these quantities.

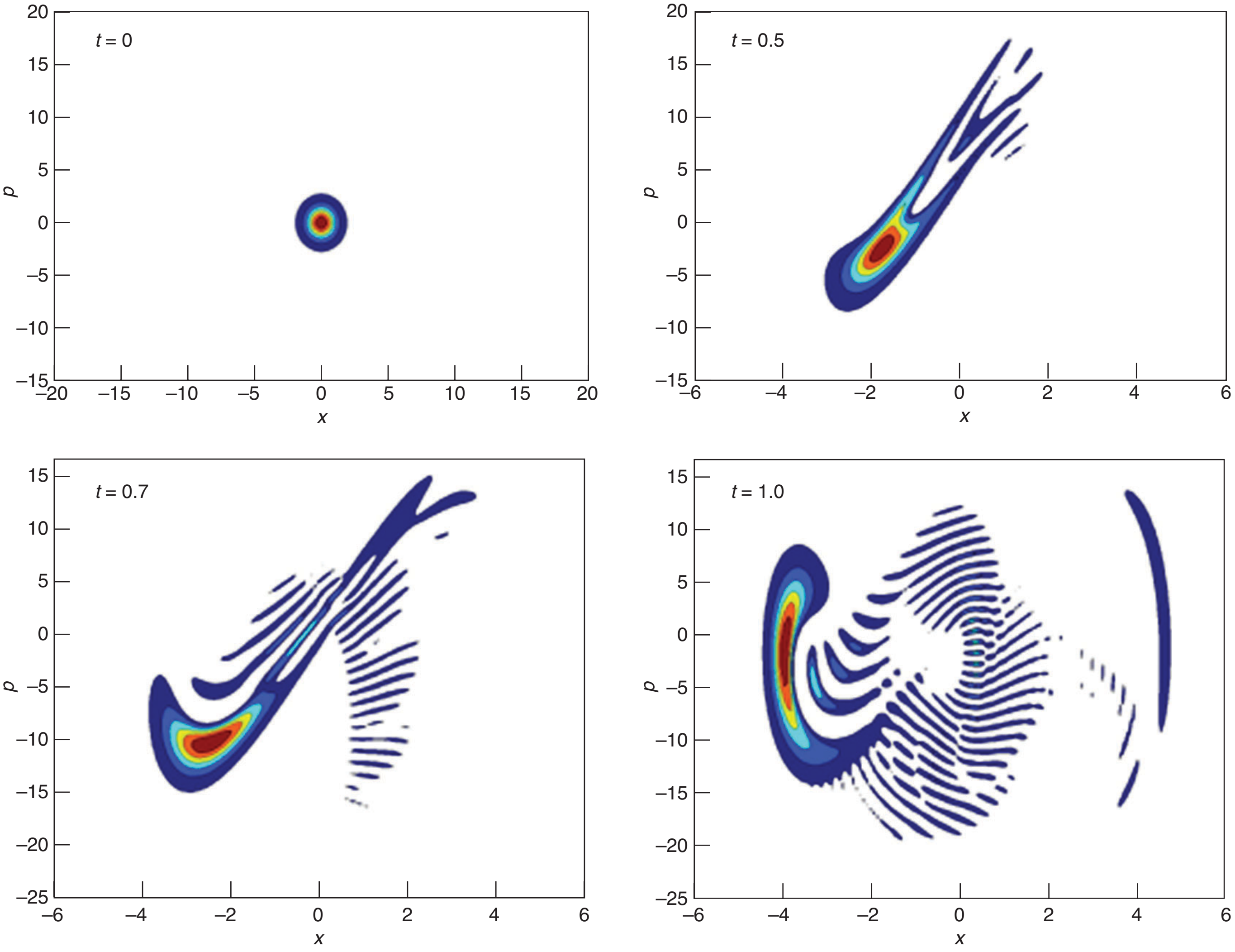

Figure 2. Evolution of the Wigner Function under a Nonlinear Force

These four snapshots show the Wigner function at different times during the simulations of the Duffing oscillator. At $t = 0$, the Wigner function is localized around a single point. As time passes, however, the Wigner function becomes increasingly delocalized under the nonlinear potential of the Duffing oscillator.

measurements, introduced in undergraduate quantum mechanics courses, are not adequate for describing continuous measurements because they yield complete information instantaneously. The proper description of measurements that extract information continuously, however, results from a straightforward generalization of von Neumann measurements (Davies 1976, Kraus 1983, Carmichael 1993). All we need to do is let the system interact weakly with another one, such as a light beam, so that the state of the auxiliary system should gather very little information about the main one over short periods and thereby the system of interest should be perturbed only slightly. Only a very small part of the information gathered by a projective measurement of the auxiliary system then pertains to the system of interest, and a continuous limit of this measurement process can then be taken. By the mid 1990s, this generalization of the standard measurement theory was already being used to describe continuous position measurement by laser beams. In our analysis, we use the methods developed as part of this effort.

A simple, yet sufficiently realistic, analogy to measuring position by direct observation is measuring the position of a moving mirror by reflecting a laser beam off the mirror and continuously monitoring the phase of the reflected light. As the knowledge of the system is initially imprecise, there is a random component in the measurement record. Classically, our knowledge of the system state may be refined to an arbitrary accuracy over time, and the random component is thereby reduced. Quantum mechanically, however, the measurement itself disturbs the system, and our knowledge cannot be improved arbitrarily. As a result, the measurement record continues to have a random component.

An equivalent way of understanding this random component is to note that the measurement process may be characterized by the rate at which information is obtained. A more powerful measurement is one in which information is obtained at a faster rate. Because of the Heisenberg uncertainty relation, if we obtain information about position, we lose information about momentum. But uncertainty in momentum turns into uncertainty in position at the very next instant. This random feedback guarantees that a continuous measurement will cause the system to be driven by noise: The higher the rate at which information is obtained, the more the noise. For a position measurement, the rate of information extraction is usually characterized by a constant, k, that measures how fast the precision in our knowledge of position, $1/\sigma_x^2$, would increase per unit time in the absence of the accompanying disturbance. In the laser measurement of position, k is determined by the power of the laser. The more powerful the laser, the stronger the measurement, and the more noise introduced by the photon collisions.

Now we are in a position to see how and under what circumstances continuous measurement transforms quantum into classical dynamics, resulting in the quantum-to-classical transition. We can include the effects of the observation on the motion of the particle by writing down a stochastic Liouville equation, that is, a Liouville equation with a random component. This equation is given in the box "Conditions for Approximate Classical Motion under Continuous Measurement" on the next page. The resulting equations of motion for the centroid of the Wigner function are

$$\langle \dot{x} \rangle = \frac{\langle p \rangle}{m} + \sqrt{8k}\sigma_x^2 \xi(t) \ , \tag{9}$$

and

$$\langle \dot{p} \rangle = F(\langle x \rangle, t) + \sqrt{8k} C_{xp} \xi(t) \ , \tag{10}$$

where $C_{xp} = (1/2)(\langle xp \rangle + \langle px \rangle - 2\langle x \rangle\langle p \rangle)$ is the covariance of x and p, and $\xi(t)$ is a Gaussian white noise.[3]

We have now reached the crux of the quantum-to-classical transition. To keep the Wigner function well localized, a strong measurement, or a large k, is needed. But Equations (9) and (10) show that a strong measurement introduces a lot of noise. In classical mechanics, however, we deal with systems in which the amount of noise, if any, is imperceptible compared with the scale of the distances traveled by the particle. We must therefore determine the circumstances under which continuous measurement will maintain sufficient localization for the classical equations to be approximately valid without introducing a level of noise that would affect this scale of everyday physics.

---

[3] White noise is random noise that has constant energy per unit bandwidth at every frequency. In reality, the actual recording of the measurement always occurs at a finite rate. So, effectively, the white noise gets filtered through a low-pass filter, which cuts out high frequencies.

Conditions for Approximate Classical Motion

The evolution of the Wigner function f_W for a single particle subjected to a continuous measurement of position is given by the stochastic Liouville equation:

$$
\begin{aligned}
f_W(x,p,t+dt) = {}& \left[1 - dt\left[\left(\frac{p}{m}\right)\partial_x + F(x,t)\,\partial_p\right] + dt\sum_{\lambda=1}^{\infty}\frac{1}{(2\lambda+1)!}\left(\frac{\hbar}{2i}\right)^{2\lambda}\partial_x^{2\lambda+1}V(x,t)\partial_p^{2\lambda+1}\right]f_W(x,p) \\
&+ \sqrt{8k}\,dt\,\xi\left(x-\langle x\rangle\right)f_W(x,p)\ , \qquad (1)
\end{aligned}
$$

where F is the force on the particle, ξ is a Gaussian white noise, and k is a constant characterizing the rate of information extraction. Making a Gaussian approximation for the Wigner function, which according to numerical studies is a good approximation when localization is maintained by the measurement, the equations of motion for the variances of x and p, σ_x^2 and σ_p^2, are

$$
\begin{aligned}
&\dot{\sigma}_x^2 = \frac{2}{m}C_{xp} - 8k\sigma_x^4\ , \quad \text{and} \\
&\dot{\sigma}_p^2 = 2\hbar^2 k - 8kC_{xp}^2 + 2\partial_x F C_{xp}\ , \quad \text{where the covariance of } x \text{ and } p \text{ is } C_{xp} = \frac{1}{2}\left(\langle xp\rangle + \langle px\rangle - 2\langle x\rangle\langle p\rangle\right)\ . \\
&\dot{C}_{xp} = \frac{1}{m}\sigma_p^2 - 8k\sigma_x^2 C_{xp} + \partial_x F\sigma_x^2\ . \qquad (2)
\end{aligned}
$$

the noise has negligible effect in these equations when the Wigner function stays Gaussian.

First, we solve these equations for the steady state and then impose on this solution the conditions required for classical dynamics to result. In order for the Wigner function to remain sufficiently localized, the measurement strength k must stop the spread of the wave function at the unstable points, $\partial_x F > 0$:*

$$
8k \gg \left|\frac{\partial_x^2 F}{F}\right|\sqrt{\frac{|\partial_x F|}{2m}}\ . \qquad (3)
$$

If noise is to bring about only a negligible perturbation to the classical dynamics, it is sufficient that, at a typical point on the trajectory, the measurement satisfy

$$
\frac{2|\partial_x F|}{s} \ll \hbar k \ll \frac{|\partial_x F|s}{4}\ , \qquad (4)
$$

where s is the typical value of the system's action† in units of $\hbar$. Obviously, as s becomes much larger than $2\sqrt{2}$ this relationship is satisfied for an ever-larger range of k. At the spot where this range is sufficiently large, we obtain the classical limit.

---

[*] If the nonlinearity is large on the quantum scale, $\hbar\left|\left(\partial_x^2 F\right)/F\right| \geq 4\sqrt{m\left|\partial_x F\right|}$, then $8k$ needs to be much larger than $\left(\partial_x^2 F\right)^2\hbar/4mF^2$ irrespective of the sign of $\partial_x F$. This observation does not change the argument in the body of the paper.

[†] We are assuming that both $[mF^2/(\partial_x F)^2]|F/p|$ and $E\,|p/4F|$ evaluated at a typical point of the trajectory are comparable to the action of the system, and we define that action to be $\hbar s$.

With analytical tools alone, this problem cannot be solved. However, one can take a semianalytical approach by accepting two important results that come from numerical simulations: (1) Any Wigner function localizes under a sufficiently strong measurement, and (2) under such a measurement, once the Wigner function becomes localized, it is approximately described by a narrow Gaussian at all later times. Therefore, we assume a Gaussian form for the Wigner function, write the equations determining how the variances and covariances change with time, and solve those equations to find their values in a steady state. Having all these ingredients, we can then find the conditions under which the noise terms are small and the system remains well localized (see the box on the opposite page). Our central conclusion is that a quantum system will behave almost classically for an ever-increasing range of measurement strengths when the action of the system is large compared with the reduced Planck constant $\hbar$.

This concept may be understood heuristically in the following way: Because of the uncertainty principle, the effective area where the localized Gaussian Wigner function is nonzero can never be less than $\hbar$. If this limiting area is so large compared with the scale of the problem that it cannot be considered localized, we certainly do not expect classical behavior. Conversely, as long as the measurement extracts information at a sufficiently low rate to avoid squeezing the Wigner function to a smaller scale than the limiting one, the quantum noise remains on the scale of the variances themselves. As a result, the system behaves almost classically.

There are systems, however, whose phase space is sufficiently small for quantum effects to be manifest or even dominant. This is true, for example, of isolated spin systems with small total angular momenta. Even when they are observed and interacting with the environment, these spin systems are expected to be indescribable by the classical laws of motion. A spin coupled to other degrees of freedom such as position is a more interesting case, especially when the position of the system would have followed a classical trajectory in the absence of that interaction. To what extent, if at all, that coupling stops position from following a classical trajectory is the subject of ongoing research (Ghose et al. 2002).

Chaos in a Quantum System under Continuous Observation

As an illustration of these general ideas, we consider the Duffing oscillator, a single particle sitting in a double-well potential and driven sinusoidally—see Figure 1(d). We chose this nonlinear system because it has been studied in depth and it allows us to choose parameters that produce chaotic behavior over most of the system's phase space. Our test will indicate whether chaotic classical motion is a good approximate description of this quantum system when it is under continuous observation. To diagnose the presence of chaos, we calculate the maximal Lyapunov exponent, the most rigorous measure of chaotic behavior,[4] and compare our calculated value for the quantum system with the classical value.

The Hamiltonian for the particle in the double-well potential is

$$H = \frac{p^2}{2m} + Bx^4 - Ax^2 + \Lambda x \cos(\omega t) , \tag{11}$$

where m, A, B, Λ, and ω are parameters that determine the size of the particle and the spatial extent of the phase space. The action should be large enough so that the particle can behave almost classically, yet small enough to illustrate how tiny it needs to be before quantum effects on the particle become dominant. Bearing this requirement in mind, we choose a mass $m = 1$ picogram, a spring constant $A = 0.99$ piconewton per meter, a nonlinearity $A/B = 0.02$ square micrometer, a peak driving force of $\lambda = 0.03$ attonewton, and a driving frequency $\omega = 60$ rad per second. Because of the weakness of the nonlinearity, the distance between the two minima of the double well is only about 206 nanometers, and the height of the potential is only 33 nano-electron-volts. The frequency of the driving force is 10 hertz. For these values, a measurement strength k of 93 per square picometer per second, which corresponds to a laser power of about 0.24 microwatt, is adequate to keep the motion classical, or the Wigner function well localized.

---

[4] The maximal Lyapunov exponent is one of a number of coefficients that describe the rates at which nearby trajectories in phase space converge or diverge.

To study the system numerically, we allow the particle's Wigner function to evolve according to the stochastic Liouville equation for approximately 50 periods of the driving force and then check that it remains well localized in the potential. We find, indeed, that the width of the Wigner function in position (given by the square root of the position variance σ_x^2) is always less than 2 nanometers. Thus the position of the particle is always well resolved by the measurement as the system evolves. In addition, an inspection of the centroid's trajectory shows that the noise is negligible. In order to verify that the motion is, in fact, that of a classical Duffing oscillator, we perform two tests. The first is to plot a stroboscopic map showing the particle's motion in phase space and then compare that map with the corresponding one of the classical Duffing oscillator driven by a small amount of noise. The observed quantum map and the classical map are displayed in Figure 3.

The two stroboscopic maps are very similar and show qualitatively that the quantum dynamics under continuous measurement exhibits chaotic behavior analogous to classical chaos. To verify this finding quantitatively, we conduct a second test and calculate the Lyapunov exponent for both systems. As we already mentioned, trajectories that are initially separated by a very small phase-space distance, $d(0)$, diverge exponentially as a function of time in chaotic systems. The Lyapunov exponent λ, which determines the rate of this exponential increase, is defined to be

$$\lambda = \lim_{t\to\infty} \lim_{d(0)\to 0} \frac{\ln d(t)}{t} \; . \tag{12}$$

To calculate this exponent, we first choose a single fiducial trajectory in which the centroid of the Wigner function starts at the phase-space point given by $\langle x \rangle = -\,98$ nanometers and $\langle p \rangle = 2.6$ picograms micrometers per second (pg μm/s). At 17 intervals along this trajectory, each separated by approximately 20 periods of the driving force, we obtain neighboring trajectories by varying the noise realization. We calculate how these trajectories diverge from the initial trajectory and average the difference over the 17 sample trajectories. We then carry out this procedure for 10 fiducial trajectories, all starting at the same initial point but differing because of different noise realizations. Plotting the logarithm of this average divergence as a function of time results in a line whose slope is the Lyapunov exponent. In Figure 4, we plot the logarithm of the average divergence for both the observed quantum system and the classical system driven with a small amount of noise. The slope of the lines drawn through the curves gives the Lyapunov exponent, which in both cases is 5.7(2) per second. To show that the noise has a negligible effect on the dynamics, we also calculate the Lyapunov exponent for the classical system with no noise, using trajectories starting in a small region around the point given by $x = -\,98$ nanometers

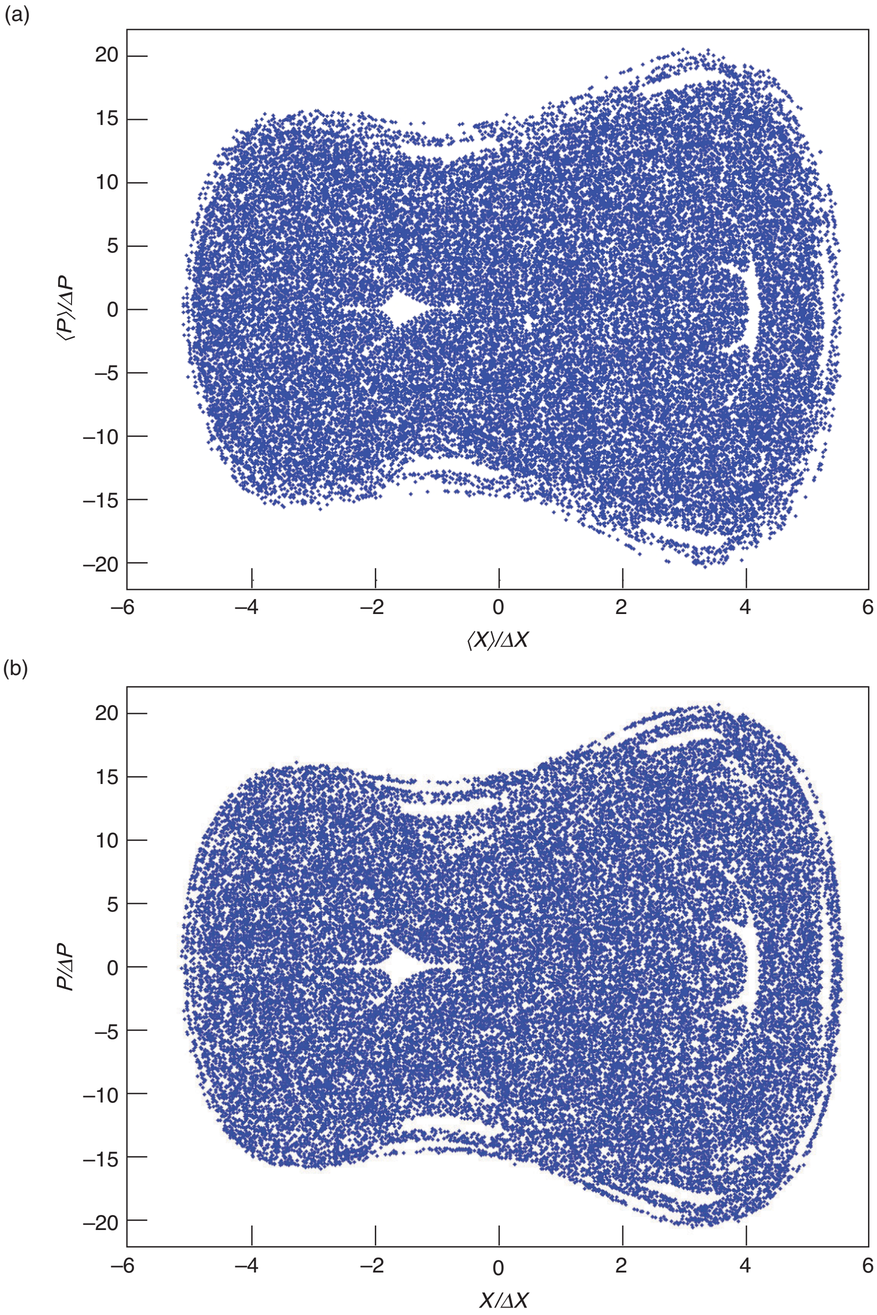

Figure 3. Stroboscopic Maps for the Quantum and Classical Duffing Oscillators

The results of the Duffing oscillator simulations are plotted as stroboscopic maps. (a) The map for the continuously observed quantum Duffing oscillator displays the centroids of the Wigner function at time intervals separated by the period of the driving force. This map is a pastiche from several different runs with different initial conditions, for a total duration of 39,000 periods of the temporal drive. (b) The map for the classical Duffing oscillator driven with a small amount of noise displays the calculated locations of particles in phase space at time intervals separated by the period of the driving force. The two maps are very similar. The quantum system under continuous measurement exhibits qualitatively the same chaotic behavior as the classical system driven with a small amount of noise. In these figures, ΔX = 33 nm, and ΔP = 324 pg nm/s.

and p = 2.6 pg µm/s. Those trajectories give a Lyapunov exponent of 5.6(1) per second, which is in agreement with the previous value.

Now we elaborate on the problem hinted at in the introduction. If observation realizes the classical world, do trees in remote forests fall quantum mechanically? Of course, the tongue-in-cheek answer is, “who knows?” At a deeper level, however, we note that even in a remote forest, trees continue to interact with the environment, and through this interaction, the components of the environment (reflected light, air molecules, and so on) acquire information about the system. According to unitarity, an important property of quantum mechanics, information can never be destroyed. The information that flowed into the environment must either return to its origin or stay somewhere in the environment—the decaying sound of the falling tree must yet record

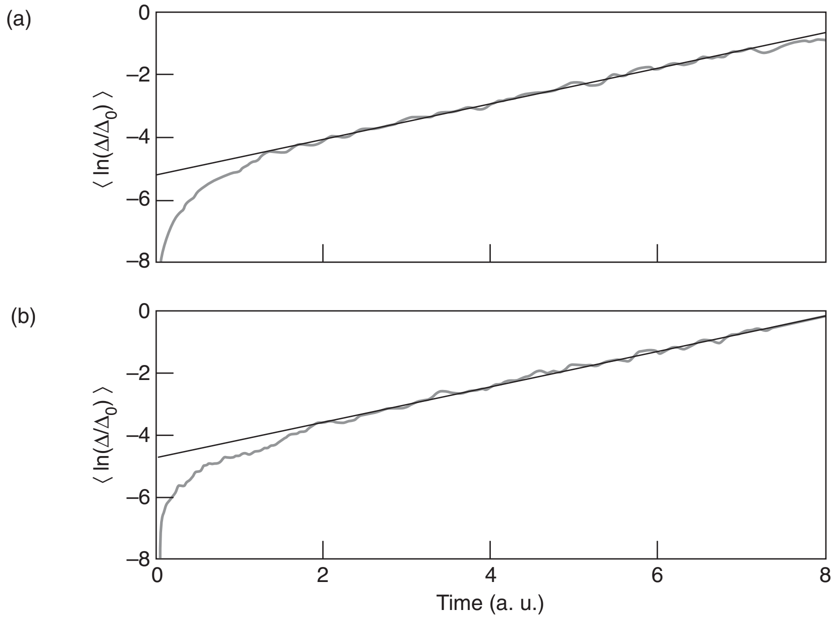

Figure 4. Lyapunov Exponents for the Quantum and Classical Duffing Oscillators
In order to calculate the Lyapunov exponents, λ, for (a) a continuously observed quantum Duffing oscillator and (b) a classical Duffing oscillator driven with a small amount of noise, we plot against time the logarithm of the average separation of trajectories that begin very close together. The parameters defining the oscillator—the continuous-measurement strength in the quantum system and the noise in the classical system—are detailed on pages 119-–120 of this article. The slope of the line drawn through the curves gives the Lyapunov exponent, which in both cases is λ = 0.57(2). Also in both cases, Δ_0 = 33 nm.

its presence faithfully, albeit perhaps only in a shaken leaf. And herein lies the key to understanding the unobserved: If a sufficiently motivated observer were to coax the information out of the environment, that action would become an act of continuous measurement of the current happenings even though actually performed in the future. But since the current state of affairs can't be influenced by what anyone does in the future, the behavior of the system at present cannot contradict anything that such a classical record could possibly postdict.

If the motion is not observed, no one knows which of the possible paths the object took, but the rest of the universe does record the path, which could, therefore, be considered as classical as any (Gell-Mann and Hartle 1993). All that happens when there is no observer is that our knowledge of the motion of the object is the result of averaging over all the possible trajectories. In that case, we are forced to describe the state of the system as being given by a probability distribution in phase space since we no longer know exactly where the system is as it evolves. This observation is, however, just as true for a (noisy) classical system as it is for a quantum system.

The Connection to the Theory of Decoherence

We can now explain how the analysis presented here relates to a standard approach to the quantum-to-classical transition often referred to as decoherence. The procedure employed in decoherence theory is to examine the behavior of the quantum system coupled to the environment by averaging over everything that happens to the environment. This procedure is equivalent to averaging over all the possible trajectories that the particle might have taken, as explained above. Thus decoherence gives the evolution of the probability density of the system when no one knows the actual trajectory.
The relevant theoretical tools for understanding this process were first developed and applied in the 1950s and 1960s (Redfield 1957, Feynman and Vernon 1963), but more recent work (Hepp 1972, Zurek 1981, 1982, Caldeira and Leggett 1981, 1983a, 1983b,

Joos and Zeh 1985) was targeted at condensed-matter systems and a broader understanding of quantum measurement and quantum-classical correspondence. It was found that averaging over the environment or over the equivalent, unobserved, noisy classical system gives the same evolution (Habib et al. 1998). In this classical counterpart, different realizations of noise give rise to slightly different trajectories, and in a chaotic system, these trajectories diverge exponentially fast. As a result, probability distributions obtained by averaging over the noise tend to spread out very fast, and our knowledge of the system state is correspondingly reduced. In other words, discarding the information that is contained in the environment or, equivalently, the measurement record, as averaging over these data implies, leads to a rapid loss of information about the system. This increasing loss of information, characterized by a quantity called entropy, can then be used to study the phenomenon of chaos with varying degrees of rigor.

Averaging over the environment to produce classical probability distributions was, however, not completely satisfactory. Not only does this averaging procedure not allow us to calculate trajectory-based quantities, but it also restricts our predictions to those derivable by knowing only the probability densities at various times. But classical physics is much more powerful than that—it can predict the outcome of many "if ... then" scenarios. If I randomly throw a ball in some direction, the probability of it landing in any direction around me is the same, but if you see the ball north of me, you can predict with pretty good certainty that it won't land south of me. In the classical world, such correlations are numerous and varied, and the measurement approach we have taken here completes our understanding of the quantum-to-classical transition by treating all correlations on an equal footing. It is easy to see, however, that if the continuous measurement approach has to get all the correlations right, it must per force get the decoherence of probability densities right!

The realization that continuous measurement was the key to understanding the quantum-to-classical transition has emerged only in the last decade. First introduced in a paper by Spiller and Ralph (1994), this idea was then mentioned again by Martin Schlautmann and Robert Graham (1995). Subsequently, the idea was developed in a collection of papers (Schack et al. 1995, Brun et al. 1996, Percival and Strunz 1998, Strunz and Percival 1998). However, the scientific community was slow to pick up on this work, possibly because the authors used a stochastic model referred to as quantum state diffusion, which may have obscured somewhat the measurement interpretation. In 2000, we published the results presented in this article, namely, analytic inequalities that determine when classical motion will be achieved for a general single-particle system, and showed that the correct Lyapunov exponent emerges (Bhattacharya et al. 2000). For this purpose, we used continuous position measurement, which is ever present in the everyday world and therefore the most natural one to consider. This accumulation of work now provides strong evidence that continuous observation supplies a natural and satisfactory explanation for the emergence of classical motion, including classical chaos, from quantum mechanics. In addition, such an analysis also makes clear that the specific measurement model is not important. Any environmental interaction that provides sufficient information about the location of the system in phase space will induce the transition in macroscopic systems. Recently, Andrew Scott and Gerard Milburn (2001) have analyzed the case of continuous joint measurement of position and momentum and of momentum alone, and they verified that classical dynamics emerges in the same way as described in Bhattacharya et al. (2000). ■

Further Reading

Bhattacharya, T., S. Habib, and K. Jacobs. 2000. Continuous Quantum Measurement and the Emergence of Classical Chaos. *Phys. Rev. Lett.* **85**: 4852.

Brun, T. A., I. C. Percival, and R. Schack. 1996. Quantum Chaos in Open Systems: A Quantum State Diffusion Analysis. *J. Phys. A* **29**: 2077.

Caldeira, A. O., and A. J. Leggett. 1981. Influence of Dissipation on Quantum Tunneling in Macroscopic Systems. *Phys. Rev. Lett.* **46**: 211.

———. 1983a. Quantum Tunneling in a Dissipative System. *Ann. Phys. (N.Y.)* **149**: 374.

———. 1983b. Path Integral Approach to Quantum Brownian-Motion. *Physica A* **121**: 587.

Carmichael, H. J. 1993. *An Open Systems Approach to Quantum Optics*. Berlin: Springer-Verlag.

Davies, E. B. 1976. *Quantum Theory of Open Systems.* New York: Academic Press.

DeWitt, B. S., and N. Graham, Eds. 1973. *The Many-Worlds Interpretation of Quantum Mechanics*. Princeton: Princeton University Press.

Einstein, A. 1917. On the Quantum Theorem of Sommerfield and Epstein. *Verh. Dtsch. Phys. Ges*. **19**: 434.

Feynman, R. P., and F. L. Vernon. 1963. The Theory of a General Quantum System Interacting with a Linear Dissipative System. *Ann. Phys (N. Y.)* **24**: 118.

Gell-Mann, M., and J. B. Hartle. 1993. Classical Equations for Quantum Systems. *Phys. Rev. D* **47**: 3345.

Ghose, S., P. M. Alsing, I. H. Deutsch, T. Bhattacharya, S. Habib, and K. Jacobs. 2002. Recovering Classical Dynamics from Coupled Quantum Systems Through Continuous Measurement. [Online]: http://eprints.lanl.gov (quant-ph/0208064).

Habib, S., K. Shizume, and W. H. Zurek. 1998. Decoherence, Chaos, and the Correspondence Principle. *Phys. Rev. Lett.* **80**: 4361.

Habib, S., K. Jacobs, H. Mabuchi, R. Ryne, K. Shizume, and B. Sundaram. 2002. The Quantum-Classical Transition in Nonlinear Dynamical Systems. *Phys. Rev. Lett.* **88**: 040402.

Hepp, K. 1972. Quantum Theory of Measurement and Macroscopic Observables. *Helv. Phys. Acta* **45**: 237.

Joos, E., and H. D. Zeh. 1985. The Emergence of Classical Properties through Interaction with the Environment *Z. Phys. B* **59**: 223.

Kraus, K. 1983. *States, Effects, and Operations: Fundamental Notions of Quantum Theory*. Berlin: Springer-Verlag.

Landau, L. D., and E. M. Lifshitz. 1965. *Quantum Mechanics*: *Non-relativistic Theory*. New York: Pergamon Press.

———. 1980. *Statistical Physics*. New York: Pergamon Press.

Omnès, R. 1994. *The Interpretation of Quantum Mechanics*. Princeton: Princeton University Press.

Percival, I. C., and W. T. Strunz. 1998. Classical Dynamics of Quantum Localization. *J. Phys. A* **31**: 1815.

Poincaré, H. *New Methods of Celestial Mechanics*. 1992. Edited by D. L. Goroff. New York: Springer.

Redfield, A. G. 1957. Theory of Relaxation Processes in Advances in Magnetic Resonance. *IBM J. Res. Dev.* **1**: 19.

Schack, R., and C. M. Caves. 1999. Classical Model for Bulk-Ensemble NMR Quantum Computation. *Phys. Rev. A* **60**: 4354.

Schack, R., T. A. Brun, and I. C. Percival. 1995. Quantum State Diffusion, Localization and Computation. *J. Phys. A* **28**: 5401.

Schlautmann, M., and R. Graham. 1995. Measurement Trajectories of Chaotic Quantum Systems. *Phys. Rev. E* **52**: 340.

Scott, A. J., and G. J. Milburn. 2001. Quantum Nonlinear Dynamics of Continuously Measured Systems. *Phys. Rev. A* **63**: 042101.

Spiller, T. P., and J. F. Ralph. 1994. The Emergence of Chaos in an Open Quantum System. *Phys.Lett. A* **194**: 235.

Strunz, W. T., and I. C. Percival. 1998. Classical Mechanics from Quantum State Diffusion—A Phase Space Approach. *J. Phys. A* **31**: 1801.

Zurek, W. H. 1981. Pointer Basis of Quantum Apparatus: Into What Mixture Does the Wave Packet Collapse? *Phys. Rev. D* **24**: 1516.

———. 1982. Environment-Induced Super-selection Rules. *Phys. Rev. D* **26**: 1862.

———. 1991. Decoherence and the Transition to Classical. *Phys. Today* **44**: 36.

Tanmoy Bhattacharya graduated from the Indian Institute of Technology in Kharagpur, India, with a master's degree in physics in 1984. He received a Ph.D. in physics from the Tata Institute of Fundamental Research in Bombay, India, in 1989. Tanmoy worked as a postdoctoral researcher at Brookhaven National Laboratory, at the Centre d'Énergie Atomique in Saclay, France, and at Los Alamos National Laboratory before becoming a staff member in the Theoretical Division at Los Alamos in 1995. Over the years, Tanmoy's research activities have diversified. Having started with an interest in the structure and interactions of elementary particles, Tanmoy has become interested in phylogenetic problems in viral evolution and fundamentals of quantum mechanics. He is currently working on the interface of quantum and classical systems.

Salman Habib received his undergraduate degree from the Indian Institute of Technology in Delhi, India, and his Ph.D. from the University of Maryland, College Park, in 1988. He then held postdoctoral fellowships at the University of British Columbia, Vancouver, and at Los Alamos National Laboratory. In 1994, he became a staff member in the Theoretical Division at Los Alamos. The central theme of Salman's research has been the study of dynamical systems covering areas that range from classical and quantum chaos to the dynamics of the Universe. In the past decade, Salman has contributed to elucidating the nature of the quantum-to-classical transition and worked on the problem of controlling quantum dynamical systems. His recent work focuses strongly on the interface between theory and experiment.

Kurt Jacobs received a bachelor of science degree from the University of Auckland, New Zealand, in 1993 and a master's degree in physics from the same institution in 1995. Three years later, Kurt received his Ph.D. in physics from Imperial College, London University. Since that time, Kurt has been working as a postdoctoral fellow in the Elementary Particles and Field Theory Group of the Theoretical Division at Los Alamos National Laboratory. His work has been mainly in the fields of quantum measurement theory, the quantum-to-classical transition, and quantum information theory.

Quantum Feedback Control

How can we control quantum systems without disturbing them?

Salman Habib, Kurt Jacobs, and Hideo Mabuchi

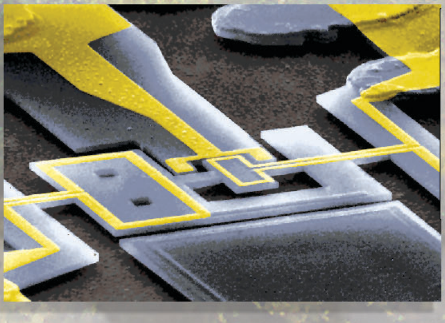

The nanomechanical electrometer shown here was built in Michael Roukes' group at Caltech. It has a demonstrated sensitivity below a single electron charge per unit bandwidth and should ultimately reach sensitivities of the order of parts per million. Its operation is based on the movement of a torsional resonator that carries a detection electrode placed in an external magnetic field. The gate electrode is seen on one side of the resonator.

Ever since Niels Bohr's first attempt at understanding the hydrogen atom, the fundamental cautionary lesson of quantum mechanics has been driven home time after time: Processes in the microworld transpire according to laws and principles that directly contradict those governing the macroworld of human experience. This radical shift in understanding is now almost a century old and has been definitively confirmed by numerous experiments. It might seem likely that the strange behaviors of quantum systems would be familiar by now and practical devices harnessing those behaviors would be commonplace. For the most part, however, we have remained mere spectators of the microphysical realm, where quantum mechanics holds sway, being forced to observe naturally occurring phenomena rather than being able to control and manipulate them. In the coming decade, however, this situation may be reversed.

Recent advances in quantum and atomic optics and condensed matter physics are providing tools to engineer practical quantum devices and perhaps even modestly complex networks of these devices. Quantum information processing, precision measurement, and development of ultrasensitive sensors are driving the present development of quantum technologies. If quantum technologies are ever to achieve the complexity of classically engineered systems such as jet aircraft and the Internet, a quantum analog of classical feedback control must be developed, since feedback control is at the heart of the stability and predictability underlying complex engineered systems.

Along these lines, recent theoretical results on error correction in quantum computation and on the dynamics of open quantum systems may be viewed as first steps in developing a theoretical formalism for practical quantum feedback control (see the articles "Introduction to Quantum Error Correction" on page 188 and "Realizing a Noiseless Subsystem" on page 260). Indeed, feedback control represents a promising new approach to mitigating quantum noise and decoherence in both quantum computation and precision measurement. If we are to apply the concepts and methods of feedback control theory to quantum dynamical systems, we must not only extend classical control concepts to new regimes but also analyze quantum measurement in a way that is useful for control systems.

The Evolution of Control Theory

Controlling natural phenomena through macroscopic engineering goes back thousands of years. Consider for a moment the ingenious ways in which early human civilizations controlled irrigation. In Mesopotamia (2000 BC), where rainfall was poor and the Tigris and Euphrates Rivers were the main sources of water, engineers constructed an elaborate canal system with many diversion dams (see the drawing to the left). In that system, the Euphrates served as a source and the Tigris as a drain. In a similar vein, the ancient Egyptians used water from the Nile and thereby allowed their civilization to flourish. On a smaller scale, machines using feedback control were developed in the Greco-Roman period, and methods for the automatic operation of windmills date back to the Middle Ages.

Perhaps the best-known example of feedback control in the industrial era is the Watt governor, which stabilizes steam engine speeds under fluctuating loads. James Clerk Maxwell provided the first dynamical analysis of this system based on differential equations. His work, which was published in 1868, founded the field of mathematics now known as control theory. In the early part of the 20th century, the idea of self-regulating machinery continued to be pushed in various directions, notably in electronic amplification. Control concepts were further developed for industrial, navigational, and military applications.

After World War II, control systems progressed to a new level of complexity. Up until that time, feedback control systems had been largely single loop, taking the feedback signal from one point and connecting the correction signal to a different point. Multiloop control systems and more-sophisticated feedback techniques emerged from progress in optimization theory and dynamical systems theory, as well as from the advent of digital computers.

After 1960, there emerged what is often referred to as "modern" (as opposed to "classical") control theory (Brogan 1990, Zhou et al. 1996), which emphasizes optimization of cost and performance. For the same control goals, it is clear that not all control strategies will be equally effective in terms of cost and performance. Determining the best strategy defines the problem of optimal control; however, optimal algorithms are often unstable to variations in system parameters and the external environment. Theorists then turned to ensuring performance bounds in the presence of uncertainty. This work resulted in the theory of "robust" control (Zhou et al. 1996). Noise in the inputs, extrinsic disturbances in the system under control, measurement errors, and modeling inadequacies—all can render control systems less effective or, in some cases, even lead to catastrophic failures. The role of robust control is to maintain adequate stability and other performance margins given the uncertainties mentioned earlier.

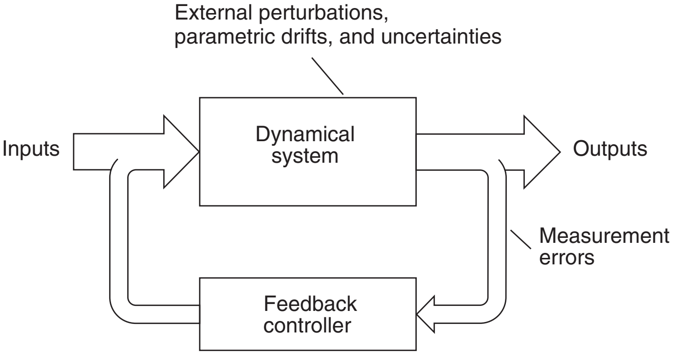

Figure 1. Classical Feedback Control
The classical dynamical system to be controlled has a set of input variables, which are processed by the system dynamics into a set of output variables. Some fraction of the set of input and output variables (possibly different for each case) is available for hookup to the controller. The controller has to perform in the presence of external fluctuations—that is, uncertainties and drifts in the parameters describing the dynamical system—and measurement errors.

Classical Control Systems

Formally speaking, a control system consists of a dynamical system interacting with a controller, a device that influences the state of the dynamical system toward some desired end. The objective may be to regulate the flow of an industrial process, money, energy, information, and so on. In a "closed-loop," or feedback, control system, the controller uses outputs from the dynamical system to monitor and influence its interaction with that dynamical system. For a linear dynamical system, for example, such a situation could be described by the following equation:

$$d\mathbf{x} = A\mathbf{x}dt + Bd\mathbf{W} + C\mathbf{u} \ , \qquad (1)$$

where $\mathbf{x}$ is a vector describing the state of the system, $d\mathbf{W}$ is a vector of Gaussian noise sources, and $\mathbf{u}$ is the vector of inputs determined by the controller. The matrix A gives the system's deterministic motion, and B and C describe, respectively, how the noise and input vectors are coupled into the system. A separate equation, namely,

$$d\mathbf{y} = H\mathbf{x}dt + Rd\mathbf{V} \ , \qquad (2)$$

describes the continuous measurement of system outputs by the controller. In each small time interval dt, the controller obtains the measurement result $d\mathbf{y}$. That result is directly related to the true state of the system by some linear transformation H, but it also includes a Gaussian noise process $\mathbf{V}$, which serves to represent imperfections in the measurement.

Examples of control systems can be found in many applications. For instance, servomechanisms are control systems that use small control inputs to produce changes in large mechanical systems. In effect, the larger systems are "slaved" to the output of the servomechanisms (for example, liquid levels in reservoirs are controlled by float valves). Feedback circuits are used in ingenious ways in electronic amplification to manipulate input and output impedances and to improve the linearity, distortion, and frequency bandwidth of the output signal relative to the input signal.

In an "open-loop" control system, the controller does not monitor the output of the dynamical system. A dynamical model for the system is assumed, and control is applied with the idea that the desired outcome will actually be achieved. Open-loop strategies are useful in situations in which the system dynamics are known precisely and vary only slowly. Processes with long measurement dead times are sometimes better suited to open-loop control methods than to feedback methods. Open-loop control strategies are applied in situations as diverse as the maximization of returns from financial investments, optimal determination of aircraft flight paths, and controlled dissociation of molecules.

Figure 1 shows how to implement closed-loop control for a dynamical system. One must be able to measure some of the dynamical variables of the system under control (the outputs) and use them to influence some other variables (the inputs). In other words, given the output variables, the controller implements a particular control strategy to influence the state of the dynamical system by appropriately varying the inputs. Robust controllers take into account variations in system parameters and fluctuations from the external environment to produce control strategies with guaranteed stability bounds.

Control systems can involve many different interacting physical systems

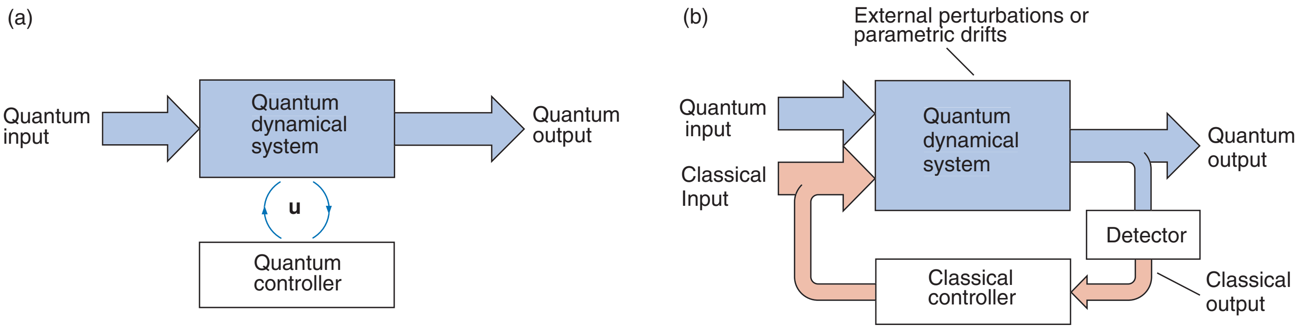

Figure 2. Directly and Indirectly Coupled Quantum Feedback

(a) Both the dynamical system and the controller are quantum systems coupled through a unitary interaction. A quantum variable is coupled to the quantum controller, and a quantum input path from the controller goes directly back to the quantum system. (b) A quantum dynamical system can be viewed as having two sets of inputs, one relating to the variation in the classical parameters describing the Hamiltonian and the other representing fully quantum inputs. Similarly, the output channel can be divided into a quantum and a classical channel. The classical channel is, in fact, a piece of the quantum channel that has become classical after observation. The controller analyzes the classical record to form an estimate of the dynamical system's state and uses this information to implement the appropriate control.

with a large number of sequential, parallel, and nested control loops that are both open and closed. For example, closed- and open-loop strategies can be combined as in the fast closed-loop systems used to stabilize the slower, inherently unstable open-loop dynamics of modern fighter aircraft.

Developing Control in Quantum Systems

The general picture of control systems outlined in the previous section appears to be extendable to quantum systems. Certainly, open-loop control problems are conceptually straightforward in the quantum context. One begins with the time evolution operator of the quantum system—the Schrödinger equation for the wave function, the Liouville equation for the density matrix, or more complicated dynamical evolution equations for the density matrix characterizing a system coupled to an environment. A theory for time-dependent variations in the evolution operator is then developed in such a way that the wave function or the density operator at some time is close to some target value. This target value does not have to be unique, nor in fact is the time evolution to that value unique. The approach just outlined applies equally well to classical probabilistic evolutions: Although quantum and classical systems are dynamically distinct, the principles for open-loop control are in fact very similar.

Controlling chemical reactions by laser-produced electromagnetic fields that are time dependent is a well-known open-loop quantum control problem. In the frequency-resolved approach to control, the quantum interference between different evolutionary paths is being manipulated; in the time-resolved approach, the dynamics of wave packets produced by ultrafast laser pulses leads to control. For some specific control of the chemical reactions, one can optimize the temporal and spectral structure of those laser pulses (Shi et al. 1988).

The fundamental differences between classical and quantum systems become real issues, however, in the field of closed-loop control. Quantum systems can have two distinct types of feedback control: directly and indirectly coupled quantum feedback (see Figure 2). As illustrated in Figure 2(a), in a system with directly coupled quantum feedback, a quantum variable of the system is coupled to the quantum controller, and a quantum input path from the controller goes directly back to the quantum system. When the quantum feedback is indirect, as shown in Figure 2(b), the quantum dynamical system under control is an observed system. It therefore generates a classical output, also known as the measurement record, which the controller may analyze to provide a best estimate of the original quantum state of the system. The controller then feeds back a classical signal to vary parameters in the quantum evolution operator in accord with the chosen control strategy. Hybrid couplings using both direct and indirect quantum feedback channels are easy to envisage: The channel from the system output to the controller input may be directly coupled whereas the channel from the controller output to the system input may be coupled indirectly through a classical path.

In both classical and quantum contexts, the main goal of closed-loop control is to enhance system performance in the presence of noise from both the environment and the uncertainty in the system parameters. To limit the effects of noise, the controller must perform an irreversible operation. Noise generates a large set of undesirable evolutions, and the controller's task is to map this large set to a much smaller one of more desirable evolutions. Mapping from the larger to the smaller set is by definition irreversible. In other words, noise is a source of entropy for the system. To control the system, the controller must extract the entropy from the system under control and put it somewhere else. The controller must therefore have enough degrees of freedom to respond conditionally upon the noise realization. In indirect quantum feedback control, the measurement process, coupled with the conditional response of the controller, is the source of entropy reduction. In direct quantum feedback control, the evolution of the system is fully unitary, or quantum mechanical. The quantum controller provides a large Hilbert space of quantum mechanical states. That is precisely where the entropy generated by the noise may be put (or where the history of the effect of the noise on the system may be stored). The quantum controller then reacts conditionally to this quantum record, keeping the entropy of the quantum dynamical system low, while the entropy of the storage location grows continually.

Inherent Noise Generation in Quantum Feedback Control

Unlike classical systems, quantum systems may be easily disturbed when information about them is extracted. Measurement disturbs a quantum system through the following intrinsic property of quantum mechanics: Obtaining accurate knowledge about one observable of a quantum system necessarily limits the information about an observable conjugate to the first. For example, particle position and momentum are conjugate observables, and the uncertainties inherent in the knowledge of both are codified by the famous Heisenberg uncertainty relation. If the chosen feedback-control strategy involves measurement, one must take into account the effects of the measurement on the evolution of the quantum system. A generally applicable model for including those effects is that of a continuous quantum measurement. This model was developed for quantum optics (Carmichael 1993), a field in which such measurements have been realized experimentally, and it was also derived in the mathematical physics literature with the help of more abstract reasoning (Barchielli 1993). In this volume, the model of a continuous quantum measurement is presented in the article "The Emergence of Classical Dynamics in a Quantum World" on page 110.

Quantum measurements may introduce unwanted noise in three more-or-less distinct ways. First, one may measure an observable conjugate to the real variable of interest and thereby introduce more uncertainty in the latter variable. More generally, one may attempt to obtain information inconsistent with the state under control. For example, to preserve a state that is the superposition of two position states, position measurements must be avoided because they will destroy the superposition. Thus, in quantum mechanics, the type of measurement chosen must be consistent with the control objectives. This condition is unnecessary in classical feedback control. Second, if trying to control the values of observables (Doherty et al. 2000), one must consider that the time evolutions of different observables necessarily affect each other over time. Observables whose values are uncertain at one time will cause other observables (perhaps more accurately known) to become uncertain at a later time. For example, a very accurate measurement of the particle position at one time introduces uncertainty into the value of the particle momentum. Because the value of momentum determines the position of the particle at a later time, the momentum uncertainty makes the future position of the particle more uncertain, hence introducing noise into the quantity that is being measured. This mechanism for introducing noise is usually referred to as the back action of a quantum measurement.

The third kind of noise involves the randomness of the measurement results. Because the state of the observed system after a measurement depends upon the outcome of the measurement, the more the result fluctuates, the more noise there is in the evolution of the system. For classical measurements, fluctuations in measurement results cannot be any more than the entropy of the system before measurement; that is, the measurement does not introduce any additional noise into the system. In quantum mechanics, however, even if the system state is known precisely, one can still make measurements that change the state in a random way, thereby actually injecting noise into the system. This observation is particularly relevant when the overall state of the system, rather than a specific observable, is being controlled. The situation is further complicated by the fact that, for certain classes of measurements, there is actually a tradeoff between the noise injected by the measurement and the information gained by the observer (Doherty et al. 2001). As a result, designing measurement strategies is far from being a trivial activity.

Strategies for Quantum Feedback Control

The differences between classical and quantum measurements profoundly affect the design of feedback control algorithms. A classical controller extracts as much information from the system as possible. In quantum control, irreducible disturbances are inherent to any measurement, and therefore the measurement strategy becomes a significant part of the feedback algorithm. For example, just as the inputs to the system change with time, the measurements too may need to be varied with time so that the best control should be achieved.

Adaptive measurement, or altering the measurement as it proceeds, was first introduced by Howard Wiseman (1995), not for control but for accuracy. The result was a more accurate measurement of some aspect of the quantum state. Nevertheless, this approach has a unique bearing on quantum feedback control algorithms. Knowing that quantum measurements can disturb the state being measured, one may want to start a continuous measurement process by measuring in a way that is not necessarily optimal but is sufficiently weak to cause minimal disturbance to the aspect of interest. As the measurement proceeds, one uses the continuously obtained information about the state to make the measurement increasingly close to optimal.

For example, consider measuring the oscillation amplitude of a harmonic oscillator when the phase of the oscillation is unknown but the oscillator is known to be in an amplitude-squeezed state; that is, the uncertainty in amplitude or energy is much smaller than the uncertainty in phase, the conjugate variable (see Figure 3). In this case, an accurate measurement of amplitude is given by a measurement of position at the moment when the particle is at its maximum spatial extent, or maximum distance from $x = 0$. On the other hand, at the moment when the particle has the most momentum (at position $x = 0$), the ideal quantity to measure is momentum. Thus, for a continuous measurement of the oscillation amplitude, a linear combination of position and momentum should be measured and the relative weighting of those two variables should be allowed to oscillate in time. However, without knowing the mean phase of oscillation, one cannot know which variable should have the most weighting in the measurement at what time. Using an adaptive measurement procedure, one can start by assuming the oscillator to have a particular phase and then adjust the relative weights of position and momentum to more desirable values as information about the phase is obtained.

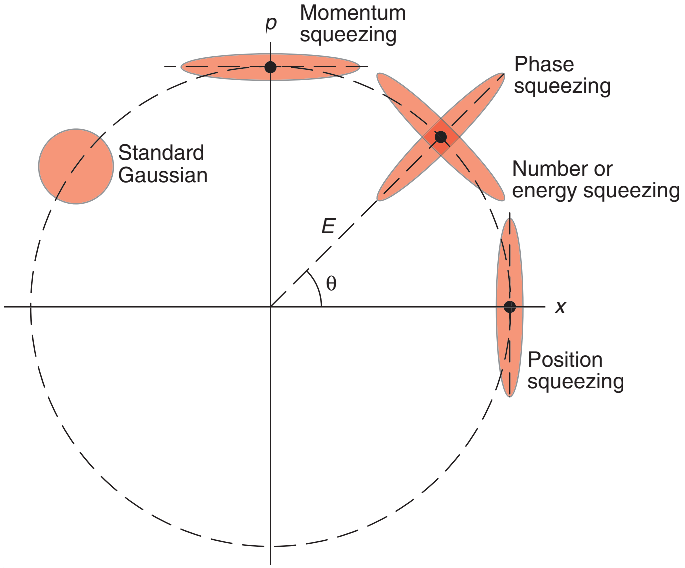

Figure 3. "Squeezed" States for a Harmonic Oscillator
Squeezing may be illustrated by considering phase-space plots of a Gaussian wave function. For a standard Gaussian state, the uncertainties in the *x*- and *p*-direction are equal, and the uncertainty ellipse takes the shape of a circle, provided appropriate position and momentum scalings are made. When states are "squeezed," the area of the uncertainty ellipse remains constant, but the ellipse is rotated and squeezed as shown. Squeezing momentum, for example, means reducing the uncertainty in momentum. The constant energy surface is the dashed circle, and the position on the circle can be specified by the angle. Squeezing phase and energy again refers to changes in shape of the uncertainty ellipse for the wave function.

Applications of Quantum Control

Atomic optics is one field in which it should be possible to test quantum feedback control in the near future. It has already been demonstrated that a single atom can be trapped inside an ultralow-loss optical cavity (mirror reflectivity is $R = 0.9999984$ in experiments at Caltech) in the strong-coupling quantum regime (Mabuchi et al. 1999). Figure 4 illustrates the experimental setup used at Caltech. The strong coupling occurs between the atom and the radiation field in the cavity and is proportional to the induced atomic dipole moment and the single-photon cavity field. Continuous measurements and real-time feedback could be used to cool such an atom to the "ground" state of the quantized mechanical potential produced by several photons in the cavity. The average number of photons circulating inside such a cavity can be kept very low (from 1 to 10 photons) if one uses a weak driving laser that barely balances the slow rate at which individual photons leak out. If the cavity mode volume is

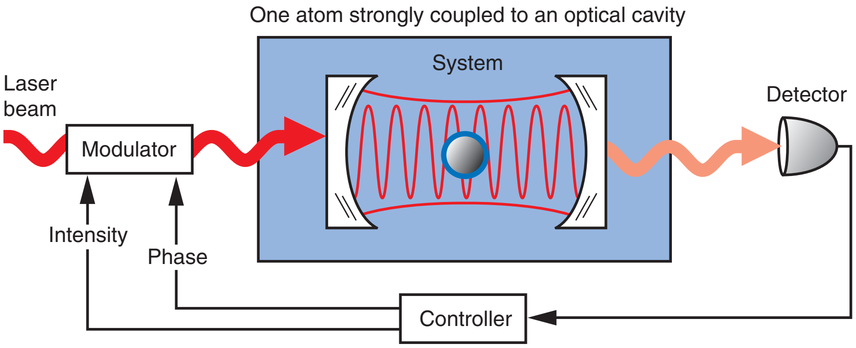

Figure 4. Quantum Feedback in a Cavity Quantum Electrodynamics Application

The dynamics between the atom and the photon field in the cavity can be modified by continuous measurement of the light transmitted through the cavity (which bears information about the evolving system state) and by continuous adjustment of the amplitude/phase of the driving laser in a manner that depends on the measurement results. Control objectives of fundamental interest include active cooling of the motion of an individual atom, feedback-stabilized quantum state synthesis, and active focusing of atomic beams for applications such as direct-write lithography.

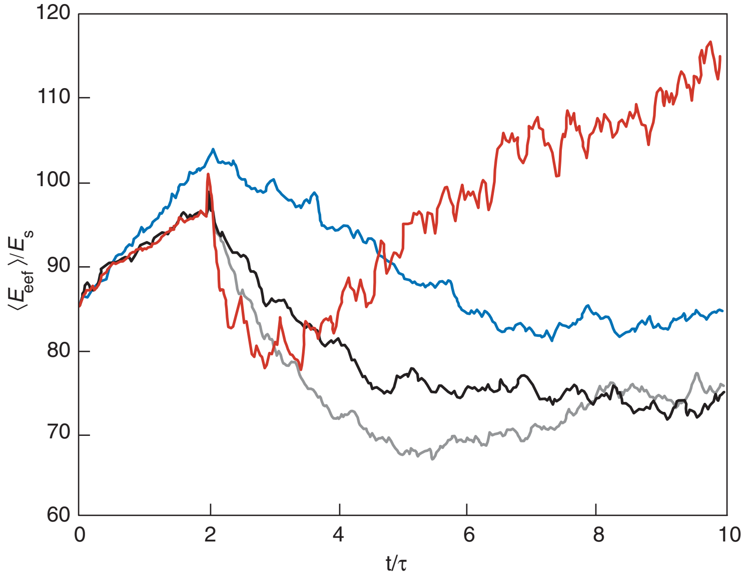

Figure 5. Simulating a Feedback Algorithm to Cool Atomic Motion in an Optical Cavity

In this simulated experiment, the light forms an effective sinusoidal potential for the atom, and the controller switches this potential between a high and a low value (separated by some ΔV) to cool the atomic motion. In this simulation, the feedback is turned on at *t* = 2, and the expected value of the atomic motion energy is plotted here as a function of time for four different values of ΔV. Although these results are still preliminary, they indicate that the effectiveness of the feedback algorithm is highly dependent on ΔV.

sufficiently small, just a few photons can give rise to dipole (alternating-current Stark shift) forces that are strong enough to bind an atom near a local maximum of the optical field distribution. At the same time, the atomic motion can be monitored in real time by phase-sensitive measurements of the light leaking out of the cavity. To a degree determined by the fidelity of these phase measurements, the information gained can be used continually to adjust the strength of the driving laser (and hence the depth of the optical potential) in a manner that tends to remove kinetic energy from the motion of the atomic center of mass.

In order to perform such a task in real time, however, it is essential to develop approximate techniques for continuously estimating the state of the atomic motion. Approximations are needed because integrating a stochastic conditioned-evolution equation to obtain a continuous estimate of the density matrix is far too complex a task to be performed in real time. While this experiment remains to be carried out, we have developed an approximate estimation algorithm[1] and used it in combination with an experimentally realizable feedback algorithm (see Figure 5).

Feedback cooling ideas can also be applied to condensed-matter systems. Some of our recent calculations predict that feedback control can be used to cool a nanoresonator below the limits set by refrigeration. This method would reduce thermal fluctuations to approximately the quantum energy level spacing of the resonator. These findings are important because nanoscale devices are interesting from a more fundamental perspective than merely sensing and actuation applications. Provided they can be cooled to sufficiently low temperatures, low-loss nanomechanical resonators would be excellent candidates for the first observation of quantum dynamics in mechanical mesoscopic systems. Yet, as mentioned above, in order achieve this goal, we must reduce thermal fluctuations to approximately the quantum energy level spacing of the resonator, a task which requires temperatures in the range of millikelvins.

---

[1] This algorithm is described in a yet unpublished paper by Salman Habib, Kurt Jacobs, Hideo Mabuchi, and Daniel Steck.

To cool the position coordinate of the nanoresonator, one needs a suitable scheme for continuous position measurement. One practical method of performing a continuous measurement of a nanoresonator's position is to use a single-electron transistor (SET)—see Figure 6. To make the measurement, one locates the resonator next to the central island of the SET. When the resonator is charged and the SET is biased so that current flows through it, changes in the resonator's position modify the energy of the central island, which produces changes in the SET current. The current therefore provides a continuous measurement of the position of the resonator, a requirement for implementing a linear feedback cooling algorithm. A feedback force can be applied to the resonator by varying the voltage on a "feedback electrode," which is capacitively coupled to the resonator (see Figure 6). The applied voltage is adjusted so as to damp the amplitude of oscillation.

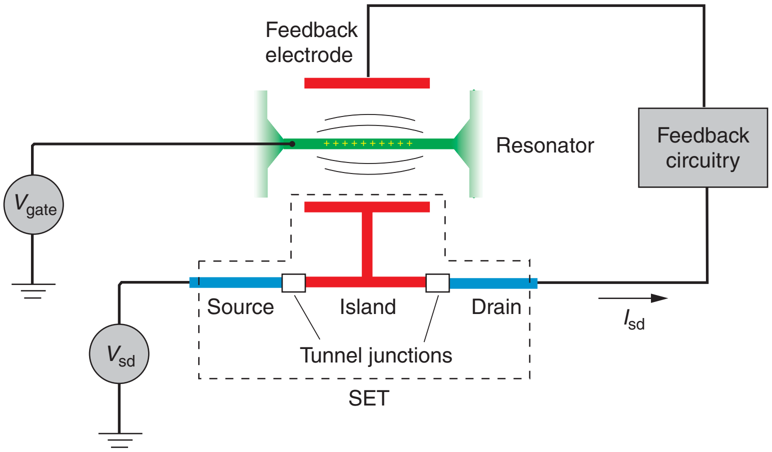

Figure 6. Cooling a Nanomechanical Resonator

This schematic diagram illustrates a concept for cooling a nanomechanical resonator to millikelvin temperatures, at which we can possibly observe quantum dynamics. An SET measures the position of the resonator, and a feedback mechanism damps (cools) the resonator's motion. The resonator, which is charged by the voltage source V_{gate} acts as the SET gate electrode. The resonator is also capacitively coupled to the SET island (red) and feedback electrode. As it moves back and forth relative to the SET island, the current I_{sd} flowing through the SET changes. Information about the changing current is used by the feedback circuitry to charge the feedback electrode. A force is generated that damps the resonator's oscillations.

Experiments on nanomechanical oscillators observed with SETs currently start at temperatures near 100 millikelvins. These oscillators have fundamental frequencies f_0 on the order of 1 to 100 megahertz. As a concrete example, consider a practical oscillator with f_0 = 10 megahertz, a length of 2 micrometers, and the other two dimensions on the order of 100 nanometers. The effective mass of such an oscillator is roughly 10^{-19} kilograms. An achievable quality factor, Q, is about 10^4. In order to observe discrete quantum passage from one oscillator energy level to another, the thermal energy should be on the order of the level spacing, that is, $k_B T \sim hf_0$, which corresponds to an effective temperature T = .24 millikelvin. Habib, Jacobs, Asa Hopkins, and Keith Schwab have shown that feedback cooling applied to this system at an initial temperature T = 100 millikelvins can yield a final temperature of T = 0.35 millikelvin. At this temperature, the aggregate occupation number lies between zero, the ground state, and one, the first excited state of the nanomechanical resonator. In other words, the system is cold enough to allow observation of quantum "jumps." Although our calculations are based on certain idealized assumptions, those assumptions are close enough to reality that experimentalists can hope to achieve similar results.

Another, seemingly paradoxical, application of quantum feedback control techniques might be in suppressing quantum dynamical effects such as tunneling. A classical memory device can be viewed as a two-state system with the two states separated by a finite energy barrier. At low temperatures, there is a finite probability of coherent or incoherent tunneling from one minimum to the other. Tunneling generates random memory errors, but continuous measurement, coupled with feedback, can suppress it. One such scheme is described and demonstrated in Andrew Doherty et al. (2000). The Hamiltonian for the double well is taken to be

$$H = \frac{1}{2}p^2 - Ax^2 + Bx^4 , \qquad (3)$$

where x and p are dimensionless position and momentum. Choosing A = 2 and B = 1/9 puts the minima of the wells at ±3 and gives a barrier height of approximately 13.5. The controller is allowed to continuously observe the position of the particle and to apply a

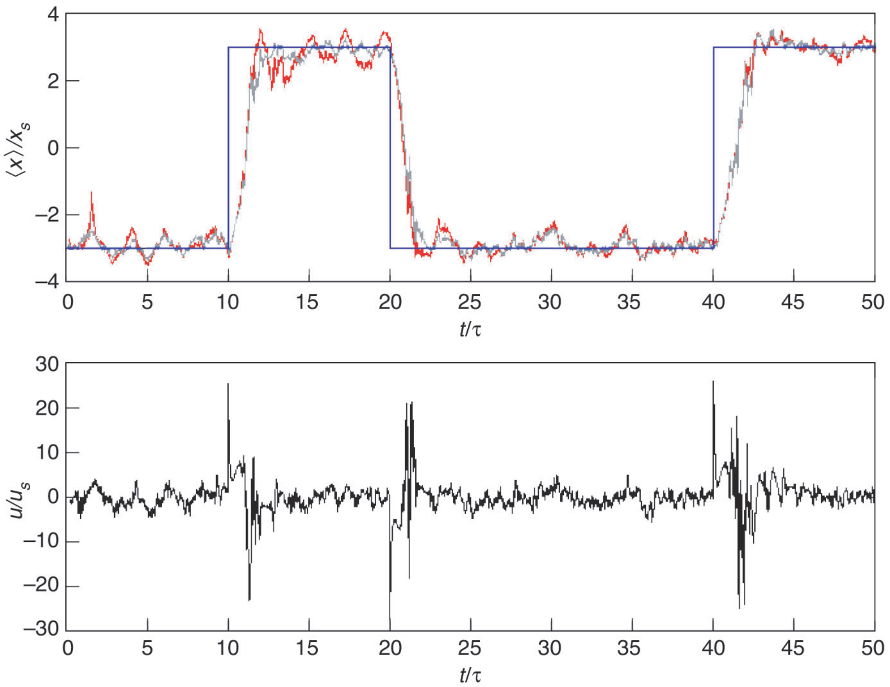

Figure 7. Particle in a Double Well Controlled by an Estimation-Feedback Scheme

(a) Shown here, as a function of time, are the target position (blue line), the 'true" mean position (red line) obtained with the stochastic master equation (in which the measurement strength k equals 0.3 and the thermal heating rate β equals 0.1), and the position obtained with the Gaussian estimator (gray line). (b) The control strength (size of applied force) is shown as a function of time.

linear force in addition to the "double-well" potential already present. The continuous observation is described by the equation

$$dq = \langle x \rangle dt + \frac{dV}{\sqrt{8k}} \quad , \qquad (4)$$

where dq is the measurement result in the time interval dt and k is a constant characterizing the accuracy, or strength, of the measurement.

The system is also driven by a thermal heat bath in the high-temperature limit. The effect of that bath is, in fact, the same as that of a continuous quantum measurement of position that ignores the measurement result. When the bath is described in this way, it is the strength of the fictitious measurement that gives the rate of thermal heating, and we will denote this constant by β.

Integrating a stochastic master equation gives the observer's state of knowledge as a result of the continuous measurement. However, since this is a differential equation for the density matrix of the single particle, it is numerically expensive to integrate. For practical purposes, one requires a simplified means for calculating a state estimate. To achieve this goal, we note that, as a result of the continuous observation, even though the dynamics are nonlinear, the density matrix remains approximately Gaussian. When a Gaussian approximation is used, the stochastic master equation reduces to a set of five equations (for all the moments of x and p up to quadratic order), and so it provides us with a practical method for obtaining a continuous state estimate. In practice, this Gaussian estimator can be shown to work quite well; that is, mean values from the approximate estimator agree very well with mean values derived from exact numerical solutions of the stochastic master equation—see Figure 7(a).

In addition to a state estimation procedure, we also require a feedback algorithm. If the system were linear, one could apply the optimal techniques of modern control theory to find a feedback algorithm. Because attempting an optimal control solution for the full nonlinear problem is computationally intractable, the idea is to linearize the system dynamics around the present estimate of the state with the further assumption that the probability density, conditioned on the measurement record, remains Gaussian. As long as position measurements are sufficiently strong, this last condition is satisfied. The importance of this condition is twofold: Having a Gaussian approximation does not only mean that a small number of moments (five) are needed to describe the distribution but also that the quantum propagator is very close to the classical propagator at each time step (for exactly Gaussian states, the two are identical), and hence techniques borrowed from classical control have an excellent chance of working. The control can fail if the measurement is too weak to maintain a localized Gaussian distribution or if it is too strong. In the latter case, the state is Gaussian, but the measurement noise is too large.

The Gaussian state estimate is now used to set the value of the feedback term in the Hamiltonian (the sign and the magnitude of the coefficient of the linear feedback term in the potential). By choosing appropriate strengths for the measurement and the feedback strength, one can show that the feedback scheme is effective in controlling whether the particle is in the desired minimum—see Figure 7(b). For this plot, the measurement strength is $k = 0.3$, and the thermal heating rate is $d\langle E \rangle / dt = \beta = 0.1$.

This scheme has limitations arising from unwanted heating due to the measurement. Although some of the heating derives directly from having to keep the state close to Gaussian, a more general limitation also contributes to heating: The measurement must be sufficiently strong to provide enough information for control to be effective. Developing new estimation and feedback schemes that can reduce the measurement-induced heating rate is an important area for future research.

Outlook for the Future

Most likely, ideas in quantum feedback control will first be tested in condensed matter physics and in quantum and atomic optics. Experiments in atomic optics have already furnished the cleanest tests and demonstrations of quantum mechanics in the last several decades. These include violations of the Bell inequalities, quantum teleportation, quantum state tomography, quantum cryptography, and single-atom interference. The ability to compare experimental results with precise theoretical benchmarks is a hallmark of these tests. As these experiments become increasingly sophisticated and complex, one can envisage a passage from "toy" demonstrations to real applications such as feedback control. The more strongly coupled systems of condensed matter physics are less amenable to accurate theoretical prediction. Nevertheless, experiments are becoming comparable in quality to early atomic optics experiments, and the time is ripe for active interaction between these two fields: Theoretical development in quantum optics, such as continuous measurement and quantum control, can be taken over to condensed matter contexts, most notably in nanotechnology. As the size of the smallest structures that can be fabricated by lithographic techniques decreases, the need for quantum mechanics becomes inevitable. Since lithography is the only way we know to create very complex systems at reasonable cost, it follows that a fundamental and predictive understanding of quantum dynamics applicable to these systems (whether coherent or incoherent) will be required. It is also clear that, for these systems to be designable and to function reliably in an engineering sense, further development of quantum control theory will be necessary.

From a "more algorithmic" perspective, the Holy Grail is the development of optimal and robust control algorithms that are generally applicable. So far, apart from the trivial case in which the system dynamics are linear and the measurement strategy is considered fixed (Doherty and Jacobs 1999), no such optimal algorithms have been found for quantum feedback control. In classical control theory, optimal and robust control algorithms exist for linear systems, but only very few for nonlinear systems despite the best effort of control theorists in the past few decades. Nonlinear classical optimal control is a very difficult problem indeed, and probably intractable in most cases. Systematic numerical search algorithms for optimal strategies exist, but these also become intractable for systems of reasonable size. Because the dynamics of noisy and measured quantum systems is inherently nonlinear, the quantum control problem may also be intractable (Doherty et al. 2000). However, in quantum dynamics, nonlinearity is of a restricted kind, and the possibility of obtaining general analytic results providing optimal and robust algorithms for the feedback control of quantum systems remains an open problem. ■

Further Reading

Barchielli, A. 1993. Stochastic Differential-Equations and a Posteriori States in Quantum-Mechanics. *Int. J. Theor. Phys*. **32** (12): 2221.

Brogan, W. L. 1991. *Modern Control Theory*. Englewood Cliffs, NJ: Prentice-Hall.

Carmichael, H. J. 1993. *An Open Systems Approach to Quantum Optics*, Lecture Notes in Physics Monograph 18. New York: Springer-Verlag.

Doherty, A. C., and K. Jacobs. 1999. Feedback Control of Quantum Systems Using Continuous State Estimation. *Phys. Rev. A* **60** (4): 2700.

Doherty, A. C., S. Habib, K. Jacobs, H. Mabuchi, and S. M. Tan. 2000. Quantum Feedback Control and Classical Control Theory. *Phys. Rev. A* **62**: 012105.

Doherty, A. C., K. Jacobs, and G. Jungman. 2001. Information, Disturbance, and Hamiltonian Quantum Feedback Control. *Phys. Rev. A* **63**: 062306.

Hood, C. J., T. W. Lynn, A. C. Doherty, A. S. Parkins, and H. J. Kimble. 2000. The Atom-Cavity Microscope: Single Atoms Bound in Orbit by Single Photons. *Science* **287**: 1447.

Mabuchi, H., J. Ye, and H. J. Kimble. 1999. Full Observation of Single-Atom Dynamics in Cavity QED. *Appl. Phys. B* **68** (6): 1095.

Maxwell, J. C. 1868. On Governors. *Proc. R. Soc. London* **16**: 270.

Shi, S., A. Woody, and H. Rabitz. 1988. Optimal Control of Selective Vibrational Excitation in Harmonic Linear Chain Molecules. *J. Chem. Phys*. **88**: 6870.

Wiseman, H. M. 1995. Adaptive Phase Measurements of Optical Modes: Going Beyond the Marginal *Q* Distribution. *Phys. Rev. Lett*. **75**: 4587.

Wiseman, H. M., and G. J. Milburn. 1993. Quantum Theory of Optical Feedback via Homodyne Detection. *Phys. Rev. Lett.* **70**: 548.

———. 1994. Squeezing via Feedback. *Phys. Rev. A* **49**: 1350.

Zhou, K., J. Doyle, and K. Glover. 1996. *Robust and Optimal Control*. Englewood Cliffs, NJ:Prentice-Hall.

Hideo Mabuchi received an A.B. in physics from Princeton University and a Ph.D. from Caltech. Upon graduating, he became Assistant Professor of Physics at Caltech but spent his first year on leave at Princeton University as a visiting fellow in chemistry. Since returning to Caltech, he has been named an A. P. Sloan Research Fellow, Office of Naval Research Young Investigator, and a MacArthur Fellow. His current research focuses on quantum measurement, quantum feedback control, control-theoretic approaches to the theory of multiscale phenomena, and optical measurement techniques for molecular biophysics.

For biographies of Salman Habib and Kurt Jacobs, see page 125.

Atom-Trap BECs

A new laboratory for studying superfluidity, quantum fluctuations, and other quantum phenomena

Eddy M. E. Timmermans

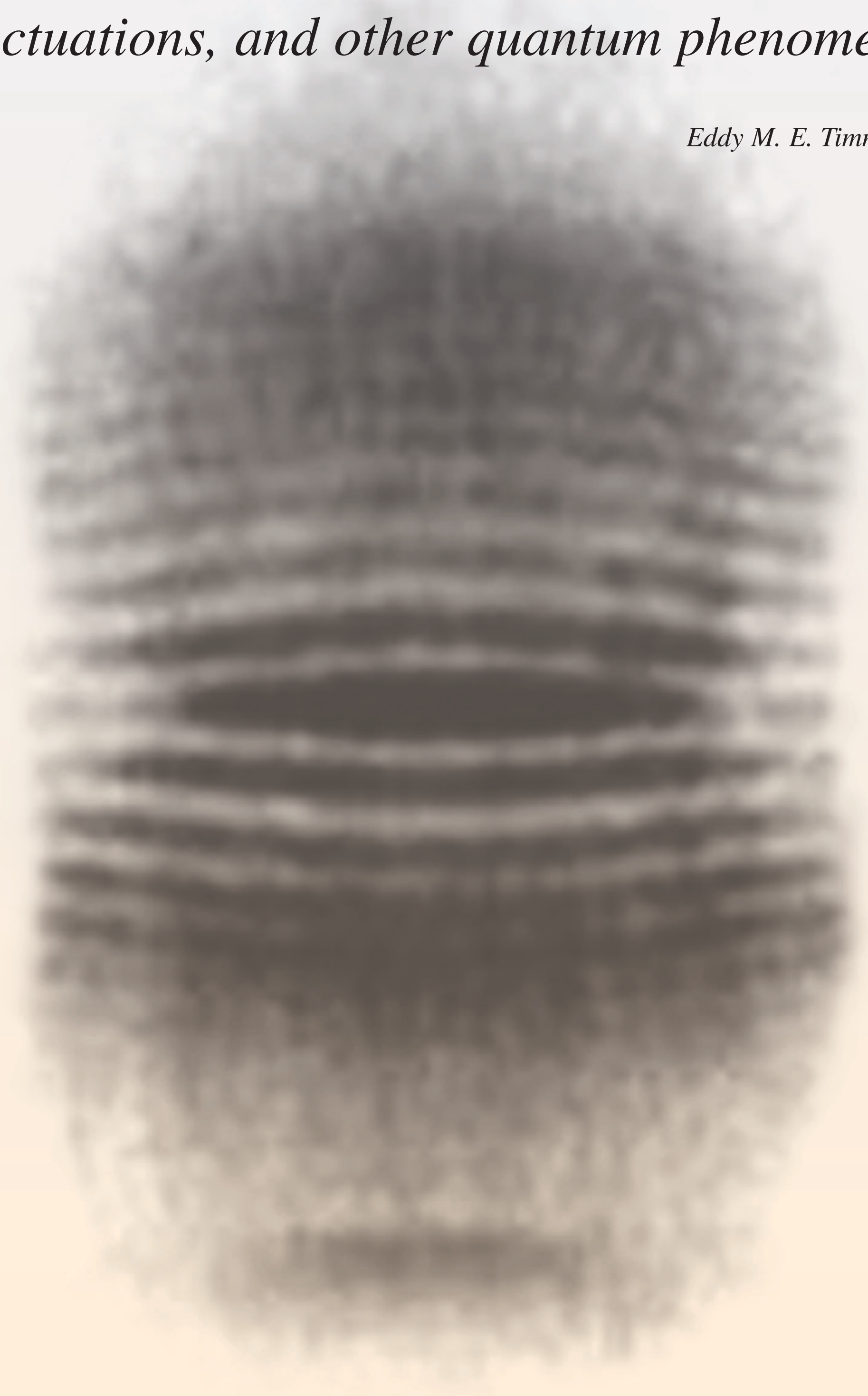

In October 2001, the field of ultracold-atom physics was honored with the Nobel Prize in physics. It was awarded to Carl Wieman, Eric Cornell, and Wolfgang Ketterle for the creation and study of dilute-gas Bose-Einstein condensates (BECs). Never before had the BEC phase transition, predicted by Einstein more than 70 years earlier, been observed in such a clear and unambiguous realization. By confining neutral atoms in a tiny magnetic trap and cooling them to temperatures only nanokelvins above absolute zero, the Nobel laureates and their colleagues had slowed the atoms down to the point at which the individual wave functions begin to overlap and many thousands of atoms suddenly occupy exactly the same single-particle quantum state. Coaxing bosonic atoms (atoms with integer spin) to condense into this coherent quantum state had been the "holy grail" of the cold-atom physics community for almost two decades. The quest had led to the development of extraordinarily clever trapping and cooling techniques, including Zeeman slowing, magneto-optical trapping, evaporative cooling, and time-orbital potential trapping. The achievement of the first atomic BECs in the summer of 1995 has led to a remarkable sequence of advances that continues unabated.

At first, this article first provides a historical perspective on atom-trap BECs and then focuses on the exciting experiments that are driving the field of cold-atom physics. Our historical overview stresses the long-range coherent properties of BECs and the role BEC physics has played in the explication of superfluidity in liquid helium. In discussing current work, we have selected a line of research and a series of experiments that illustrate the enormous flexibility of the new atom-trap BEC technologies. These experiments were carried out at the Massachusetts Institute of Technology (MIT), Yale University, and Max Planck Institute of Physics in Munich, Germany. Their achievements suggest intriguing prospects for future work in ultracold atomic physics in general and at Los Alamos in particular. In fact, several Los Alamos scientists have already contributed to the development of this field on an individual basis, and we briefly mention those in the concluding section.

The opening figure, produced by Ketterle's group at MIT, is taken from the paper (Andrews et al. 1997) that provides the starting point for our discussion of the new avenues introduced by these advances. The figure is a direct optical image of two ballistically expanding BECs showing a spatial interference pattern on a macroscopic scale. This pattern is a stunning confirmation that the phase coherence in atom-trap BECs is as complete as in optical lasers, and therefore these condensates can be manipulated and used as atomic lasers, that is, as coherent sources of atomic-matter waves. This is a unique prospect for phase-coherent matter.

After we introduce and resolve an intriguing puzzle regarding the origin of the interference pattern, we turn to a BEC experiment by the group of Mark Kasevich at Yale. This experiment is interesting from a theoretical point of view because the BECs display both laserlike and superfluid aspects of long-range phase coherence. The former is usually reserved for a nonequilibrium system of noninteracting photons, whereas the latter is usually reserved for an equilibrium or near-equilibrium fluid of strongly interacting helium atoms. Specifically, adjacent weakly linked BECs display laserlike spatial interference in a manner that implies Josephson-junction-like phase dynamics between the BECs (Orzel et al. 2001).

The purpose of the Yale experiment was not to probe coherent behavior but to induce and observe quantum fluctuations in the conjugate variables of long-range phase versus localized atom number. The group loaded the BECs into an optical lattice in which the potential barriers separating the lattice wells serve as junctions. By gradually freezing out the motion of the bosons through the junctions and observing the subsequent loss of phase coherence, the scientists were able to infer an increased certainty in the number of atoms in each well, that is, the formation of number-squeezed states. A few months later, the group of Theodore Hänsch in Munich, Germany (Greiner et al. 2002), conducted a beautiful experiment that took this process to its limit. They observed the sudden disappearance of all phase coherence in a BEC trapped in an optical-lattice potential, a direct demonstration of the Mott-insulator phase transition in which a partly coherent state becomes an all-localized state and the tunneling between wells completely stops. This transition is somewhat analogous to the well-known Mott transition from a conducting phase to an insulating phase of electrons in a crystal lattice.

The success of these experiments is due in part to the fact that dilute-gas BECs, with their long coherence lengths and slow evolution times, are readily manipulated and observed with high-precision atomic and optical technologies. Atom-trap BECs have become a remarkably flexible and transparent system for exploring complex many-body phenomena.

In introducing a theoretical view of these developments, we use a "pedestrian" approach to the condensate description, drawing the comparison to single-particle quantum mechanics wherever possible. This approach will make some of the more subtle points of many-body condensate physics accessible to the nonspecialist. We end with an assessment of the atom-trap BEC system for investigating fundamental issues in many-body physics.

Atom-Trap BECs—A Realization of Einstein's Condensate

Einstein was the first to understand the quantum concept of particle indistinguishability and to realize some of its far-reaching implications. He made the following prediction: When a gas of noninteracting bosons, or particles with integer spin, is cooled below a critical temperature, a significant fraction of the particles will suddenly find themselves in the same lowest-energy single-particle state. (This is an example of a many-body system that is "quantum degenerate," a term signifying that the system's behavior is dominated by quantum statistics—that is, the statistics of indistinguishable particles, either Bose statistics for particles with integer spin or Fermi statistics for particles with half-integer spin—as opposed to the Boltzmann statistics of classical systems.) In the limit of zero temperature, all the noninteracting bosons would occupy exactly that same ground state yielding a many-body state that we now call a BEC.

Similarly, in the ground state of a dilute gas of bosons, almost all particles find themselves in the same single-particle quantum state. Much attention has been devoted over the years to the study of such dilute-gas BECs because they are believed to provide a model for studying superfluidity in a more direct way. The term "superfluidity" denotes a host of low-temperature fluid phenomena such as inviscid, or dissipationless, flow and quantized vortices, all of which contradict our intuition for classical fluid behavior. Interestingly, all condensed-matter superfluids such as helium-4, its fermion cousin helium-3, and the superconductors consist of strongly interacting particles and do not resemble dilute-gas BECs in most of their particulars. However, we believe that their superfluid nature arises from the property of long-range phase coherence, which they share with the dilute-gas BECs. The concept of long-range phase coherence will be discussed later. For now, simply stated, it implies the existence of a complex-valued, single-particle-like wave that characterizes the entire many-body system.

In the case of a dilute BEC, the single-particle-like quantum wave (a wave function that depends on the position of a single particle) can be identified with the wave function of the single-particle state that is occupied, on average, by more than one boson and is also known as the multiply occupied single-particle state.[1] Because almost all particles occupy that single-particle state at zero temperature, the dilute BEC exhibits almost complete coherence. The dilute BEC is then the simplest superfluid system. In contrast, the precise description of the quantum wave coherence of a strongly interacting superfluid is not straightforward. Although it is tempting, for instance, to associate the fraction of the fluid that is superfluid (and can flow without dissipation) with the fraction of the atoms that occupy the lowest-energy single-particle state, that assumption turns out to be wrong. At zero temperature, the helium-3 fluid is all superfluid, whereas only 10 percent of the atoms occupy the zero-momentum state.

Questions regarding the strong interaction effects and the role of quantum fluctuations in reducing the phase coherence and superfluid fraction remain of interest. Against this backdrop, it may be worth noting that the optical-lattice BEC experiments described below give unprecedented control of such quantum fluctuations.

The current atom-trap BECs are dilute in a sense that we will specify shortly. Their experimental achievement represented the first unambiguous realization of dilute BECs. They are made from neutral alkali atoms (sodium, rubidium, lithium, and more recently, hydrogen) that are trapped and cooled with a combination of optical and magnetic fields. (See "Experiments on Cold Trapped Atoms" on page 168 for a description of trapping and cooling processes.) The alkali atoms chosen consist of an even number of fermions (protons, neutrons, and electrons) giving a total spin that has an integer value. These "composite" bosons exhibit the same type of "gregarious" behavior that Einstein predicted for noncomposite bosons. Indeed, the experimenters knew that a BEC had formed when they saw evidence for a sudden increase in the number of atoms occupying the same single-particle ground state at the center of the trap (see Figure 1). This "condensation" is quite different from the familiar liquid-vapor phase transition seen in water, for example. The particle wave functions overlap perfectly, and the behavior of this degenerate Bose-Einstein gas, or condensate, becomes exquisitely sensitive to the interparticle interactions even if the system is dilute. The spatial extent of the multiply occupied single-particle wave function is determined by the competition of the effective interparticle repulsion and the trapping potential that confines the atoms. In present-day experiments, the size of the BEC can be as large as one-tenth of a millimeter. In other words, the multiply occupied single-atom wave function describing the BEC is macroscopic.

Although Bose-Einstein condensation had never been directly observed before 1995, this phase transition served as a textbook example in statistical mechanics (Huang 1987) because it is one of the few phase transitions that can be described analytically. As Einstein himself stressed (Pais 1979), this remarkable transition follows solely from the quantum-mechanical concept of particle indistinguishability, unlike the usual phase

---

[1] A multiply occupied single-particle state is mathematically expressed in Equation (1) of this article.

Figure 1. The First Atom-Trap BECs
Some of the first signatures of Bose-Einstein condensation were obtained in a dilute gas of trapped rubidium atoms in the groups of Wieman and Cornell. Shown in (a) are the shadow (absorption) images of the density profile of the trapped atoms and in (a′) the cross sections of the local density. Both data sequences were obtained with varying values of the cutoff energy used in the evaporative cooling, the final stage in cooling the trapped atoms. In evaporative cooling, atoms of energy above the cutoff, indicated in megahertz, were removed from the trap. As the cutoff energy decreases, the final temperature to which the system equilibrates is lowered. Below a critical value, a sharp peak appears in the density profile, a signal that Bose-Einstein condensation has occurred. As the gas was contained in an asymmetric (cigar-shaped) trap, the shape observed in (a) provides an independent signature. The leftmost frame shows a spherically symmetric thermal cloud; the middle frame shows an asymmetric density spike corresponding to the condensate surrounded by a thermal cloud; and the rightmost frame shows the final density spike in which most of the atoms have Bose-condensed. (b) These shadow images from Ketterle's group show a BEC in sodium. The number of trapped atoms is greater than that in (a) by about a factor of 100. The density of the condensate grows with decreasing temperature from left to right. (b′) These density plots show cuts through an atomic cloud as the condensate develops. Note that the spatial extent of the condensate is about 0.1 mm. The size reflects the macroscopic nature of the system. It increases with the scattering length defined in the text.

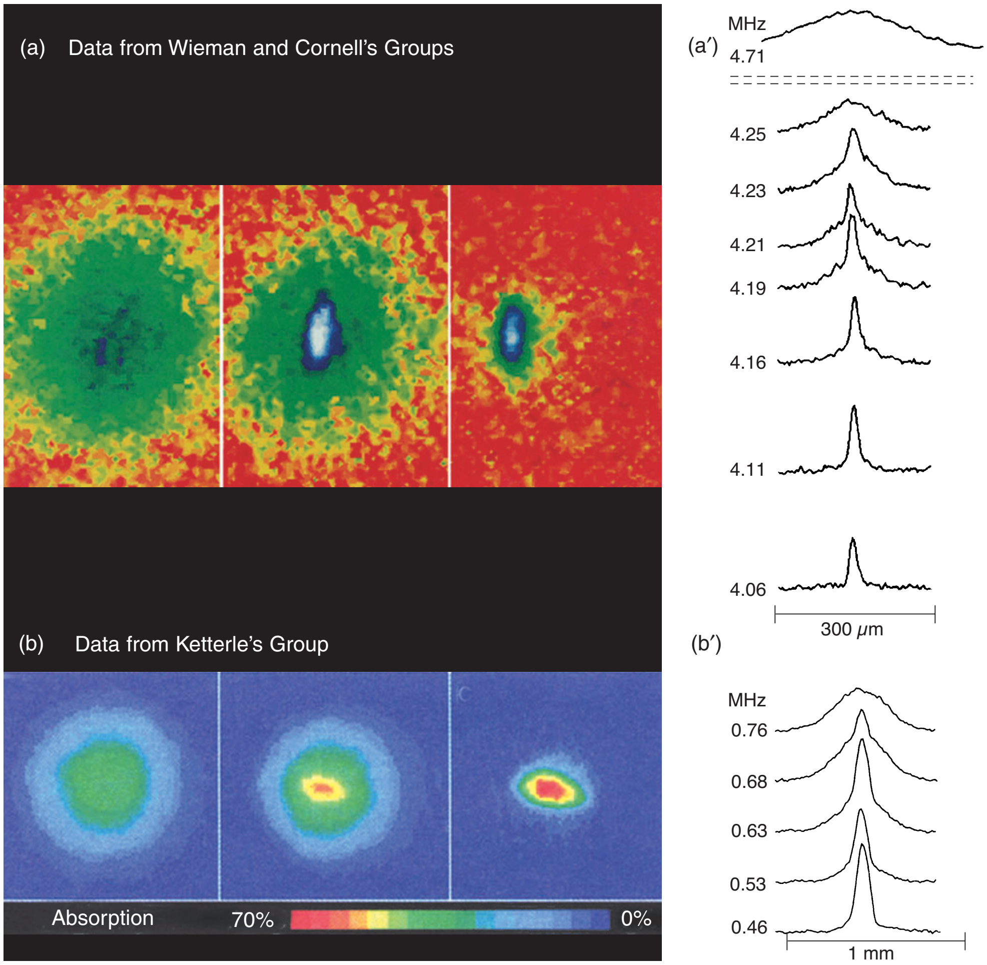

[Figures 1(a) and 1(a′) are reprinted with permission from Anderson et al. *Science* 269, page 199. Copyright 1995 American Association for the Advancement of Science. Figures 1(b) and 1(b′) are reproduced with permission from the American Physical Society.]

transitions, which result from a competition between interactions and entropy (disorder).

The neutral atom-trap systems are extremely dilute. Like billiard balls, they feel each other's presence only when they are separated by a distance equal to or less than a particular length. This length, known as the scattering length a, takes on different values for different atomic species—or even for the same species in different atomic states—but for most of the trapped neutral alkali atoms, its value is positive (reflecting an effectively repulsive force between the particles), and it tends to be about 1 nanometer. We characterize the "diluteness" of the gas by visualizing the atoms as hard spheres of radius a and computing the fraction of the total volume occupied by the spheres, $(4\pi/3)na^3$, also called the "packing fraction." In the current atom-trap BECs, the packing fraction ranges from one part in a million to one part in a billion.

At that diluteness, almost all atoms are phase coherent in the zero-temperature Bose-condensed state, somewhat in the manner that the photons produced through stimulated emission into a single mode of an optical-laser cavity are phase coherent. That is, all particles behave according to the same coherent wave function, and the particles can exhibit macroscopic interference. Contrary to the optical-laser system, the BECs consist of mutually interacting particles that are conserved (that is, the total number of atoms remains constant) and that can relax to an equilibrium state, in which case the long-range phase coherence gives rise to superfluid behavior. Indeed, in the last three years, experiments have definitively shown that the atom-trap BECs exhibit the defining behavior of a superfluid such as sustained superflow (or dissipationless flow), zero resistance to an object moving through the condensate, and quantized vortices.

Most BEC experiments are carried out with no more than a hundred thousand to a few million atoms. The difficulties encountered in increasing the particle number currently limits the prospects for practical applications somewhat. On the other hand, the atom-trap BEC technology has become fairly routine—more than 20 experimental groups have achieved BECs by now. The extraordinary flexibilities offered by the available atomic, molecular, and optical technologies, as well as by the imaging techniques, provide the BECs with advantages that are unique in low-temperature physics.

Aspects of BEC Dynamics

We will explore a bit further the two quantum concepts that are central in understanding BECs and the sense in which superfluid behavior of the BECs represents the behavior seen or inferred in liquid helium and other systems, including nuclei, subnuclear systems produced in accelerators, and neutron stars. Those two central concepts are particle indistinguishability and coherent wave behavior.

Particle Indistinguishability. It was Einstein who realized that the statistics Bose devised to understand the Planck spectrum of black-body radiation involved counting the number of ways in which particles (in that case, photons) can be distributed over single-particle states (called "subcells" in Einstein's thermodynamic treatment). The Bose counting presumed the particles to have a distinctly nonclassical quality. Whereas the trajectories of classical particles can always be followed so that the particles can be distinguished from each other, Bose counting assumed particles to be fundamentally indistinguishable. Einstein extended the counting technique for photons, whose particle number is not conserved, to a gas of conserved noninteracting particles, and he showed that the indistinguishability implies a sudden increase in the number of particles occupying the specific subcell/single-particle state of lowest energy: the BEC phase transition.

Coherent Wave Behavior. A BEC's coherent wave behavior follows directly from the time evolution of the multiply occupied single-particle state. In quantum mechanics, the one-particle system evolves according to Schrödinger's wave equation. As a consequence, the single-particle system can exhibit the type of interference seen in Young's classic double-slit experiment, which proved that light was a wave phenomenon (see the box "The Double-Slit Experiment"). In the quantum interpretation, light and atoms exhibit both particle and wave behavior, and the interference results from the uncertainty in knowing which of two possible trajectories the particle or the photon followed in reaching the detector. (Put another way, the particle can simultaneously follow two different paths to reach the screen; that is, it can exist in a superposition of probability amplitudes A_1 and A_2, one for each path. The probability of finding the particle at the detector is given by the square of the amplitude $|A_1 + A_2|^2$, which exhibits interference that is due to the $A_1A_2^* + A_1^*A_2$ contribution.) Depending on the location at which the particles hit the detector, the probability amplitudes for each path add up constructively or destructively, respectively increasing or decreasing the probability.

As explained in the box, the observation of an interference pattern, even with light, can represent an experimental challenge. Many particles (or photons) must pass through the slits for the pattern to be seen, and if the particles (photons) occupy different single-particle states, the interference washes out, and the probability becomes a single blob without the spatial oscillations that signal interference. In the BEC case, as in an optical-

The Double-Slit Experiment—A Quantitative Measure of Coherence

In 1802, Young devised and performed the double-slit experiment, which disproved Newton's particle theory of light and established unequivocally that light is a wave phenomenon. In that experiment, two holes punched in a screen allowed incident light to pass through. The light intensity reaching a second screen located behind the first was then recorded, and under the right conditions, it was possible to observe interference fringes (an intensity pattern that oscillates in space), giving unmistakable proof of the wave nature of light.

To understand the origin of the interference fringes, we imagine the light to be perfectly monochromatic (characterized by a single wavelength or frequency) and to be emitted in a direction perpendicular to the screens from a point source an infinite distance away (see Figure A). In that case, the incident light consists of plane waves with wave fronts parallel to the screen. The light reaching a specific position on the second screen has traveled in a straight line from either hole, and the difference in distance traveled determines the difference in phase of both light rays reaching the screen. If the difference in distance traveled by each ray is equal to an integer number of wavelengths, the waves originating from each hole are in phase, which means that their instantaneous electric-field vectors point in the same direction. The total electric field, which is the vector sum of both fields, then has a magnitude equal to the sum of the magnitudes. In contrast, if the difference in distance is equal to an odd number of half-wavelengths, the waves are out of phase, meaning that the electric-field vectors of the rays that passed through the different slits point in opposite directions and that the magnitude of their vector sum is less than that of the light from a single hole. In fact, they can completely cancel each other out, giving a vanishing intensity. In the first case, the waves are said to add up constructively, and the intensity, which is proportional to the square of the magnitude of the total electric-field vector, appears bright; in the latter case, the waves add up destructively, and the intensity appears dim. Varying the position on the second screen causes the difference in distance from both holes to vary and the intensity to go through a series of maxima and minima, corresponding to, respectively, constructive and destructive interference.

In a realistic two-slit experiment, the incident waves are not perfectly monochromatic, and the source of light is not a perfect point source. Whether the interference pattern can be distinguished in the recorded intensity actually depends on the details of the experiment, such as the distance between the slits. Loosely speaking, optical coherence refers to the ability of the light to exhibit such interference. Mathematically, the contrast is specified by measurements of the highest (I_{max}) and lowest (I_{min}) intensities. The visibility of the fringes, defined as the ratio $(I_{max} - I_{min})/(I_{max} + I_{min})$, provides a measure of light coherence. For laser light, the slits can be as far apart as the width of the laser beam and still produce an interference pattern with a visibility near unity. In the quantum description of the laser, nearly all photons are said to be in the same state. In contrast, thermal light contains photons in different states, each of which would give a different interference pattern with interference fringes at different positions. The recorded pattern is a sum of all the interference patterns, and the fringes at different positions can wash each other out.

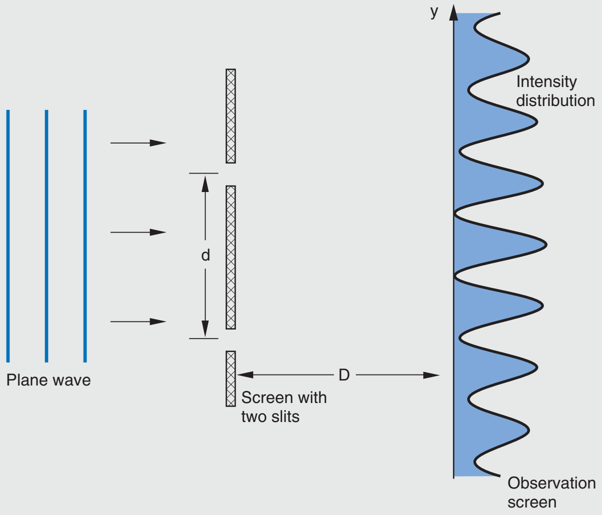

Figure A. Diagram of Double-Slit Experiment
A plane wave incident on the first screen passes through the two slits and is stopped by the second screen. The light intensity at a specific position on the second screen depends on the difference in the path lengths traveled by the light waves emanating from the two slits to that position. If the path length difference is equal to an odd number of half wavelengths, the spot appears dim (low intensity); if it is equal to an integer number of wavelengths, the spot appears bright (high intensity). The path length difference varies along the straight line shown in the plane of the second screen. Along this line, the intensity passes through positions of constructive and destructive interference, giving an oscillatory intensity variation, called interference fringes.

laser system, most particles occupy the same state so that the many-particle system exhibits the interference pattern of the single-particle system. We call this property "coherent wave behavior." As mentioned previously, it is the essential property that the weakly interacting BEC has in common with the strongly interacting superfluids such as helium.

Classical or Mean-Field Description of BEC Dynamics. Current atom-trap BECs have packing fractions of about one part in a million to one part in a billion. At that diluteness, almost all the neutral atoms of a near-equilibrium system at near zero temperature occupy the same single-particle state. The many-body system can therefore be approximated by an N-particle wave function consisting of a product of single-particle wave functions:

$$\Psi\left(\mathbf{r}_1,\mathbf{r}_2,\ldots,\mathbf{r}_N;t\right) \approx \chi\left(\mathbf{r}_1;t\right)\chi\left(\mathbf{r}_2;t\right)\ldots\chi\left(\mathbf{r}_N;t\right) , \tag{1}$$

where the single-particle χ-function is a complex-valued quantity:

$$\chi\left(\mathbf{r};t\right) = \left|\chi\left(\mathbf{r};t\right)\right|\exp\left(i\theta\left(\mathbf{r};t\right)\right) . \tag{2}$$

In 1927, shortly after the discovery of quantum mechanics, Erwin Madelung pointed out that the behavior of the single-particle wave function was analogous to that of a fluid in which $|\chi(\mathbf{r};t)|^2$ plays the role of the single-particle density and $(\hbar/m)\nabla\theta$ is associated with a velocity. Similarly, in BEC physics, where the single-particle wave function is multiply occupied, the phase of the single-particle wave function, θ, plays a crucial role in the theory as the single phase that gives rise to all the coherent wave phenomena discussed below. In particular, its gradient describes the velocity associated with the dissipationless flow observed in superfluid systems.

The product state in Equation (1) is a special case of the Hartree-Fock Ansatz for the many-body wave function of identical particles, and it evolves according to a Hartree-Fock equation of motion. If the boson particles of mass m experience an external trapping potential V, so that the potential energy of a single boson at position $\mathbf{r}$ is $V(\mathbf{r})$, and if the bosons interact with each other through an interaction potential v, so that a pair of bosons located respectively at $\mathbf{r}$ and $\mathbf{r}'$ experience an additional energy $v(\mathbf{r} - \mathbf{r}')$, then the Hartree-Fock equation takes on the following form:

$$i\hbar\frac{\partial\chi}{\partial t} = \left[-\frac{\hbar^2\nabla^2}{2m} + V\left(\mathbf{r}\right)\right]\chi + \left[N-1\right]\int d^3\mathbf{r}'\, v\left(\mathbf{r}-\mathbf{r}'\right)\left|\chi\left(\mathbf{r}';t\right)\right|^2 . \tag{3}$$

Because the interaction between neutral atoms in a BEC has a much shorter range than the length scales on which the atom-trap BECs vary, we can approximate the interparticle potential by an effective contact interaction, $v(\mathbf{r} - \mathbf{r}') \rightarrow \lambda\delta(\mathbf{r} - \mathbf{r}')$, where the interaction strength λ is proportional to the scattering length a: $\lambda = (4\pi\hbar^2/m)a$. In addition, the number of particles is large enough to allow approximating $(N - 1)$ by N. We then introduce the condensate field Φ as $\Phi = N^{1/2}\chi$ so that $|\Phi|^2$ represents the particle density, as it does in the single-particle case. With these quantities, the Hartree equation for atom-trap BECs takes on the form of the celebrated Gross-Pitaevski equation:

$$i\hbar \frac{\partial}{\partial t}\Phi = \left[-\frac{\hbar^2\nabla^2}{2m} + V + \lambda\left|\Phi^2\right|\right]\Phi \ . \qquad (4)$$

This equation, first derived by Pitaevski to treat superfluid vortices in a full quantum description, has been very popular in many fields of physics (and even biology). In spite of its simplicity, it has solutions that exhibit crucial nonlinear physics phenomena such as solitary waves, self-focusing, and self-trapping. As a result, the atom-trap BECs can also be regarded as new laboratories for studying nonlinear dynamics.

Describing the physics of BECs by means of the Gross-Pitaevski equation—Equation (4)—is known as "making the mean-field approximation" or "working in the classical approximation." The term "classical" may appear out of place because Equation (4) implies that matter has wavelike behavior, and it implicitly contains the Planck constant. Nevertheless, this equation also follows from the Lagrange equations of the corresponding classical field theory without any quantization condition. The Gross-Pitaevski equation gives a classical description of BECs in the same sense that Maxwell's equations provide a classical description of photon dynamics. Perhaps most significantly, the Gross-Pitaevski equation provides the simplest possible description of a superfluid system, and the mean-field approximation (which for BECs is equivalent to assuming a product wave-function solution) captures many of the essential features of superfluidity. For instance, the mean-field treatment predicts a dispersion relation, or excitation spectrum, that satisfies Landau's criterion for dissipationless flow (a criterion to which we refer below). On the other hand, the Gross-Pitaevski equation is certainly not as general as the phenomenon of superfluidity. Although some long-range behavior of the helium superfluids and superconductors can be qualitatively understood when this equation is invoked, the atom-trap BECs are the only systems quantitatively described by it. Moreover, the classical description also breaks down for BECs, for example, when quantum fluctuations become important, as they do in the experiments described at the end of this article. Those experiments involve number-squeezed states and the Mott transition from a coherent, or superfluid, state to a localized state.

The Coherent Wave Nature of Superfluidity

The term "superfluidity" was first applied to a very low temperature phase of liquid helium. In 1938, Peter Kapitza and, independently, John Allan and Donald Misener discovered that below a critical temperature of 2.2 kelvins, liquid helium-4 flows without measurable dissipation through capillary tubes. It seemed that this low-temperature phase of helium-4, called $\mathrm{He}_{\mathrm{II}}$, is not governed by the usual laws of classical fluid dynamics. Subsequent experiments uncovered other counterintuitive phenomena in $\mathrm{He}_{\mathrm{II}}$, including the fountain effect, perfect heat conductivity, and persistent circular flow. Superfluidity is now the name for both this collection of phenomena and the state of matter responsible for them.

The superfluid state was so unusual and its mechanism so difficult to discern in the relatively inaccessible medium of a strongly interacting fluid that its origin remained a matter of continuing controversy for more than two decades.

Is He_{II} like a BEC? Noting that helium-3, the fermion cousin of helium-4, did not undergo a phase transition to a superfluid at similar temperatures, Fritz London suggested in 1938 that the He_{II} transition is intimately related to the boson nature of the helium-4 atoms. He further proposed that the He_{II} superfluid is, in a generalized sense, a BEC. Of course, being a strongly interacting fluid, the helium system cannot be characterized by the assumption that all atoms occupy the same single-particle state. Nevertheless, London (1938) argued that "some of the general features of the degenerate ideal Bose-Einstein gas remain intact, at least qualitatively, for this liquid." He also offered support for his thesis by calculating the BEC critical temperature for the helium density, which came out to 3.13 kelvins, remarkably close to the He_{II} transition temperature of 2.12 kelvins, measured in 1933. Although the latter agreement is largely fortuitous, London's words sound almost prophetic in retrospect: He hinted that the superflow in He_{II} was a macroscopic quantum current brought about by changes in the boundary conditions.

The Two-Fluid Description of He_{II}. Following a different track, Lev Landau and, independently, Laszlo Tisza (who was, in fact, partly motivated by London's views) proposed the two-fluid model of He_{II}, in which one component is an inviscid, irrotational superfluid that does not carry entropy. This model explained the observed effects and also correctly predicted new superfluid phenomena, such as second sound. Landau used very general assumptions to derive a criterion for superfluidity and an expression for the critical velocity above which dissipation would set in. The critical-velocity calculation, although ultimately incorrect, captured the main features of persistent flow, and a generalized form of the Landau criterion is still of great use in explaining critical velocities for superfluidity. Nicolai Nicolaevich Bogoliubov showed that a weakly interacting BEC satisfies Landau's criterion for superfluidity, but Landau continually resisted the notion that the superfluid should be associated with a BEC.

The BEC Description Revisited. Finally, Oliver Penrose (1951) and then Penrose and Lars Onsager (1956) proposed the currently accepted point of view that superfluidity is a macroscopic manifestation of coherent (hence, single-particle-like) quantum-wave behavior. This description does not contradict the two-fluid model but supersedes it in the sense that the coherent quantum-wave behavior includes phenomena, such as quantized vortices and Josephson effects, which find no explanation in the two-fluid model.

As previously mentioned, the single-particle quantum wave behavior, which is compatible with and can be described as fluidlike behavior, had been pointed out by Madelung in 1927. In his pioneering paper of 1951, Penrose derived the equation for the off-diagonal density matrix of the many-body helium fluid and then drew on Madelung's analysis of the single-particle wave function to associate the long-range part of that off-diagonal density matrix with the superfluid component of the two-fluid model. In essence, Penrose identified quantum wave coherence as the essential feature responsible for both superfluidity and the BEC-like behavior conjectured by London.

As the understanding grew that superfluidity was an outcome of quantum wave coherence, the intimate connection between superfluidity and superconductivity was realized. We now understand both phenomena to be caused by coherent quantum-wave behavior, that is, many identical particles or units whose behavior can be described by the same single-particle wave function. For a superfluid, the single unit that exhibits the quantum wave behavior is a boson particle; for a superconductor, it is a pair of fermions. Much as we regard a superfluid as a BEC of boson particles, we can regard a superconductor as a BEC of fermion pairs. Not surprisingly, therefore, the fields of

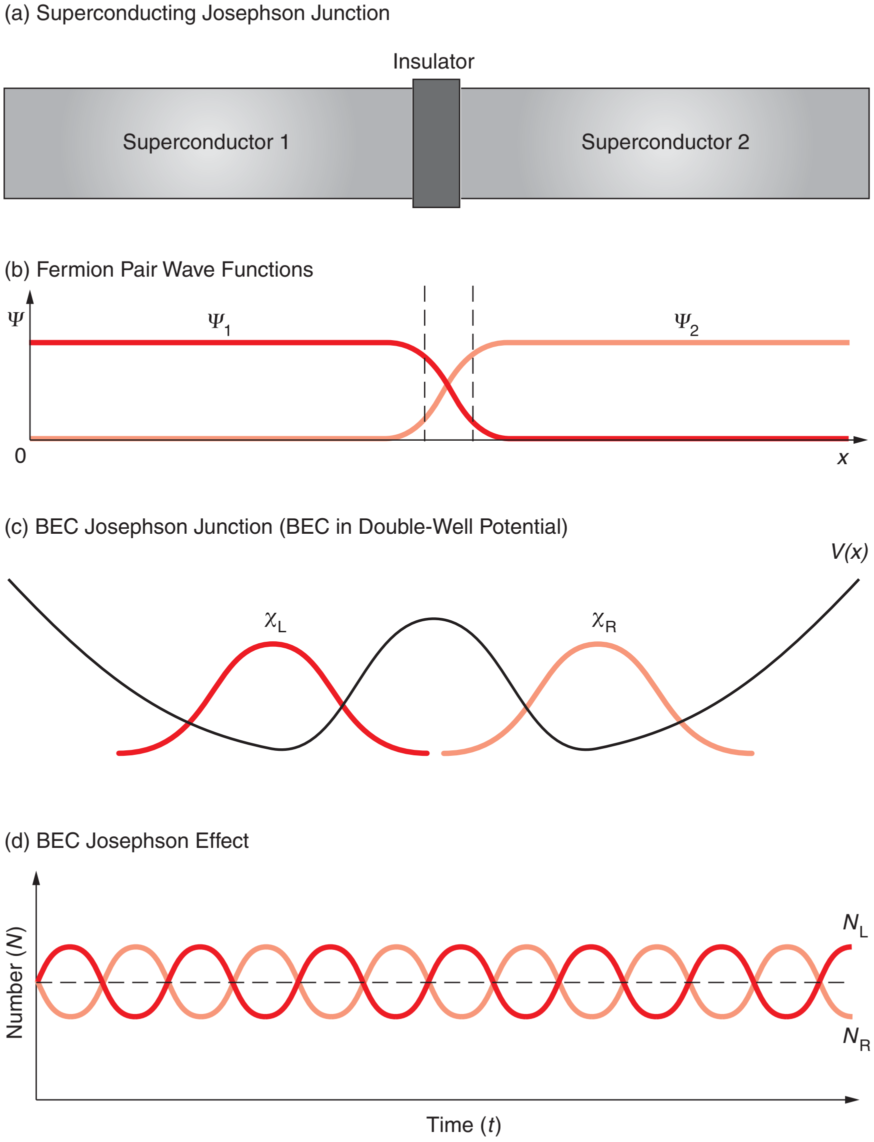
(a) Superconducting Josephson Junction
Insulator
Superconductor 1
Superconductor 2
(b) Fermion Pair Wave Functions
Ψ
Ψ1
Ψ2
0
x
(c) BEC Josephson Junction (BEC in Double-Well Potential)
V(x)
χL
χR
(d) BEC Josephson Effect
Number (N)
NL
NR
Time (t)

Figure 2. Josephson Junctions and the Josephson Effect for BECs
The diagrams show (a) two superconductors separated by a thin barrier and (b) the overlap of the coherent single-particle wave functions that describe each superconductor in the neighborhood of the junction. In 1962, Brian Josephson showed that, under certain conditions, quantum mechanical tunneling of electron pairs could occur through the barrier. If the two wave functions differ by a phase, a direct current of electron pairs will flow through the barrier, or junction. If a voltage is placed across the junction, the phase difference varies periodically in time, causing an alternating current to flow across the junction. (c) A neutral-atom BEC trapped in a double-well potential behaves like a superconducting Josephson junction. The potential barrier created by a laser beam acts like the insulating barrier between the superconductors. (d) The BEC junction is predicted to exhibit the Josephson effect. For instance, a sudden change in the chemical potential of one of the BECs would initiate an oscillation in the number of particles in each well. The frequency of the oscillation is determined by the difference of the chemical potentials.

superfluidity and superconductivity share a number of phenomena that stem directly from their coherent wave nature. Two of these coherent phenomena, Josephson junctions and quantized vortices, have recently been studied in atom-trap BECs and are briefly described next.

Josephson Junctions. In the 1960s, the physics of superconducting Josephson junctions provided evidence for the coherent wave nature of superconductors. The Josephson junction is a weak link, such as a thin insulator, connecting two indistinguishable superfluids or superconductors—see Figures 2(a) and 2(b). One manifestation of the Josephson "effect" is an alternating current flowing through the weak link when both sides of the junction are kept at different chemical potentials by, for instance, the introduction of a potential difference over the junction.

In an ordinary electronic circuit, the potential difference sets up a direct current (dc), which flows from the region of high chemical potential to that of low chemical potential. In contrast, in a coherent-wave superfluid system, the rate for bosons or fermion pairs to tunnel through the potential barrier of the junction depends sinusoidally on the phase difference between the single-particle-like wave function on either side of the junction. That phase difference increases linearly with time in the presence of a potential difference, giving an alternating current that oscillates at the frequency corresponding to the chemical potential difference.

In the original condensed-matter Josephson junctions, the superfluids were superconductors. In such cases, the bosons tunneling through the junction are electron pairs, and the current is a charge current, which is easily and accurately measured. In helium superfluids, on the other hand, the weak link is difficult to make, and the observation of a weak neutral current presents a nontrivial experimental challenge, which was only recently met (Packard 1998).

The direct analogue of the Josephson junction in atom traps is an atomic BEC trapped in a double-well potential—see Figures 2(c) and 2(d). The challenge of observing the Josephson effect in this system, however, is similar to the problem encountered in observing Josephson oscillations in helium superfluids: How can one measure small-amplitude oscillations of neutral-particle populations? In the last section, we show how atom-trap BEC technology made possible a unique solution to the problem of observing Josephson phase dynamics.

Quantized Vortices. Quantized vortices are another coherent wave phenomenon unique to superfluids and superconductors. In classical fluids, vortices are long-lived flow patterns in which the particles whirl around an axis, all with the same angular momentum. In a superfluid, a superflow that similarly whirls around an axis can be set up by a characteristic variation of the coherent wave function: the phase of the wave function varies cylindrically around the vortex axis. For the wave function to be single-valued, it must return to its initial value after a full rotation around the axis; that is, its phase must have changed by 2π or by $2\pi n$, where n represents an integer number. This constraint implies that the angular momentum of superfluid vortices is quantized with allowed values equal to $n\hbar$—see Figure 3(a).

Quantized vortices in helium were observed by William Vinen and by George Rayfield and Frederick Reif, and their observations provided further support for the coherent wave behavior of the helium superfluid. In atom-trap BECs, the long-lived metastable vortex structures were created and studied in laboratories at the Joint Institute for Laboratory Astrophysics (JILA) at Boulder, Colorado, in the groups of Wieman and Cornell; at the École Normale Supérieure in Paris, in the group of Jean Dalibard; at MIT in the group of Ketterle; and at Oxford University, England, in the group of Chris Foot—see Figure 3(b). A direct measurement of the angular momentum of the vortices, by Dalibard's group, experimentally confirmed the quantization of BEC vortices. In addition, at MIT, rapid advances in BEC technology led to the creation of vortex lattices (also called Abrikosov lattices) in atom-trap BECs with up to 160 vortices and to the detailed observation at both MIT and JILA of the intricate dynamics of vortex formation and decay.

BEC Interference—A Demonstration of Wave Coherence

In optical systems, long-range phase coherence is easily demonstrated through the double-slit experiment. In fact, the sharpness of the interference fringes produced in that experiment is used as the standard measure of optical coherence. In contrast, condensed-matter systems give mostly indirect signatures of wave coherence—quantized vortices and Josephson effects—although observations and applications of temporal interference in superconductors do exist (for example, in superconducting quantum interference devices, or SQUIDS).

Figure 3. Quantized Vortices

(a) In a superfluid, the phase of the wave function for a vortex must increase by 2π on each revolution, which implies that the angular momentum of the vortex must be an integer multiple of $\hbar$, or $n\hbar$. (b) Several experimental groups have created and imaged quantized vortices in atom traps. The transverse absorption images (Madison et al. 2000) are of a condensate of about 10^5 rubidium-87 atoms at a temperature below 80 nK. This condensate has been stirred with a laser beam at various rotational frequencies. Above a critical rotational frequency, vortex filaments appear. Plots 1 and 2 show the variation in optical thickness along the horizontal axes of the clouds imaged in plots 3 and 4, respectively. The cloud stirred at 145 Hz (shown in plot 3) contains no vortex filament, whereas the cloud stirred at 152 Hz (shown in plot 4) contains one vortex filament. In plots 5, 6, and 7, the condensate was stirred at rotational frequencies of 169, 163, and 168 Hz, respectively.

(Reproduced with permission from *The American Physical Society*.)

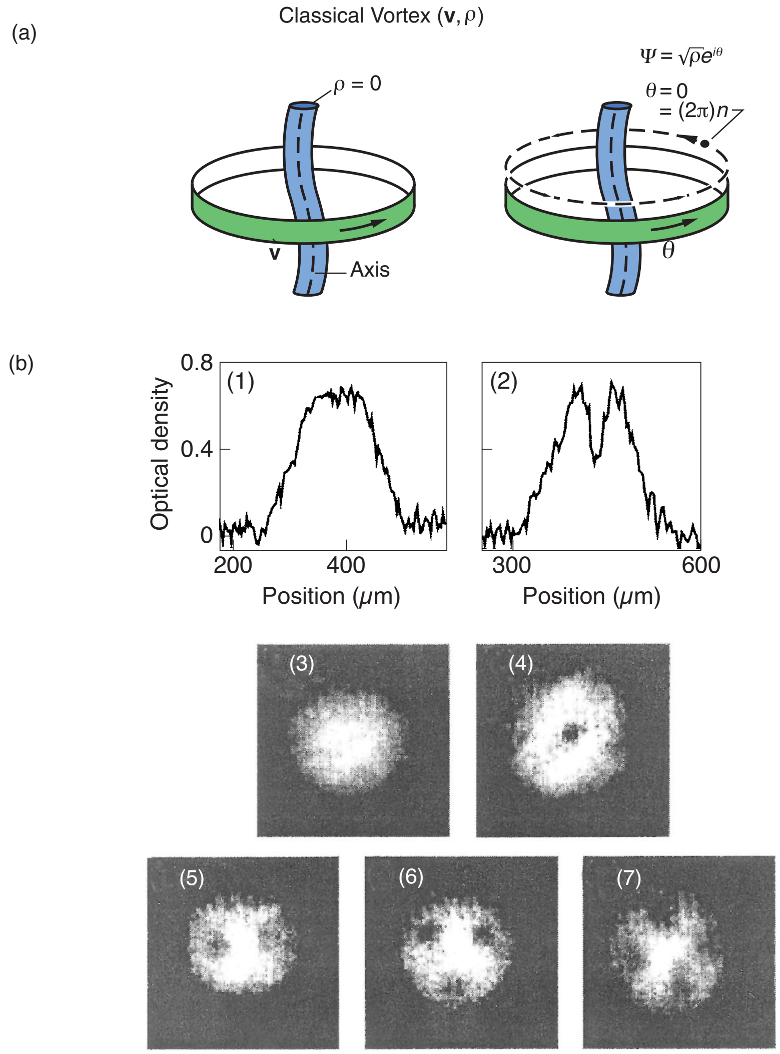

Thus, when Ketterle's group at MIT observed the spectacular interference pattern shown in the opening illustration, they brought an unusual message: BECs are superfluids that can manifest their long-range phase coherence in an optical-laser-like manner of spatial interference. Michael Andrews and collaborators later (1997) argued that the interfering BEC experiment demonstrated the first atom laser (albeit in a form that, as of yet, is not necessarily useful to applications). Their demonstration suggests that the simultaneous appearance of superfluid and laserlike aspects of long-range phase coherence might one day yield particularly potent applications of BECs.

The MIT Experiment. Figure 4 outlines the experimental procedure used by the MIT group. First, an off-resonant laser beam is passed through the center of an atom trap, which effectively creates a double-well potential. The atoms are then cooled and Bose-condensed into two BECs, one on either side of the potential barrier—see Figure 5(a). Because the height of the barrier significantly exceeds the chemical potential of either BEC, the two BECs are independent.

When the trapping potential was switched off, the two BECs expanded freely and started overlapping spatially. Using two laser pulses in succession, the MIT group imaged the local density of atoms in a 100-micrometer-thick slice within the region of

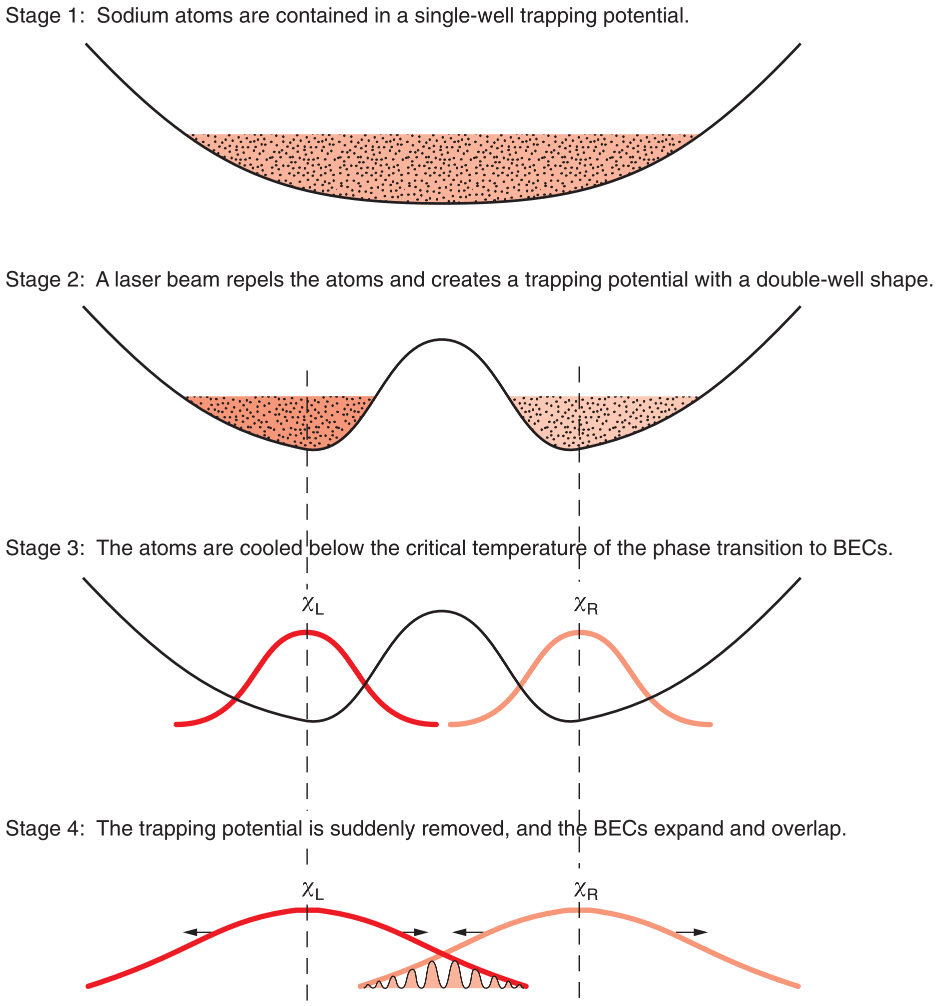
Stage 1: Sodium atoms are contained in a single-well trapping potential.
Stage 2: A laser beam repels the atoms and creates a trapping potential with a double-well shape.
Stage 3: The atoms are cooled below the critical temperature of the phase transition to BECs.
χL
χR
Stage 4: The trapping potential is suddenly removed, and the BECs expand and overlap.
χL
χR

Figure 4. Procedure for Creating BEC Interference
In the BEC interference experiment conducted at MIT (Andrews et al. 1997), sodium atoms were contained in a cigar-shaped trap (stage 1). In the second stage, a laser beam focused on the center of the initial trap repelled the atoms from that region, creating an overall atomic potential that has a double-well shape. In the third stage, the atoms were cooled below the critical temperature T_C of the BEC phase transition. The height of the potential barrier separating the wells greatly exceeded the thermal energy k_BT_C (where k_B denotes the Boltzmann constant) and the chemical potentials of the BECs that are formed in the left (L) and right (R) wells. (The wave functions for the two BECs are labeled χ_L and χ_R.) Under these conditions, the two BECs are independent of each other in the sense that they cannot "know" each other's phase. When the trapping potential is suddenly removed in stage 4, both BECs expand and then overlap. Images of the atomic density of the overlapping BECs show macroscopic interference fringes of high visibility.

overlap. The first laser pulse pumped the BEC atoms in the selected slice from state $|1\rangle$ to a different hyperfine state $|2\rangle$. The second laser, tuned near a resonant transition from state $|2\rangle$ to state $|3\rangle$ and pointing more or less perpendicular to the plane of the slice, imaged the density of atoms in state $|2\rangle$. The image showed a highly visible, regular pattern of clearly separated interference fringes of macroscopic size (40 micrometers)—see Figure 5(b). The visibility of the fringes (defined in the box "The Double-Slit Experiment") ranged from 20 to 40 percent. By characterizing their optics, the experimentalists inferred that the actual visibility of the density fringes ranged from 50 to 100 percent. The density fringes are defined as $(\rho_{\max} - \rho_{\min})/(\rho_{\max} + \rho_{\min})$, where $\rho_{\max}$ and $\rho_{\min}$ denote the maximum and minimum densities if observed with an ideal imaging technique. The high visibility of the observed fringes indicates that the entire many-body system behaves as a coherent wave.

What Produces the Interference Fringes? Unquestionably (by definition, in fact), macroscopic interference fringes indicate coherence in the usual optical sense. But how the observed interference fringes relate to the coherence of the expanding BECs is a matter of considerable subtlety, as will be explained. Under the experimental conditions of independent BECs, the single-particle density matrix, as we show below, does not

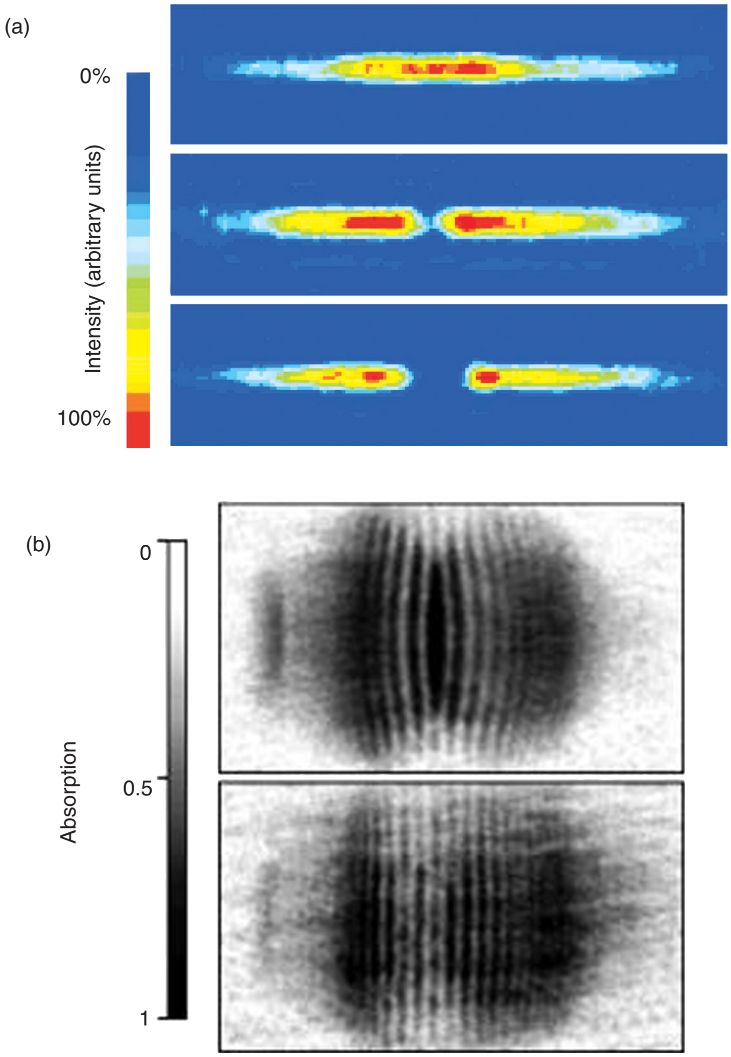

Figure 5. Sodium Atom BECs and Their Interference
(a) Phase contrast images of a single Bose condensate (upper panel) and double Bose condensates were taken in the magnetic trap of the MIT group. An argon ion laser that was focused into the center of the trap created a double-well potential. Changes from 7 to 43 mW in the power of the laser-light sheet caused the distance between the two condensates to vary. (b) The interference pattern of two expanding condensates was observed after a 40-ms time of flight for two different powers of the argon-laser-light sheet (raw-data images). The periods of the fringes were 20 and 15 μm; the laser powers were 3 and 5 mW; and the maximum absorptions were 90% and 50%, respectively, for the left and right images. The fields of view were 1.1 mm horizontally by 0.5 mm vertically. The horizontal widths were compressed fourfold, a condition that enhances the effect of the fringe curvature. For the determination of the fringe spacing, the dark central fringe on the left was excluded.
(Reprinted with permission from Andrews et al. *Science* 275, pages 638 and 639. Copyright 1997 American Association for the Advancement of Science.)

exhibit interference. Why then does the recorded image show fringes? The resolution, as we show for a special case, depends on the fact that the image does not record the single-particle density.

The Case of BECs with Definite Particle Number. As reported by Andrews et al. (1997), the potential barrier separating the two BECs was five times higher than the energy corresponding to the critical temperature for the BEC phase transition and 50 times higher than the chemical potentials of the BECs in each well. Under those conditions, the state of the double-well BEC system is indistinguishable from that of two BECs that were condensed in separate traps at an infinite distance from each other and then brought together. In principle, we can therefore know exactly how many particles occupy each of the two BECs. That is, the system is in a number state. The single-particle density of this double-well number state $\rho_{1(N)}$ does not exhibit interference, a point we now demonstrate for a simplified double-well number state with only two particles.

We call the single-atom state centered in the right well $\chi_R(\mathbf{r})$ and the single-atom state centered in the left well $\chi_L(\mathbf{r})$, where $\mathbf{r}$ denotes the center-of-mass position of the trapped atom. Thus, a two-particle number state with one atom in each well is represented by a wave function $\Psi_{(N)}$:

$$\Psi_{(N)}(\mathbf{r}_1,\mathbf{r}_2;t) = 2^{-1/2}\left[\chi_{\mathrm{L}}(\mathbf{r}_1;t)\chi_{\mathrm{R}}(\mathbf{r}_2;t) + \chi_{\mathrm{R}}(\mathbf{r}_1;t)\chi_{\mathrm{L}}(\mathbf{r}_2;t)\right] . \qquad (5)$$

When the external potential is switched off, the two-particle wave function, to a close approximation, remains of the form in Equation (5), with χ_{L} and χ_{R} evolving as freely expanding single-particle wave functions that are mutually orthogonal. The corresponding single-particle density $\rho_{1(N)}$ at a given time *t*,

$$\begin{aligned}\rho_{1(N)}(\mathbf{r};t) &= \int d^3r_2 \left|\Psi_{(N)}(\mathbf{r},\mathbf{r}_2;t)\right|^2 \\ &= \frac{1}{2}\left[\left|\chi_{\mathrm{L}}(\mathbf{r};t)\right|^2 + \left|\chi_{\mathrm{R}}(\mathbf{r};t)\right|^2\right], \qquad (6)\end{aligned}$$

is equal to an incoherent average of the densities of the individual expanding single-particle wave functions. Generally, the single-particle densities expand smoothly—a free-particle Gaussian wave function (for instance, if the χ-wave-functions start out as ground-state functions of harmonic oscillator potentials) remains Gaussian—so that $\rho_{1(N)}(\mathbf{r}; t)$ does not exhibit spatial oscillations.

The Case of a Mutually Coherent State of the Double-Well System. In contrast, had a single-well system containing both particles in its center-of-mass ground state been split adiabatically, the resulting double-well system would be in a mutually coherent state. This particular mutually coherent state would be a product of single-particle wave functions of the type $2^{-1/2}[\chi_{\mathrm{L}}(\mathbf{r}; t) + \exp(i\alpha)\,\chi_{\mathrm{R}}(\mathbf{r}; t)]$, where α denotes the phase

$$\Psi_{(\mathrm{C})}(\mathbf{r}_1,\mathbf{r}_2;t) = \frac{1}{2}\left[\chi_{\mathrm{L}}(\mathbf{r}_1;t) + \exp(i\alpha)\chi_{\mathrm{R}}(\mathbf{r}_1;t)\right]\left[\chi_{\mathrm{L}}(\mathbf{r}_2;t) + \exp(i\alpha)\chi_{\mathrm{R}}(\mathbf{r}_2;t)\right], \qquad (7)$$

difference that evolved between the right and left wave functions during the adiabatic splitting of the wells. This two-particle, mutually coherent wave function takes the form where the label C stands for coherent. The mean field or classical description—see Equation (1)—of the double-well BEC assumes such mutual coherence. The single-particle density of the mutually coherent, freely expanding two-particle system reads

$$\rho_{1(\mathrm{C})}(\mathbf{r};t) = \frac{1}{2}\left[\left|\chi_{\mathrm{L}}(\mathbf{r};t)\right|^2 + \left|\chi_{\mathrm{R}}(\mathbf{r};t)\right|^2 + \left(\chi_{\mathrm{L}}(\mathbf{r};t)\chi_{\mathrm{R}}^*(\mathbf{r};t)\exp(i\alpha) + \text{c.c.}\right)\right], \qquad (8)$$

where c.c. is the complex conjugate of the previous term. Far from the potential minima of the initial wells, the amplitudes of the expanding wave functions vary slowly in space, so that we can approximate those amplitudes as $\chi_{\mathrm{R}}(\mathbf{r}; t) \approx \chi \exp[i\theta_{\mathrm{R}}(\mathbf{r}; t)]$ and $\chi_{\mathrm{L}}(\mathbf{r}; t) \approx \chi \exp[i\theta_{\mathrm{L}}(\mathbf{r}; t)]$, and the single-particle density in the far region becomes

$$\rho_{1(\mathrm{C})}(\mathbf{r};t) = \chi^2\left\{1+\cos\left[\theta_{\mathrm{R}}(\mathbf{r};t) - \theta_{\mathrm{L}}(\mathbf{r};t) + \alpha\right]\right\} . \qquad (9)$$

Thus, in addition to the densities of the expanding single-particle wave functions, $\rho_{1(\mathrm{C})}(\mathbf{r};t)$ also contains an α-dependent term—namely, the interference fringes—that varies sinusoidally with the difference of the position-dependent phases of the overlapping χ_{R} and χ_{L} functions. The expression in Equation (8) is quite general; the single-particle density of an *N*-particle BEC distributed over two wells in a mutually coherent state takes on the form of Equation (9) in the far region.

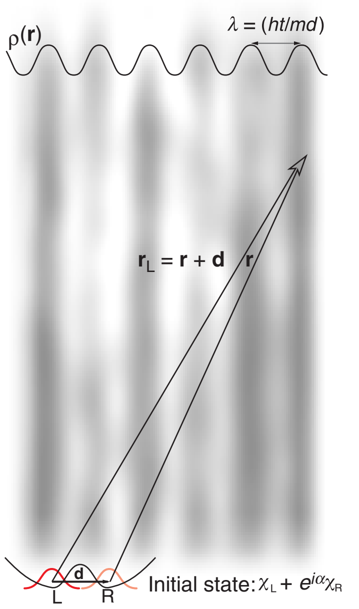
$\rho(\mathbf{r})$
$\lambda = (ht/md)$
$\mathbf{r}_L = \mathbf{r} + \mathbf{d}$
$\mathbf{r}$
d
L
R
Initial state: $\chi_L + e^{i\alpha}\chi_R$

Figure 6. Geometry of Interference Fringes
The diagram shows the interference fringes in the image of two expanding BECs that were initially trapped in the right (R) and left wells (L) of a double-well potential. As defined in the text, the r-vector denotes the position relative to the center of the right well, and the d-vector denotes the relative position of the centers of both wells. The high-density regions of the interference fringes are planes oriented perpendicular to *d*. At a time *t* after releasing the BECs, the interference fringe planes are separated by a distance $\lambda = ht/(md)$. The actual positions of the fringes depend on the phase difference α of the initial BECs (if the BECs are phase coherent, $\chi = \chi_L + e^{i\alpha}\chi_R$).

Heuristic Derivation of the Interference Fringe Pattern. What is the geometry and spacing of the interference fringes that would be produced by this mutually coherent state? We offer a heuristic derivation of the phase of a freely expanding single-particle state. Classically, a particle that has traveled a distance r in a time t has a velocity $v = r/t$. In the spirit of the Madelung description, we associate the gradient of the phase θ with $mv/\hbar$, and we find $d\theta/dr = (mr/\hbar t)$, so that $\theta = (m/2\hbar)(r^2/t) + C$, where C denotes a constant, independent of $\mathbf{r}$. Now we suppose that the left and right BECs are sufficiently alike so that we can assume that their phases in the expansion evolve with the same constant C. In that case, the difference between the phases of the amplitudes χ_R and χ_L evaluated at a vector distance $\mathbf{r}$ from the center of the right well and $\mathbf{r}_L$ from the center of the left-well is

$$\theta_R - \theta_L = (m/2\hbar t)[r^2 - r_L^2\,]^2 = -\,(m/2\hbar t)[2\mathbf{d}\cdot\mathbf{r} + d^2]\ , \tag{10}$$

where the vector distance $\mathbf{d}$ separates the centers of the potential wells and $r^2 - r_L^2 = -2\mathbf{r}\cdot\mathbf{d} - d^2$ (see Figure 6). The high-density regions of the interference fringes are planes perpendicular to $\mathbf{d}$ at a regular spacing of $\lambda = \hbar t/(md)$. The measured density pattern for the density in Equation (9) is

$$\rho_{1(C)}(\mathbf{r};t) = \chi^2\left\{1 + \cos\left[(m/\hbar t)(\mathbf{r}\cdot\mathbf{d}) + (m/2\hbar t)d^2 - \alpha\right]\right\}\ , \tag{11}$$

and the value of α can be inferred from the positions of the interference fringe planes. A more careful derivation of the phases $\theta_{R(L)}$ gives corrections, but the above expressions are essentially correct in the regions imaged in the interfering BEC experiment. The experimental images do indeed reveal planar interference fringes, separated by a distance $\lambda = ht/(md)$.

Resolving the Origin of the Interference. The experiment clearly indicated coherence, and the image agrees with the single-particle density of the mutually coherent double-well system. However, the experimental system was prepared not in a mutually coherent state, but in a number state analogous to that described by Equation (5). In that state, given that the single-particle density $\rho_{1(N)}$ in Equation (6) does not exhibit interference, why does the recorded image show fringes like those from the coherent single-particle density in Equation (11). The resolution of this apparent puzzle lies in the fact that the image does not record the single-particle density. Instead, the experiment probes the multiparticle density. Specifically, we cannot interpret the image of the N-particle system as N independent measurements of the single-particle density. But we can assume that the measurement captures the N-body system in a "likely" configuration; that is, the observation of a particle at $\mathbf{r}_1$, another at $\mathbf{r}_2$, and so on, indicates that the state of the system corresponding to the N-particle density $\rho_N(\mathbf{r}_1, \mathbf{r}_2, \ldots, \mathbf{r}_N) = |\Psi(\mathbf{r}_1, \mathbf{r}_2, \ldots, \mathbf{r}_N)|^2$ has a relatively high probability.

We use the special case of two particles in a double-well potential to illustrate the difference in probing the N-particle rather than the single-particle density. We assume the two-particle double-well system is prepared in the number state of Equation (5). We detect the particles at a time t during a period that is short on the time scale on which the single-particle wave functions χ_L and χ_R expand. The probability that one particle is recorded at $\mathbf{r}_1$ and the other at $\mathbf{r}_2$ is proportional to the two-particle number-state density:

$$\rho_{2(N)}(\mathbf{r}_1,\mathbf{r}_2;t) = \left|\chi_L(\mathbf{r}_1;t)\right|^2\left|\chi_R(\mathbf{r}_2;t)\right|^2 + \left|\chi_L(\mathbf{r}_2;t)\right|^2\left|\chi_R(\mathbf{r}_1;t)\right|^2 + \left[\chi_L(\mathbf{r}_1;t)\,\chi_R^*(\mathbf{r}_1;t)\,\chi_R(\mathbf{r}_2;t)\,\chi_L^*(\mathbf{r}_2;t) + \text{c.c.}\right]\ . \tag{12}$$

(a) Initial State

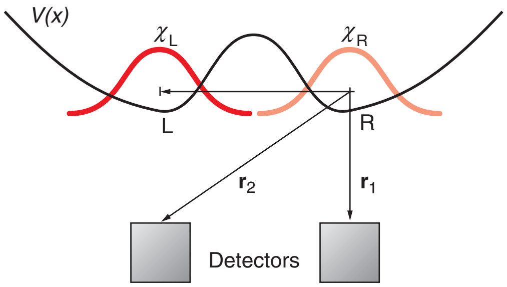

(b) Released Trap, Event 1

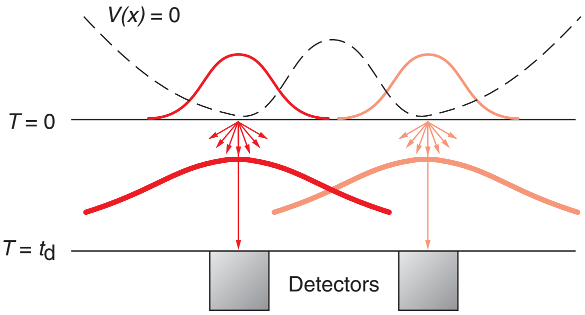

(c) Released Trap, Event 2

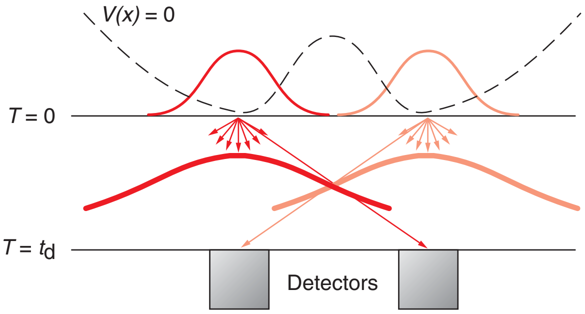

Figure 7. Origin of the Two-Particle Interference in Equation (13)

This schematic illustrates the origin of the interference pattern in the two-particle density for an expanding two-particle system that originates in a number state of a double-well potential. (a) The origin of the coordinate system is the center of the right potential well. (b) In event 1, the particle detected at $\mathbf{r}_1$ originates from the right well; the particle detected at $\mathbf{r}_2$, from the left well. (c) In event 2, the particle detected at $\mathbf{r}_1$ originates from the left well, whereas the particle detected at $\mathbf{r}_2$ originates from the right well. Because the two-particle wave function consists of a superposition of terms that correspond to the classical trajectories shown in (b) and (c), these events can interfere.

Assuming that $\mathbf{r}_1$ and $\mathbf{r}_2$ are located in the region where $|\chi_L(\mathbf{r}_1;\, t)| \sim |\chi_L(\mathbf{r}_2;\, t)| = \chi$, the two-particle density defined in Equation (12) takes on the form

$$\rho_{2(N)}(\mathbf{r}_1,\mathbf{r}_2;t) \approx \chi^4\left\{1 + \cos\left[\theta_R(\mathbf{r}_1;t) - \theta_L(\mathbf{r}_1;t) - \left(\theta_R(\mathbf{r}_2;t) - \theta_L(\mathbf{r}_2;t)\right)\right]\right\}, \qquad (13)$$

which contains the typical oscillatory contribution seen in Equation (9) describing an interference pattern. Thus, although the system is in a number state and the single-particle density does not exhibit interference, the two-particle density $\rho_{2(N)}$ does show interference.

The sinusoidal contributions in Equation (13) arise from the interference of the two distinct two-particle events illustrated in Figure 7. In one event, the particle detected at $\mathbf{r}_1$ was initially in the right well, whereas the particle detected at $\mathbf{r}_2$ originated from the left well. In the second event, the situation is reversed: The particle detected at $\mathbf{r}_1$ originated from the left well, whereas the particle detected at $\mathbf{r}_2$ originated from the right well.

Using Equation (10) for the phase difference between the two single-particle wave functions at a position $\mathbf{r}$, $\theta_R(\mathbf{r}) - \theta_L(\mathbf{r}) \approx -(m/2\hbar t)[2\mathbf{d}\cdot\mathbf{r} + d^2]$, we find that the two-particle distribution depends only on the relative position $\mathbf{r}_1 - \mathbf{r}_2$,

$$\rho_{N,2}(\mathbf{r}_1,\mathbf{r}_2;t) \approx \chi^4\left\{1 + \cos\left[(m/\hbar t)\,\mathbf{d}\cdot(\mathbf{r}_1 - \mathbf{r}_2)\right]\right\} . \tag{14}$$

Whereas the likelihood of detecting the first particle at position $\mathbf{r}_1$ is independent of $\mathbf{r}_1$ in the far region $\rho_{1(N)} \approx \chi^2$, the likelihood of detecting a second particle at $\mathbf{r}_2$ is greater near the planar regions $\mathbf{d} \cdot (\mathbf{r}_1 - \mathbf{r}_2) = n(ht/m)$, where n denotes an integer. Note that the planar regions of maximal $\rho_{2(N)}$-values resemble the interference fringes of $\rho_{1(C)}$ in Equation (11), namely, the single-particle density of the expanding, mutually coherent two-particle double-well system. In fact, the fringe patterns for the two-particle density will be identical to those of an equivalent mutually coherent system, provided the relative phase α is chosen so that the fringes of that equivalent system overlap the position where the first particle was detected. Because the position of the first particle is undetermined until measured, we can say that it is the act of determining the first particle's position that fixes the value of the relative phase of an equivalent mutually coherent system. The two-particle number-state probability distribution then resembles the product of one-particle probability distributions of the equivalent mutually coherent system. That equivalence is a general feature: The more particles detected in the image of an expanding number-state double-well BEC, the more the outcome of such measurement resembles that performed on a mutually coherent double-well BEC. The relative phase of the equivalent mutually coherent BEC system can be extracted from the image but cannot be determined beforehand.

The equivalence to a mutually coherent state with a value of the phase difference that is established by the act of measurement is familiar from the observation of interference of independent lasers (Pfleeger and Mandel 1967) and of the dc Josephson effect (Anderson 1986).

Relative Phase Dynamics for Two *N*-Particle BECs. Our derivation of the number-state two-particle density and its equivalence to a mutually coherent state density of undetermined relative phase is not easily generalized to a number-state double-well system with larger particle numbers. Instead, we can apply the elegant description developed for the relative phase dynamics of Josephson junctions. In this description, the dynamics between the two weakly linked superfluids is cast in terms of only two variables: α, the relative phase, and m, half the difference of the number of particles contained in each well. In fact, m and α are quantum numbers, and the number states are the eigenstates of m. We denote by $|m\rangle$ the number state of a double-well system with N-particles per well, of which $N - m$ occupy the left well and $N + m$, the right well.

An alternative set of basis functions is provided by states of good relative phase $|\alpha\rangle = N^{-1/2}\sum_m \exp(i\alpha m)|m\rangle$. The transformation from the $|m\rangle$-basis to an $|\alpha\rangle$-state representation is therefore a Fourier transform, somewhat analogous to the transformation between the traditional momentum and coordinate representations. Just as coordinates and momenta are conjugate to each other, m and α are conjugate variables. The many-body state can be expanded in either the $|\alpha\rangle$-states or the $|m\rangle$-states, $|\Psi\rangle = \int d\alpha \Psi(\alpha)|\alpha\rangle = \sum_m \Psi_m|m\rangle$, where $\Psi(\alpha)$ and Ψ_m are equivalent to the coordinate (x) and momentum (p) representations of a single-particle state. Generally, the Ψ wave function implies a spread both in the m and α variables: $\Delta m = (\langle(m - \langle m\rangle)^2\rangle)^{1/2}$, $\Delta\alpha = (\langle(\alpha - \langle\alpha\rangle)^2\rangle)^{1/2}$, where $\langle\ \rangle$ denotes the expectation value. As conjugate variables, Δm and $\Delta\alpha$ satisfy the

Heisenberg uncertainty relation $\Delta m \times \Delta\alpha \geq 1$, whereas Δx and Δp satisfy the relation $\Delta x \times \Delta p \geq \hbar$ in single-particle quantum mechanics.

To continue our comparison of BEC interference experiments with single-particle quantum mechanics, we note that the establishment of a relative phase between interfering BECs is the analogue of a position measurement on a particle in a plane-wave state. When the plane wave has a well-defined momentum, then $\Delta p = 0$ and $\Delta x \rightarrow \infty$. The latter expression means that the coordinate has maximum uncertainty, and therefore, a measurement of x could yield any value. Likewise, in the initial state of the interfering BEC experiment, $\Delta m = 0$, and the determination of α achieved by the imaging of the expanding BECs could yield any value. When the measurement is performed, however, the wave function collapses to an eigenstate of α.

Squeezing the Numbers in BECs—Macroscopic Quantum Fluctuations

As mentioned previously, the number-phase description in terms of the α or m quantum eigenvalues is familiar from the treatment of Josephson junctions. The application of the number-phase description to the problem of double-well BECs then reveals an intimate connection between the physics of BEC interference and Josephson physics. However, the BEC interference experiment conducted at MIT lacks the weak link through which the superfluids can exchange their boson particles. Consequently, it is not exactly a BEC-Josephson experiment. In a subsequent effort, the Kasevitch group at Yale used a related setup and succeeded in inducing and controlling such reversible superflow between multiple BECs. The Yale experimentalists achieved this goal by trapping the BECs in the potential minima of an optical lattice—a trapping potential that oscillates sinusoidally in space as $|E_0|^2 \sin^2(kx)$—and by lowering and raising the potential barriers separating the BECs through variations of $|E_0|^2$. Most important, the Yale group probed Josephson physics by observing variations in the interference pattern of the expanding BECs after switching off the optical-lattice potential.
The sharpness of the interference fringes revealed the uncertainty in relative phase, $\Delta\alpha$, of the expanding BECs. In particular, when the barrier height had been sufficiently increased before the BECs were released, the fringes observed in the image of the expanding BECs became fuzzy, an indication that the uncertainty in the phase values of the initial BECs had increased markedly. This increase is expected as the number uncertainty decreases. As we argue below, this is a genuine quantum fluctuation effect observed in a macroscopic system. To set the stage, we start by elucidating the role of the quantum fluctuations in multiple-well BEC physics.

Quantum and Classical Physics of Double-Well BECs. As in Equation (1), the classical or mean-field description of the N-particle double-well system, the many-body wave function is a product state: $\Psi(\mathbf{r}_1, \mathbf{r}_2, \ldots, \mathbf{r}_N;t) \approx \chi(\mathbf{r}_1;t)\ldots, \chi(\mathbf{r}_N;t)$, where each single-particle wave function is a linear superposition of left-well (χ_L) and right-well (χ_R) wave functions,

$$\chi(\mathbf{r};t) = 1/(2N)^{1/2}[(N - m(t))^{1/2}\chi_\mathrm{L} + e^{i\alpha}(N + m(t))^{1/2}\chi_\mathrm{R}] \ , \qquad (15)$$

and α and m are well-defined parameters. We use the same notation as in the number-phase description because the physical interpretation of α and m is the same as that of the quantum eigenvalues introduced above. In fact, $\alpha(t)$ and $m(t)$ in Equation (15) are the expectation values of the quantum treatment of the number-phase dynamics. The classical treatment can then describe superfluid effects, the essence of which relies on

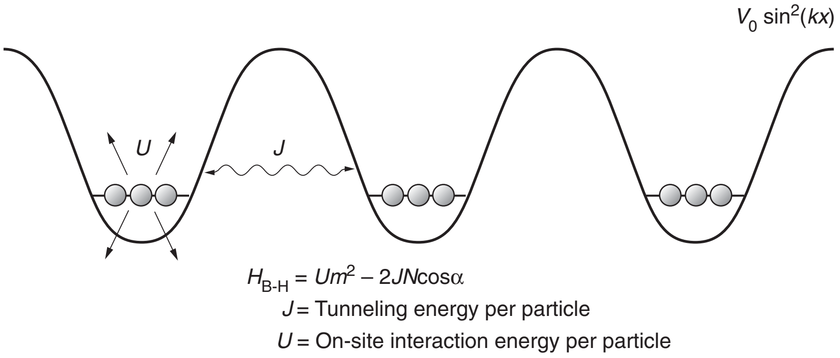
$V_0 \sin^2(kx)$
U
J
$H_{\text{B-H}} = Um^2 - 2JN\cos\alpha$
J = Tunneling energy per particle
U = On-site interaction energy per particle

Figure 8. The Bose-Hubbard Model
The diagram shows an optical-lattice potential occupied by atoms of integer spin. The interactions between the atoms include a hopping or tunneling interaction and a repulsive interaction between atoms at the same site.

the existence of a well-defined phase—see Equations (1) to (4) and the section “The Coherent Wave Nature of Superfluidity”—but it cannot account for behavior such as the collapse to a random value of the relative phase in the imaging of interfering BECs. More generally, contrary to predictions of classical mechanics, the quantum treatment predicts different outcomes of identical measurements on identically prepared systems. Measures of such quantum randomness are the standard deviations, such as the deviations $\Delta\alpha$ and Δm introduced earlier, that quantify the range of quantum fluctuations. For sufficiently large numbers of atoms, Δm can take on values that are large enough for the fluctuation range to be called “macroscopic.”

Weakly Linked BECs. When the barrier separating the two potential wells in the double-well BEC is lowered to an appropriate value, atoms can penetrate the barrier, which thereby provides the weak link that allows the left and right BECs to exchange particles. As in the description of BEC interference, we define a phase for each BEC and describe the possible particle exchange in terms of the canonically conjugate variables that represent the difference of the condensate phases, α, and half the difference of the particle population, m, occupying the individual BECs. The inter-BEC particle exchange gives rise to an effective tunneling energy of the usual Josephson form,

$$E_{\text{tun}} = -E_J \cos(\alpha) \quad . \tag{16}$$

We expect the value of E_J to be roughly proportional to the number of particles (N) per well, to depend weakly on the number difference m, and to be extremely sensitive to the height of the potential barrier separating the BECs. As the barrier height increases, the tunneling of particles is restricted, a limitation corresponding to a decrease in the value of the E_J-parameter in Equation (16). In what follows, we write $E_J = 2NJ$, where J denotes the tunneling energy per particle. The tunneling energy, minimized by putting $\alpha = 0$, favors a well-defined value of the phase difference in the ground state and, hence, favors the establishment of a definite phase difference (the superfluid limit). In contrast, the usual interparticle interactions, if repulsive, favor a well-defined value of m. To see that, we note that the interparticle interaction energy scales as the number of interactions. The N_L-particles (in the left BEC) experience $N_L(N_L - 1)/2 \approx N_L^2/2$ interactions. Similarly, the N_R-particles (contained in the right well) undergo $N_R^2/2$ interactions. Assuming that the interaction energy per particle, U, is approximately the same in each well and using $N_L = N - m$ and $N_R = N + m$, we write the total interaction energy as

$$E_{\text{int}} = (U/2)\left[N_{\text{R}}^2 + N_{\text{L}}^2\right] \approx U\left[N^2 + m^2\right] . \tag{17}$$

In contrast to the tunneling energy, E_{int} takes on its minimum value at $m = 0$, corresponding to the BEC number state with $N_{\text{R}} = N_{\text{L}} = N$. The contribution to the energy that stems from the phase-number dynamics (the sum of interaction and tunneling energies after the constant UN^2-term has been discarded) is then equal to

$$H = Um^2 - 2JN\cos(\alpha) . \tag{18}$$

Classically, the position of lowest energy is $m = 0$, $\alpha = 0$. Quantum mechanically, it follows from Heisenberg's uncertainty principle that m and α, being conjugate variables, cannot be determined simultaneously to absolute certainty. We now use the double-well Bose-Hubbard Hamiltonian in Equation (18) as a starting point to indicate how weakly linked BECs can be regarded as a laboratory for exploring both the classical dynamics and the quantum nature of Josephson junctions. A schematic representation of the individual terms that contribute to this Hamiltonian is shown in Figure 8.

Probing Josephson Physics in Weakly Linked BECs. The Bose-Hubbard Hamiltonian in Equation (18) is the generic form of the Hamiltonian that governs the physics of Josephson junctions. We can expect, therefore, that the atom trap becomes a new laboratory for studying Josephson effects. Although this physics has been studied intensely in condensed-matter environments, the new parameter range and technology of the BEC traps give a new twist to the study of Josephson-junction physics and other known phenomena, as well as the opportunity to study quantum fluctuations and, perhaps, to discover novel applications.

A sudden change in the depth of one of the wells or in its particle number can "nudge" the many-body system out of equilibrium, initiating a collective excitation in which the expectation value of the well populations oscillates. This phenomenon is called Josephson oscillations. On the topic of probing quantum behavior, it is interesting that the parameters in Equation (18) can be controlled experimentally: Variations in the trapping potential can alter the values of U and J. Clearly, the atom-trap technology gives unusual control over the Josephson junction, providing new knobs that can both initiate Josephson oscillations and vary the quantum fluctuations. The crucial question of whether oscillations and fluctuations can be measured in cold-atom BECs was answered, in part, by the Yale experiment.

What are the obstacles that the BEC technology faced in probing Josephson physics? In superconductors, Josephson effects are routinely studied by measurements of the weak supercurrent. Such measurement of a charged particle can be achieved relatively simply and accurately. In systems of neutral particles, on the other hand, the observation of a weak current represents a much greater challenge, and in helium fluids, a Josephson current was only recently observed (Packard 1998). By the same token, in the neutral-atom traps, current atom-counting techniques are not sufficiently accurate to allow observing small-amplitude population oscillations. Numbers of atoms in a typical BEC are measured with a relative accuracy of only about 10 percent. This low accuracy renders the technique unsuitable for observing Josephson oscillations of atomic-trap populations in the linear regime (number oscillations with a magnitude of 1 percent or less of the total number of trapped atoms). Instead of measuring a population imbalance,

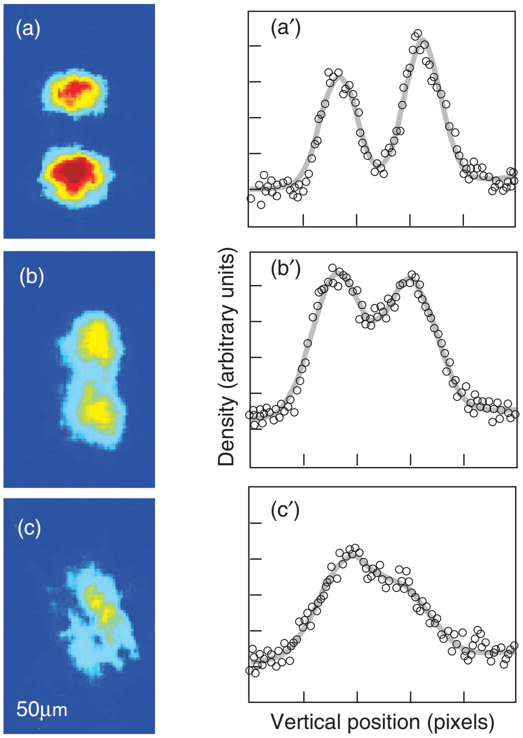

Figure 9. Formation of Number-Squeezed States in an Atom-Trap BEC

The sequence of absorption images, (a)–(c), and the associated density cross sections, (a′)–(c′), show atoms released from optical lattices of increasing depth: $U_0 = 7.2E_{\text{recoil}}$, $U_0 = 18E_{\text{recoil}}$, and $U_0 = 44E_{\text{recoil}}$, respectively. In (a), the two-peaked structure is due to interference between atoms released from different lattice sites. As the well depth increases and the tunneling rate decreases, the interference pattern becomes progressively blurred, reflecting greater phase uncertainty and the formation of number-squeezed states.

(Reprinted with permission from Orzel et al. *Science* 291, page 2389. Copyright 2001 American Association for the Advancement of Science.)

we might try to observe the relative phase of BECs, which gives a complementary view of the physics; for instance, the expectation value of the relative phase oscillates at the same frequency as the population imbalance or current in the Josephson oscillation. The BEC interference experiment conducted at MIT illustrated that the relative phase can be measured from recorded images of expanding BECs. This measurement, however, is destructive and yields a value for the phase at a single time. Whether this technique could be used to probe the time evolution of the phase is not evident. In addition, the imaging of BEC interference in the double-well system gives only a single value of the phase, whereas a measurement of the range of quantum fluctuations requires a record of the phase distribution.

The Yale experiment resolved the problem of probing the phase distribution by imaging the interference of many simultaneously expanding BECs, which had been weakly linked before the trapping potential was released. The resulting image is sensitive to the distribution of the complex phase values of the BECs. If the phases of the BECs are strongly correlated—they all have approximately the same value, for instance—then the interference of each pair of BECs can add up in phase and give an overall pattern with bright and sharp fringes. In contrast, if the phases of the weakly linked BECs are randomly distributed, then their values, determined by the act of imaging, differ widely. As a consequence, the fringes corresponding to the interference of different pairs of BECs do not overlap, so that interference washes out. The Yale experiment imaged the density of 12 expanding BECs that had been initially trapped in the adjacent potential wells of a linear optical lattice and weakly linked before the optical-lattice potential was released (see Figure 9). In such an optical lattice, the centers of mass of adjacent BECs are all separated by the same distance (half the wavelength of the light that creates the standing wave pattern of the lattice potential). By measuring the amplitude and fringe sharpness (defined as the ratio of spatial width to the distance separating the fringes) observed in imaging the expanding BECs, the Yale group quantified the uncertainty of the relative phase values.

As they had ramped up the height of the potential barriers before releasing the BECs, the Yale group observed a marked decrease in the sharpness of the fringes in the expanding-BEC images. The measured sharpness was in quantitative agreement with numerical simulations that were based on the ground-state phase uncertainty. The assumption that the many-body system has reached its ground state before the trapping potentials are switched off is reasonable because the change in potential barrier was effected adiabatically in the experiments. In a ground state, the uncertainties of conjugate variables generally reach the Heisenberg limit, which in this case would mean that $\Delta m \times \Delta\alpha \approx 1$. Thus, from their measurements and the agreement with the predicted values of phase uncertainty, the Yale group inferred that their observed

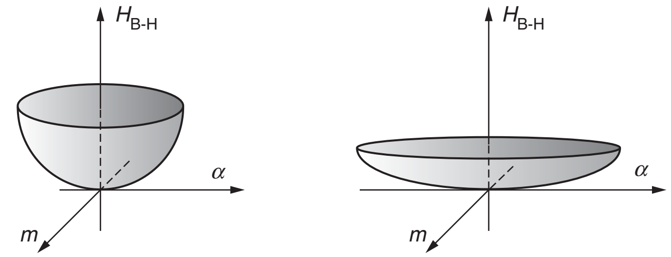
(a) Energy Surface

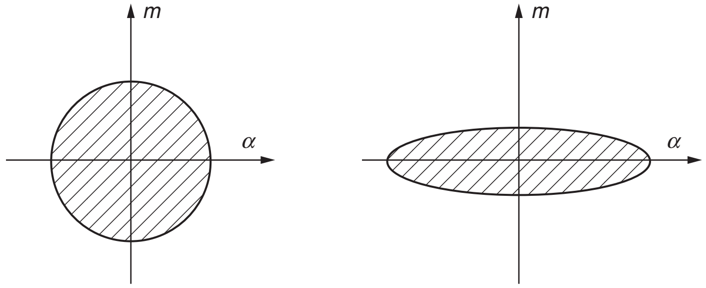
(b) Region of Wigner Distribution, $W(m, \alpha) > p_0$

Figure 10. Number Squeezing in Phase Space
This graph illustrates the physics of number squeezing by showing the effect of an increase in the potential barrier on the number phase (m, α) Wigner distribution of the double-well BEC discussed in the text. The graphs show the area in which the Wigner distribution of the many-body ground state exceeds a minimal value. An increase in the potential barrier lowers the tunneling rate J, which reduces the {tightness of confinement in the α-direction of the (m, α) phase space. The word "confinement" refers to the potential energy-like term in the energy expression of Equation (18) that depends on α. As a result of lowering J, the ground-state Wigner distribution stretches out in the α-direction. In accordance with the Heisenberg uncertainty principle ($\Delta m \Delta \alpha \approx 1$), the area of high Wigner distribution value remains constant in the process of stretching and the number uncertainty Δm decreases accordingly.

increase in phase uncertainty implied a similar decrease in number uncertainty Δm. By analogy with a similar reduction of uncertainty in optical field intensities, the process of reducing $\Delta m << N^{1/2}$ is called "squeezing." In Figure 10, we further illustrate the aptness of this term by sketching the effect of varying the parameters of the Hamiltonian in Equation (18) on the Wigner distribution function.

The experimental increase of the potential barrier height lowers the value of J, which greatly reduces the tightness of the confinement in the α-direction of the (α, m)-phase space. In response, the Wigner distribution stretches out farther in the α-direction. Since the area of high probability shown in Figure 10 remains of order 1, the uncertainty in the m-direction is tightly squeezed. Thus, as the hopping motion of particles between adjacent wells is "frozen out," each well contains a better-defined number of particles. To further support their claim of having observed quantum fluctuations, the Yale group also demonstrated that the trend of decreased fringe sharpness may be turned around by reversal of the variation in potential barrier height.

Quantitative Treatment of Number Squeezing. We now revisit the description of the double-well BEC to provide a quantitative understanding of the number uncertainty squeezing illustrated in Figure 10. We introduce a dimensionless parameter, or coupling constant Γ, that characterizes the competing interactions in the system: $\Gamma = UN/2J$ is the ratio of the interparticle interaction energy per well ($UN^2/2$) to the tunneling energy per well NJ (the latter plays a role somewhat analogous to that of kinetic energy in other systems). We minimize the Hamiltonian described by Equation (18) in the α-representation. To convert Equation (18) from the number representation to the α-representation, we replace the m-operator by $-(1/\mathrm{i})\partial/\partial\alpha$. Then, we calculate the expectation value of the Hamiltonian by using the Gaussian state for the wave function ψ, $\psi(\alpha) \propto \exp(-\alpha^2/(4x)$. The expectation values are simplified when expressed in terms of the width parameter x, which is related to the uncertainty in phase difference as $\Delta\alpha = (2x)^{1/2}$: $\langle m^2 \rangle = -\langle \partial^2/\partial\alpha^2 \rangle = 1/(2x)$ and $\langle \cos(\alpha) \rangle = \exp(-x)$.

The expectation value of the Hamiltonian is then equal to

$$\langle H \rangle = \frac{U}{2}\left[\frac{1}{x} - \frac{2N^2}{\Gamma}\exp(-x)\right] \tag{19}$$

and we obtain the value of the width parameter x by minimizing Equation (19):

$$x = \sqrt{\frac{\Gamma}{2N^2}}\exp(x/2) \ . \tag{20}$$

In the weakly coupled regime $\Gamma << 2N^2$, the minimum expectation value occurs at a value $x << 1$, in which case $\exp(x/2) \approx 1$ and Equation (20) yields the width parameter $x \approx (\Gamma/2)^{1/2}/N$. In other words, the weakly coupled case yields a very small phase uncertainty,

$$\Delta\alpha = (2x)^{1/2} \approx (2\Gamma)^{1/4}/N^{1/2} << 1 \ , \tag{21}$$

and therefore corresponds to the superfluid limit. Most superconducting Josephson junctions find themselves in this limit. Because the number uncertainty is small, $\Delta\alpha \sim N^{-1/2}$, the classical (or mean-field) approximation successfully describes these Josephson experiments. The uncertainty in particle number $\Delta m \approx N^{1/2}/2\Gamma^{1/4}$ appears Poissonian ($\Delta N \approx N^{1/2}$) if we write it in terms of the coupling constant. The small phase uncertainty in this regime is not easily measured with appreciable accuracy.

In contrast, as the value of J is lowered by an increasing barrier height, the coupling constant $\Gamma = [UN/2J]$ increases accordingly, and the phase uncertainty can increase to give a measurable decrease in fringe sharpness. In the Yale experiment, the increase in the potential barrier was sufficient to allow the system to approach the strong coupling regime $\Gamma \sim N^2$ or $U/J \sim N$. In that regime, the value of x at the minimum energy can become of order 1, in which case we cannot replace $\exp(x/2)$ by 1. Instead, we must solve Equation (20). By the time the potential barrier has been increased to the point that, say, $U/J = (4/e)N$, the variation becomes $\Delta m = (1/2)^{1/2}$, and the uncertainty in atomic population of each well has dwindled to less than one particle. At that point, $\Delta m << N^{1/2}$, and we say that the number distribution has become sub-Poissonian. The phase-difference uncertainty, $\Delta\alpha$, also becomes of order unity. Well before that point, say, when U/J is increased to only 10 percent of N, or $U/J = 0.1N$, the uncertainty in phase difference in the double-well BEC has grown to half a radian. In the multiple-well BEC system, the uncertainty in phase between nonadjacent wells under that same condition, $U/J = 0.1N$, is greater, and the loss of fringe sharpness in the interference of 12 BECs is quite noticeable.

From Superfluid to Mott Insulator

By illustrating number squeezing, the Yale group demonstrated that BEC technology can engineer and observe quantum fluctuations of an almost macroscopic system. On the other hand, technical constraints in the Yale experiment limited the height to which the potential barrier could be raised and, hence, the range to which the number uncertainty could be squeezed. These limitations prevented the Yale group from venturing further into the strong-coupling regime. By pushing this frontier, Hänsch's group in Munich were able to observe a very interesting phase transition (Figures 11 and 12). As they squeezed the number uncertainty below a value of order 1—it would be $(1/2)^{1/2}$

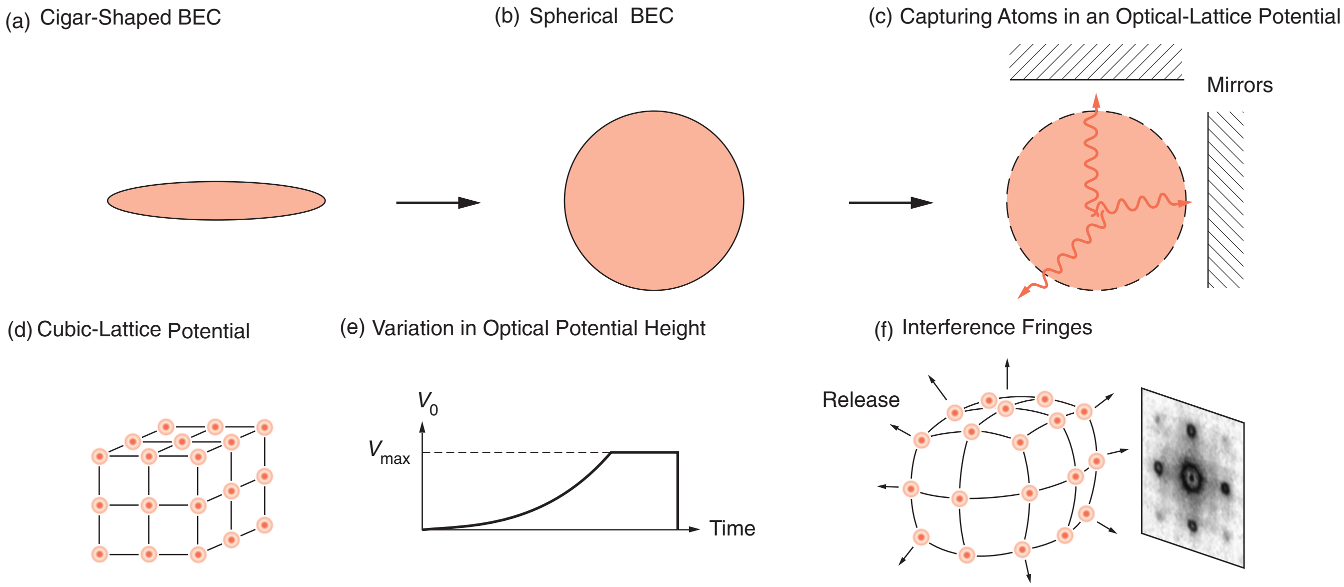
(a) Cigar-Shaped BEC
(b) Spherical BEC
(c) Capturing Atoms in an Optical-Lattice Potential
Mirrors
(d) Cubic-Lattice Potential
(e) Variation in Optical Potential Height
V_0
V_{max}
Time
(f) Interference Fringes
Release

Figure 11. Demonstration of a Transition from a Superfluid to a Mott Insulator

In the BEC experiment that demonstrated the quantum phase transition from a superfluid to a Mott insulator (Greiner 2002), the experimentalists started with a cigar-shaped BEC (a) that was relaxed to a spherical BEC (b), distributing the atoms more evenly over a larger region of space. By shining in three laser beams, detuned from each other and reflected by mirrors, the researchers created a standing-wave pattern that captures the atoms in an optical-lattice potential (c): $V(x, y, z) = V_0[\sin^2(kx) + \sin^2(ky) + \sin^2(kz)]$, where k denotes the wave vector of the laser light. Gradual increases in laser intensity and, hence, in the potential V_0 trap one to three atoms per potential minimum, or well. These minima form a cubic lattice (d). In (e) we show a typical variation of the optical potential height V_0: The potential height is ramped up "slowly" for 80 ms and kept constant for another 20 ms; then the trapping potential is suddenly switched off, at which point the atoms in the BEC begin to expand. In (f), the atomic wave functions from different wells begin to overlap, and the atomic density imaged in a plane shows interference fringes.

in the approximations introduced previously—the ground state abruptly changes to a Fock or number state with $\Delta m = 0$. This phenomenon is a true phase transition: Many-body properties change suddenly as $U/J \sim N$. In addition to the change in number statistics, the system's conductivity alters discontinuously as the system takes on a number state. In the number state, a finite amount of energy is required to transfer atoms between wells; therefore, the transition to the number state abruptly alters the nature of the many-body system from a conductor with superfluid properties to a Mott insulator. This many-body phenomenon is an example of a transition driven by the competition between different interactions, rather than by the competition between order and disorder, which is responsible for usual phase transitions. If they involve quantum fluctuations, the former transitions (which occur at zero temperature) are called quantum phase transitions.

If we can trust the tunneling energy in Equation (16) and the interaction energy in Equation (17) to accurately describe the many-body physics, then the BEC in an optical lattice is an example of a Bose-Hubbard system. The theory of the phase transition from superfluid to Mott insulator in such systems has been explored in great detail. Experimentally, this transition was first observed in an array of superconducting Josephson junctions. In BEC physics, the experimental study of the transition by the Munich group demonstrated, once again, that the BEC technology gives an unusual degree of control.

Figure 12. Absorption Images Showing a Transition to a Mott Insulator in a BEC

The BEC absorption images (a)–(h) were recorded in a particular plane 15 ms after the trapping potential was switched off. The images reflect different maximum values V_{max} of V_0. In units of the recoil energy, $E_{recoil} = \hbar^2k^2/2m$ (capital R was used for "right"), V_{max} took on the values (a) 0, (b) $3E_{recoil}$, (c) $7E_{recoil}$, (d) $10E_{recoil}$, (e) $13E_{recoil}$, (f) $14E_{recoil}$, (g) $16E_{recoil}$, and (h) $20E_{recoil}$. Notice that the interference pattern completely disappears between $V_0 = 14E_{recoil}$ and $V_0 = 16E_{recoil}$, in agreement with the prediction that all phase information would be lost as the potential barriers increase and the atoms become localized in their respective potential wells.

(This figure was reproduced courtesy of *Nature*.)

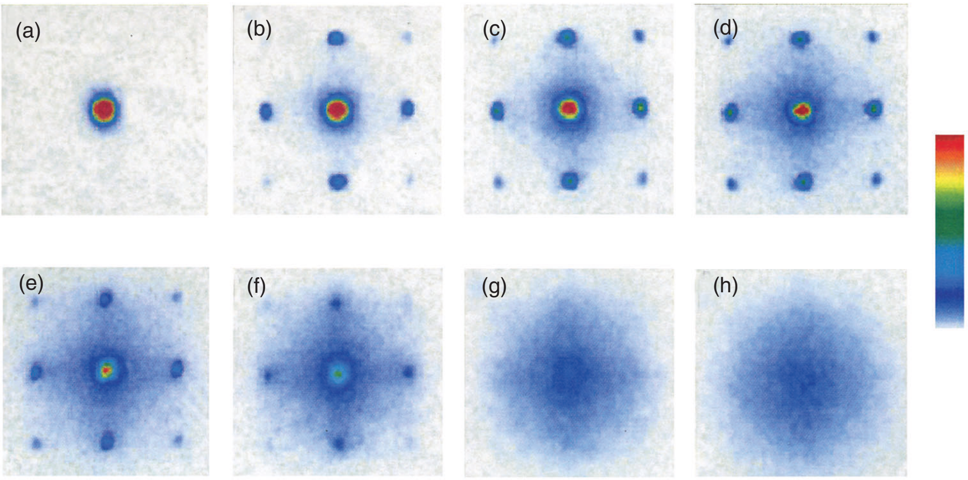

Before describing the experiment, we demonstrate the transition in the double-well BEC system. From Equation (19), we see that, in the limit of large phase uncertainty ($x \to \infty$), the expectation value of the number-phase energy—Equation (18)—vanishes. Consequently, when the local minimum of $\langle H \rangle$ takes on a positive value, the true minimum of the system is found at $x \to \infty$, as we illustrate in Figure 13. As the value of U/JN increases, the value of the local minimum increases until, at $U/J = (4/e)N$, corresponding to $\Delta\alpha = 2^{1/2}$ and $\Delta m = 2^{-1/2}$, the value of the minimum turns positive and the real minimum is at $x \to \infty$, corresponding to $\Delta\alpha \to \infty$ and $\Delta m = 0$.

A significant difference between the Yale and Munich experiments lies in the number of potential wells created in the optical lattices. The trapping potential in Hänsch's group was a three-dimensional lattice of 65 sites in each dimension. The large number of lattice sites in the Munich experiment, 65^3 in total, is significant because it allows experimentalists to trap one to three particles per site while still having a sufficiently large total number of atoms to image the interference of the expanding BECs. By lowering the value of N (N was about 10,000 in the Yale experiment), the Munich group could reach the critical ratio of $U/J \sim N$ with a much smaller increase in barrier height. Actually, the simple (α, m) treatment of the number-phase dynamics in the double-well BEC becomes invalid for small values of N and a different description, such as the one presented by Subir Sachdev (1999), is necessary. Nevertheless, the (α, m) description still captures the main features and predicts the correct order of magnitude of the transition point. Hänsch's group also probed the excitations of this system and found evidence for the insulator property of a finite energy (or "gap") necessary to allow transferring atoms between wells. Again, these experiments illustrate the unprecedented tools offered by the cold-atom technology.

Los Alamos Achievements and Future Work

With regard to fundamental physics, we have shown that BEC experiments can probe beyond the confines of traditional condensed-matter Josephson-junction studies by exploring and engineering quantum fluctuations. We have also emphasized that atom-laser systems with superfluid properties (long-range phase coherence in an equilibrium as opposed to a nonequilibrium state) may offer unique opportunities for application. For instance, the BECs may find novel uses in atom interferometry and sensing applications.

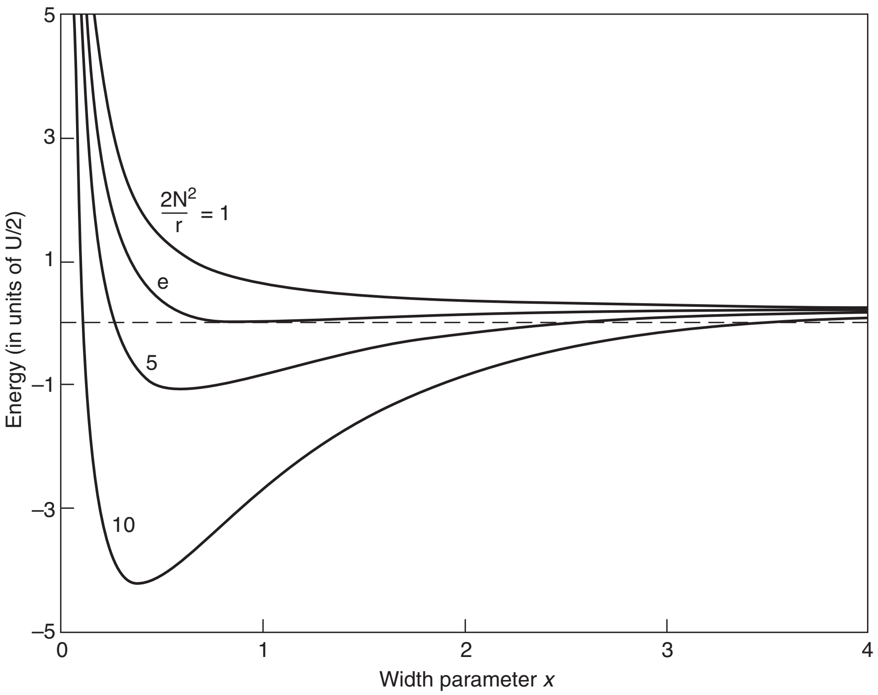

Figure 13. Number-Phase Energy for Different Interaction Parameters

The expectation values of the number-phase energy of Equation (18) are calculated with a Gaussian trial wave function $\psi(\alpha) \propto \exp(-\alpha^2/[4x])$ and are plotted as a function of the width parameter x, which is related to the phase uncertainty $\Delta\alpha$ as $x = (\Delta\alpha)^2/2$. The different curves show $H(x)$ for different values of the interaction parameter $(2N^2/\Gamma)$. From bottom to top, those values are 10, 5, e, and 1. For $(2N^2/\Gamma) < e$, the local minimum is also the global minimum, whereas for $(2N^2/\Gamma) > e$, the global minimum occurs in the limit $x \to \infty$, corresponding to a complete uncertainty of the phase.

Hopefully, this historical perspective has also conveyed a sense of the flexibility of the cold-atom-trap technology. That flexibility has led to a host of other avenues being pursued or contemplated: for instance, schemes to alter and control the nature and strength of the interparticle interactions, already successful searches for superfluid properties in BECs, demonstrations of nonlinear physics effects in superfluids (vortices, solitons, and "quantum shocks"), the study of mutually coherent BECs, the demonstration of atom-molecule BECs, and the prospect of using BECs for the study of quantum measurement theory.

Los Alamos National Laboratory has been active in exploring several of the above aspects. The following are some of the Los Alamos contributions and ongoing projects that we are aware of. On the experimental side, David Vieira and Xinxin Zhao are working toward the use of an atomic BEC to cool down fermion atoms (see the article "Experiments with Cold Trapped Atoms" on page 168). On the theoretical side, Peter Milonni was the first to point out that external electric fields can be used to control the interparticle interactions in the atom-trap systems (Milonni 1996). Diego Dalvit, Jacek Dziarmaga, and Wojciech Zurek resolved the puzzle of the lifetime of the proposed Schrödinger cat states in BEC-like systems, and they have proposed schemes to reduce the effect of decoherence and increase the cat's longevity (see the article "Schrödinger Cats in Atom-Trap BECs" on page 166). In collaboration with experimentalist Roberto Onofrio (visiting from the University of Padua, Italy), they continue to explore the possible use of BECs in studies of measurement theory. Lee Collins has explored the vortex and soliton dynamics in BECs, working closely with the experimental group of Bill Philips at the National Institute of Standards and Technology (Denschlag et al. 2000). Gennady Berman and Augusto Smerzi are exploring the possibility of using BECs to study the boundary between quantum and classical behavior (Berman et al. 2002), as well as using BECs in optical lattices for interferometry purposes (Dziarmaga et al. 2002).

Since 1996, I have also been active in BEC research. The prediction for the phase separation of BECs under specific conditions (Timmermans 1998) has been confirmed by experiments in Ketterle's group at MIT. This same group also confirmed our predictions for the reduction of scattering slow distinguishable particles by the BEC (Timmermans and Côté 1998) and for the excitation rate of phonon modes in two-photon scattering experiments. Recently, the group of Wieman at JILA found evidence for a prediction by Timmermans et al. (1999) of the formation of an atom-molecule BEC in the Feshbach resonance scheme that was initially proposed to alter the effective interparticle interactions. In a recent collaboration with Milonni of Los Alamos and Arthur Kerman of MIT, I pointed out the possibility of creating a fermion-boson superfluid (Timmermans et al. 2001) by bringing an ultracold fermion gas mixture near a Feshbach resonance. Finally, I discovered the heating mechanism that explains the temperature limit encountered by efforts in fermion atom cooling and provides the main obstacle for the current experiments to reach fermion superfluidity in atom traps (Timmermans 2001a).

The variety of approaches and cold-atom research topics at Los Alamos is yet another measure of the richness of this field. By now, numerous experiments have established the cold-atom trap as a new kind of laboratory in which to study interesting fundamental issues in low-temperature, many-body, and nonlinear physics. The unusual control and the variety of experimental knobs also hint at the possibility of practical applications. Hopefully, Los Alamos can continue to play a significant role in the ongoing cold-atom physics adventure. ■

Further Reading

Anderson, P. W. 1986. Measurement in Quantum Theory and the Problem of Complex Systems. In *The Lesson of Quantum Theory*. p. 23. Edited by J. D. Boer, E. Dal, and O. Ulfbeck. Amsterdam: Elsevier.

Anderson, M. H., J. R. Ensher, M. R. Matthews, C. E. Wieman, and E. A. Cornell. 1995. Observation of Bose-Einstein Condensation in a Dilute Atomic Vapor. *Science* **269**: 198.

Andrews, M. R., C. G. Townsend, H. J. Miesner, D. S. Durfee, D. M. Kurn, and W. Ketterle. 1997. Observation of Interference between Two Bose Condensates. *Science* **275**: 637.

Berman, G. P., A. Smerzi, and A. R. Bishop. 2002. Quantum Instability of a Bose-Einstein Condensate with Attractive Interaction. *Phys. Rev. Lett.* **88**: 120402.

Bradley, C. C., C. A. Sackett, J. J. Tollett, and R. G. Hulet. 1995. Evidence of Bose-Einstein Condensation in an Atomic Gas with Attractive Interactions. *Phys. Rev. Lett.* **75**: 1687.

Davis, K. B., M.-O. Mewes, M. R. Andrews, N. J. van Druten, D. S. Durfee, D. M. Kurn, and W. Ketterle. 1995. Bose-Einstein Condensation in a Gas of Sodium Atoms. *Phys. Rev. Lett.* **75**: 3969.

Denschlag, J., J. E. Simsarian, D. L. Feder, C. W. Clark, L. A. Collins, and J. Cubizolles. 2000. Generating Solitons by Phase Engineering of a Bose-Einstein Condensate. *Science* **287**: 97.

Dziarmaga, J., A. Smerzi, W. H. Zurek, and A. R. Bishop. 2002. Dynamics of Quantum Phase Transition in an Array of Josephson Junctions. *Phys. Rev. Lett.* **88**: 7001.

Greiner, M., O. Mandel, T. Esslinger, T. W. Hänsch. and I. Bloch. 2002. Quantum Phase Transition from a Superfluid to a Mott Insulator in a Gas of Ultracold Atoms. *Nature* **415**: 39.

Huang, K. 1987. *Statistical Mechanics*. Second Edition. New York: John Wiley & Sons.

London, F. 1938. The λ-Phenomenon of Liquid Helium and the Bose-Einstein Degeneracy. *Nature* **141**: 643.

Madison, K. W., F. Chevy, W. Wohlleben, and J. Dalibard. 2000. Vortex Formation in a Stirred Bose-Einstein Condensate. *Phys. Rev. Lett.* **84**: 806.

Milonni, P. W., and A. Smith. 1996. van der Waals Dispersion Forces in Electromagnetic Fields. *Phys. Rev. A* **53**: 3484.

Orzel, C., A. K. Tuchman, M. L. Fenselau, M. Yasuda, and M. A. Kasevitch. 2001. Squeezed States in a Bose-Einstein Condensate. *Science* **291**: 2386.

Packard, R. E. 1998. The Role of the Josephson-Anderson Equation in Superfluid Helium. *Rev. Mod. Phys.* **70**: 641.

Pais, A. 1979. Einstein and the Quantum Theory. *Rev. Mod. Phys.* **51**: 861.

Penrose, O. 1951. On the Quantum Mechanics of Helium II. *Philos. Mag.* **42**: 1373.

Penrose, O., and L. Onsager. 1956. Bose-Einstein Condensation and Liquid Helium. *Phys. Rev.* **104**: 576.

Pfleegor, R. L., and L. Mandel. 1967. Interference of Independent Photon Beams. *Phys. Rev.* **159**: 1084.

Rayfield, G. W., and F. Reif. 1964. Quantized Vortex Rings in Superfluid Helium. *Phys. Rev.* **136**: A1194.

Sachdev, S. 1999. Chapter 10 in *Quantum Phase Transitions*. Cambridge: Cambridge University Press.

Timmermans, E. 1998. Phase Separation of Bose-Einstein Condensates. *Phys. Rev. Lett.* **81**: 5718.

———. 2001a. Degenerate Fermion Gas Heating by Hole Creation. *Phys. Rev. Lett.* **87**: 240403.

———. 2001b. Superfluids and Superfluid Mixtures in Atom Traps. *Contemp. Phys.* **42**: 1.

Timmermans, E., and R. Côté. 1998. Superfluidity in Sympathetic Cooling with Atomic Bose-Einstein Condensates. *Phys. Rev. Lett.* **80**: 3419.

Timmermans, E., K. Furuya, P. W. Milonni, and A. K. Kerman. 2001. Prospect of Creating a Composite Fermi-Bose Superfluid. *Phys. Lett. A* **285**: 228.

Timmermans, E., P. Tommasini, R. Côté, M. Hussein, and A. Kerman. 1999. Rarified Liquid Properties of Hybrid Atomic-Molecular Bose-Einstein Condensates. *Phys. Rev. Lett.* **83** (14): 2691.

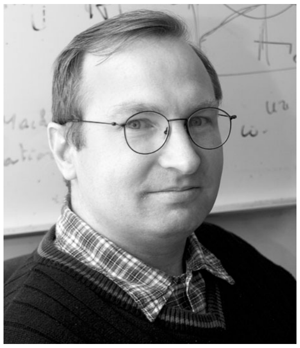

Eddy Timmermans is currently an Oppenheimer postdoctoral fellow at Los Alamos National Laboratory and will soon join the permanent staff of the Theoretical Division. He received his Ph.D. in condensed-matter theory from Rice University (1995) and then became a fellow at the Harvard-Smithsonian Institute for Theoretical Atomic and Molecular Physics (1995–1998). There, he became interested in the physics of ultracold-atom systems. His most recent research has explored issues of and prospects for fermion pairing in ultracold-atom systems.

Schrödinger Cats

in Atom-Trap BECs

Diego A. R. Dalvit and Jacek Dziarmaga

Microscopic quantum superpositions are routinely observed in experiment. Macroscopic quantum superpositions, on the other hand, are still encountered rarely despite nearly a century of experimentation with quantum mechanics. Fast decoherence of macroscopic states is to blame for this state of affairs (see the articles "Decoherence and the Transition from Quantum to Classical" and "The Emergence of Classical Dynamics in a Quantum World" on pages 86 and 110). And yet, the past few years have witnessed several breakthroughs in the macroscopic regime. To name a few, superposition states of macroscopic numbers of photons and atoms have been produced in cavity quantum electrodynamics, matter-wave interference in fullerene carbon-60 has been observed, and controlled decoherence due to engineered environments has been measured in ion traps. Recently, the first detection of a macroscopic Schrödinger cat state in a radio-frequency (rf) superconducting quantum interference device, or SQUID (a superposition of clockwise and counterclockwise superconducting current flow), was reported. All these achievements tempt one to try similar investigations of basic quantum mechanics in the rapidly growing field of Bose-Einstein condensates (BECs).

In the article "Atom-Trap BECs" on page 136, Eddy Timmermans describes the possible emergence of nonclassical behavior by number squeezing in a dilute BEC. For a double-well configuration, the ground state of the condensate is determined by the competition between the tunneling energy $E_{\rm tun} = -\gamma E_{\rm J} \cos\alpha$, which favors states with a well-defined relative phase between the wells, and the interaction energy $E_{\rm int} = (U/2)(N^2 + m^2)$, which favors number states in each well. When the interaction energy is repulsive ($U > 0$), the ground state corresponds to $m = 0$, and $\alpha = 0$, that is, an equal number of particles in the two wells with zero relative phase. However, for attractive interactions ($U < 0$), the ground state is very different: It corresponds to a superposition of states with $m = +N$ and $m = -N$, namely,

$$|\Psi\rangle = \frac{1}{\sqrt{2}} \begin{bmatrix} |N_{\rm L} = N, N_{\rm R} = 0\rangle \\ +|N_{\rm L} = 0, N_{\rm R} = N\rangle \end{bmatrix} \quad .$$

This state is clearly nonclassical, all N bosons being simultaneously in the left well and in the right well. It corresponds to a macroscopic quantum superposition—a BEC Schrödinger cat—analogous to Schrödinger's Gedanken experiment of a cat in the weird superposition of being both dead and alive.

Various schemes have been proposed for building macroscopic superpositions in BECs. For example, for a BEC in a double-well potential with an attractive interparticle interaction, one can in principle create the cat state through adiabatically cooling down the BEC until the ground state is reached. Another option is to confine bosons that have an attractive interaction between atoms in two hyperfine levels (A and B) in a single potential well. Initially, all atoms in the BEC are in a given hyperfine state, say A, and then a resonant rf pulse is applied to the system to transfer (or rotate) the atoms part of the way between state A and B. The duration of the pulse is much shorter than the self-dynamics of the condensate. At this stage, each atom is in a superposition of levels A and B, and the corresponding many-body quantum state is a product of single-particle superpositions of A and B, that is, it is still a microscopic superposition. However, as this initial state evolves under the nonlinear Hamiltonian that governs the BEC with its attractive interparticle interactions, it reaches a macroscopic superposition in which all atoms are simultaneously in level A and level B, $|\Psi\rangle = (1/\sqrt{2})[|N_A, 0_B\rangle + |0_A, N_B\rangle]$. An even weirder superposition state has been proposed, namely, a coherent superposition of atomic and molecular BECs. It must be stressed that, to date, no experiment has been carried out that attempts to produce any of the aforementioned superposition states.

The condensate is an open quantum system, that is, it is in contact with an environment mainly composed of noncondensed thermal particles. The interaction between that environment and the BEC cat state may cause the loss of coherence between the components of the quantum superposition. If the decoherence time were very small, then the existence of these states in a BEC would be merely of academic interest because there would be no chance of observing them in the laboratory. Therefore, it is important to understand how the thermal cloud affects the longevity of BEC cat states. In principle, a single noncondensed atom colliding with the condensed superposition state and taking away information

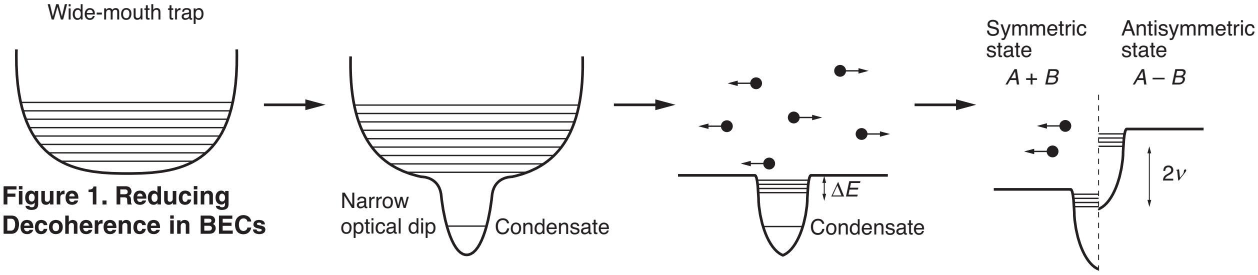

Figure 1. Reducing Decoherence in BECs

about the phase of the state is enough to kill the atomic coherence. Estimated decoherence times for the proposed BEC cat states are inversely proportional to the product of N_E (the number of noncondensed bosons) and N^2 (where N is the number of bosons in the condensate), that is, $t_{\text{dec}} \approx 10^5$ seconds/$(N_E N^2)$. For N_E from 10^0 to 10^4 and N from 10^1 to 10^7, the decoherence times can range over 16 orders of magnitude, from 1000 seconds down to 10^{-13} second. Given that macroscopic cats require big values of N, it is clear that, for the sake of the cat's longevity, one must go beyond the standard trap settings.

In what follows, we concentrate on a BEC cat formed with two hyperfine states A and B. We show that, by using a combination of trap engineering and what we call "symmetrization" of the environment, as illustrated in Figure 1, one can decrease decoherence rates. First, one prepares the condensate inside a wide magnetic trap and then superimposes a narrow optical dip. The parameters of the traps are chosen such that only a single bound state lies within the dip. The bosons are forced to adiabatically condense into that state. Then the magnetic trap is opened, and most of the noncondensed atoms are allowed to disperse away. The aim of this procedure is to eliminate as much of the thermal cloud as possible. However, atoms occupying bound states within an energy band of width ΔE at the mouth of the dip may not disperse away, but the occupation numbers of those states before the opening of the wide trap may subsist. Those atoms would stay in contact with the condensate and continue to monitor its quantum state and thereby destroy any chance of the condensate to form a superposition. Even if such a truncated environment is relatively harmless, there are ways to better protect the condensate from it.

What we call "symmetrization" of the environmental states can further reduce the decoherence rate. To produce symmetrization, one applies an rf pulse with frequency ν that induces coherent transitions between states A and B of all atoms, both condensed and thermal ones. On the one hand, the state of the condensate is still a macroscopic superposition but slightly different from the original one $(1/\sqrt{2})[|N_A,0_B\rangle + |0_A,N_B\rangle]$ because the rf pulse produces a small increase in the variance of the number of atoms in each well. On the other hand, the single-particle energy spectrum of the noncondensed bosons is modified. It is now composed of two energy-level ladders shifted with respect to each other by 2ν. One ladder is shifted down, corresponding to states symmetric under the interchange $A \leftrightarrow B$, and the other is shifted upwards, corresponding to states antisymmetric under such interchange. When the energy bandwidth near the mouth of the dip $\Delta E << 2\nu$, only symmetric environmental states are occupied. A collision between atoms occupying those states and the condensate does not affect the phase coherence of the latter because both states and the interaction Hamiltonian are symmetric under the interchange $A \leftrightarrow B$. In other words, a symmetric environmental state affects the components $(|N_A,0_B\rangle$ and $|0_A,N_B\rangle)$ of the BEC cat in exactly the same way, multiplying them by a common phase factor, which obviously does not affect the phase coherence of the condensate. When the relation $\Delta E << 2\nu$ does not hold, some atoms will occupy antisymmetric environmental states and can cause decoherence. However, since that occupation number can be controlled by the intensity of the laser field inducing the coherent transitions between the states A and B, the method of symmetrization can still significantly extend the longevity of the BEC cat. ■

Diego A. R. Dalvit graduated from the Universidad de Buenos Aires, Argentina, in 1993 with a Master's degree in physics and received a Ph.D. in physics from the same university in 1998. Diego has been working as a postdoctoral researcher in the Theoretical Division at Los Alamos since 1999. He is the author of a book on problems in statistical mechanics. He is currently working on the dynamical Casimir effect, decoherence theory, and Bose-Einstein condensation.

Jacek Dziarmaga graduated from the Jagellonian University in Kraków, Poland, in 1994 with a Master's degree in physics and received a Ph.D. in physics from the Jagellonian University in 1995. He has been working as a Senior Research Assistant in the Department of Mathematical Sciences at the University of Durham in the United Kingdom, then as a Director-funded postdoctoral fellow at Los Alamos National Laboratory, and now he is an adjunct professor at the Jagellonian University in Kraków. He is currently working on phase transitions, decoherence theory, and Bose-Einstein condensates.

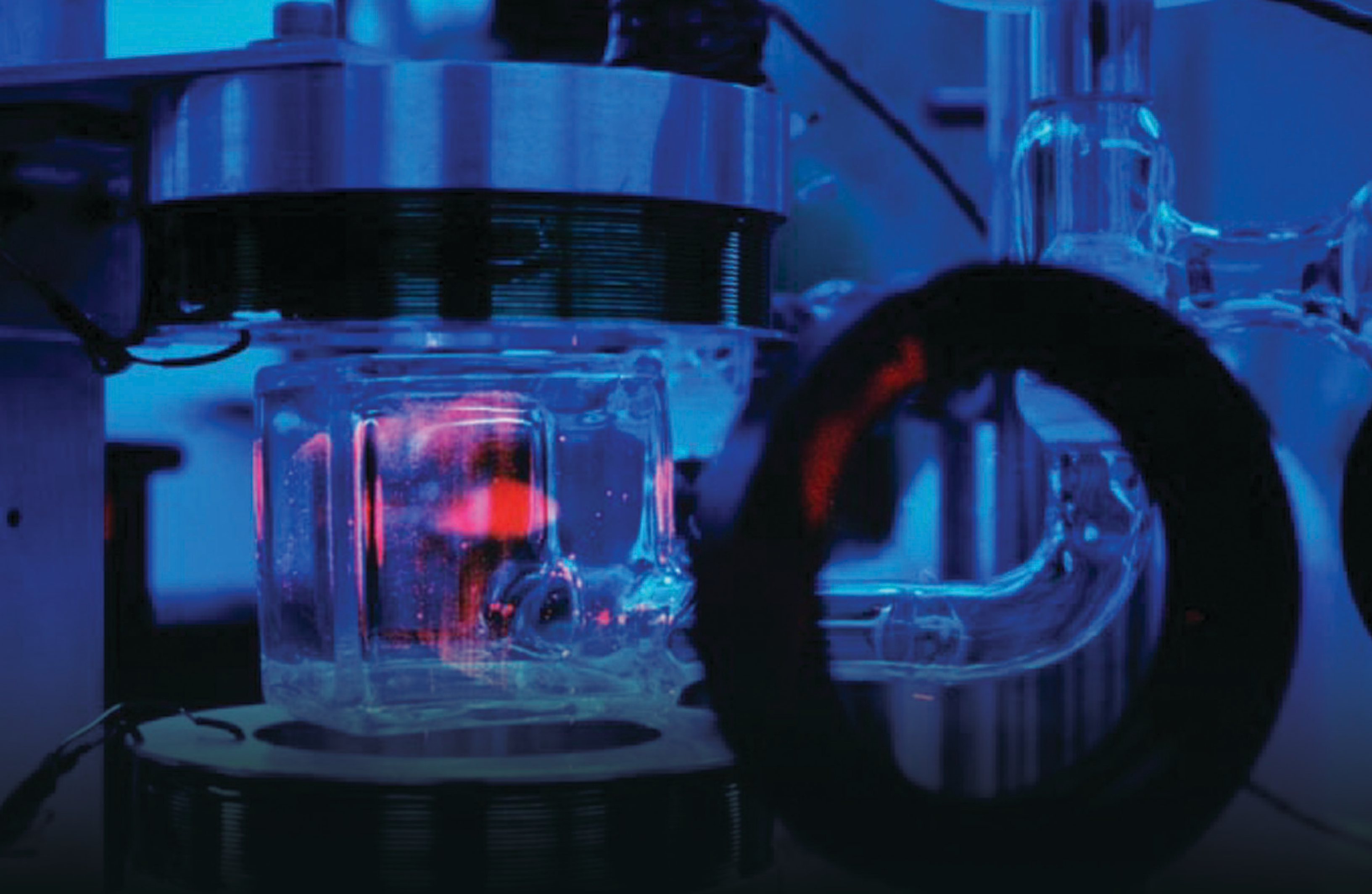

Experiments on Cold Trapped Atoms

David J. Vieira and Xinxin Zhao

Those of us who have fun trying to take a picture of a fast moving object usually end up with a blurry, imprecise image. Something similar happens when we try to make precision measurements on moving atoms—the movement results in a broadening of intrinsic atomic line widths, and we end up with an imprecise understanding of the subtle atomic processes that produce those lines. Likewise, detailed studies of the interactions between atoms are hindered by motion because energetic collisions between atoms tend to complicate the system's dynamics and/or mask quantum effects. In general, if we are interested in making precision measurements on the individual or collective properties of free atoms, we have to slow the atoms down.

Kinetic theory tells us that the velocity of an atom in a gas is proportional to the square root of the temperature and inversely proportional to the atom's mass. The atoms and small molecules in the air that we breathe, for example, move about at astonishingly high velocities at room temperature—about 4000 kilometers per hour. Because the velocity varies only as the square root of the temperature, one must make a gas very cold in order to substantially slow the atoms. At one degree above absolute zero (1 kelvin), atoms still cruise at a few hundred kilometers per hour. Only when temperatures of a few millionths of a kelvin (a few microkelvins) are reached do free atoms move slowly enough that we can make high-precision spectroscopic measurements.

Several methods have been developed that use laser light to cool gases to the microkelvin temperature range. The cold atoms can then be contained within different kinds of atom traps, where they can be studied very accurately or cooled to even lower temperatures. The traps also allow us to concentrate a large number of atoms into a small volume. As the number density increases, the individual atoms begin to "feel" one another, and we can begin to study the transition from individual to collective behavior. With certain "bosonic" atomic species, cooling and trapping techniques enable us to create one of the most fascinating—and fragile—states of matter in the universe, the Bose-Einstein condensate (BEC). See the box "The Bose-Einstein Condensate" on the next page and the article "Atom-Trap BECs" on page 136.

The atom-trapping team at Los Alamos National Laboratory has adapted cooling and trapping techniques to radioactive atoms for both fundamental and applied research. We are in the process of making sensitive measurements of parity violation in nuclear beta-decay as a means to test the Standard Model of electroweak interactions. We are also trying to cool a dilute gas of fermions to a degenerate quantum state (degenerate Fermi matter), where the density is comparable to that found in a BEC. Aside from displaying interesting quantum mechanical properties, ultracold fermions could undergo a phase transition to a superfluid state, and our apparatus should give us unprecedented control in forming and studying this system. Finally, we are using atom-trapping technology to trap and measure isotopic ratios of selected nuclear species at ultrasensitive levels for nonproliferation treaty verification and environmental studies.

Cooling and Trapping Techniques

Laser cooling of neutral atoms was proposed in 1975 by Theodore Hänsch and Arthur Schawlow, both then at Stanford University. The basic idea was to use the momentum transfer between a photon and an atom to slow the atom down.

When an atom absorbs a photon, its momentum is reduced by an amount $p = h\nu/c$ where h is Planck's constant, ν is the frequency of the light, and c is the speed of light. When the atom emits a photon, it gains momentum of the same magnitude (a so-called momentum kick). If, as in laser light, all the absorbed photons come from the same direction, then after many photon scattering events (rapid absorption and emission events), the net change in momentum will be unequal, since the fluorescent photons are emitted in all directions and the sum of the momentum kicks averages to zero. The result is a net loss of momentum.[1]

To get laser cooling to work, we use the Doppler effect to ensure that only those atoms moving into the laser beam will absorb photons. The Doppler effect relates the intrinsic frequency of a source to the frequency "sensed" by an observer moving relative to the source. The pitch of a siren, for example, sounds higher when we move quickly toward it (or it moves quickly toward us) and lower when we move rapidly away. Similarly, an atom "sees" the frequency of a photon increase when the atom moves toward the photon. Thus, if we tune a laser to have a slightly lower frequency than the resonance frequency of an atom's

---

[1] The change in momentum due to light scattering means that the atom feels a pressure, which can be quite large (up to 10,000 times larger than the force of gravity). Radiation pressure provides a very effective means of moving atoms around.

(a) Momentum Transfer

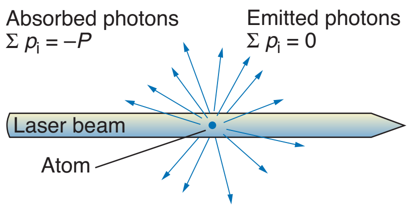

(b) Atom Moving into Laser Beam

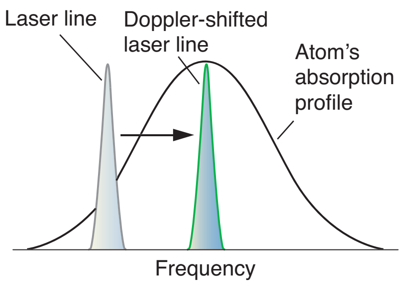

(c) Atom Moving with Laser Beam

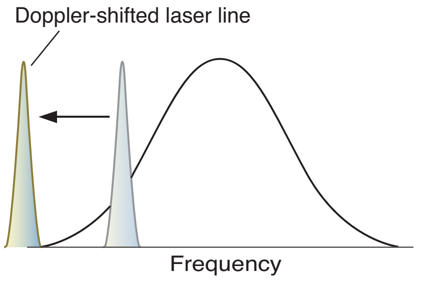

Figure 1. Laser Cooling
(a) An atom illuminated by laser light will absorb and reemit (scatter) many photons. (b) If the laser frequency is tuned below the atomic resonance line (red detuned), then an atom moving against the laser beam "sees" a laser frequency that is Doppler-shifted closer to the absorption maximum. It absorbs the low-energy laser photons. The atom then emits a higher-energy photon at the resonance frequency of its transition line. The atom loses energy with each absorption/emission event and begins to cool. (c) An atom moving in the same direction as the laser beam "sees" the detuned laser frequency Doppler-shifted still farther away from its absorption maximum. The atom absorbs few photons and is not cooled.

The Bose-Einstein Condensate

Elementary particles—and collections of particles such as nuclei and atoms—are either fermions (and have half integer spin) or bosons (and have integer spin). In the mid-1920s Albert Einstein, building on the work of Satyendra Nath Bose, predicted that, at exceptionally low energies, an ensemble of massive bosons should undergo a transition into a state that is described by a single, coherent wave function. This coherent state—now called the Bose-Einstein condensate (BEC)—would be as different from ordinary matter as laser light is from sunlight.

Physicists believed that a dilute gas of bosons could form a BEC, but the conditions needed to produce one are extreme. In order to become coherent, or establish a common phase relationship amongst themselves, the atomic wave functions must overlap significantly with one another. The spatial extent of the atomic wave function is given by its de Broglie wavelength λ, and it can be shown that the BEC will form if the atom density, expressed as the number of atoms in a λ-sided cube, exceeds 2.6. Both the de Broglie wavelength and the density of a gas depend on temperature, and one can calculate how cold it must be to achieve the critical density in a cold boson gas. The answer is, on the order of a few hundred billionths of a kelvin.

Certainly, one problem in creating a BEC was to find a gaseous system that would not coalesce into a solid as the temperature plunged toward absolute zero. The solution was to use certain alkali atoms (atoms from group I of the Periodic Table). When spin-polarized, these atoms have a weak repulsive force between them that would ensure that the system remained a gas. A BEC of rubidium-87 atoms was finally created and observed in 1995 by Carl Weiman's and Eric Cornell's group at the University of Colorado / JILA (Joint Institute for Laboratory Astrophysics). Four months later, Wolfgang Ketterle's group from the Massachusetts Institute of Technology created a BEC from sodium-23 atoms. Since that time, a BEC has been observed in several other bosonic alkali species, such as hydrogen-1 and lithium-7. All the efforts involved cooling the atoms (except hydrogen atoms) to less than a millikelvin in what is called a magneto-optical trap (MOT), reducing the temperature by another order of magnitude by laser cooling, and then transferring the atoms to a magnetic trap. There, the atoms are cooled by a technique known as evaporative cooling to less than 200 nanokelvins to create a BEC.

absorption line (detuning), only atoms that happen to be moving against the beam see the frequency of the photon Doppler-shift into resonance (see Figure 1). These atoms lose momentum and are slowed down (cooled). Atoms moving in the same direction as the detuned laser beam are Doppler-shifted farther away from resonance. They do not readily absorb photons and are consequently unaffected.

To cool the atoms in three dimensions requires six intersecting laser beams—one pointing in each of the six directions ±x, ±y, and ±z. Then any atom that emerges from the intersection region will be moving against a properly tuned laser beam and will be cooled.

The force experienced by an atom during laser cooling is velocity dependent; that is, its magnitude

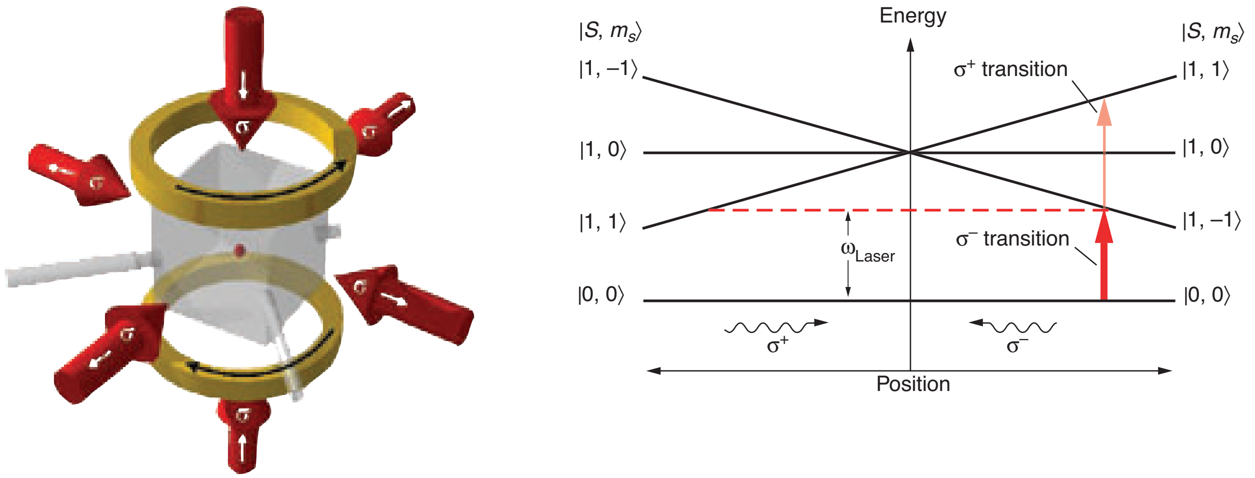

Figure 2. The Magneto-optical Trap (MOT)

(a) The MOT consists of six circularly polarized laser beams that intersect at the zero point of a magnetic field (produced by the set of anti-Helmholtz magnetic coils). The tube projecting from the left is used to bring atoms into the evacuated glass cell located between the coils. (b) This schematic energy diagram indicates why trapping occurs. The σ^- polarized light induces a transition from the ground state $|S, m_s\rangle = |0, 0\rangle$ to the $|1, -1\rangle$ excited state, whereas the σ^+ polarized light will induce a transition from $|0, 0\rangle$ to $|1, +1\rangle$. The atom's magnetic substates are Zeeman-split by the magnetic field. As the atom drifts away from the center of the MOT, say, to the right of the diagram, an atomic transition to the $m_s = -1$ substate shifts onto resonance with the σ^- polarized laser and starts to preferentially absorb these photons over the σ^+ polarized laser coming from the opposite direction. The resulting laser-induced pressure "pushes" the atom back toward the center. The result is the same if the atom moves out in any direction from the center of the trap.

[Part (b) of the figure was adapted from *Phys. Rev. Lett.* 59 (1987), p. 2631, with permission from the authors.]

depends on the atom's velocity as it moves toward the laser beam. (The three-dimensional laser cooling is often called an optical molasses because velocity-dependent forces are viscous forces and the atom behaves as if it were entrained in a viscous liquid. The term optical molasses was coined by Steven Chu of Stanford University.) Velocity dependence means that the cooling rate decreases as the atom slows down. When the velocity gained by the atom as it emits a photon (the atom recoil) equals the loss of velocity due to the scattering process, the cooling ceases altogether. The minimum velocity of the atom at the "recoil limit" translates into a minimum temperature.[2] For sodium atoms, the recoil limit is 2.4 microkelvins and for somewhat heavier cesium atoms it is about 0.2 microkelvin.

The Magneto-optical Trap (MOT). Although optical molasses cools atoms down to very low temperatures, the atoms can diffuse out of the laser region through random Brownian motion. The MOT was invented to prevent this loss and to confine the atoms. The idea behind the MOT is to combine the optical molasses with an external magnetic field and thereby create a spatially dependent force that acts only on atoms that wander from the trap's center. The MOT was fully developed in David Pritchard's laboratory at MIT in 1987. Because of its relative ease of construction and great utility, it is perhaps the most commonly used atom trap.

For this trap, three pairs of counterpropagating, circularly polarized laser beams (σ^+ and σ^- polarizations) establish an optical molasses within a vacuum chamber, as seen in Figure 2. Outside the molasses region are two magnetic coils. The current in each coil runs in opposite directions (anti-Helmholtz configuration) and creates a "quadrupole" magnetic field, which has zero field value at the center between the two coils. The field gradient increases linearly as one moves out from the center in any direction.

The trap works because an atom's magnetic substates (*m*-states) have different energies in a magnetic field (the Zeeman effect), and due to the field gradient, the *m*-state energy increases (or decreases) as the atom moves out from the center of the MOT. With reference to Figure 2(b), an atom in the trap will be illuminated with both σ^+ and σ^- circularly polarized laser light. Suppose the atom moves away from the center of the trap, say, in the $(+z)$-direction, so that it moves into the σ^- laser beam, but in the same direction as the σ^+ laser beam. Both lasers are tuned slightly below the $|S = 0\rangle \rightarrow |S = 1\rangle$ resonance frequency. At some distance from the MOT center, the drifting atom will come into resonance with the incoming σ^- radiation (but not with the σ^+ light). Similar to the way in which it absorbs light in an optical molasses, the atom will begin to absorb more of the σ^- light and will feel a pressure that pushes it back toward the center of the MOT. Likewise, an atom moving in the ($-z$)-direction (or $\pm x$, $\pm y$ directions) will preferentially absorb photons from the inward-directed laser beam and will be pushed back toward the trap's center. Because the magnetic field is symmetric, the atom becomes trapped in three dimensions.

---

[2] There are also subrecoil laser-cooling mechanisms that can cool atoms below the recoil limit.

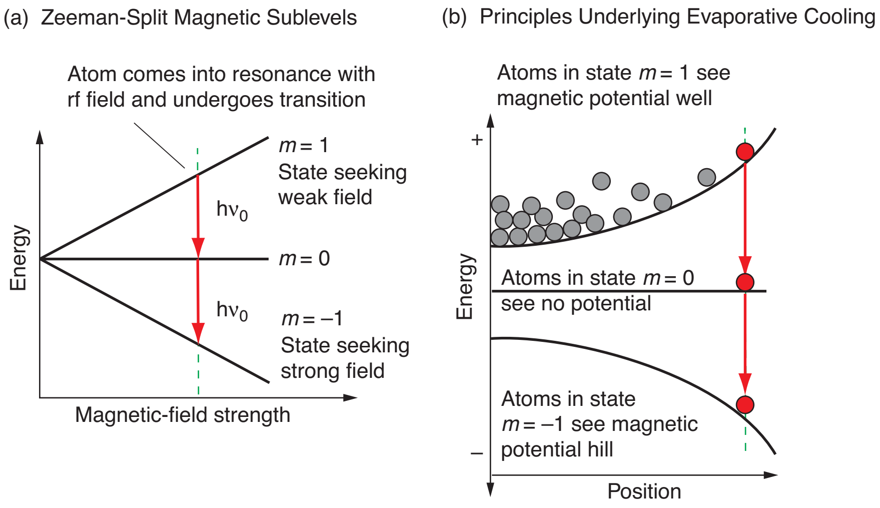
(a) Zeeman-Split Magnetic Sublevels

(b) Principles Underlying Evaporative Cooling

Figure 3. Evaporative Cooling

(a) The figure shows the magnetic sublevels of an atom as a function of magnetic-field strength. An atom in the state |*m* = 1⟩ is diamagnetic because it has lower energy in weaker magnetic fields. (Therefore the atom is attracted to regions of weaker field.) Conversely, atoms in the state |*m* = –1⟩ are paramagnetic (that is, attracted to regions of higher magnetic fields). If the atom is illuminated by an rf radiation of frequency ν_0, then at some magnetic-field value, the atom can come into resonance with the radiation and undergo a transition from |*m* = 1⟩ to |*m* = 0⟩, and then from |*m* = 0⟩ to |*m* = –1⟩. The diamagnetic atom converts into a paramagnetic one. (b) The evaporative cooling technique removes the most energetic atoms from a magnetic trap. Atoms in the trap are polarized in the |*m* = 1⟩ (diamagnetic) state and are trapped by the quadrupole magnetic field. The most energetic atoms make the greatest excursions from the trap center and move into regions of higher magnetic field. These atoms come into resonance with an rf field and are converted to paramagnetic atoms, which are ejected from the trap. (They move to high-field regions outside the trapping volume.) After reequilibration through atomic collisions, the remaining atoms reach a lower temperature.

Magnetic Traps, Evaporative Cooling, and the Time-Orbiting Potential (TOP). While the MOT requires lasers to trap the atoms, magnetic fields alone can create a trapping potential. A pure magnetic trap makes use of the fact that atoms will experience a magnetic dipole force in a magnetic field gradient $\mathbf{F} = -\boldsymbol{\mu}\cdot\nabla\mathbf{B}$, where $\boldsymbol{\mu}$ is the atom's magnetic moment and $\nabla\mathbf{B}$ is the magnetic field gradient. If the atom is polarized into the $|m = 1\rangle$ substate, the force will be toward lower magnetic-field values. The atom is diamagnetic and can be trapped by a simple magnetic quadrupole field, which has a zero magnetic-field value at the center.

Magnetic traps are easy to construct, but they have fairly weak trapping potentials (about 1000 times weaker than found in a MOT). They can only trap atoms that are already very cold, with thermal energies equivalent to 1 millikelvin or less. Once inside a magnetic trap, the atoms can be cooled to the limits of laser cooling. To reach the temperatures needed to create a BEC, however, we need another cooling technique, namely, evaporative cooling.

Temperature is a measure of the average kinetic energy of a system, and in a gas, the energy is distributed amongst the atoms according to a Maxwell-Boltzmann distribution. This means that some atoms always have greater than the average energy. We can efficiently cool a gas by removing the highest-energy atoms. After the remaining gas re-equilibrates, it will have a lower average energy. The common name for this process is evaporation. A liquid that is evaporating (say a steaming cup of coffee) cools down because the most energetic atoms leave (and form the rising steam).

To further cool the already cold atoms, we actively eject the most energetic particles. We stated that the magnetic trap holds onto diamagnetic atoms. But atoms polarized in the $|m = -1\rangle$ substate are paramagnetic and will be attracted to the higher magnetic fields outside the trapping region. A radio-frequency (rf) field can be used to induce transitions between magnetic substates and convert an atom that is diamagnetic to one that is paramagnetic, at which point it is ejected from the trap. The frequency of the rf field is chosen such that only atoms with enough energy to move to the edge of the magnetic potential well come into resonance with the rf field (see Figure 3). After ejecting the most energetic atoms from the trap, the rf frequency is readjusted so that once again the most energetic atoms of the now

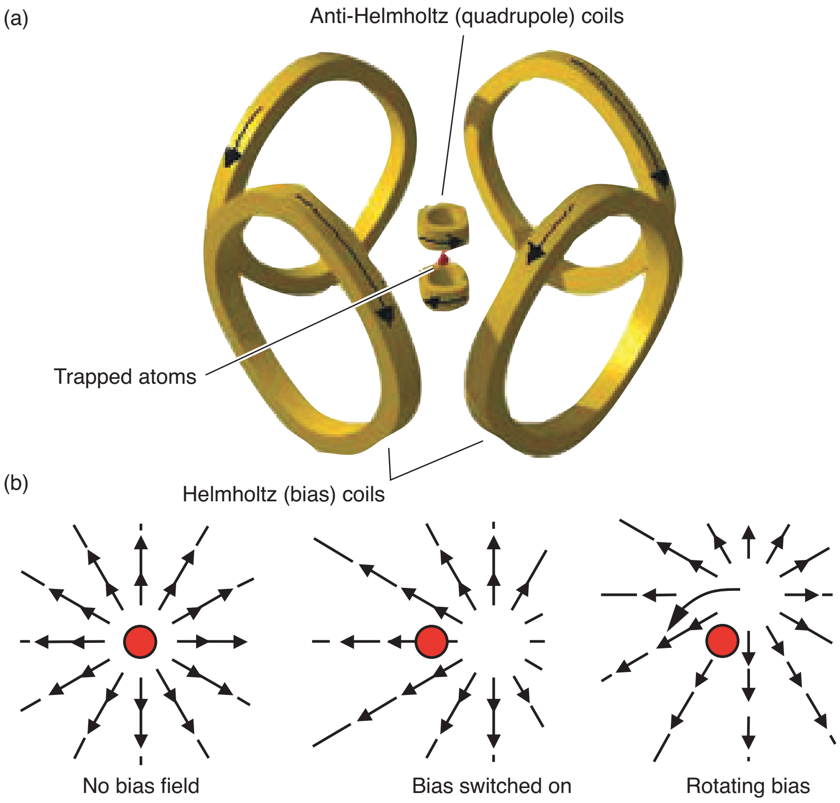

Figure 4. The Time-Orbiting-Potential (TOP) Trap
(a) The TOP trap is a magnetic trap that combines two magnetic fields: a quadrupole field (produced by the central, anti-Helmholtz coils) and a bias field (produced by the outer Helmholtz coils). (b) With the addition of the bias field, the potential minimum of the magnetic trap shifts off-axis. By adjusting the current in the Helmholtz coils, we make the bias field rotate around the trap axis and produce a time-averaged total field with a positive field strength at the center of the trap. As long as the bias field rotates fast enough, the atoms will remain polarized and stay trapped.

colder gas are ejected. In this way, it is possible to successively skim off the hottest atoms and thereby evaporatively cool the atoms.

One problem with this cooling scheme is that the quadrupole field has zero field strength at the center of the trap. Consequently, the magnetic substates are not Zeeman-split at the center of the trap, so polarized atoms can undergo spontaneous spin-flip transitions to the $|m = 0\rangle$ or $|m = -1\rangle$ substates in this region. The loss rate by this mechanism increases as the atoms become colder, making it difficult to achieve the critical BEC conditions of high atom density and low temperature.

The TOP trap, developed by Eric Cornell and collaborators, eliminates this problem by adding an off-axis bias field to the static quadrupole field. As seen in Figure 4, the minimum of the total magnetic field becomes shifted away from the trap center. By rotating the bias field, the time-averaged total field still retains its basic quadrupole configuration, but now it has positive field strength at the center, so the atoms remain polarized. The bias field must rotate faster than the atoms can respond,[3] but this objective is easily achieved. The TOP trap allows the density of atoms in the trap to increase sufficiently as the atoms are evaporatively cooled to reach the conditions for a BEC.

Atom Trapping at Los Alamos

Having cold, almost frozen, atoms at our disposal allows us to perform high-precision experiments to test quantum theories of ultracold ensembles of atoms and the nature of fundamental forces. Our system at Los Alamos, illustrated in Figure 5, combines several of the techniques and traps discussed above. A high-efficiency MOT that is coupled to an off-line mass separator is used for trapping radioactive atoms. Once the atoms are trapped, they can be counted with high sensitivity (via fluorescence detection) or transferred to another trap, where various experiments can be performed. At present, we are pursuing a number of research initiatives.

Parity Violation in Nuclear Beta-Decay. Spatial reflection symmetry, otherwise known as parity conservation, maintains that the fundamental processes of nature should be the same under a spatial inversion of all vector parameters. Parity conservation was verified in electromagnetic and strong interactions, but as a startled physics community discovered in the

---

[3] The atoms oscillate within the harmonic potential well of the TOP trap. If the atoms are to experience the time-averaged magnetic field, the bias field must rotate faster than the atoms' period of oscillation.

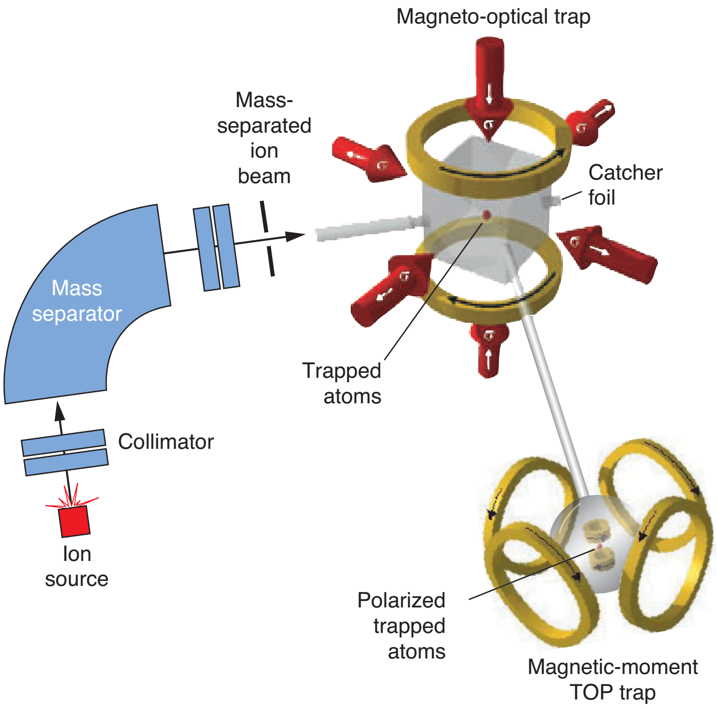

Figure 5. Los Alamos Setup to Trap Radioactive Atoms

Cooling atoms to ultralow temperatures must be done in stages, with several traps and laser configurations. In the setup at Los Alamos, energetic, radioactive atoms from an ion source are implanted into a thin metal foil that sits within an evacuated glass cell, around which are the MOT field coils. Heating the foil releases the atoms into the cell where they are trapped in the MOT and cooled to about 100 μK. The MOT is turned off, and a laser pushes the atomic cloud into the evacuated chamber of a second MOT, where the atoms are recaptured. The magnetic field of this second MOT is turned off and an optical molasses is established by detuning the frequency of the laser further to the red (that is, to lower frequency). Within a few milliseconds, the atoms have cooled to approximately 20 μK, and then they are optically pumped into a diamagnetic substate with a polarized laser beam. The optical pumping beam is then turned off, and the magnetic field is quickly ramped up in a TOP configuration. We plan to use evaporative cooling to bring the atoms to a final temperature of a few hundred nanokelvins.

1950s, not in the weak interaction. Despite the astounding progress that has been made in understanding fundamental forces over the past fifty years, the origin of parity violation in the weak interaction remains a mystery of modern science. We hope to make a very precise measurement of the degree of parity violation in rubidium-82 as a means to test current theories.

One way the weak interaction manifests itself is through a type of nuclear beta-decay, whereby a proton in a parent nucleus decays to a neutron, a positron (also known as a beta particle) and an electron neutrino. A daughter nucleus with a different atomic number is created in the process. For example, in rubidium-82 decay,

$$^{82}\text{Rb} \longrightarrow {}^{82}\text{Kr} + e^+ + \nu \ .$$

For the initial and final states of interest, this decay involves pure Gamov-Teller transitions that proceed solely through the axial-vector (parity-violating) component of the weak interaction and is predicted by the Standard Model to be maximally parity violating. If the rubidium-82 nucleus is polarized by a magnetic field, then parity violation would manifest itself as an asymmetry in the angular distribution of the emitted positrons relative to the nuclear spin direction. For the primary beta-decay branch (in which the rubidium-82 nucleus decays to the 0^+ ground state of krypton-82), the positron is emitted in the direction of the nuclear spin. (In a secondary, less probable decay branch, the positron comes out in a direction opposite to that of the nuclear spin.)

We have recently demonstrated the trapping of polarized, radioactive rubidium-82 atoms. A radiochemically separated sample of strontium-82 ($t_{1/2}$ = 25 days) is loaded into the ion source of a mass separator. The strontium-82 decays by electron capture to rubidium-82 ($t_{1/2}$ = 76 seconds). The rubidium-82 atoms are thermally ionized, electrostatically extracted, mass separated, and implanted into a zirconium catcher foil located inside a glass cell that sits at the center of a high-efficiency MOT. Heating the foil releases the atoms as a dilute vapor into the glass cell where they are trapped and cooled.

The atoms are rapidly transferred to a second chamber by resonant laser light “pushing” on them. In the second chamber, the atoms are retrapped in a second MOT, further cooled, optically pumped into a specific magnetic substate, and loaded into a TOP magnetic trap. Being in a stretched state, the nuclear spin is aligned with the overall spin of the atom. Consequently, the nuclei are polarized and aligned with the local field. In the center of the TOP, the strongest field is in the direction of the bias field, so the direction of the nuclear spin rotates with the bias field.

By keeping track of the varying currents in the bias coils of the TOP trap, we can reconstruct the direction of the bias field, hence the spin alignment, as a function of time. We can

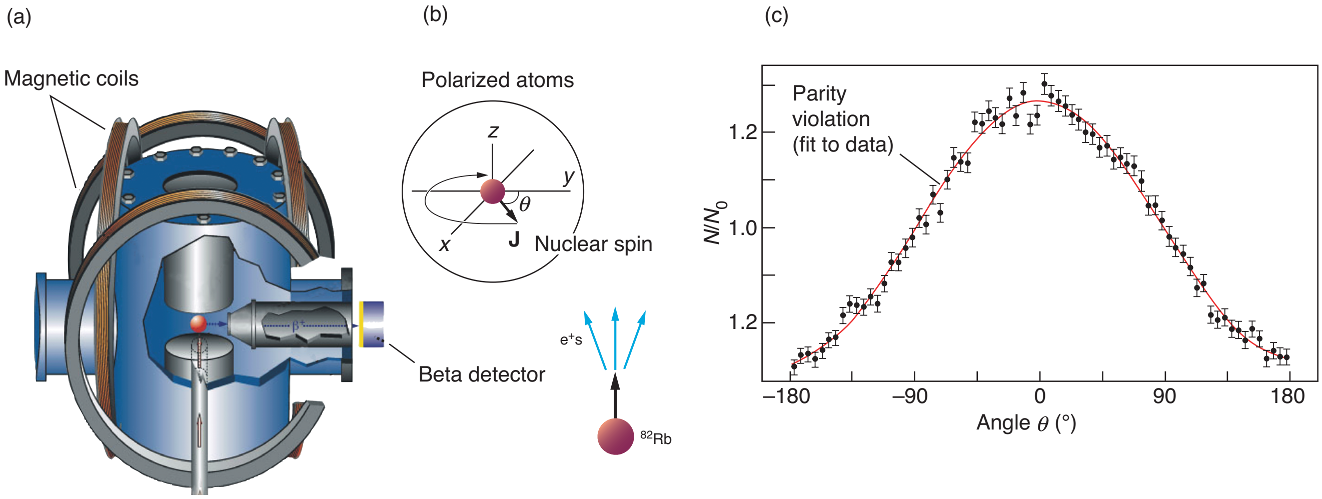

Figure 6. Measurement of Parity Violation

(a) The figure shows the TOP trap of our experimental system. The nuclei of the trapped rubidium-82 atoms are spin polarized and always point in the direction of the TOP's rotating bias field. By monitoring the currents that produce the bias field at any given time, we can reconstruct the magnetic-field orientation; hence, we know the nuclear spin direction. A plastic scintillator is used to detect the emitted positrons. When a positron is detected, we reconstruct the nuclear-spin direction and can determine the angle θ between it and the positron emission direction. (b) Because parity is not conserved in the weak interaction, the spin-polarized rubidium-82 nuclei will decay by preferentially emitting positrons in the direction of the nuclear spin. (c) This plot of rubidium-82 beta-decay data, accumulated over a period of 6 hours for positrons with energies above 800 keV, shows the parity violating the angular distribution of the positrons. The red line is a cosine fit to the distribution.

then correlate each beta event with the orientation of the nuclear spin, and record the angle between the beta and the nuclear-spin direction. In Figure 6, we show our initial proof-of-principle results, which indicate that parity is, as expected, violated in the beta decay of polarized rubidium-82 atoms. This is the first time that the entire angle-dependent parity-violating amplitude has been measured.

We are in the process of making a 1 percent measurement of this correlation in order to place stringent limits on the maximal parity-violating nature of the weak interaction. We hope to extend that measurement to 0.1 percent and to search for new physics beyond the Standard Model.[4]

Ultracold Atoms / Quantum Degenerate Matter. The ability to trap and cool different isotopes enables us to explore mixed fermionic and bosonic systems. In particular, we are working to produce a BEC of bosonic rubidium-87 and overlap it with a magnetically trapped cloud of radioactive, fermionic rubidium-84. In doing so, we hope to sympathetically cool, via atomic collisions, the rubidium-84 atoms down to the Fermi degenerate regime (approximately 10 to 100 nanokelvins). We want to study the fermion-fermion and fermion-boson collision dynamics at temperatures approaching absolute zero.

Recent calculations show that rubidium-84 is a good fermionic candidate for sympathetic cooling because it has a large and positive scattering length with rubidium-87. Calculations also indicate, however, that, in the presence of a relatively low magnetic field (**B** ~ 100 gauss), a Feshbach resonance should be present in rubidium-84. This resonance allows two colliding atoms to form a temporary molecule before separating, and by adjusting the magnetic-field value, we can fine-tune the energy at which the resonance occurs. In doing so, we can control the collision cross section and effectively "tune" the temperature at which a phase transition to a superfluid state will occur.

The radioactive rubidium-84 atoms ($t_{1/2}$ = 33 days) for our experiments are produced by proton spallation reactions on a molybdenum target at the Los Alamos Neutron Scattering Center. The rubidium is chemically extracted from the molybdenum and loaded into the ion source of a mass separator. The rubidium-84 is implanted and captured in the MOT in a similar procedure to that described in the previous section.

As an initial step toward achieving our goal, we have demonstrated the trapping of rubidium-84. Figure 7(a) shows the time-dependent trapping signal from roughly one million trapped rubidium-84 atoms. At high atom densities, the losses from the trap are dominated by laser-light-assisted collisions between trapped atoms.

By overlapping a cloud of 3×10^5 cold atoms of rubidium-84 with a large cloud of 7×10^7 atoms of stable rubidium-87, we have also been able to set a limit on the inelastic-collision

---

[4] This work is done in collaboration with scientists from the Chemistry and Physics Divisions at Los Alamos. See Crane et al. 2001.

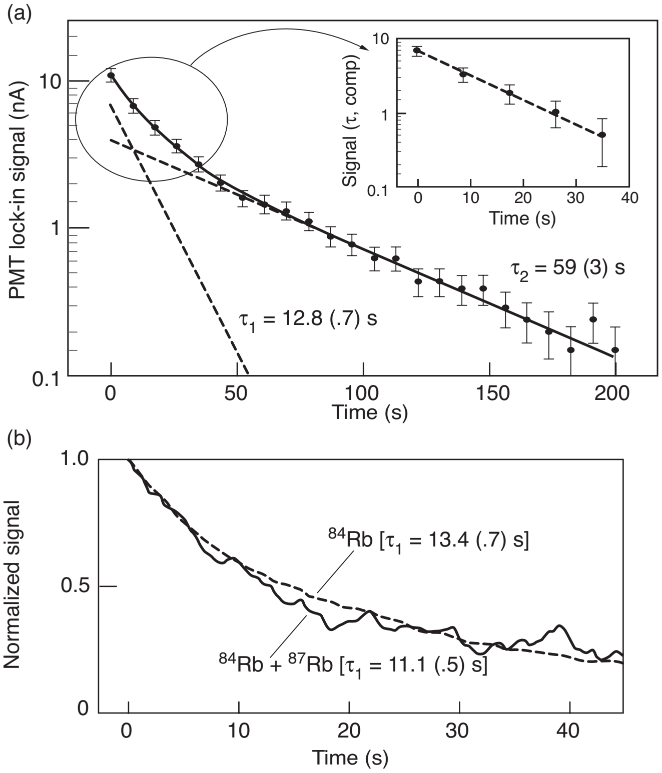

Figure 7. Lifetimes in a MOT: Rubidium-84 with and without an Overlapping Cloud of Rubidium-87

How long will a MOT confine half a million rubidium-84 atoms? The data indicates that the answer depends on the atomic density. (a) At high densities (short times), light-assisted collisions between trapped atoms dominate. These give rise to the short-lived component (t_1 = 12.8 s) of the overall trap lifetime. (The inset shows a fit to the short-lived component.) As the number of trapped atoms decreases and the density goes down, light-assisted losses become negligible and only collisional losses between the cold atoms and the hot background gas remain. The collisional losses correspond to the long-lived component, with a lifetime of about 59 seconds. (b) Introducing rubidium-87 atoms into the trap could lead to collisions between the rubidium isotopes and an enhanced loss rate. This figure shows the normalized lifetime in the trap of rubidium-84 atoms with and without an overlapping cloud of rubidium-87 atoms (solid line and dashed line, respectively). The additional loss rate is sufficiently small that it does not present a problem for the sympathetic cooling experiment discussed in the text.

loss rate of the atoms from the trap, which could affect the rubidium-84 trapping lifetime—see Figure 7(b). Fortunately, this loss rate was found to be sufficiently small and did not present a problem for the sympathetic cooling experiment. We are currently optimizing the evaporative-cooling process to achieve quantum degeneracy for the bosonic rubidium-87 and to study its cooling of rubidium-84 (Crane et al. 2000).

Ultrasensitive Detection. As a result of fallout from atmospheric nuclear tests, the two radioactive isotopes cesium-135 ($t_{1/2} = 2.3 \times 10^6$ years) and cesium-137 ($t_{1/2} = 30$ years) are ubiquitous in the environment, at a relative abundance of roughly 1 part per billion with respect to stable cesium-133. (The fission product isotopes are man-made, that is, anthropogenic.) Cesium adsorbs strongly and rapidly to soil particles, and because the heavier isotope cesium-137 is relatively easy to detect through gamma-ray spectrometry, it has served as a chronometer and tracer in a diverse array of scientific endeavors, including studies of soil erosion and lake sedimentation.

The long radioactive lifetime of cesium-135, however, severely limits its detection by gamma-ray spectrometry. This is unfortunate, since a measurement of the cesium-137/cesium-135 isotope ratio would lead to a relatively unambiguous determination of a sample's age. Furthermore, that particular ratio is of interest for nonproliferation and treaty verification because the cesium-137/cesium-135 content of nuclear-fuel effluent can provide valuable information about nuclear-reactor operations.

Detecting both isotopes, especially from random environmental samples, requires that we have a highly sensitive, highly selective technique. Several advanced technologies, including resonant ionization mass spectrometry (RIMS), have been successfully applied to the problem, with the RIMS method achieving a detection limit of about 1×10^8 atoms, an estimated isotopic selectivity of about 10^{10}, and an overall efficiency (from source size to detectable sample size) of 2×10^{-6}.

We recognized that, when coupled to a mass separator, a MOT could do even better. Because the trapping potential of a MOT derives from a multiphoton, near-resonant absorption process, it is very species selective (atomic, isotopic, and isomeric) with respect to what it traps. The mass separator also has high isotopic selectivity, so a mass separator/MOT system affords a huge suppression of signals from unwanted species. A MOT "detector" should also have high sensitivity. Each trapped atom can scatter (rapidly absorb and emit) about 10^7 photons per second, so even small numbers of atoms can be detected.

We are the first group to have succeeded in trapping and detecting cesium-135 and cesium-137 in a MOT. A sample containing both isotopes was placed in the source of a mass separator, and each isotope was sequentially measured with a MOT. Trapped-atom numbers in the case of either isotope ranged from 10^4 to 10^7, as determined from the MOT fluorescence signal. Over this trapped-atom range, the MOT fluorescence signal was found to increase linearly with the number of atoms implanted into the foil with no sign of an isotopic dependence to within 4 percent.

Direct measurement of the cesium fluorescence signals should yield the cesium-137/cesium-135 ratio. In principle, our mass separator/MOT technique can make that determination to within 10 percent of uncertainty. Currently, the system has a detection limit of about 10^6 atoms, an isotopic selectivity of greater than 10^{12}, and an overall efficiency of 0.5 percent. As such, our work represents a significant advance in efficiency and isotopic selectivity among other methods applied to the detection of cesium radioisotopes (Di Rosa et al. 2002.). More important, our results demonstrate the advantages of applying atom-trapping techniques to the general problem of ultrasensitive detection.

Conclusions

Over the last decade, advances in the laser cooling and trapping of atoms have revolutionized the prospects of fundamental research and applied quantum-based projects. In atomic physics, scientists have gained unprecedented control over quantum ensembles, as witnessed by the creation and wide study of BECs today. But the new trapping and cooling techniques should not be viewed as simply a workhorse for quantum optics and atomic physics. Their use has spread to nuclear physics (as in our rubidium-82 experiment), biophysics, condensed-matter physics, quantum information, and environmental science (as demonstrated by our cesium experiments). The results of this “cross-fertilization” have in turn enriched the field of atomic physics. We believe the atom-trapping revolution is just beginning and that in the years to come there will be many new exciting interdisciplinary opportunities. ■

Further Reading

Crane, S. G., X. Zhao, W. Taylor, and D. J. Vieira. 2000. Trapping an Isotopic Mixture of Fermionic ^{84}Rb and Bosonic ^{87}Rb Atoms. *Phys. Rev. A* **62**: 011402(R).

Crane, S. G., S. J. Brice, A. Goldschmidt, R. Guckert, A. Hime, J.J Kitten, D. J. Vieira, and X. Zhao. 2001. Parity Violation Observed in the Beta Decay of Magnetically Trapped ^{82}Rb Atoms. *Phys. Rev. Let.* **86**: 2967.

Di Rosa, M. D., S. G. Crane, J. J. Kitten, W. A. Taylor, D. J. Vieira, X. Zhao. 2002. Magneto-Optical Trap and Mass Separator System for the Ultrasensitive Detection of ^{135}Cs and ^{137}Cs, Los Alamos National Laboratory document, LA-UR-02-3926. (Submitted to *Appl. Phys. B*).

Inguscio, M., S. Stringari, and C. E. Wieman, eds. 1999. *Bose-Einstein Condensation in Atomic Gases*, *Proceedings of the International School of Physics Enrico Fermi*. Amsterdam: IOS Press.

DeMarco, B. 2001. “Quantum Behavior of an Atomic Fermi Gas.” Ph.D. thesis, University of Colorado.

Metcalf, H. and R. van der Straten. 1994. Cooling and Trapping of Neutral Atoms. *Physics Reports* **244**: 203.

Greiner, M., O. Mandel, T. Esslinger, T. W. Hänsch, and I. Bloch. 2002. Quantum Phase Transition from a Superfluid to a Mott Insulator in a Gas of Ultracold Atoms. *Nature* **415**: 39.

Roberts, J. L. 2001. “Bose-Einstein Condensate with Tunable Atom-Atom Interactions: The First Experiments with ^{85}Rb BECs.” Ph.D. thesis, University of Colorado.

David J. Vieira is the nuclear chemistry team leader in the Isotope and Nuclear Chemistry Group at Los Alamos. He obtained his Ph.D. in nuclear chemistry from the University of California, Berkeley, in 1978, after which he came to Los Alamos. He has been an Adjunct Professor of Physics at the Utah State University since 1984 and was an Alexander von Humboldt Fellow (1990–91). David received a Los Alamos Distinguished Team Performance Award in 1993 for the development of a He-jet system at the Los Alamos Neutron Science Center (LANSCE) and the Fellows Prize (1998) for the development of the time-of-flight isochronous (TOFI) recoil spectrometer, the study of exotic nuclei using TOFI, and the trapping of radioactive atoms. David’s current interests include fundamental atomic and nuclear physics experiments involving trapped radioactive atoms, ultrasensitive detection, quantum information and control using trapped atoms, as well as fundamental symmetries, radioactive beams, and neutron-induced cross section measurements.

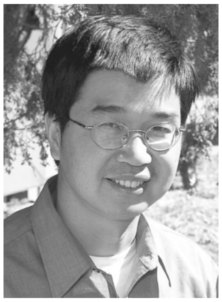

Xinxin Zhao received his Ph. D. from Rice University in 1993. After three years of postdoctoral research on single-ion high-precision spectroscopy at the University of Washington, he came to Los Alamos National Laboratory to work on laser cooling and trapping of radioactive atoms. In 1999, he became a technical staff member at the Laboratory. He has over ten years of experience in the areas of atom/ion trapping, laser cooling, and high-resolution laser spectroscopy. Together with David Vieira and collaborators, Xinxin has demonstrated the trapping of a record number of radioactive atoms and observed the first beta-decay asymmetry spectrum from magnetically trapped polarized atoms. His current research interests are application of laser cooling and trapping to fundamental and applied physics.

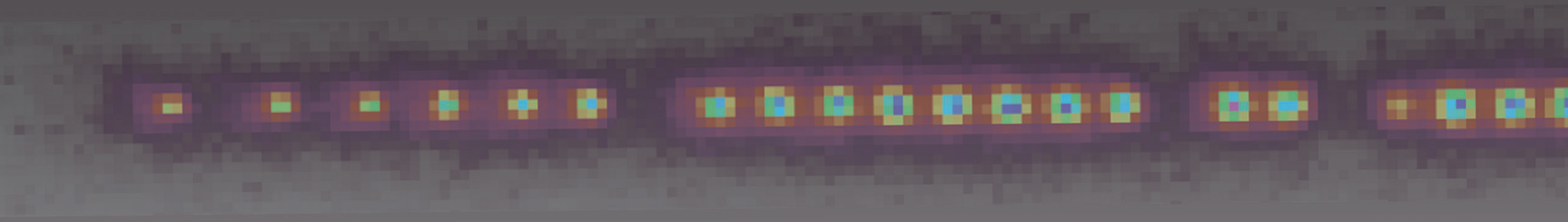

Quantum Information with Trapped Strontium Ions

Dana J. Berkeland

Something wonderful happens when small numbers of ions are trapped in a linear Paul (radiofrequency, or rf) trap and laser-cooled. The ions become nearly motionless and line up neatly along the trap axis—each confined to its own tiny space of about 100 micrometers or less in any direction. Because the ions are frozen in place, experimental physicists can continually observe them for up to months at a time and gain uncommon insight into the quantum realm.

For example, single ions exhibit quantum-mechanical effects that could never be observed in a large ensemble of ions or neutral atoms. A large field of study in quantum optics has in fact emerged with the development of ion traps (Thompson et al. 1997). In addition, the internal transitions of a nearly motionless ion are only slightly affected by Doppler shifts, and the ion can be superbly isolated from unwanted electric fields and noisy magnetic fields. This characteristic makes a trapped ion a useful testing ground for many physical theories that predict very small shifts of the atomic energy levels (Berkeland et al. 1999). Finally, a focused laser beam can interact first with one specific ion, then a different one—a capability that means we can control complicated interactions between states of a particular ion and between different ions. For this reason, the ion trap has shown considerable promise as the basis for a quantum computer. (See the article "Ion-Trap Quantum Computation" on page 264.)

In this article, I discuss some of our activities with trapped and laser-cooled ions. I focus on an experiment that provides a fundamental test of quantum-mechanical randomness but also mention a spectroscopy experiment that is a prerequisite to the development of a quantum logic gate. For background material, see the previously mentioned article, "Ion-Trap Quantum Computation," which discusses the operational principles of a linear Paul trap and laser cooling.

We conduct our experiments using singly ionized strontium atoms. Figure 1(a) is an illustration of our linear Paul trap (Berkeland 2002). Most of the trap has been created with off-the-shelf components and requires no precise or otherwise demanding machining to assemble. This feature is significant because it shows that ion trapping with linear traps can be an accessible technology for groups with limited resources.

Figure 1(b) shows the transitions we use in the strontium ion $^{88}\mathrm{Sr}^+$. We use the 422-nanometer transition to Doppler-cool the ions. We also collect the 422-nanometer fluorescent light from the decay of the $P_{1/2}$ state and focus it onto a detector to image the ions. Light at 1092 nanometers drives the $D_{3/2} \leftrightarrow P_{1/2}$ transition to prevent the atoms from pooling in the long-lived $D_{3/2}$ state, in which they would not scatter any 422-nanometer light. A 674-nanometer diode laser drives transitions between the $S_{1/2}$ ground state and the $D_{5/2}$ state, which lives an average of 0.35 seconds. This transition can be used to couple the $S_{1/2}$ and $D_{5/2}$ states of the ion with its motional states, any of which may be used as qubits in a quantum computer. The $S_{1/2} \leftrightarrow D_{5/2}$ transition is also driven

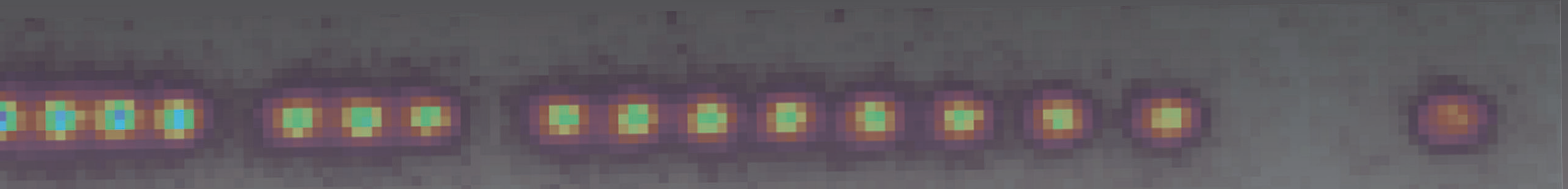

About forty strontium ions lined up in our linear Paul trap are visible because they scatter laser light. The apparent gaps are due to other ions that do not scatter the light.

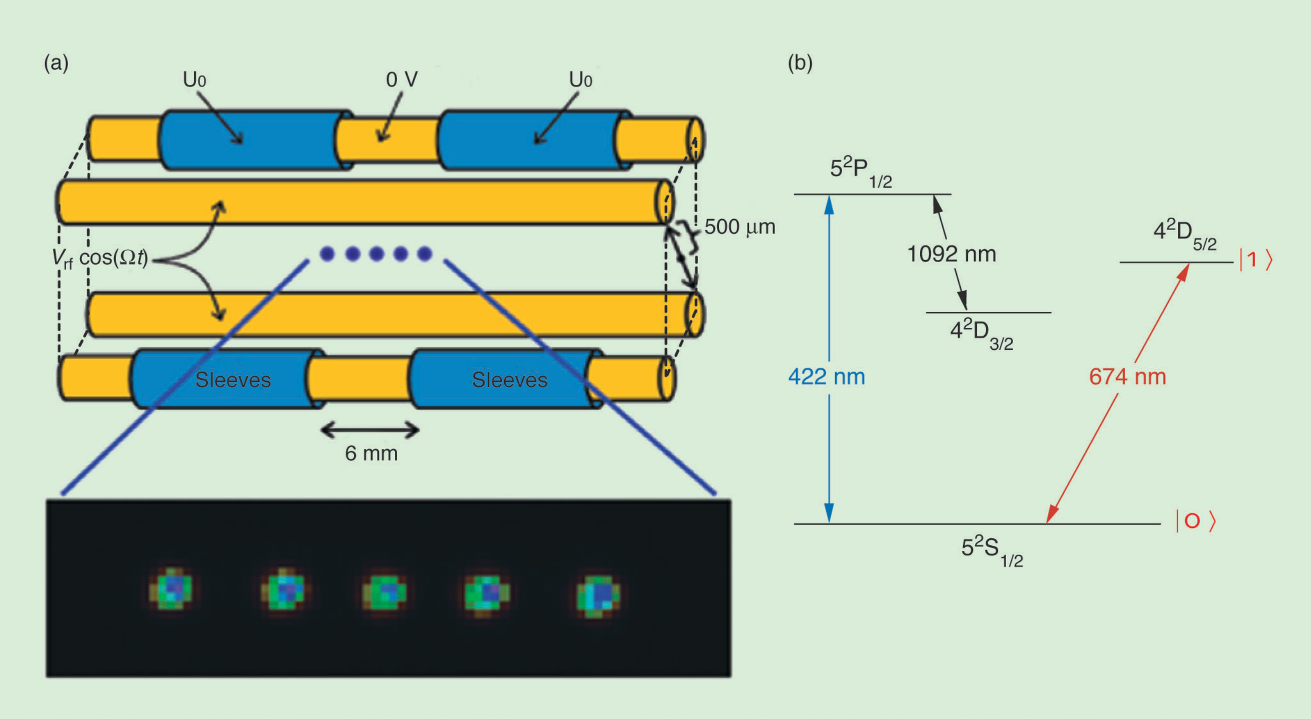

Figure 1. Strontium Ion Linear rf Paul Trap

(a) A schematic of the linear trap depicts five $^{88}Sr^+$ ions along its axis (not to scale). The ions in this trap are confined radially in a time-averaged potential that is created by applying 100 V at a frequency of 7 MHz to the two electrodes shown. The other two electrodes are held at a constant potential. The tubular electrodes (labeled "sleeves") are held at constant potentials up to 100 V, relative to the other electrodes, to stop the ions from leaking out of the ends of the trap. The picture of five Sr^+ ions was made by focusing the 422-nm light scattered from the ions onto an intensified charge-coupled-device camera. The ions are spaced about 20 μm from each other.

(b) The diagram shows the relevant energy levels of Sr^+ and the corresponding transitions (not to scale). We use 422-nm light from a frequency-doubled diode laser to Doppler-cool the ions and collect the scattered 422-nm light to detect the ions. A fiber laser generates 1092-nm light that keeps the ions from becoming stuck in the long-lived $D_{3/2}$ state. A very stable diode laser at 674 nm drives the narrow $S_{1/2} \leftrightarrow D_{5/2}$ transition.

so that quantum jumps can be observed in the experiments discussed next.

Quantum Randomness

In the article "A New Face for Cryptography" on page 68, the authors describe the quantum cryptography project at Los Alamos. Cryptography applications, whether classical or quantum, require strings of numbers (typically 1s and 0s) that are as random as possible. Generating random numbers, however, is not a trivial matter. In fact, the random number generators found in various computer programs are do not yield very random numbers because they are based on algebraic processes that are intrinsically deterministic.

It is generally accepted that producing strings of truly random numbers requires measuring the random outcome of a quantum-mechanical process. One example of a random

(a) An ion excited to the short-lived $4^2P_{1/2}$ state scatters millions of photons per second

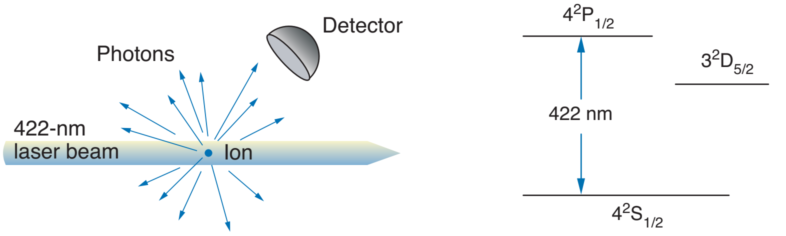

(b) The scattering stops when the ion jumps to the long-lived $3^2D_{5/2}$ state

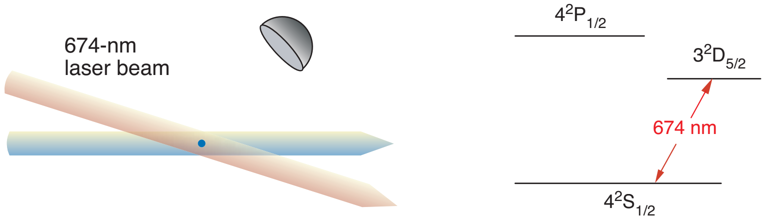

(c) Data from a quantum-jump experiment

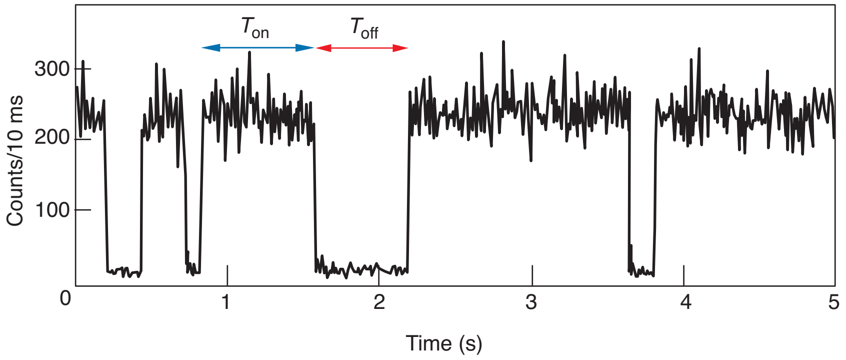

Figure 2. Quantum Jumps in a Single Trapped $^{88}Sr^+$ Ion

(a) When illuminated by 422-nm radiation, a single strontium ion will cycle between the $S_{1/2}$ and $P_{1/2}$ states and will scatter millions of photons per second. Some of the scattered light can be collected with a simple optical detector in order to monitor the state of the ion. (b) If the ion is simultaneously illuminated with 674-nm radiation, it will occasionally undergo a transition ("quantum jump") from the $S_{1/2}$ state to the long-lived $D_{5/2}$ state. The scattered light then disappears. (c) This plot shows typical data from the quantum-jump experiment. When the count rate is over 50 counts per 10 ms, the atom is cycling between the $S_{1/2}$ and $P_{1/2}$ states. When the count rate suddenly falls to less than 50 counts per 10 ms, the atom has made a transition into the $D_{5/2}$ state. We continuously monitor the ion's scattering rate for nearly an hour to observe tens of thousands of these transitions.

outcome is a photon hitting a beam splitter (Jennewein et al. 2000). The photon has a probability to either pass through the optic or reflect off it, and only a measurement determines its fate. Another example is the decay of radioactive nuclei, which emit, say, alpha particles at unpredictable times (Silverman et al. 2000). Although both those processes are believed to be random, they suffer from one major drawback in a test of their statistics: As in any experimental setup, all the detectors have physical limitations. Therefore, we cannot be sure that we would detect every photon or alpha particle. It is possible that some nonrandom processes might be overlooked in analyzing the incomplete data set.

In contrast, a very clean way to test the statistical nature of quantum processes is to analyze the behavior of an atom undergoing quantum jumps (Erber 1995). Quantum jumps are the sudden transitions from one quantum state to another. As Figure 2 shows, a strontium ion in the $S_{1/2}$ ground state will absorb a photon from a laser tuned to 422 nanometers and "jump" to the $P_{1/2}$ excited state. Because the $P_{1/2}$ state is short-lived, the ion quickly returns to the $S_{1/2}$ state by emitting a 422-nanometer photon in a random direction. Once it returns to the $S_{1/2}$ state, the ion can absorb and emit another photon, and because the lifetime of the $P_{1/2}$ excited state is so short, the ion will scatter millions of photons per second. We can detect enough of the scattered light with an optical system to observe the ion but not enough to determine every time the ion jumps to and from the $P_{1/2}$ state.

To directly observe quantum jumps, we simultaneously illuminate the ion with a 422- and a 674-nanometer laser light. In addition to jumping to the $P_{1/2}$ state, now the ion can also jump to the $D_{5/2}$ state. As soon as that transition occurs, the ion will stop scattering 422-nanometer light. The scattered light will return the moment the ion has left the $D_{5/2}$ state. As Figure 2 shows, we can very easily record every time a single ion makes a transition to the $D_{5/2}$ state and every time it returns to the $S_{1/2}$ state. According to quantum theory, the exact times of those transitions are completely unpredictable. Surprisingly, this prediction has not been tested with data sets comprising much more than about a thousand consecutive events. It is important to test very large sets of data because it is harder to make a nonrandom series of numbers appear random if the series is very long.

Many tests can be used to determine the degree of randomness in a string of data. Figure 3(a) shows the result of one such test applied to our quantum-jump data (Itano et al. 1990). A single atom was continuously monitored until it had made over 34,000 transitions in and out of the $D_{5/2}$ state. We record the length of each time period $T_{\mathrm{on},i}$, during which the atom continually scatters 422-nanometer photons, and the length of each subsequent time period $T_{\mathrm{off},i}$, during which the ion scattered no photons because it was in the $D_{5/2}$ state. For example, in the figure, the values of T_{off} are $T_{\mathrm{off},1} = 0.23$ second, $T_{\mathrm{off},2} = 0.1$ second, $T_{\mathrm{off},3} = 0.61$ second, and $T_{\mathrm{off},4} = 0.17$ second.

We then sift through the data to determine the number of times a particular pair of values ($T_{\mathrm{off},i}$, $T_{\mathrm{off},i+1}$) occurs and make the color-coded plot shown in Figure 3(a). The symmetry and shapes of these graphs reflect several important characteristics of the data. For example, a pair of values, say ($T_{\mathrm{off},i}$, $T_{\mathrm{off},i+1}$) = (0.23 second, 0.1 second), is just as likely to occur as the pair (0.1 second, 0.23 second)—a long period of fluorescence is no more likely to be followed by a short one than a short period is likely to be followed by a long one. Essentially, plots like these indicate that the ion has no memory of what it was doing just the briefest moment before it fluoresces. This fundamental feature of quantum processes has not previously been tested precisely. It is also exactly what one would like to see in a random number generator.

We can easily convert the quantum-jump data into a string of 1s and 0s. If $T_{\mathrm{on},i}$ is more than a set amount of time, we assign to that event the value 0. Likewise, if $T_{\mathrm{on},i}$ is less than this time, we will assign the value 1 to the event. Figure 3(b) gives an

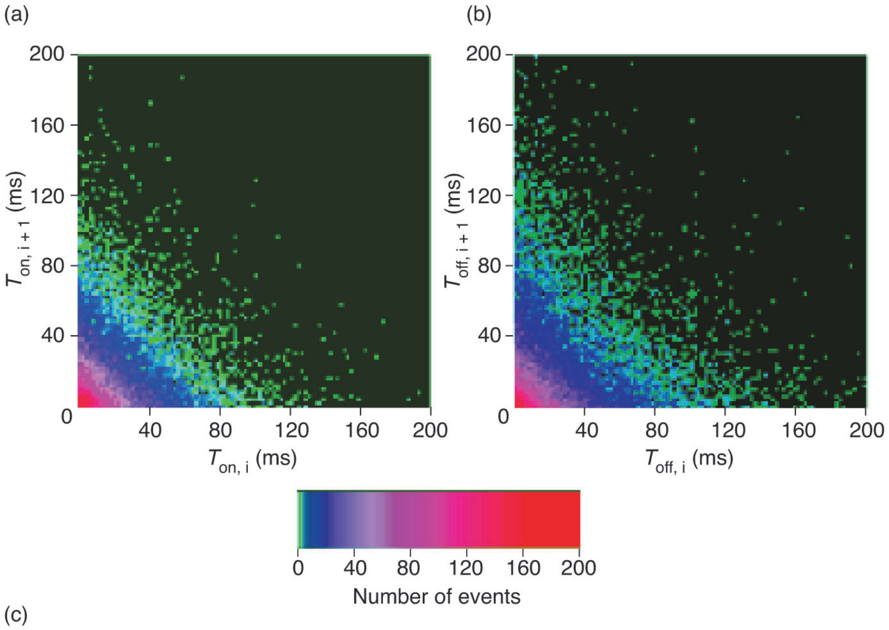

(c)

Set 1

4	2	18	86	14	8	52
16	10	10	22	78	146	196
180	84	134	6	52	2	32
72	34	76	112	12	16	2
82	28	6	54	4	170	38
22	42	78	6	22	2	186
32	82	66	48	30	54	32
4	16	32	28	126	34	74

Set 2

1	1	1	0	1	1	0
1	1	1	1	0	0	0
0	0	0	1	0	1	0
0	0	0	0	1	1	1
0	1	1	0	1	0	0
1	0	0	1	1	1	0
0	0	0	0	0	0	0
1	1	0	1	0	0	0

Figure 3. Analyzing Quantum-Jump Data

The scatter plots show consecutive periods that the ion spends (a) scattering 422-nm photons ($T_{\mathrm{on},i}$, $T_{\mathrm{on},i+1}$) and (b) not scattering 422-nm photons ($T_{\mathrm{off},i}$, $T_{\mathrm{off},i+1}$). Because these graphs are symmetric about their diagonal axis, we can tell that the ion is just as likely to spend a long time scattering photons followed by a short time scattering photons as it is to spend a short time followed by a long time scattering photons. This is one of many indications that the ion has no memory of when it has made a transition between the $S_{1/2}$ and $D_{5/2}$ states. (c) The quantum-jump data can also be converted to digital data. The first set of numbers shows a string of consecutive times spent in the $D_{5/2}$ state ($T_{\mathrm{off},i}$). If the ion spends 30 ms or more in the $D_{5/2}$ state, the event is assigned a value of 0. Otherwise, the event is assigned a value of 1. These assignments are shown in set 2. With strings of tens of thousands of these digital numbers, we can use established protocols to test the randomness of our quantum-jump data.

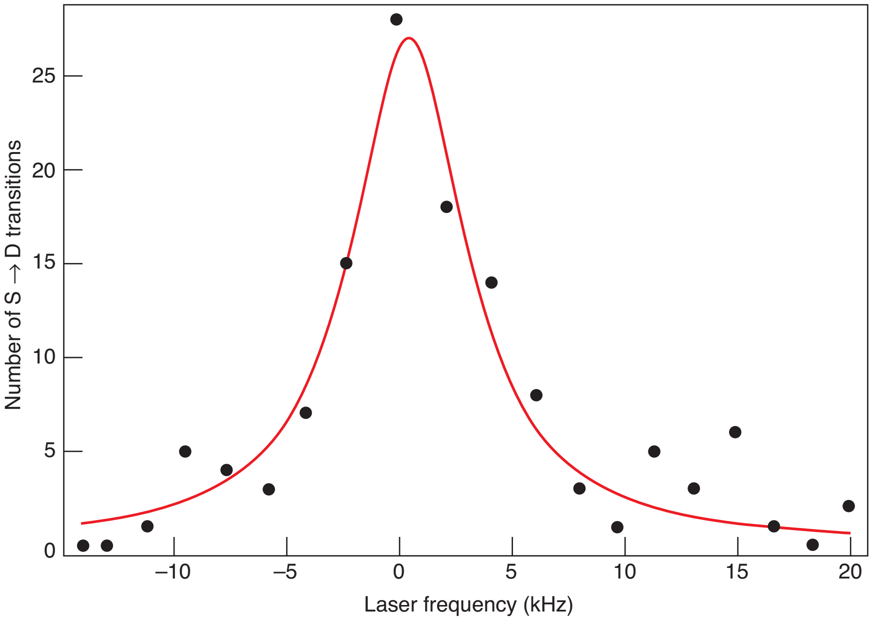

Figure 4. Measurement of the Laser Linewidth

The plot shows data taken from the narrow sideband of the $S_{1/2} \leftrightarrow D_{5/2}$ transition in a single trapped $^{88}Sr^+$ ion. The solid line is a Lorentzian line shape that is fitted to the data. In one laser probe cycle, the atom starts in the $S_{1/2}$ state. Next, the cooling light is turned off while the 674-nm light is pulsed on for 0.001s. Then the cooling light is turned on again, and we see if any 422-nm light is scattered into the detector. If not, then the 674-nm laser has successfully transferred the ion to the $D_{5/2}$ state. This process is repeated 100 times for each laser frequency.

example of this conversion for a typical set of data.

Digitizing our data lets us use some of the established protocols that test the randomness of digital data. (One such standard is outlined in the U.S. Federal Information Processing Standards publication 140-2). An example of such a test is the following: In a string of 1s and 0s, we count how many times the two-digit patterns (0,0), (0,1), (1,0) and (1,1) appear. We then compare these numbers with the values expected for an ideal, random sequence. It is easy to calculate how likely it is that the measured sets of values differ from the expected ones, so that we can decide whether or not our quantum-jump data are random according to the given protocol. We are collecting continuous sequences of data, tens of thousands of events long, that can be used for these tests.

Quantum Computing

We are also beginning some of the tasks that are prerequisites to making a quantum logic gate with a trapped ion. Perhaps the most critical step is coherently driving transitions between specific qubit states. In the experiments we are considering, the strontium $S_{1/2}$ ground state corresponds to the qubit state $|0\rangle$, whereas the $D_{5/2}$ excited state corresponds to the $|1\rangle$ qubit state. The stable 674-nanometer diode laser couples the qubit states to each other and to states of the ion's quantized external motion that would also be qubit states (Monroe et al. 1995).

The stability of the laser is one of several parameters that can limit the performance of a quantum computer. If the laser frequency and phase were constant, we could almost always complete quantum logic operations perfectly. For example, starting with the ion in the $S_{1/2}$ state, we could reliably create a specific superposition of the $S_{1/2}$ and $D_{5/2}$ states:

$$\left|S_{1/2}\right\rangle = \frac{\left|S_{1/2}\right\rangle + i\left|D_{5/2}\right\rangle}{\sqrt{2}} \quad . \qquad (1)$$

However, if the phase or frequency of the laser is not perfectly stable while this operation is taking place, the result of the operation may be, for example,

$$\left|S_{1/2}\right\rangle = \frac{0.99\left|S_{1/2}\right\rangle + i1.01\left|D_{5/2}\right\rangle}{\sqrt{2}} \qquad (2)$$

In this case, the new wave function has a small phase error. If this operation is repeated many times, the accumulations of these small errors could invalidate the results of a quantum computation. Because every laser has a nonzero linewidth (proportional to the laser's frequency), such errors are inevitable. One way to reduce the likelihood of introducing the errors is to perform the logic operation quickly, that is, faster than the typical time scales of the frequency fluctuations of the laser, although it is easier to perform a quantum-gate operation slowly. Thus, it is critical that the laser be very stable with its linewidth as small as possible.

We have measured our laser linewidth using a procedure related to the quantum-jump experiment described earlier. First, we turn off the 422-nanometer light, letting the ion decay to the $S_{1/2}$ state. Then we illuminate the ion with a pulse of 674-nanometer laser light. (The 422-nanometer light remains off during this step, because that light will perturb the $S_{1/2}$ state and broaden the $S_{1/2} \leftrightarrow D_{5/2}$ transition.) We then determine whether or not the laser has driven the atom from the $S_{1/2}$ to the $D_{5/2}$ state by shining the

422-nanometer light on the ion. We detect light scattered by the ion if it is not in the $D_{5/2}$ state, but only background light (the small amount of light scattered off the trap and vacuum chamber) if the ion is in the $D_{5/2}$ state. Figure 4 shows the number of times the 674-nanometer laser transfers the ion to the $D_{5/2}$ state as the laser frequency is scanned over one of the motional sidebands of the $S_{1/2} \leftrightarrow D_{5/2}$ transition. The figure also shows the result of fitting a Lorentzian-shaped curve to these data. From the shape of the fitted curve and from a few key experimental parameters, we can determine that the laser linewidth is about 4 kilohertz or less, which is about one percent of one billionth of the absolute frequency of the laser light (445 terahertz).

This laser linewidth is sufficiently narrow so that we can perform specific, coherent operations on qubit states. However, to perform the operations needed for a quantum logic gate, the ions must be cooled much more than they are at present, so that the quantum state of the ion can be initialized to the ground state of its motion. We are currently working toward this goal and on further narrowing the linewidth of the 674-nanometer laser. In addition, we are working on or anticipate performing several other quantum-optics experiments. The apparatus presented here, along with ion traps in general, can facilitate significant contributions to the field of quantum information and quantum computation. ■

Acknowledgments

I would like to thank Richard Hughes for suggesting the study of the randomness of quantum jumps and for his indispensable role in bringing ion-trap technology to the field of quantum information and quantum computation at Los Alamos. In addition, I am grateful to Daisy Raymondson for her work on some of the laser systems used in this experiment and to the Los Alamos Summer School for initially bringing her to Los Alamos.

Further Reading

Berkeland, D. J., A Linear Paul Trap for Strontium Ions. (To be published in *Rev. Sci. Instrum.*)

Berkeland, D. J., J. D. Miller, F. C. Cruz, B. C. Young, R. J. Rafac, X.-P. Huang et al. 1999. High-Resolution, High-Accuracy Spectroscopy of Trapped Ions. In *Atomic Physics 16. Proceedings of the International Conference*. Edited by W. E. Baylis and G. W. F. Drake, 29. New York: AIP Press.

Erber, T. 1995. Testing the Randomness of Quantum-Mechanic: Natures Ultimate Cryptogram. *Ann. N. Y. Acad. Sci.* **755**: 748.

Itano, W. M., J. C. Bergquist, F. Diedrich, and D. J. Wineland. 1990. Quantum Optics of Single, Trapped Ions. In *Coherence and Quantum Optics VI*, 539. Edited by J. H. Eberly, et al. New York: Plenum Press.

Jennewein, T., U. Achleitner, G. Weihs, H. Weinfurter, and A. Zeilinger. 2000. A Fast and Compact Quantum Random Number Generator. *Rev. Sci. Instrum.* **71** (4): 1675.

Monroe, C., D. M. Meekhof, B. E. King,, W. M. Itano, and D. J. Wineland. 1995. Demonstration of a Fundamental Quantum Logic Gate. *Phys. Rev. Lett.* **75**: 4714.

Silverman, M. P., W. Strange, C. Silverman, and T. C. Lipscombe. 2000. Tests for Randomness of Spontaneous Quantum Decay. *Phys. Rev. A* **61**: 042106.

Thompson, R. C., K. Dholakia, J.-L. Hernandez-Pozos, G. Zs. K. Horvath, J. Rink, and D. M. Segal. 1997. Spectroscopy and Quantum Optics with Ion Traps. *Physica Scr.* **T72**: 24.

Dana J. Berkeland has performed a wide variety of experiments in atomic and optical physics. She received her Ph.D. from Yale University in 1995 after precisely measuring Stark shifts in lithium and cesium and measuring the ground-state Lamb shift in hydrogen to an accuracy of 6 parts per million. This measurement, performed with Malcolm Boshier, was at the time the most precise measurement of the quantity. Dana spent three years as a National Research Council postdoctoral fellow at the National Institute of Standards and Technology in Boulder, Colorado, where she evaluated a trapped-mercury-ion microwave frequency standard to a fractional accuracy of 3×10^{-15} (making it one of the most accurate frequency standards in the world). In 1998, she came to Los Alamos National Laboratory as a J. Robert Oppenheimer postdoctoral fellow to build a laboratory for quantum-optics experiments with trapped strontium ions and became a technical staff member in 2000. She has over a decade of experience in building and developing laser systems and related optics. Dana has over seven years of experience in building and working with ion trapping systems.

Theory of Single-Spin Detection with a Scanning Tunneling Microscope

Alexander V. Balatsky and Ivar Martin

No fundamental principle precludes the measurement of a single spin, and therefore the capability to make such a measurement simply depends on our ability to develop a detection method of sufficient spatial and temporal resolution. The standard electron spin detection technique—electron spin resonance—is limited to a macroscopic number of electron spins (10^{10} or more) (Farle 1998). A state-of-the-art magnetic resonance force microscope has recently detected about a hundred fully polarized electron spins (Bruland et al. 1998). We argue that scanning tunneling microscopy offers a powerful technique to detect a single spin and propose the theoretical basis for the new spin-detection technique, which we call spin precession by scanning tunneling microscopy.

The capability to routinely detect and manipulate a single spin would be remarkably useful, with applications ranging from the study of strongly correlated systems to nanotechnology and quantum information processing. For example, we could investigate magnetism on the nanoscale in a strongly correlated system by detecting changes in the spin behavior as the system enters the magnetically ordered state (Heinze et al. 2000). We could also fully explore the magnetic properties of a single paramagnetic atom in the Kondo regime (Manoharan et al. 2000). Magnetic properties of spin centers in superconductors are another area where a single spin plays an important role, since it can generate intragap impurity states (Salkola et al. 1997, Yazdani et al. 1997). With regard to nanotechnology, the ability to manipulate a single spin could open the door to single-spin-based information storage devices, whereas in the realm of quantum computing, it could help bring to fruition several specific computing architectures (Kane 1998, Loss and DiVincenzo 1998).

Our theoretical investigation of spin precession–scanning tunneling microscopy has in part been motivated by the experiments of Yshay Manassen et al. (1989), in which a defect structure (an oxygen vacancy) in oxidized silicon was interrogated with a scanning tunneling microscope (STM). The STM operated in the presence of an external magnetic field, and a small alternating current (ac) signal in the power spectrum of the tunneling current was detected at the spin's precession, or Larmor, frequency. The ac signal was spatially localized at distances of about 5–10 angstroms from the spin site. The extreme localization of the signal and the linear scaling of its frequency with the magnetic field prompted Manassen to attribute the detected ac signal to the Larmor precession of a single-spin site. Whereas that interpretation was somewhat controversial, the later work by Manassen et al. (2000) and more recent work by Colm Durkan and Mark Welland (2002) support the notion that STM can indeed sense a single spin.

From a theoretical perspective, it was not clear how the spin could generate an ac component in the STM's tunneling current. As outlined below, however, the precessing spin causes an ac modulation of the surface density of states near the spin site, provided a dc current flows through the surface. In fact, that current can be the tunneling current that flows between the STM tip and the surface. Thus, the tunneling current, which is proportional to the surface density of states, plays two roles in spin detection by scanning tunneling microscopy: It provides a means to couple the precessing spin to

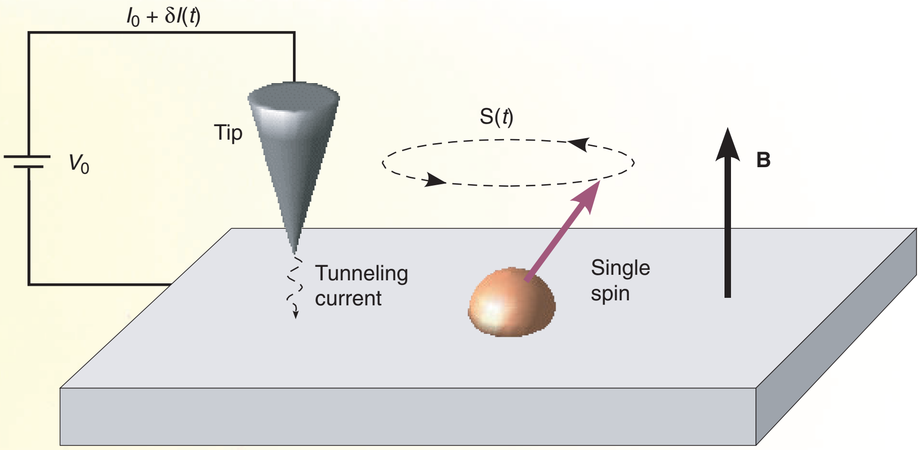

Figure 1. Experimental Setup for Electron Spin Precession by Scanning Tunneling Microscopy
In the applied magnetic field B, the spin of the magnetic atom (for example, gadolinium, shown in gold) is precessing around the field line. The STM tip is precisely positioned within a few angstroms of the spin site. The dc tunneling current I_0, between the STM tip and the sample, can acquire an ac component, $\delta I(t)$, that signals the presence of the precessing spin.

the density of states and a means to detect the ac modulation of those states. The experimental setup that we consider is shown in Figure 1. A general discussion of the principles underlying scanning tunneling microscopy can be found on page 303.

Before analyzing the effect of the STM, consider a localized magnetic site with spin **S** (spin 1/2), on the surface of a substrate. In the presence of a magnetic field, **B**, the energy levels of the spin-up and spin-down states (denoted by $E_\uparrow$ and $E_\downarrow$, respectively) are Zeeman-split. At a finite temperature, or as a result of an external excitation, the spin may be driven into the mixed state characterized by the wave function

$$|\psi(t)\rangle = \alpha(t)\,|\uparrow\rangle + \beta(t)\,|\downarrow\rangle \ , \tag{1}$$

where

$$\alpha(t) = |\alpha| \exp(-iE_\uparrow t) \ , \text{ and}$$
$$\beta(t) = |\beta| \exp(-iE_\downarrow t + i\phi(t)) \ .$$

The phase $\phi(t)$ determines the spin coherence time τ_ϕ and is related to the spin relaxation time T_2 measured by electron spin resonance.

In the state given by Equation (1), the spin, with an expectation value of

$$\frac{\langle \psi(t)|\mathbf{S}|\psi(t)\rangle}{\langle \psi(t)|\psi(t)\rangle} \ , \tag{2}$$

will precess around a magnetic field line at the Larmor frequency ω_L,

$$\hbar\omega_L = E_\uparrow - E_\downarrow = \gamma B \tag{3}$$

where γ is the gyromagnetic ratio. (See the box “Spin Manipulation with Magnetic Resonance” on page 288.) In a magnetic field of 100 gauss, this frequency is 280 megahertz for a free electron.

If we consider what happens on the surface, then the precession of the local moment will be coupled to the orbital motion of electrons via the spin-orbit interaction. The details of the spin-orbit coupling depend on the specific material. In general, however, the interaction of the conduction electrons with the local impurity spin can be described by the Hamiltonian

$$H = H_0 + J\,\mathbf{S}\cdot\sigma(0) \quad , \tag{4}$$

where J is the strength of the exchange interaction between the local spin $\mathbf{S}$, and the spin density of the conduction electrons, $\sigma(0) = \sigma_{\alpha\beta}\, c^{\dagger}_{\alpha}(0)\, c_{\beta}(0)$, on the impurity site. Here, $c^{\dagger}_{\alpha}(0)$, $c_{\beta}(0)$ are the electron creation/destruction operators with spin α and β, respectively, and $\sigma_{\alpha\beta} = (\sigma^{x}_{\alpha\beta}, \sigma^{y}_{\alpha\beta}, \sigma^{z}_{\alpha\beta})$ is a vector of Pauli matrices. The unperturbed Hamiltonian H_0 describes the surface without the spin impurity. Based on symmetry, the energy of the unperturbed surface states contains a spin-orbit part that is linear both in the conduction-electrons' spin, σ, and their momentum, $\mathbf{k}$ (Bychkov and Rashba 1984).

$$\varepsilon(\mathrm{k}) = \frac{k^2}{2m^*} + \gamma_{\mathrm{SO}}\left[\mathbf{n} \times \mathbf{k}\right] \cdot \hat{\sigma} \quad , \tag{5}$$

where m^* is the band mass of electrons in the substrate, $\mathbf{n}$ is a unit vector normal to the surface, and γ_{SO} is a parameter that characterizes the strength of the surface spin-orbit coupling. The problem specified by Equations (4) and (5) can be solved for each instantaneous value of the precessing spin $\mathbf{S}(t)$. The solution, however, does not lead to a time-dependent conduction-electron density of states $N(\mathbf{r}, t)$ because the effects of the precessing spin average to zero. In that case, the tunneling current would remain constant.

To extend the model, we account for the fact that the tunneling current injects electrons into the sample, and those electrons can flow to the spin site. In the presence of a current density $\boldsymbol{j}$ flowing through the surface, the equilibrium momentum distribution $\mathbf{k}$ is shifted by an amount, $\mathbf{k}_0 = \boldsymbol{j}m^*/ne$, where n is the carrier density and e is the electron charge. This shift can be introduced into a Green's function matrix for the conduction electrons, $\hat{G}_0(\mathbf{k},\omega)$,

$$\hat{G}_0(\mathbf{k},\omega) = \left[\omega - \frac{(\mathbf{k} - \mathbf{k}_0)^2}{2m^*} - \gamma_{\mathrm{SO}}\left[\mathbf{n} \times \mathbf{k}\right] \cdot \hat{\sigma}\right]^{-1} \quad . \tag{6}$$

We expand the matrix in γ_{SO} relative to the Fermi energy. Then, to first order in both the exchange coupling J and γ_{SO}, we obtain an $\mathbf{S}$-dependent contribution to the density of the surface states:

$$\frac{\delta N}{N} = \gamma_{\mathrm{SO}}\, J\, \frac{dN}{dE}\, J_0^2(k_F r)\left[\mathbf{k}_0 \times \mathbf{S}\right]_n \quad . \tag{7}$$

This correction depends on the distance from the spin center, r, through the Bessel function of the first kind, $J_0(x)$. The correction is time dependent in the presence of a magnetic field because the projection of $\mathbf{S}$ oscillates at the Larmor frequency. The magnitude of the correction is proportional to the current density in the system (through $\mathbf{k}_0$).

The total (ac plus dc) tunneling current I, between the STM tip and the sample is proportional to the single-electron density of states in the substrate. Therefore, the ac component $\delta I(t)$, normalized to the tunneling current, can be estimated as

$$\frac{\delta I(t)}{I} = \frac{\delta N(t)}{N} \ . \tag{8}$$

We have focused on the case in which an STM injects current into the system, but in principle, the current can also be provided externally (through extra leads attached to the substrate), and the ac current can be detected with some ultrasensitive current measurement device.

It is also important to note that the electron density of states $N(\mathbf{r}, t)$ is a scalar and should be invariant under time reversal, whereas $\mathbf{S}$ is odd under time reversal. Hence, $\delta N(\mathbf{r}, t)$ can depend only on the product of the spin vector with some other vector that is odd under time reversal. In Equation (7), that vector is the current density, that is, $\delta N \sim [\mathbf{k}_0 \times \mathbf{S}]_n$. Another possibility is that the correction to the density of states depends on the time derivative of the spin vector, that is, $\delta N \sim \partial_t \mathbf{S}(t)$. We have also found a mechanism for this possibility.

Our conjecture of how an STM can detect single spins is based on the ac modulation of the density of surface states that results from a current-induced spin-orbit coupling to the precessing local spin. The changing state density is observed as the ac component to the tunneling current. ■

Alexander Balatsky received his Ph.D. in 1987 from the Landau Institute for Theoretical Physics, where he then worked as a researcher until 1989. From 1989 to 1991, he was at the University of Illinois at Urbana-Champaign, where he became a visiting resident assistant professor in 1990. In 1991, he joined Los Alamos National Laboratory as a J. R. Oppenheimer Fellow and is currently a technical staff member in the Theoretical Division.

Ivar Martin is a technical staff member in the Theoretical Division at Los Alamos National Laboratory. He received his Ph.D. from the University of Illinois at Urbana-Champaign in 1999. His research interests include the theory of strongly correlated systems, development of novel local probes, and the theory of quantum measurement and computation.

Further Reading

Balatsky, A. V., and I. Martin. 2001. Theory of Single Spin Detection with STM. [Online]: http://eprints.lanl.gov (cond-mat/0112407).

Bruland, K. J., W. M. Dougherty, J. L. Garbini, J. A. Sidles, and S. H. Chao. 1998. Force-Detected Magnetic Resonance in a Field Gradient of 250 000 Tesla per Meter. *Appl. Phys. Lett.* **73** (21): 3159.

Bychkov, Y. A., and E. I. Rashba. 1984. Properties of a 2D Electron Gas with Lifted Spectral Degeneracy. *JETP Lett.* **39** (2): 78.

Durkan, C., and M. E. Welland. 2002. Electronic Spin Detection in Molecules Using Scanning-Tunneling-Microscopy-Assisted Electron-Spin Resonance. *Appl. Phys. Lett.* **80** (3): 458.

Farle, M. 1998. Ferromagnetic Resonance of Ultrathin Metallic Layers. *Rep. Prog. Phys.* **61** (7): 755.

Heinze, S., M. Bode, A. Kubetzka, O. Pietzsch, X. Nie, S. Blugel, and R. Wiesendanger. 2000. Real-Space Imaging of Two-Dimensional Antiferromagnetism on the Atomic Scale. *Science* **288** (5472): 1805.

Kane, B. E. 1998. A Silicon-Based Nuclear Spin Quantum Computer. *Nature* **393**: 133.

Loss, D., and D. P. DiVincenzo. 1998. Quantum Computation with Quantum Dots. *Phys. Rev. A* **57**: 120.

Manassen, Y., I. Mukhopadhyay, and N. R. Rao. 2000. Electron-Spin-Resonance STM on Iron Atoms in Silicon. *Phys. Rev. B* **61** (23): 16223.

Manassen, Y., R. J. Hamers, J. E. Demuth, and A. J. Castellano Jr. 1989. Direct Observation of the Precession of Individual Paramagnetic Spins on Oxidized Silicon Surfaces. *Phys. Rev. Lett.* **62**: 2531.

Manoharan, H. C., C. P. Lutz, and D. M. Eigler. 2000. Quantum Mirages Formed by Coherent Projection of Electronic Structure. *Nature* **403**: 512.

Salkola, M. I., A. V. Balatsky, and J. R. Schrieffer. 1997. Spectral Properties of Quasiparticle Excitations Induced by Magnetic Moments in Superconductors. *Phys. Rev. B* **55**: 12648.

Wiesendanger, R., H.-J. Güntherodt, G. Güntherodt, R. J. Gambino, and R. Ruf. 1990. Observation of Vacuum Tunneling of Spin-Polarized Electrons with the Scanning Tunneling Microscope. *Phys. Rev. Lett.* **65**: 247.

Yazdani, A., B. A. Jones, C. P. Lutz, M. F. Crommie, and D. M. Eigler. 1997. Probing the Local Effects of Magnetic Impurities on Superconductivity. *Science* **275** (5307): 1767.